SHOCK TUBE INVESTIGATION AND MODELING OF DICYCLOPENTADIENE: FUNDAMENTAL TO APPLICATION

KUNAL VISHWANATH DHOKE

Ph.D. Thesis

October 2021

Department of Inorganic and Physical Chemistry,
Indian Institute of Science
Bengaluru – 560016 (India)

SHOCK TUBE INVESTIGATION AND MODELING OF DICYCLOPENTADIENE: FUNDAMENTAL TO APPLICATION

A thesis
submitted for the degree of
DOCTOR OF PHILOSOPHY
in the faculty of Science
by

KUNAL VISHWANATH DHOKE

Department of Inorganic and Physical Chemistry
Indian Institute of Science
Bengaluru- 560 012
India

OCTOBER - 2021

Dedicated to my late Mother

DECLARATION

I hereby declare that the work embodied in this thesis has been carried out by me for the degree of Doctor of Philosophy and no part of it has been submitted for any degree of any institution previously. Wherever the contribution from others is involved in any form, every effort is made to indicate it clearly, with due reference and acknowledgment. I hereby permit the Indian Institute of Science to use, display or transfer any of the thesis details furnished by me to other institutions or individuals for the purpose of scholarly research.

Department of Inorganic and Physical Chemistry, Kunal V. Dhoke
Indian Institute of Science, October 2021
Bangalore-560012, India.

CERTIFICATE

We hereby declare that the work presented in this thesis entitled "**Shock Tube Investigation and Modeling of Dicyclopentadiene: Fundamental to Application**" is the result of original research work performed by Kunal V. Dhoke at the Department of Inorganic and Physical Chemistry, Indian Institute of Science, Bangalore, India under our supervision and any part of it has not been carried submitted for any degree of any institution previously. The work presented by him in this thesis is, to the best of our knowledge and belief, original except as acknowledged in the text.

Prof E. Arunan
(Research Supervisor)
Dept. of Inorganic and Physical Chemistry,
Institute of Science,
Bangalore-560012, India.

Prof K P J Reddy
(Co-Supervisor)
Dept. of Aerospace Engineering
Institute of Science,
Bangalore-560012, India.

ACKNOWLEDGEMENTS

I am grateful to numerous "peers" who have contributed towards shaping this thesis. First and foremost, I would like to express my appreciation to **Professor E Arunan** and **Professor K P J Reddy** for their advice during my doctoral research endeavor for the past seven years. I am deeply grateful to them for their constant encouragement, guidance, and forced me to remain focused on achieving my goal. I am very grateful to Professor E Arunan as a teacher, a friend, a role model, and pillar support in my guide. I thank him for introducing me to the fascinating world of shock tube and its application in chemical kinetics. Beyond the discussion on chemical kinetics, the insight and perspective on many aspects apart from research are things that I will keep close to my heart.

I am very grateful to Professor K P J Reddy for his mentorship and the opportunity that he offered to me to work in the Laboratory for Hypersonic and Shock Wave Research (LHSR), a unique lab of its own kind at the Indian Institute of Science, Bangalore. I would like to express my deepest sense of gratitude to him for allowing me to be a part of this community. His unique traits such as a passion for innovative research which benefits every common man will be an inspiration for life.

I am very grateful to **Professor G Jagadeesh** for his continuous encouragement throughout my stay at IISc and the invaluable comments and suggestions at critical stages were major motivations.

I would like to express my sincere thanks to the Chairmen (present and past) of the Inorganic and Physical Chemistry Department for providing me the facilities to carry out my research. I thank all the faculty members of the department for their encouragement and support.

I am grateful to Dr. Tarandeep Singh for contributing scientifically towards the incorporation of insert in the driver section of the shock tube. He has helped me greatly and been a source of knowledge with remarkable programming skills.

I would like to thank my lab-mates Kiran, Subharaj, Snehal, Balaji, Lakhan, Pradeep, Sudarshan, Ramji, Gopalkrishna, Snehdeep, Ankit are always helpful and appreciated. I thank all my friends, batchmates, and well-wishers for their constant support and valuable suggestions.

I thank IISc for providing the Supercomputer Education and Research Center facility during my stay in IISc.

I would like to thank my parents which forms an important foundation for this accomplishment and without them, it would certainly have been a more challenging path. To achieve this success, my ravenous curiosity was nurtured by the sacrifice, encouragement, and love of my parents. My family's love has always provided me a great source of inspiration, words would not be enough to express my full gratitude, other than to say thank you.

I would like to express my sincere thanks to an important pillar of LHSR, Mr. Jeevan (official storekeeper of LHSR), Mr. Gangadhar Moorthy, Mr. Rajajgopal, Mr. N Kumar, Mrs. Shashikala, and Mr. Raghu for their assistance and help. A special thanks to Mr. K Nagashetty for his encouragement and suggestions are

highly acknowledged. I would like to thank my senior Chintoo, Janardhan, Anbuselvan, Abhishek, Balakalyani, and Srinath for their support and help.

I thank IISc for the travel grant for attending the ISSW-30 conference in Tel Aviv, Israel.

I am extremely grateful to all my teachers and well-wishers. Finally, I would like to thank everybody who was directly or indirectly behind the accomplishment of my thesis.

Above all, I would like to thank God Almighty for the blessings he has showered upon me and for giving me wisdom, strength, and ability to undertake this beautiful journey of research.

Kunal Vishwanath Dhoke

NOMENCLATURE

P	Pressure (bar)
T	Temperature (K)
v	Velocity (m/s)
a	Velocity of sound (m/s)
ρ	Density (kg/m^3)
M	Molecular weight (g)
γ	Specific heat ratio
R	Universal gas constant($m^3Pamol^{-1}K^{-1}$)
τ	Dwell time or Reaction time (sec)
ϕ	Equivalence ratio
M_s	Mach number
W_s	Shock wave speed
dP_5^*/dt	Rate of change of P_5 with time
Λ	Shock wave attenuation rate
$'g'$	Equivalence factor
k_B	Boltzmann constant
$k(T)$	Rate constant
E_a	Activation energy
A	Pre-exponential factor
Q	Total partition function

CONTENTS

LIST OF FIGURES

LIST OF TABLES

ABSTRACT

Research into energy sources remains an important field of activity and requires detailed investigation. Over the last 90 years, fuel has been leading primary research work in the field of combustion. There is a large class of fuels that are currently used in automobiles and almost all are made of hydrocarbons and/or alcohol. Once energy is supplied to a fuel/oxygen(or air) mixture, the fuel will undergo cracking generating the radicals that propagate the reaction with oxygen. Understanding the combustion chemistry of hydrocarbon fuel and the process of soot formation is one of the growing areas of research. In particular, polycyclic aromatic hydrocarbon (PAHs), which are considered to be combustion-generated pollutants, and their role in the formation of soot is of greater interest due to its adverse effect on the environment. The work presented in this thesis tries to address the above issue and provide a better understanding of the combustion process.

Dicyclopentadiene (DCPD), a homodimer of cyclopentadiene (C_5H_6) was chosen for the present study. DCPD can be obtained by dehydrogenation of JP-10 (jet propellant $C_{10}H_{16}$) which is currently used as aviation fuel. The combustion chemistry for JP-10 is well established. Very few studies are present in the literature on the thermal decomposition of dicyclopentadiene. Hence, to begin with, the thermal decomposition of DCPD was carried out in a single pulse shock tube. The shock tube is incorporated with the step size driver insert to correct the non-ideal pressure rise due to non-ideal effects. Hence it facilitates the near-ideal behavior behind the reflected shock wave region. The experiments were performed behind the reflected shock wave in the temperature range of 1250-1550 K and pressure range of 13-16 atm. Also, Ab-initio calculations were carried out to

find the minimum energy pathway that can lead to the formation of observed products. Thereupon the detailed kinetic modeling was carried out to simulate the concentration profile of different observed products.

Ab-initio calculations were carried for the dissociation reaction of dicyclopentadiene to cyclopentadiene conversion. Quantum theory of atoms in molecule (QTAIM) which is based upon electron density topology provides insight into the reaction. AIM analysis along the reaction coordinate was carried out which provides information about bond breaking and bond making phenomenon occurring during chemical transformation. In addition, AIM analysis was used to identify the various types of non-covalent interactions present in the structures along the reaction coordinate from reactant to product.

Ignition delays were measured for DCPD using the modified chemical shock tube (CST3) to characterize it as a fuel. The measurement of ignition delay times were performed for three different equivalent ratios 0.5, 1, and 1.5. A comparison of ignition delay times between JP-10 and DCPD has been made. Furthermore, a detailed kinetic mechanism was developed for a better understanding. In addition, a comparison was made between the calculated and experimental observed ignition delay times.

SYNOPSIS

Dicyclopentadiene ($C_{10}H_{12}$), a homodimer of cyclopentadiene (cy-C_5H_6), a molecule that has attracted greater interest in the high-temperature gaseous environment such as combustion, flame, etc. A cyclopentadienyl radical (cy-C5H5) [*Int. Sym. on Combustion, 26, 1, 1996, 685-692*], produced during the combustion of hydrocarbons leads to the formation of polycyclic aromatic hydrocarbons (PAHs) and soot. DCPD has received considerable attention for ROMP (ring-opening metathesis polymerization) in solid propellant due to its high polymerization rate, and its ability to provide thermal, chemical, and mechanical stability to its polymer [*Macromolecules, 35, 2002, 7878-7882*]. The hydrogenation of DCPD gives TH (endo-tetrahydridodicyclopentadiene) dimer, which has been used as a fuel in liquid rocket propellant for missiles and jet propellant (JP-10, $C_{10}H_{16}$, currently used as an aviation fuel).

The thesis begins with a brief introduction to the current research topic and moves on to describe the work done in subsequent chapters. In Chapter 2, we discuss the foundation of understanding shockwave-based research and their wide ranges of applications in various interdisciplinary fields. The application of shock wave in chemical kinetics is highlighted along with different methods presently available along with a brief introduction about generating shock wave in a laboratory scale. Also, it discusses non-ideal effects occurring in the shock tube and its consequences on the reflected shock pressure. The non-ideal phenomena such as incident shock wave attenuation, boundary layer growth, and other non-ideal effects can cause a gradual rise in pressure behind the reflected shock wave region. This rise in pressure introduces grave uncertainties in the reflected shock temperature and the result of chemical kinetic studies. In some cases, the rise in

pressure may exceed more than 15%. To overcome this, we have incorporated the step size insert in the driver section. With the proper design of an insert, it is possible to eliminate the non-ideal pressure rise in reflected shock pressure caused by non-ideal effects. The detailed modeling and final insert design used to counterpart non-ideal pressure rise are also presented. Finally, the reflected shock temperature (T_5) calibration study of our chemical shock tube (CST-3) was performed using ethyl chloride as an external standard is discussed. Chapter 3 begins with the experimental investigation on the thermal decomposition of DCPD using a modified shock tube incorporated with the driver insert. The experiments were performed behind the reflected shock wave in the temperature range of 1250-1550 K and pressure range of 13-16 atm. The major products observed during pyrolysis are methane, acetylene, cyclopentadiene, and benzene whereas the minor products include ethylene, propylene, propyne, allene, 1,3-butadiene, vinyl acetylene, toluene, styrene, and phenylacetylene. Whereas benzene, indene, methyl-indenes, and naphthalene are major species formed during cyclopentadiene pyrolysis. Also, Ab-initio calculations help to locate the transition state. We performed the ab-initio calculation for the dissociation reaction of dicyclopentadiene to cyclopentadiene monomer. A kinetic mechanism consisting of 82 reactions and 35 species has been derived for the DCPD thermal decomposition based upon the experimental and theoretical results. Chapter 4 forms the theoretical background for the dissociation reaction of dicyclopentadiene to cyclopentadiene conversion. Quantum theory of atoms in molecule (QTAIM) which is based upon electron density topology provides insight into the reaction. AIM analysis along the reaction coordinate was carried out which provides information about bond breaking and bond making

phenomenon occur during chemical transformation. AIM study shows that the dissociation is initiated by breaking on one C-C bond first and even at the TS only one of the two bridging bonds are broken. Also, a new C-C bond is formed at the transition state characterized by a bond critical point that forms a cage-like structure. In addition, AIM analysis was used to identify various types of non-covalent interactions. DCPD shows the non-bonding interactions correspond to the positive value of sign of $(\lambda_2)\rho$. The transition state exhibit attractive as well as non-bonding interactions correspond to the negative and positive value of sign of $(\lambda_2)\rho$ respectively. Whereas near product geometry shows the nonbonding interactions correspond to a positive value sign of $(\lambda_2)\rho$. For DCPD, gradient isosurfaces represented at the center of the ring signify the steric repulsion between the bridge carbon atoms whereas the isosurfaces present in between the norbornene ring and cyclopentene ring shows repulsive interaction. For the transition state, isosurfaces show a region of non-covalent interaction at the center of two cyclopentadiene rings where Π-stacking is expected. In the case of the near product geometry, the isosurfaces are similar to the transition state geometry. Chapter 5 focuses on the measurement of ignition delay times of dicyclopentadiene (DCPD) in a modified chemical shock tube (CST3). The measurement of ignition delay times were carried out for three different equivalent ratios 0.5, 1, and 1.5. Furthermore, a detailed kinetic mechanism was developed for a better understanding of the oxidation mechanism. In addition, a comparison was made between the calculated and observed ignition delay. The mechanism fairly replicated the observed ignition delay. The comparison between ignition delays of DCPD and JP-10 showed that DCPD resembles almost the same fuel characteristics as that of JP-10. The activation energy for JP-10 and DCPD

oxidation are found to be 37.58 kcal/mol and 36.92 kcal/mol respectively. Chapter 6 forms the comprehensive description of the entire work and emphasizes the salient features of the present work. Also, it presents some suggestions regarding future directions of research related to this work.

1 INTRODUCTION

CHAPTER OVERVIEW

This chapter will form the foundation of understanding the fascinating area of the shockwave. The shockwave-based research and its wide range of applications in various interdisciplinary fields are presented here. In particular, the application of shock wave in chemical kinetics is highlighted along with different methods presently available. Also, the importance of the thermal rate constant is presented. Towards the end of the chapter, the reasons that have been a motivating factor for the present work are enumerated. The chapter concludes with the objectives of the present work along with the organization of the thesis.

1.1 HISTORY

Chemical Kinetic study deals with the determination of the rate of a chemical reaction which provides the information needed for many practical applications. Furthermore, the identification of molecular mechanisms and pathways for chemical reactions are the major cornerstones and goals of physical chemistry. The first key step in this direction was the discovery by Arrhenius [1-2], who proposed the empirical relation which gives the dependence of the rate constant of a chemical reaction on the absolute temperature, a pre-exponential factor, and activation energy of the reaction. According to Arrhenius, before the reactants transform into products, they must first acquire a minimum amount of energy called the activation energy E_a. Later, Eyring, Evans, and Polanyi [3-4] developed the transition state theory (TST) in the 1930s, providing a solid foundation for the empirical Arrhenius equation. According to TST, the rate of reaction can be studied by examining the activated complexes (identified as transition states in recent literature) at the saddle point of the potential energy surface. TST has been most successful in its original goal of calculating absolute reaction rate constants. However, as a notable exception to TST, Arthur Suit, Joel Bowman, and coworkers [5] proposed a roaming pathway for a reaction that bypasses the conventional saddle point transition state to form molecular products. In the roaming mechanism [6-8], the reaction path visits the plateau region of the potential surface near dissociation to radical product followed by intramolecular abstraction to give instead close shell products.

The kinetic modeling of combustion of fuel, and thermal decomposition of hydrocarbon require accurate measurement of thermal rate constant. Understanding the process of formation of polycyclic aromatic hydrocarbons

(PAHs) and soot in a high-temperature gaseous environment has been a subject of investigation due to its scientific and practical importance. PAHs are important intermediates generated during the process of combustion which leads to the formation of soot and even more importantly because of their inherent mutagenic and carcinogenic activity [9-12]. Kinetics of thermal decomposition of lower hydrocarbons such as acetylene [13], ethylene [12], propyne [17], allene [16], and 1,3-butadiene [14] have been studied to understand the initial ring formation and bond-breaking process. Previous studies on higher hydrocarbons like cyclopentadiene [18-19], toluene [20-25], xylene [26-28], JP-10 [29-32], cyclohexane [33-36], cyclohexadiene [37-41], benzene [42-48], styrene [49-50], etc. have been reported.

Over time, advancements in technologies enable us to provide more depth in our understanding and also refinement of kinetic mechanism even when the problems addressed in the 1960s and 2000s may be similar. For example, consider cyclohexane pyrolysis carried out by Ogunye et al. [34] in 1981 and Kiefer et al. [12] in 2009. If one can neglect the experimental range and products formed in both experimental studies, we can see that the earlier study mainly focused on determining the product concentration at various temperatures and the latter one tried to explain in detail the possible pathways leading to the observed products. This may be attributed to the facts like improvisation in detection techniques, theoretical methods, etc. In some way, these improvements have led to a greater understanding of the kinetics of molecules.

1.2 METHODS

Many experimental techniques are currently available which help to study the rate of a reaction. The most common way of activating a molecule for chemical

kinetics studies is by heating and photolysis. For the reactions initiated by heating, reaction time will depend upon the heating procedure as well as the configuration of the reactor. Similarly, the products formed during chemical transformation can be detected and analyzed using different techniques. Some of these methods which are useful for studying chemical reactions occurring in the gas phase even following very rapid reactions are outlined below.

1.2.1 FLOW REACTOR

In kinetic investigations, those mainly concerned with obtaining the fundamental information, it is common to use a static system with reactant confined to reactant vessel and concentration changes are followed. However, in some cases, it is more convenient to allow the reaction mixture to flow through a reaction vessel known as a flow reactor. Such a flow system may be useful when it is desired to study a reaction at low pressure or concentration and study very rapid reactions. As an example, we consider a turbulent adiabatic flow reactor. The flow reactor consists of a cylindrical quartz tube, 10 cm in diameter in which hot inert carrier gas, N_2, flowing with very large velocity is a new type of solution performing chemical reactions. The initial experiments were carried out on the oxidation of methane and carbon monoxide for the temperature range 1100 -1400 K [53]. Nitrogen or air was used as carrier gas and pre-heated by passing through a firebrick red. The oxygen was introduced using the valve in the nitrogen/air flow. The pre-heated carrier gas and oxygen mixture was then mixed with fuel (which in this case is methane or carbon monoxide) at the entrance of the reaction chamber. The reaction chamber was heated by four electrical heaters to maintain the temperature in and around the quartz chamber. The temperature in the reaction zone is measured using a thermocouple. The mixture coming from the

exit of the reactor was collected using a water-cooled sample probe. Typically, the reaction time was in the range of 10-25 sec.

Another example of the flow reactor which was used to carry out kinetic measurements is a tubular flow reactor described by Foulds et al. [55] The first experiment was carried out on H_2S decomposition studies using a tubular flow reactor. The premixed mixture of argon and H_2S maintained at room temperature were passed through the heated quartz tube placed in an electrically heated furnace. A temperature controller equipped with a thermocouple was used to maintain the temperature of the furnace. The linearity of reactant conversion was found to break after 0.2 min. Samples were collected from the exit of the quartz tube for further analysis.

Another type of flow reactor called a jet-stirred reactor can be used to carry out homogeneous gas-phase reactions. James et al. [51] have described a jet-stirred reactor with its primary focus to study the oxidation of the fuel. The spherical reactor is made from a fused silica interface with four nozzles for admission of the sample. The mouth of four nozzles is collectively attached to a convergent cone with a cone ending on the surface of a sphere. On the other side, a divergent cone is joined to the surface of a sphere with the divergent face pointing in an outward direction. The outlet from the reactor is collected from the divergent cone for further analysis. The flow rates of the hydrocarbon and the oxygen admitted in the reaction chamber are measured and regulated by thermal mass-flow controllers. The flow of carrier gas (nitrogen) is measured using flow rotameters. The gases are preheated using an electrically insulated resistor before their admission into the reactor chamber which is also heated using the same type of resistor. The mean reaction time of the mixture in this reactor ranges from 0.01- 3.00 sec. The working

temperature for this reactor was mentioned as 900-1200 K whereas the maximum pressure of 1MPa could be achieved.

Another type of flow reactor called a variable pressure flow reactor was described by Mueller et al. [52] in their H_2/O_2 kinetic modeling studies. The working principle is like that of other flow reactors which were explained above. In brief, the preheated mixture of nitrogen and oxygen mixture was passed over a silica foam diffuser. Diluted hydrogen gas was introduced at the entrance of the diffuser allowing it to mix with the preheated mixture of nitrogen and oxygen. Then it was introduced into the quartz tube to allow it to react which was maintained at the desired temperature. A thermocouple mounted on another side of the quartz tube was used to measure the reaction chamber temperature. Few other flow reactors [53-54] which are also reported in the literature have similar working conditions. Because the working principle of most of the flow reactors are somewhat similar, other reactors are not described.

1.2.2 RAPID COMPRESSION MACHINE (RCM)

An important experimental device called rapid compression machine (RCM) was described by Sung et al. [56] and used to understand low-to-intermediate autoignition chemistry. RCMs are primarily used to measure ignition delay times of the fuel as a function of temperature, pressure, and equivalence ratio; further, they can be equipped with diagnostics to determine temperature and flow fields inside the reaction chamber and to measure the concentration of reactant, intermediate and product species produced during the process of combustion. It is made of a reaction cylinder, hydraulic chamber, and piston assembly. The piston assembly is made of driver piston, hydraulic piston, and reactor piston attached with steel and aluminum rods, respectively. The reaction

mixture under study is enclosed in the reaction chamber and compressed to very high pressure and temperature in few milliseconds and allows to proceed in a constant volume, constant mass chamber. Typically, the pressure achieved after compression is greater than 50 bars and a temperature greater than 1000 K can be obtained. The different experimental conditions can be achieved by maintaining the compression ratio, initial pressure, temperature, and composition of the mixture. The typical reaction time of around 20-40 ms is obtained using RCM. The other end of the reactor can be modified and equipped with a diaphragm which can be ruptured using a needle to provide access for the product mixture for further analysis.

1.2.3 SiC REACTOR

This is another useful experimental device employed to investigate the fast reaction described by Ellison et al. [57]. In it, 2-3 cm long SiC tube of 1 mm inner diameter is used to perform flash photolysis experiments. The experiments were carried out by passing a dilute mixture of reactant entrained in a stream of buffer gas generally helium or argon through the reactor which was resistively heated to a specific temperature. A thermocouple was used to measure the temperature of the reactor. The characteristic residence time in the reactor is of the order of 100-200 μsec. The exit of the SiC reactor is implemented with diagnostics such as photoionization mass spectroscopy (PIMS), matrix isolation infra-red spectroscopy for identification of reactant, intermediates, and products. Thus, time profile histories of different species are obtained using this technique.

1.2.4 SHOCK TUBE

The shock tube is the most widely used experimental device to study chemical kinetics at elevated temperature and pressure. A very high temperature

(typically > 1000 K) is obtained which is far beyond that obtained using the conventional method. In a shock tube, high-pressure driver gas is separated from a low-pressure driven gas by a thin metal diaphragm. The reactant is usually diluted with an inert gas (generally argon), heated to the desired temperature behind the reflected shock wave. Homogeneous gas-phase reactions that have half-lives between 10^{-3} to 10^{-6} sec are studied conveniently using a shock tube at elevated temperature. Kineticists all over the world used a shock tube as a high-temperature wave reactor to measure the thermal rate coefficient data [58]. The working principle of the shock tube is explained in detail in chapter 2.

1.3 DETECTION TECHNIQUE

There are many techniques available that can be employed to detect reactant, intermediates, and products species formed during the reaction. These techniques are categorized into two namely, offline and online techniques. Offline techniques include gas chromatography (GC-FID, GC-MS, GC-TCD) and Fourier transforms infrared spectroscopy (FTIR) [59-60]. In addition, various online detection techniques have been used to monitor the time profile history of different species. It includes atomic resonance absorption spectroscopy (ARAS) [61-62], photoionization mass spectroscopy (PIMS), matrix isolation infra-red spectrometry, Laser absorption spectroscopy, laser-induced fluorescence (LIF), and chemiluminescence methods [63-65]. The ARAS is commonly used for the detection of H-atom. Michael et al. [66] have investigated the thermal decomposition of environmentally hazardous compounds including halogenated hydrocarbons (CH_3Br, CH_3I) using the ARAS technique.

Another commonly used technique coupled to shock tube for chemical kinetic measurement which offers high sensitivity and resolution is known as laser

schlieren (LS) [67]. This technique is especially useful for those reactions which can occur in a very short time typically about 10μs. This technique is useful in measuring vibrational relaxation times, incubation times, and dissociation rate constants for the reactions. Experimental investigations have been performed on the measurement of the vibrational relaxation of H_2, D_2, HD, N_2, O_2, F_2, HCl, DCl, etc. [68-75]. However, this technique is useful only if the mechanism of thermal decomposition of the test gas has been well established.

A shock tube coupled with emission spectroscopy can be used for the measurement of ignition delay times of the fuel at elevated temperature and pressure. The ignition delay of the fuel can be measured from CH emission, OH emission, or C_2 emission [76-79]. Measurement of ignition delay studies on hydrocarbon fuel with its focus on chemical kinetic modeling gives a better understanding of the decomposition process.

1.4 IMPORTANCE OF SHOCK TUBE

The shock tube is a well-known experimental device used for the determination of the thermal rate constants. This technique is useful to study the thermal decomposition of a wide range of molecules such as aliphatic and aromatic hydrocarbons, heterocyclic compounds, halogenated compounds as well as compounds containing other functional groups. The characteristic feature of the shock tube enables its use for the present investigation. This can be illustrated using the following examples.

The experimental observation showed that C-Cl bond scission was found to be an initial step towards the thermal decomposition of 1,2-dichloroethane using the static cell studies [80]. However, HCl elimination was observed to be the major decomposition channel in chemical activation studies [81-84]. These two results

show a great deviation from the fundamental aspects of microcanonical RRKM and transition state theory (TST). It showed that the results obtained using the static cell reactor are highly affected by heterogeneous reactions. To overcome this problem, a single pulse shock tube (SPST) technique was established in our laboratory to carry out the thermal decomposition of 1,2-dichloroethane [85-86]. The experimental observation showed that pyrolysis of 1,2-dichloroethane proceed through HCl elimination and there was no difference between chemical and thermal activation.

Schott and Kinsey [87] demonstrated successfully that the exothermic reaction such as $H_2 + O_2 \rightarrow$ products, diluted with an inert gas like argon, could be satisfactorily resolved using a shock tube. The gas-phase homogeneous reactions carried out previously using shock tubes are characterized by high dilution of the reactant with inert gas and high sensitivity of the diagnostic techniques coupled to shock tube for monitoring different species. The dilution of the reactant does not alter the endothermicity or exothermicity of the reactant to a greater extent, hence provides constant temperature conditions during the experimental investigation. Secondly, using a very low concentration of the initial reactant, interference from the secondary reactions can be eliminated or reduced completely in some cases. Roth and coworkers [88] have made a significant contribution towards heterogeneous shock tube chemical kinetics for studying dispersed systems. Shock tube provides an ideal platform for the study of nucleation and growth of particles from the vapor phase at high temperatures. Frenklach et al. [89] have performed shock tube investigation of silicon particle nucleation and particle growth during thermal decomposition of silane in the temperature range of 900-2000 K. A similar study was performed by Mick et al. [90] behind reflected

shock wave on pyrolysis of disilane (Si_2H_6) entrained with different additives to study the formation of Si atom. Herzler et al. [91] have made an investigation on the formation of TiN molecule using $TiCl_4/NH_3/ H_2$ system in the shock tube.

Phenomenons such as combustion, detonation, and many other processes can be effectively studied using shock tubes. Gas-phase combustion synthesis of nanoparticles is a well-established process using shock tubes. Roth and co-workers [92] have investigated the formation of soot particles behind a reflected shock wave in the oxidation of different hydrocarbon fuels. A shock tube can be used to study the process of incineration. As an example, the compounds chlorofluorocarbons (CFCs) are the main cause of ozone depletion in the stratosphere. These chemicals are non-biodegradable and are destroyed by incineration. Hence, it is important to have knowledge of the complete mechanism of the incineration of these compounds for detail kinetic modeling.

1.5 PRESENT STUDY

Present work is the continuation of previous work carried out at the Laboratory for Hypersonic and Shock Wave Research (LHSR). A chemical shock tube (CST-3) was used for the present experimental investigation. CST-3 was modified as a single pulse shock tube for chemical kinetic measurement. The offline techniques such as gas chromatography (GC-FID, GC-MS), FTIR techniques have been used for the identification of species formed during the reaction. The previous study including 1,2-dichloroethane [85], 2-chloroethanol [86], 2-bromoethanol [86], propargyl alcohol [95], 3-carene [96] pyrolysis were carried using a chemical shock tube at LHSR. Also, ignition delay times measurement for ethane [94], JP-10 [93], and 3-carene [96] were investigated to understand the combustion chemistry of fuels.

As described in the previous section, understanding of reaction mechanism are essential in the field of chemical kinetics. This thesis presents the result from the following investigations: (1) Modification of shock tube by incorporating driver insert to achieve constant pressure behind the reflected shock wave. (2) Experimental investigation and kinetic modeling study of pyrolysis and oxidation on dicyclopentadiene. (3) Theoretical investigation of the dissociation reaction of dicyclopentadiene to cyclopentadiene.

1.5.1 MODIFICATION OF SHOCK TUBE

The shock tube provides near-ideal behavior behind the reflected shock wave region which helps to study kinetics at elevated temperature and pressure. However, this ideal behavior will be perturbed by the presence of the non-ideal phenomenon such as incident shock wave attenuation, boundary layer growth, etc. This perturbation can cause a gradual rise in reflected shock wave pressure. In 1972, Dumitrescue [97] used a cone shape obstacle called an insert in the driver section to cancel the non-ideal rise in pressure behind the reflected shock wave. A strategy put forward by Dumitrescue and methodology by Hanson [98] was adapted to design a step-size obstacle called a driver insert. When driver inserts designed properly, incorporated in the driver section, rarefaction waves generated at the diaphragm section are reflected partially from the surface of the insert. The magnitude of the decrease in the pressure by partially reflected rarefaction waves and the pressure rise caused by non-ideal phenomenon is equal in magnitude and superimposed. Thus, the driver insert will effectively reduce or in some cases completely eliminate the non-ideal pressure rise behind the reflected shock wave. Hence, the constant pressure profile is obtained behind the reflected shock wave which is the necessity for chemical kinetic measurement.

1.5.2 KINETIC INVESTIGATION ON DICYCLOPENTADIENE

The process of formation of polycyclic aromatic hydrocarbons (PAHs) and soot in high-temperature gaseous environments such as flame is a growing area of research. However, this process can be initiated through various species which have been proposed as potential precursor such as methyl, propargyl, and cyclopentadienyl radical. Cyclopentadienyl radical is one of the most abundant radicals present in flame responsible for the formation of polycyclic aromatic hydrocarbons (PAHs), which is considered as combustion generated pollutants [99-100] and its role in the formation of soot is of greater interest due to its adverse effect on the environment.

Dicyclopentadiene (DCPD), a homodimer of cyclopentadiene (C_5H_6), can be obtained by dehydrogenation of JP-10 (Jet Propellant) which is presently used as aviation fuel. The molecular structure of DCPD is represented in Figure 1.1. DCPD can exist as an endo (a) and exo (b) isomer. As commercially available DCPD is greater than 95% endo, most of the applications of the DCPD involved an endo isomer [101].

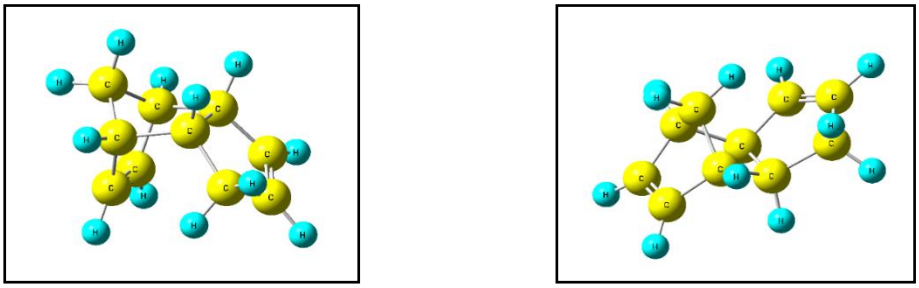

Figure 1.1. *The molecular structure of DCPD (a) endo-DCPD (left) (b) exo-DCPD (right)*

Studies on thermal decomposition of cyclopentadiene (CPD) by Burcat et al. [102] were carried out in a single pulse shock tube for the temperature range 1080-1550 K, the observed products were acetylene, ethylene, methane, allene, propyne, butadiene, propylene and benzene. Colket et al. [103] performed a shock tube

study on CPD pyrolysis and found for the reaction $c\text{-}C_5H_6 = H + c\text{-}C_5H_5$; $k = 2\times10^{15}$ $\exp(-81000/RT)s^{-1}$ in the temperature range of 1100-2000 K and pressure range of 10-13 atm. Butler [104] and Bruisma [105] carried out experiments in a flow reactor. According to Butler, CPDyl radical undergoes ring opening and produces straight chain aliphatic compounds.

Over the past decades, dicyclopentadiene (DCPD), has been researched for many reasons in combustion for various purposes such as fuel, binder, etc. [106] The binder performs a dual function of binding fuel and oxidizer as well imparting enough mechanical strength to the solid propellant grain. DCPD is also capable of forming a highly crossed-linked polymeric structural network through ring opening metathesis polymerization (ROMP). Moore et al. [101] have investigated kinetics for ring opening metathesis polymerization on endo and exo DCPD. They found that the exo isomer of DCPD is more reactive (one order of magnitude higher) than the endo isomer. To our knowledge, very few studies are available in the literature on the thermal decomposition of DCPD.

The pyrolysis and oxidation of dicyclopentadiene were performed behind a reflected shock wave in a modified shock tube. The ignition delay time was measured using the increase in pressure recorded by the PCB transducer as well as CH-emission for three equivalence ratios (ϕ = 0.5, 1, and 1.5) when the concentration of the fuel is the same. Also, kinetic modeling is carried out to validate experimentally observed ignition delay. Experimental observations on thermal decomposition of DCPD showed that the formation of cyclopentadiene constitutes the initial step towards decomposition. Ab-*inito* calculations were carried out to locate the transition state of the chemical reaction involved. The decomposition pathway of dicyclopentadiene to cyclopentadiene has been studied

using the B3LYP/6-311G+(2d, p) level of theory. Also, an Atoms in Molecules (AIM) analysis which is based upon electron density topology is carried out along the reaction coordinate which provides insight into the decomposition process.

1.6 STRUCTURE OF THE THESIS

The chapters presented in this thesis are outlined in the following manner:

- *Chapter 1* begins with an overall background of the present study. It introduces the problem at hand and presents the literature review pertaining to this area of research. The motivation and objective of the study are highlighted.
- *Chapter 2* covers a brief introduction to shock tube. The working principle of the shock tube and different diagnostic methods pertaining to the current research are presented. Also, the consequences of the non-ideal effects on reflected shock pressure are presented. Moreover, it provides the solution to overcome this issue by incorporating insert in the driver section. Thereupon it describes the present investigation of CST-3 calibration using ethyl chloride as an external standard.
- *Chapter 3* describes the experimental investigation on the thermal decomposition of dicyclopentadiene performed in a modified shock tube. Also, ab-*initio* calculations were performed to find the minimum energy pathway to the observed products, and the details are presented.
- *Chapter 4* describes the theoretical investigation on the dissociation of dicyclopentadiene to cyclopentadiene. Also, quantum theory of atoms in molecule (QTAIM) analysis, was carried out along the IRC path.
- *Chapter 5* describes the ignition delay measurement study performed on DCPD for three equivalent ratios (ϕ = 0.5, 1, and 1.5) when the concentration

of the DCPD is the same. Also, an oxidation mechanism has been used to fit the experimentally observed ignition delay times of DCPD. Comparison between experimental and calculated ignition delay times of DCPD was also presented.

- *Chapter 6* final chapter of thesis summarizes the finding from the present study also put forward future road map in the direction of the field combustion and PAHs formation.

1.7 REFERENCES

1. K. J. Laidler, Theories of Chemical Reaction Rates. 1969, McGraw-Hill.
2. K. J. Laidler, C. King, Journal of Physical Chemistry, 87 (15), 1983, 2657.
3. H. Eyring; Journal of Chemical Physics, 3 (2), 1935, 107–115.
4. J. I. Steinfeld, J. S. Francisco, W. L. Hase, Chemical Kinetics and Dynamics, Prentice-Hall. 1999, 289–293.
5. D. Townsend, S. A. Lahankar, S. K. Lee, S. D. Chambreau, A. G. Suits, X. Zhang, J. Rheinecker, L. B. Harding, and J. M. Bowman, Science, 306, 2004, 1158-1161.
6. P. L. Houston, and S. H. Kable, Proceedings of the National Academy of Sciences, 103, 44, 2006, 16079-16082.
7. L. B. Harding, S. J. Klippenstein, and A. W. Jasper, Journal of Physical Chemistry A, 116, 2012, 6967-6982.
8. R. Sivaramakrishnan, J. V. Michael, L. B. Harding, and S. J. Klippenstein, Journal of Physical Chemistry A, 116, 2007, 5981-5989.
9. W. Tsang, and A. Lifshitz, Annual Review of Physical Chemistry, 41, 1990, 559–599.
10. R. Sivaramakrishnan, R.S. Tranter, and K. Brezinsky, Journal of Physical Chemistry, 110, 2006, 9388–9399.
11. M. H. Back, Canadian Journal of Chemistry, 49, 13, 1971, 2199-2204.
12. J. H. Kiefer, S. S. Sidhu, R. D. Kern, K. Xie, H. Chen and L. B. Harding, Combustion Science and Technology, 82, 1-6, 1992, 101-130.
13. N.E. Sanchez, A. Callejas, A. Millera, R. Bilbao, and M. U. Alzueta, Energy, 43, 2012, 30-36.

14. R. D. Kern, H. J. Singh, and C. H. Wu, International Journal of Chemical Kinetics, 20, 9, 1988, 731-747.
15. P. R. Westmoreland, A. M. Dean, J. B. Howard, and J. P. Longwell, Journal of Physical Chemistry, 93, 1989, 8171-8180.
16. C. H. Wu and R. D. Kern; Journal of Physical Chemistry, 91, 24, 1987, 6291-6296.
17. Y. Hidaka, T. Nakamura, A. Miyauchi, T. Shiraishi, and H. Kawano, International Journal of Chemical Kinetics, 21, 1989, 643-666.
18. D. Wang, A. Violi, D. H. Kim, and J. A. Mullholland, Journal of Physical Chemistry A, 110, 2006, 4719-4725.
19. C. Cavallotti, D. Polino, A. Frassoldati and E. Ranzi, Journal of Physical Chemistry A, 116, 2012, 3313-3324.
20. G. da-Silva, and J. W. Bozzelli, Journal of Physical Chemistry A, 113, 44, 2009, 12045-12048.
21. V. Detilleux, and J. Vandooren, Journal of Physical Chemistry A, 113, 2009, 10913-10922.
22. G. da-Silva, A. J. Trevitt, M. Steinbauer, and P. Hemberger, Chemical Physics Letters, 517, 2011, 144-148.
23. K. M. Pamidimukkala, R. D. Kern, M. R. Patel, H. C. Wei, and J. H. Kiefer, Journal of Physical Chemistry, 91, 1987, 2148-2154.
24. R. Sivaramakrishnan, R. S. Tranter, and K. Brezinsky, Journal of Physical Chemistry A, 110, 2006, 9388-9399.
25. G. da-Silva, Chiung-Chu Chen and J. W. Bozzelli, Journal of Physical Chemistry A, 111, 2007, 8663-8676.

26. J. L. Emdee, K. Brezinsky and I. Glassman, Journal of Physical Chemistry, 95, 1991, 1626-1635.

27. Hsi-Ping S. Shen, and M. A. Oehlschlaeger, Combustion and Flame, 156, 2009, 1053-1062.

28. S. Gudiyella, T. Malewicki, A. Comandini, and K. Brezinsky, Combustion and Flame, 158, 2011, 687-704.

29. P. N. Rao and D. Kunzru, Journal of Analytical and Applied Pyrolysis, 76, 2006, 154-160.

30. S. Nakra, R. J. Green, and S. L. Anderson, Combustion and Flame, 144, 4, 2006, 662-674.

31. K. Chenoweth, Adri C. T. van Duin, S. Dasgupta, and W. A. Goddard III, Journal of Physical Chemistry A, 113, 2009, 1740-1746.

32. S. R. Smith and A. S. Gordon, Journal of Physical Chemistry, 65, 7, 1961, 1124-1128.

33. N. M. Vandewiele, G. R. Magoon, K. M. Van Geem, M. F. Reyniers, W. H. Green, and G. B. Marin, Energy Fuels, 2014, 28, 4976–4985.

34. D. S. Aribike, A. A. Susus and A. F. Ogunye, Thermochimica Acta, 47, 1981, l-14.

35. F. Billaud, P. Chaverot, M. Berthelin, and E. Freundg, Industrial & Engineering Chemistry Research, 27, 1988, 759-764.

36. J. P. Orme, H. J. Curran, and J. M. Simmie, Journal of Physical Chemistry A, 110, 2006, 114-131.

37. J. H. Kiefer, K. S. Gupte, L. B. Harding, and S. J. Klippenstein, Journal of Physical Chemistry A, 113, 2009, 13570-13583.

38. S. Granata, T. Faravelli and E. Ranzi, Combustion and Flame, 132, 2003, 533-544.

39. W. Li, M. E. Law, P. R. Westmoreland, T. Kasper, N. Hansen, and K. K. Hoinghaus, Combustion and Flame, 158, 2011, 2077-2089.

40. C. M. Gong, Z. R. Li, and Xiang-Yuan Li, Energy Fuels, 26, 2012, 2811-2820.

41. F. Berho, M. T. Rayez, and R. Lesclaux, Journal of Physical Chemistry A, 103, 1999, 5501-5509.

42. S. G. Davis, H.Wang, K. Brezinsky and C. K. Law, Twenty-Sixth Symposium (International) on Combustion/The Combustion Institute, 1996, 1025-1033.

43. M. G. Brioukov, J. Park and M. C. Lin, International Journal of Chemical Kinetics, 31, 8, 1999, 577-582.

44. H. Bohm, and H. Jander, Physical Chemistry Chemical Physics, 1, 1999, 3775 - 3781.

45. H. Richter, S. Granata, W. H. Green, and J. B. Howard, Proceedings of the Combustion Institute, 30, 2005, 1397-1405.

46. R. Sivaramakrishnan, K. Brezinsky, H. Vasudevan and R. S. Tranter, Combustion Science and Technology, 178, 1-3, 2006, 285-305.

47. S. G. Davis, C. K. Law, and H. Wang, Journal of Physical Chemistry A, 103, 1999, 5889-5899.

48. O. Herbinet, B. Sirjean, R. Bounaceur, R. Fournet, F. Battin-Leclerc, G. Scacchi and P. M. Marquaire, Journal of Physical Chemistry A, 110, 2006, 11298-11314.

49. M. A. Grela, V. T. Amorebieta, and A. J. Colussi, Journal of Physical Chemistry, 1992, 96, 9861-9865.

50. S. Hu, W. Sun, J. Fu, L. Zhang, Q. Fan, Z. Zhang, W. Wu, and Y. Tang, Journal of Molecular Modeling, 23, 2017, 179-189.

51. P. Dagaut, M. Cathonnet, J. P. Rouan, R. Foulatier, A. Quilgars, J. C. Boettner, F. Gaillard, and H. James, Journal of Physics E: Scientific Instrument, 19, 1986, 207-209.

52. M. A. Mueller, T. J. Kim, R. A. Yetter, and F. L. Dryer, International Journal of Chemical Kinetics, 31, 2, 1999, 113-125.

53. M. Golubitsky and B. L. Keytz, SIAM Journal on Mathematical Analysis, 11, 2, 1980, 316-339.

54. G. Rabai, K. Kustin, and I. R. Epstein, Journal of American Chemical Society, 111, 1989, 3870-3874.

55. P. J. Dowding, J. W. Goodwin, and B. Vincent, Colloids and Surfaces A: Physicochemical Engineering Aspects, 180, 2001, 301-309.

56. G. Mittal and C. J. Sung, Combustion science and technology, 179, 3, 2007, 497-530.

57. A. G. Vasiliou, M. R. Nimlos, J. W. Daily and G. B. Ellison, Journal of Physical Chemistry A, 113, 2009, 8540-8547.

58. A. G. Gaydon and I. R. Hurle, The Shock Tube in High Temperature Chemical Physics, 1963.

59. A. V. Friderichsen, E. J. Shin, R. J. Evans, M. R. Nimlos, and D. C. Dayton Fuel, 80, 2001, 1747-1755.

60. K. H. Weber and J. Zhang, Journal of Physical Chemistry A, 111, 2007, 11487-11492.

61. A. Lifshitz, Y. Cohen, M. B. Unkhon, and P. Frank, In International Symposium on Combustion, 26, 1, 1996, 659-667.

62. R. Sivaramakrishnan, M. C. Su, J. V. Michael, S. J. Klippenstein, L. B. Harding and B. Ruscic, Journal of Physical Chemistry A, 114, 2010, 9425-9439.

63. V. D. Knyazev and I. R. Slagle, Journal of Physical Chemistry A, 105, 2001, 3196-3204.

64. J. D. Desain and C. A. Taatjes, Journal of Physical Chemistry A, 107, 2003, 4843-4850.

65. E. V. Shanr, I. R. Slagle and V. D. Knyazev, Journal of Physical Chemistry A, 107, 2003, 8893-8903.

66. T. Ko, A. Fontijn, K. P. Lim, and J. V. Michael, Symposium (International) on Combustion, 24, 1, 1992, 735-742.

67. J. H. Klefer, M. Z. Al-Alaml, and K. A. Budach, Journal of Physical Chemistry, 86, 1982, 808-813.

68. J. E. Dove, D.G. Jones, and H. Tellelbaum, 14th International Symposium on Combustion, Combustion Institute, Pittsburgh, 1973, 177-188.

69. J. E. Dove, and H. Tellelbaum, Journal of Chemical Physics, 6, 1974, 431-446.

70. J. H. Kiefer, and R. W. Lutz, Journal of Chemical Physics, 44, 1966, 658-669.

71. P. F. Bird, and W. D. Breshears, Chemical Physics Letter, 13, 1972, 529-534.

72. C. J. Simpson, S. M. Price, and I. J. Crowther, Chemical Physics Letter, 34, 1975, 181-196.

73. J. A. Bander, and G. Sanzone, Review of Scientific Instrument, 45, 1974, 949-959.

74. W. D. Breshears, and P. F. Bird, Journal of Chemical Physics, 48, 1968, 4768-4778.

75. G. J. Diebold, R. J. Santoro, and G. J. Goldsmith, Journal of Chemical Physics, 60, 1974, 4170-4189.

76. D. F. Davidson, D. C. Horning, J. T. Herbon, and R.K. Hanson, Proceedings of Combustion Institute, 28, 2000, 1687-1699.

77. D. F. Davidson, D.C. Horning, and R.K. Hanson, AIAA; 99, 1999, 2216-2228.

78. M. B. Colket, and L. J. Spaddaccini, Journal of Propulsion and Power, 17, 2001, 315-329.

79. E. Olchansky, and A. Burcat: 21st International Symposium on Shock Waves, 2001, 5962-5978.

80. D. H. R. Barton, and K. E. Howlett, Journal of Chemical Society, 155, 1949, 165-178.

81. J. C. Hassler, D. W. Setser, and R. L. Johnson, Jornal of Chemical Physics, 45, 1966, 3231-3247.

82. J. C. Hassler, and D. W. Setser, Journal of Chemical Physics, 45, 1966, 3246-3259.

83. K. Dees, and D. W. Setser, Journal of Chemical Physics, 49, 1968, 1193-1209.

84. P. B. Roussel, P. D. Lightfoot, F. Carlap, V. Catoire, R. Lesclaux, and W. Forst, Journal of Chemical Society Faraday Transaction, 87, 1991, 2367-2381.

85. B. Rajakumar, K. P. J. Reddy, and E. Arunan, Journal of Physical Chemistry A, 106, 2002, 8366-8379.

86. B. Rajakumar, K. P. J. Reddy, and E. Arunan, Journal of Physical Chemistry A, 107, 2003, 9782-9799.

87. G. L. Schott, and J. L. Kinsey, Journal of Chemical Physics, 29, 5, 1958, 1177-1183.

88. K Bhaskaran, and P. Roth, Progress in Energy and Combustion Science, 28, 2002, 151-171.

89. A. Lifshitz, M. Frenklach, A. Burcat, Journal of Physical Chemistry, 80, 1976, 2437-2449.

90. H. J. Mick, M. W. Markus, P. Roth, and V. N. Smirnov, Reports of the Bunsen Society for Physical Chemistry, 99, 6,1995, 880-890.

91. J. Herzler, R. Leiberich, H. J. Mick, and P. Roth, Nanostructured Materials. 10, 7, 1998, 1161-1171.

92. T. Just, P. Roth, and R. Damm, 16th International Symposium on Combustion, Combustion Institute, Pittsburgh, 1977, 961-979.

93. H. K. Chakravarty, Ph.D Thesis on Thermal Decomposition of Haloethanols and Ignition of JP-10., August 2011.

94. M. Nagaboopathy, C. Vijayanand, G. Hegde, K.P.J. Reddy and E.Arunan, Current Science, 95, 1, 2008, 78-82.

95. N. Sharath, K. P. J. Reddy, and E. Arunan, Journal of Physical Chemistry A, 118, 2014, 5927–5938

96. N. Sharath, Ph.D Thesis Kinetics of 3-carene at High Temperatures and High Pressure., August 2015.

97. L. Z. Dumitrescu, Physics of Fluids 15, 1972, 207–209.

98. E. L. Petersen, and R. K. Hanson, Shock Waves 10, 2001, 405-420.

99. D. Wang, A. Violi, D. H. Kim, J. A. Mullholland, Journal of Physical Chemistry A, 110, 2006, 4719-4725.

100. D. H. Kim, J. A. Mulholland, D. Wang, and A. Violi, Journal of Physical Chemistry A, 114, 47, 2010, 12411-12428.

101. J. D. Rule and J. S. Moore, Macromolecules, 35, 2002, 7878-7882.

102. A. Burcat, and M. Dvinyaninov, International Journal of Chemical Kinetics 29, 1997, 505 – 514.

103. M. B. Colket, The Pyrolysis of Cyclopentadiene, Eastern States Section of Combustion Institute annual meeting, Orlando, 1990, Paper 1.

104. R. G. Butler, MSc. Thesis, Princeton University, 1992.

105. O. S. L. Bruisma, P. J. J. Tromp, H. J. J. de Sauvage Nolting and J. A. Moulijn, Fuel, 67, 1988, 334-349.

106. S. Reshmi, E. Arunan, and C. P. Reghunadhan Nair, Industrial Engineering & Chemical Research, 53, 2014, 16612−16620.

2

EXPERIMENTAL AND COMPUTATIONAL METHODS

CHAPTER OVERVIEW

This chapter will form a foundation for an understanding of shock waves. The shock tube is well known for its uniqueness which is an important and desirable shockwave generator to study chemical kinetics at elevated temperature and pressure. Thereupon, the details of the driver insert which was needed to ensure that the pressure behind the reflected shock wave remained constant, are enumerated. Towards the end of the chapter, the importance of uncertainty analysis in the reflected shock temperature (T_5) for obtaining accurate kinetics data is presented. A recent temperature (T_5) calibration study of our chemical shock tube (CST-3) using ethyl chloride as an external standard for a temperature range from 960-1190 K is reported in the present study.

2.1. INTRODUCTION

A shock tube-based research, over the last six decades, has discovered many potential areas for experimental investigation. The major focus of shock tube research has been on its application to aerodynamic, and high temperature chemical kinetic studies. Various interdisciplinary areas have also been investigated (see Figure 2.1). It includes the usages of a shock wave for medical applications, to study shock wave phenomena in geoscience and astrophysics related research, shock wave in condensed matter physics, and shock wave induced reactions for material synthesis [1].

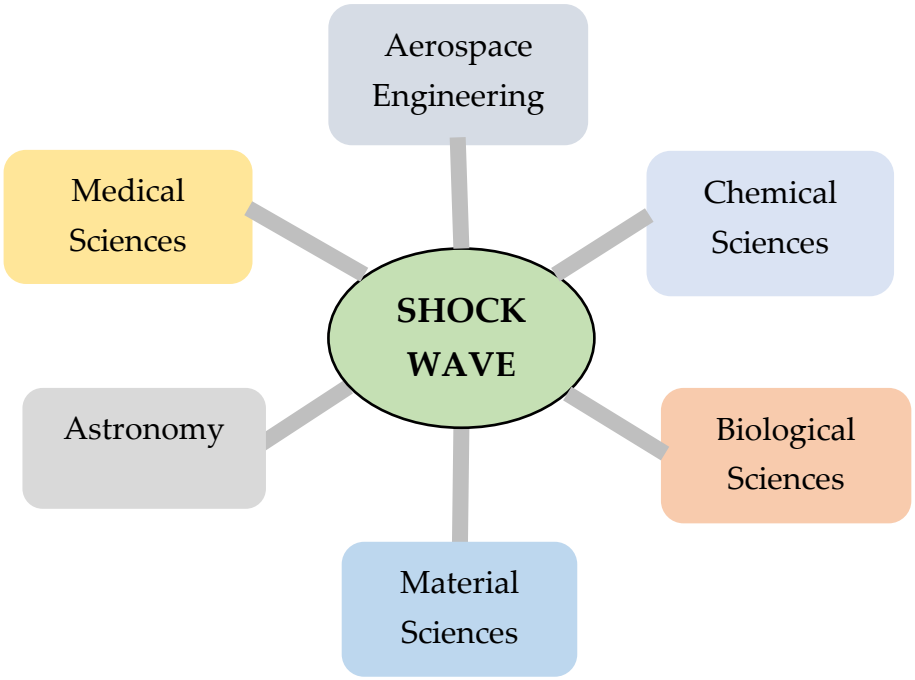

Figure 2.1. *The flowchart of shockwave applications in various modules.*

Paul Vieille [2] who introduced the first shock tube in 1899 to carry out the gas explosions in mines could not have foreseen the potential application of the shock wave. High-temperature gas-phase reactions that have half-lives between 10^{-3} to 10^{-6} sec are studied conveniently using a shock tube. Kineticists use the shock tube to perform chemical kinetics experiments at elevated temperature and

pressure for obtaining rate coefficient data under diffusion-free conditions. The temperature range under which the reaction could be studied can be extended far beyond that of a conventional flow reactor (typically > 1000 K).

2.2 SHOCKWAVE

A sound wave is the pattern of disturbance propagated through a medium caused by the movement of energy traveling in the direction of propagation producing weak adiabatic compression waves at the local speed of sound. A train of such compression waves traveling through a medium with increasing speed greater than the local speed of sound, coalesces to form a shock wave. The formation of shock waves in a medium can be illustrated using the following examples (1) by using high explosives (2) an object traveling at supersonic/hypersonic speed or a supersonic/hypersonic flow in a medium is obstructed by an obstacle in the path of it (see Figure 2.2).

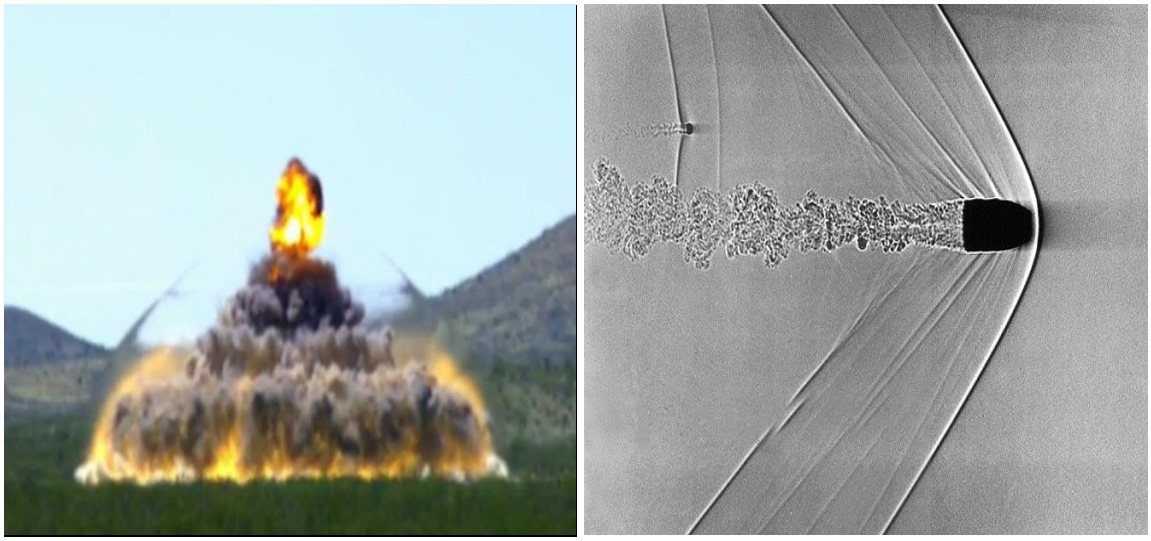

(a) ***(b)***

Figure 2.2. *Examples of shockwaves produced by (a) explosion using gunpowder (ref 3) and (b) object traveling at supersonic speeds (ref 4)*

In other words, shockwaves are non-linear waves, unlike a sound wave, which is an irreversible process that carries energy and propagates through a medium with more than the speed of sound. An inherent property of the shock wave that distinguishes it from the sound wave is that there is an abrupt rise in pressure, temperature, density, and velocity of the fluid. The phenomenon of the shock wave has occurred frequently in nature which may be either natural or artificial in origin. The natural sources of the generation of shock waves include earthquake, volcanic eruption, meteorite impact, thunderclap, etc. and artificially it can be produced using shock tubes, supersonic aircraft, explosives, etc.

2.3. FORMATION OF SHOCKWAVE

The formation of shockwaves can be well explained using a piston analogy first described by Becker [5] in 1922 (see Figure 2.3). Consider a long tube filled with a gas having a piston at the other end and let the piston be capable of acceleration to a constant velocity v. Here velocity v is much greater than the velocity of sound 'a' in that gas.

The final velocity v is attained by small increments in the velocity (dv) for a short finite time. The first increment dv generates the weak compression wave to propagate in the gas at the speed 'a'. At this stage, the gas between the piston and wavefront has been compressed uniformly and adiabatically and has achieved the velocity dv. Now let the piston achieve another small velocity increment dv, a second compression leads to an incremental increase in the velocity of gases compressed. After many such increments, the piston achieved the final velocity v. At this stage a series of waves of increasing strengths generated in the area between the initial wave and the piston. The flow velocity of the gas in the individual wave increases from dv (for the first wave) to v (at piston face) and the

separation between successive waves decreases with time. As these are weak compression waves, it is physically impossible for them to overtake one another. They are traveling at the local speed of sound and due to the differing degree of adiabatic heating in each successive compression which is increasing from front to the piston. However, the train of waves must ultimately coalesce to form a single steep wave front across which there exist large gradients of pressure, temperature, and density. This is called a shock front which moves with a velocity W_s. Any sudden release of energy will lead to the formation of shock waves within a few μs as they are one of the efficient mechanisms of energy dissipation found in nature. Shockwave can also be produced by the dissipation of mechanical, electrical, nuclear, and chemical energy in a limited case.

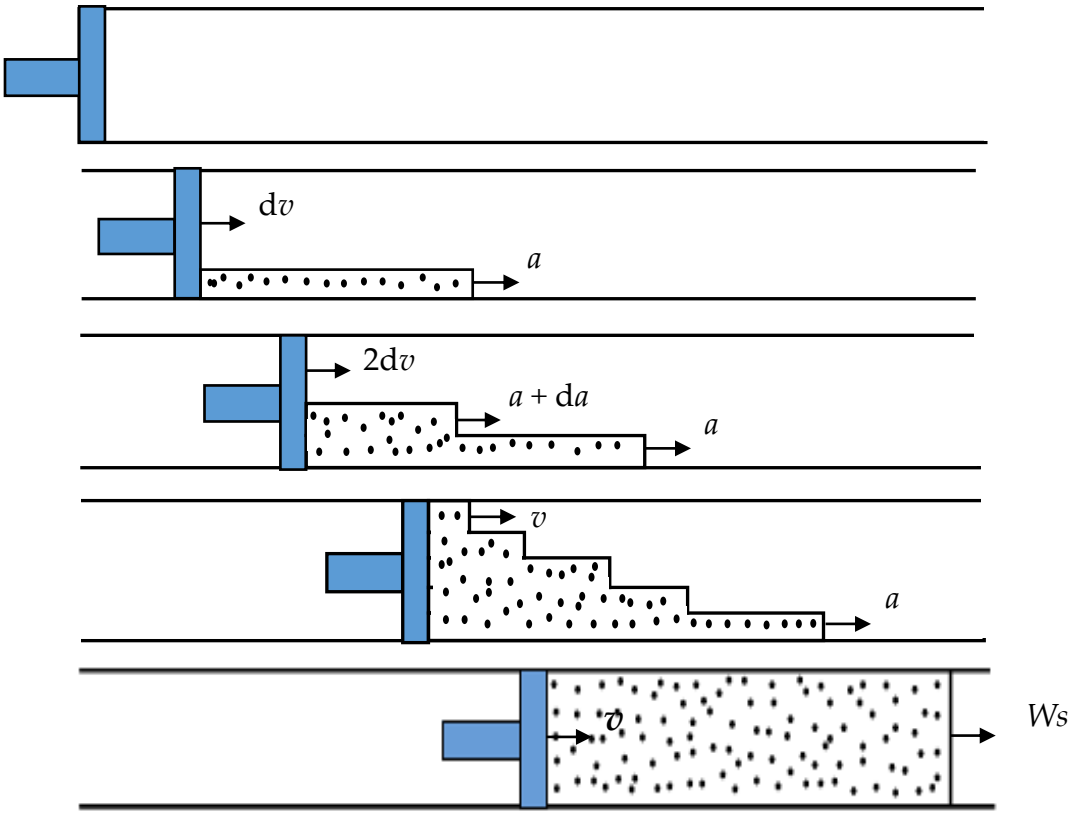

Figure 2.3. *A schematic representation for the shock wave formation using piston analogy.*

2.4 SHOCK TUBE

The shock tube is a well-established technique for the determination of the thermal rate constant. Though this technique has great potentialities in high temperature chemical research, it has some severe limitations which were reviewed by Belford and Srehlow [6]. However, this limitation was removed considerably by the consistent effort of Lifshitz, Bauer, Tsang, Tschuikow-Roux, and others. This technique is useful to study the thermal decomposition of a wide range of molecules such as aliphatic and aromatic hydrocarbons, heterocyclic compounds, halogenated compounds as well as compounds containing other functional groups [7-14].

On the laboratory scale, a shock wave is produced in the shock tube by means of rupturing a metal diaphragm. In its simplest form, a conventional shock tube comprises of two sections namely a high-pressure driver section and a low-pressure driven section separated by a thin metal diaphragm. Upon the bursting of the metal diaphragm separating these two sections results in the formation of a shockwave that propagates downstream along the driven section. A contact surface which is an interface between the driver and the driven gas follows the shockwave. The incident shockwave travels back again in the driven section after its reflection at the end wall of the driven section, leading to further compression of the test gas. Just as a compression wave propagates in the driven section in the form of a shockwave, there are rarefaction waves that propagate in the driver section of the shock tube (see Figure 2.4) with local speed of sound. The topmost diagram in Figure 2.4 shows the x-t diagram while the position of the corresponding waves in the shock tube at a given time instants are shown below in the bottom figures. Many different types of shock tubes have been developed at

our laboratory and used to suit the requirement of the research. Some of them are summarized below:

- Chemical shock tube
- Magnetically driven shock tube
- Explosive piston shock tube
- Free piston (Diaphragm less) shock tube
- Variable cross-section shock tube
- Conical shock tube
- Pressure-driven shock tubes
- Combustion-driven and detonation-driven shock tubes
- Multiple diaphragm shock tubes

Consider Figure 2.4 which defines the gas parameters in the different regions associated with the shock tube. Define, P, ϱ and T be the pressure, density, and temperature of the gas respectively and v be the velocity of the gas molecule relative to the shock tube. W_s is the velocity of the shock front relative to the shock tube. It is usual to denote conditions in the undisturbed low-pressure test gas by subscript 1. Initial pressure and temperature in this region are represented as P_1 and T_1 respectively. The region between the shock front and contact surface is denoted by 2, with pressure and temperature in this region are represented by P_2 and T_2. The region between the contact surface and the rarefaction fan is referred to as 3. The corresponding pressure and temperature of the cold driver gas in this region are denoted by P_3 and T_3 respectively. The initial conditions on the high-pressure region are denoted by 4. The corresponding pressure and temperature are denoted by P_4 and T_4. Generally, P_4 is much greater than P_1 but in the simple shock tube, it is usual for $T_4 = T_1$. If the primary shock wave is permitted to undergo

reflection at the end wall of the driven section, there is a further rise in pressure and temperature, and this region is represented by 5. In simple cases, T_5 is about twice that of T_2.

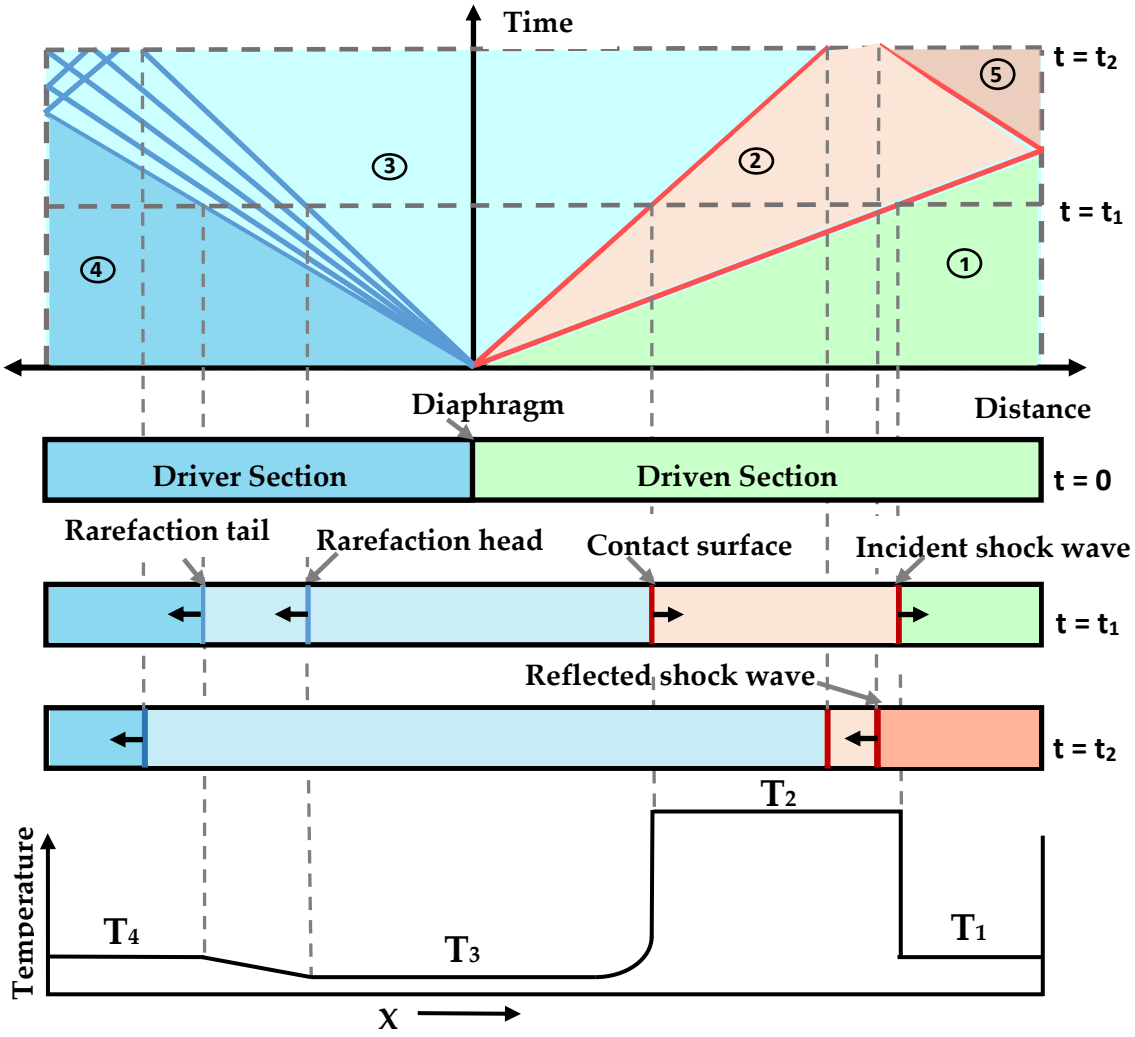

Figure 2.4. *The x-t diagram of shock wave propagation in a conventional shock tube.*

The variation of pressure, density, and temperature in the shock tube as a function of time can be calculated numerically for a one-dimensional inviscid flow using Riemann Solver. Figure 2.5 represents the variation of the pressure along the shock tube with the time. In this figure, each ribbon strand represents the pressure along the tube at a given time instant. Similarly, Figure 2.6 and Figure 2.7 represent

the variation of density and velocity along the shock tube for different time instants.

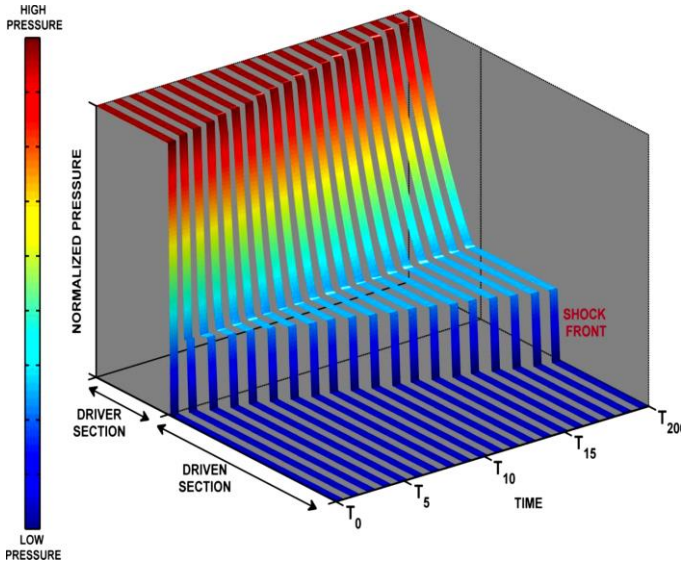

Figure 2.5. *A three-dimensional representation of variation in pressure along a shock tube with time (Figure adapted from reference 3 with permission)*

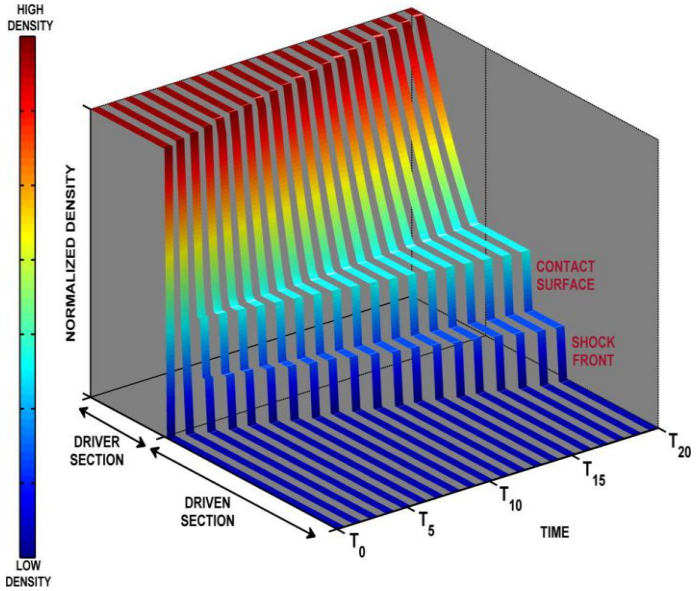

Figure 2.6. *A three-dimensional representation of variation in density along a shock tube with time. (Figure adapted from reference 3 with permission)*

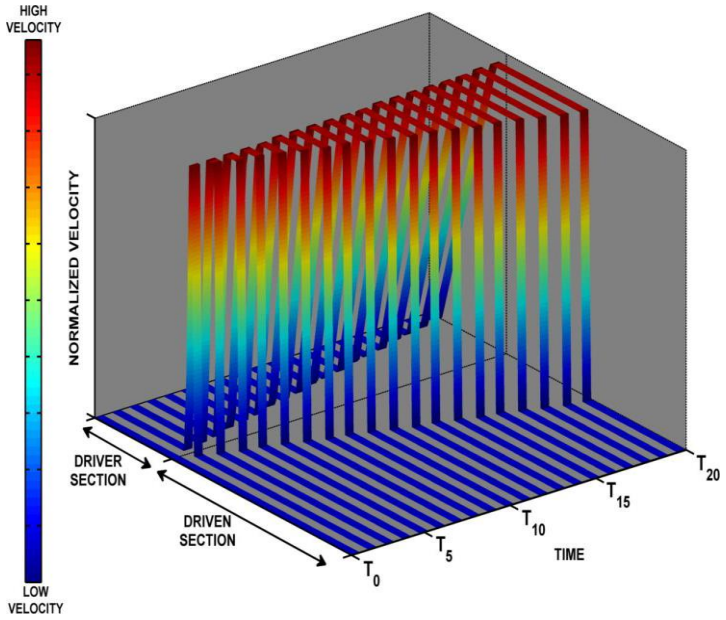

Figure 2.7. *A three-dimensional representation of variation in velocity along a shock tube with time. (Figure adapted from reference 3 with permission)*

It is important to introduce the quantity Mach number which is the ratio of the velocity of a disturbance in a gas to the local speed of sound in the gas given by,

$$M_s = \frac{W_s}{a} \qquad \text{-------- 2.1}$$

Where 'a' is the speed of sound in the medium.

Many unique features of the shock tube enable us to use it for high-temperature chemical kinetic study over a conventional reactor. The test gas molecule is heated instantaneously to desired temperature (generally >1000 K) without any interference from the surface which is an essential requirement to obtain an accurate rate constant. In some respect the result obtained with a shock tube should resemble those given by the other methods such as flash photolysis [15-18]; in flash photolysis heating is induced by sudden absorption of ultra-violet light and subsequent reactions are being followed by absorption spectroscopy. However, sudden absorption of ultra-violet light leads to the formation of free atoms and radicals, and hence the chemical processes are of a non-thermal type.

In addition to this, the heated gas molecules are rapidly quenched in about a millisecond time scale by controlled rarefaction waves traveling from another end inside the shock tube. The cooling rate commonly obtained in the shock tube is of order 0.5 to 5 K per μs. Hence very well-defined reaction time (typically a few milliseconds) is obtained with a shock tube. The characteristic feature of the shock tube is the gas temperature is raised to a very high value without a ramp whereas the shock tube remains at room temperature. The concentration of the test gas molecule under observation can be extremely low. This would prevent any secondary reaction that can occur during the thermal decomposition process. The study of important combustion processes can well be extended.

2.5 CALCULATION OF SHOCK PARAMETERS

The gas parameters in the different regions associated with a shock wave can be directly calculated from the thermodynamics which is based on conservation of mass, momentum, and energy respectively. The governing equations for shock wave parameters are given by Rankine-Hugoniot which describes the change in pressure, density, and temperature across the shock wave. For the kineticist, the conditions behind the incident and reflected shock waves are ordinarily calculated from experimental parameters including initial temperature, pressure, and composition of the driven section gas (T_1, P_1, and X_1), measured shock velocity, and the standard normal shock wave equations:

$$\frac{P_2}{P_1} = \frac{\{2\gamma M^2 - (\gamma - 1)\}}{\gamma - 1} \qquad \text{-------- 2.2}$$

$$\frac{T_2}{T_1} = \frac{[2\gamma M^2 - (\gamma - 1)][M^2(\gamma - 1) + 2]}{(\gamma - 1)^2 M^2} \qquad \text{-------- 2.3}$$

$$\frac{T_5}{T_1} = \frac{[2(\gamma - 1)M^2 - (3\gamma - 1)][M^2(3\gamma - 1) - 2(\gamma - 1)]}{(\gamma + 1)^2 M^2} \qquad \text{-------- 2.4}$$

where M = incident shock Mach number, γ = specific heat capacity ratio.

However, these equations are derived from the ideal gas condition and the attenuation in the shock tube caused by the boundary layer is neglected. This ideal behavior of the shock waves may be valid up to relatively modest initial conditions where the assumptions, as well as the equations, are valid. Thus, the reflected shock temperature computed from the above equation would generally differ from the temperature experienced by the test gas. However, this non-ideal behavior that occurred in the shock tube was extensively discussed by Belford and Strehlow [6]. As the rate constant varies exponentially with the temperature, any deviation in the measurement of temperature can induce large error in kinetics measurements. One of the approaches to overcome this problem is to calibrate the shock tube for reflected shock temperature (T_5) in terms of the kinetics of the known reaction. We used the same approach in a single pulse shock tube (SPST) to calibrate the T_5. In the present study, we performed the calibration of our chemical shock tube using ethyl chloride as an external standard as discussed in section 2.12.

2.6. CHEMICAL SHOCK TUBE

A single pulse chemical shock tube-3 (see Figure 2.8) has been used to carry out an experimental investigation of dicyclopentadiene. The shock tube is a cylindrical tube made of high purity stainless steel (grade-304) having an inner diameter of 54 mm and a wall thickness of 23 mm. The inner wall of the shock tube was honed to get a micron finish to eliminate the frictional force. The length of the driver section is 2 m whereas the length of the driven section is 5 m. These two sections are separated by a thin aluminum diaphragm. An aluminum diaphragm of varying thickness 0.7-1.0 mm was used to produce a shock wave. A diaphragm

is scored with a groove of different depths to create different reaction conditions. Generally, argon (purity > 99.9993 %) is used as driven gas whereas helium (purity > 99.9993 %) is used as driver gas. In some cases, nitrogen and hydrogen have been used. When nitrogen is used as a driver as well as driven gas, it can increase the test time compared to helium and argon as the driver and driven gas. However, it lowers the shock velocity thereby decreasing the temperature and pressure. Hydrogen can be used as a driver gas, but it is avoided due to the danger of handling it.

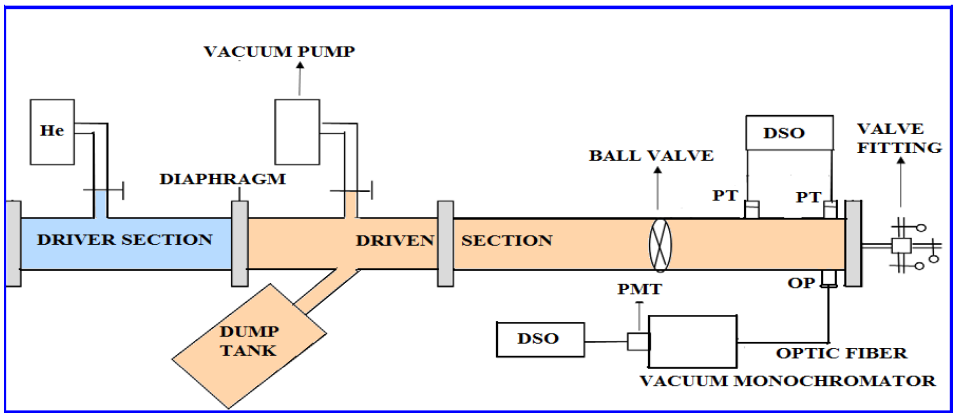

Figure 2.8. *A schematic of a chemical shock tube (CST-3) at the laboratory for hypersonic and shock wave research (LHSR).*

A suitable arrangement was made for the admission of gases into both sections. The end wall of the driven section is fitted with a four-way connector with a 6.35 mm diameter ball valve (Swagelok) which was used to introduce the sample in the test section. A similar arrangement is made in the driver section for admission of high-pressure driver gas. This arrangement is used for evacuating the shock tube down to 10^{-5} Torr. The driven section vacuum system consists of a turbo molecular pump (Edward turbo-molecular pump TIC model) to achieve ultimate pressures of 10^{-8} Torr. By using a turbo molecular pump an ultimate combined leak rate of 10^{-7} Torr per minute can be achieved with an hour of

pumping. The driver section is evacuated using a diffusion pump down to 10^{-5} Torr. Two flanges were introduced at the diaphragm section which holds the aluminum diaphragm sealed perfectly with the help of a silicon rubber 'O' ring.

2.6.1 DUMP TANK

The shock tube is operated in single pulse mode by incorporating a dump tank near the diaphragm section in the driven section at an angle of 45^0. When the dump tank is incorporated in a shock tube, it quenches the multiple reflections which leads to shocks of smaller strength. According to Bauer and Lifshitz [19], the main reason for using the dump tank is to swallow the cold driver gas that was not heated in the shock tube hence quenching the multiple reflections. Thus, the dump tank provides a very well-defined dwell time and uniform temperature during the progress of a reaction. Generally, the volume occupied by the dump tank is much higher than that of the driver section. A dump tank (made of stainless steel-304) of diameter 100 mm having the length of 1560 mm was introduced near to the diaphragm section in the driven section.

2.6.2 BALL VALVE / GATE VALVE

A shock tube can be used as a single pulse using the proper choice of driver and driven length along with incorporating dump tank, however, the dwell time experienced by test gas is the maximum at the end flange and it reduces as the reflected wave travels backward. It has been clear from the x-t diagram, expansion fan would be arriving from the opposite direction and it reaches the end flange last. As a result, only a part of the test gas present in the driven section experienced the reflected shock temperature and was heated by it. This issue can be overcome by mounting the ball valve or sliding gate valve at a certain distance away from the end flange. This can produce a third section in the shock tube which separates

from the rest of the driven section referred to as the test section. In 1970, Tschuikow-Roux and coworkers [20] have introduced the ball valve in the shock tube. Thus, the test gas constrained to the test section has nearly uniform reaction conditions. This method is called constrained reaction volume (CRV) wherein small a part of the driven section from the end wall is isolated from the rest of the driven section and filled with reactive test gas while the rest of the driven section is filled with non-reactive inert gas. A customized ball valve with an inner diameter of 54 mm of the ball was incorporated into the shock tube which separates the test section from the rest of the driven section.

2.7 INCORPORATION OF DRIVER INSERT

The shock tube can be operated in the single pulse mode with the sample confined to the test section which is highly diluted with an inert gas such as argon. It provides the near-ideal behavior behind the reflected shock wave region with an instantaneous increase in temperature (T_5) and pressure (P_5). It is based upon the assumption that in an ideal shock tube the effect caused by viscosity and heat conduction is considered to be negligible. However, this near-ideal behavior provided by the ideal shock tube is highly perturbed by the presence of non-ideal phenomena such as incident shock wave attenuation, boundary layer growth, and other non-ideal effects [21-22]. It can cause a gradual rise in pressure behind the reflected shock wave region. Figure 2.9 represents the non-ideal pressure rise of 0.07207 /ms observed behind the reflected shock wave region when both the sections are at initial temperature of 300 K. This rise in pressure introduces grave uncertainties in the reflected shock temperature and the result of chemical kinetic studies. In some cases, the rise in pressure may exceed more than 15%.

To overcome this, we have incorporated the step size insert in the driver section. With the proper design of an insert, it is possible that one can eliminate or in some cases completely remove the non-ideal pressure rise in reflected shock pressure caused by non-ideal effects.

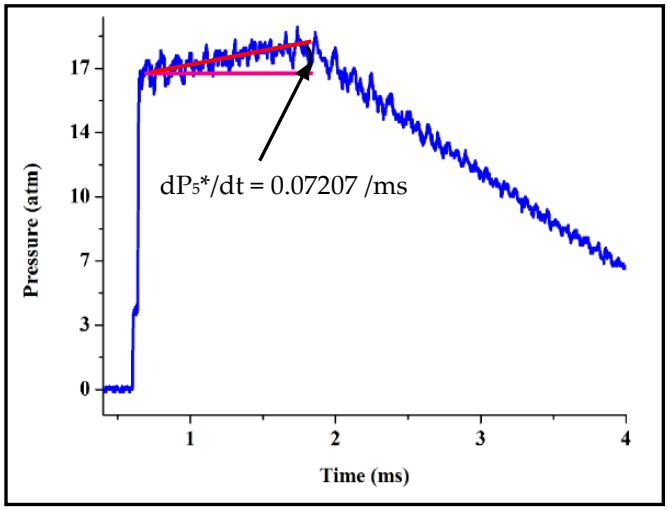

***Figure 2.9**. A non-ideal pressure-rise of 0.07207 /ms for 1.11 ms occurs in a 54 mm inner diameter shock tube of uniform cross-sectional area for both driver and driven sections. T_5 = 1261 K and P_5 = 17.0 atm when both the sections are at an initial temperature of 300 K.*

The non-ideal rise in P_5 as the rate of change of pressure due to non-ideal effects is denoted as dP_5^*/dt and given by

$$dP_5^*/dt = (dP_5/dt)/P_5 \qquad \text{-------- 2.5}$$

From Figure 2.9, the dP_5^*/dt value is found to be 0.07207 ms^{-1} when both driver and driven sections are maintained at room temperature of 300 K. However, it will require the shock tube modification to eliminate a non-ideal rise in P_5 for kinetic measurement to produce accurate experimental data.

2.7.1 METHODOLOGY

Dumitrescu [23] in 1972, proposed an idea of incorporating the cone-shaped obstacle into the driver section of the shock tube to counter the non-ideal

rise in P_5, dP_5^*/dt (see Figure 2.10). When a properly designed insert is incorporated into the driver section, rarefaction waves that are generated upon bursting of the diaphragm at the diaphragm section, reflected partially from the surface of the driver insert and propagate to the driven section. It is assumed that the decrease in the pressure by partially reflected rarefaction waves from the driver insert and the pressure rise caused by non-ideal effects is equal in magnitude and superimposed. Many methods can be used to counter the non-ideal rise in P_5 such as varying driver gas composition etc. However, we used the method of incorporation of driver insert to existing shock tubes which is found to be the most reliable method to study kinetic measurement. Using the driver insert method, the driven section remains unmodified which provides access for kinetics measurements such as CH emission, OH measurement, etc. whereas the insert can be incorporated easily in the driver section.

***Figure 2.10**. Schematic plot of modified driver section with insert in a shock tube used by Dumitrescu. It can effectively reduce the non-ideal pressure rise behind the reflected shock wave.*

Using Dumitescue's [23] idea and methodology followed by Hanson [21], we have developed an algorithm to design the shock tube driver insert. However, we have used a step size insert which was simpler to fabricate. When this step size insert is introduced in the driver section it effectively reduces non-ideal pressure rise behind the reflected shock wave. Hence uniform reflected shock pressure can be achieved which is an essential requirement for chemical kinetic measurement.

To illustrate the non-ideal effects occurring in the shock tubes, an example of two different cases is presented here. In the first case, both the driver section

and driven section remains at room temperature whereas in other case driven section is heated to a temperature of 353 K. Generally, the driven gas is chosen to be argon, which is commonly used to study high-temperature chemical kinetics whereas helium is used as driver gas.

2.7.2 PROBLEM SOLUTION AND INSERT MODELING

This method is based upon the assumption that the pressure rise in P_5 is because of non-ideal effects and that of pressure decrease caused by expansion waves can be of the same magnitude and superimposed. Hence the two pressure changes propagating in opposite directions with the same magnitude, their effects on temperature and pressure behind reflected shock wave region are effectively reduced. Since there is no direct model available which provides the relation between the rate of incident shock wave attenuation and boundary layer growth to that of dP_5^*/dt. It is difficult to calculate dP_5^*/dt analytically or numerically Hence the non-ideal rate of change in pressure is determined empirically.

To optimize the design of a driver insert it is important to address the following two problems: 1) The time taken for information about the expansion waves get reflected off from the surface of the driver insert to reach the test section and the area change in the driver section. 2) The extent of pressure changes at the test section varies with the area change in the driver section. As these two phenomena are coupled with each other, finding the exact solution is more difficult. The solution to this can be obtained separately with an approximation that these two problems will not be interfering with a grave error. A new parameter was introduced called the 'equivalence factor *g*' defined by Resler et al. [24], which provides the relation between the incident shock strength (hence the pressure at the test section) and the cross-sectional area of the driver section.

According to Alpher and White [25-26], the equivalence factor is a function of area change in the driver section. Since the area occupied by the driver insert does not change, it is easy to decouple these two problems and solve them independently.

2.7.3 FINDING THE LOCATION OF AREA CHANGE IN DRIVER SECTION

The time taken by the rarefaction waves to reflect from the surface of the driver insert and reach the test section can be determined using the method of characteristics. It will provide the time delay before the information about a variation in the pressure due to an area change in the driver section reaches the end wall of the test section. The time delay is measured from the reference point for which time zero is to be considered and defined as a time instant when the reflected shock wave passes the test section location close to the end wall of the driven section. The arrival of the reflected shock wave at the test section is taken to be at time t_0 and the arrival of reflected rarefaction waves happens at a later time t_1. Then time interval between the two is calculated as $\Delta t = t_1 - t_0$.

The one-dimensional code (Riemann solver WiSTL) developed at the University of Wisconsin [27] can be used for predicting shock wave propagation in a shock tube. It is specially developed for shock tubes having a uniform driver/driven cross-sectional area and does not account for any area changes in the driver section. At the same time, it helps in calculating the time delay before the arrival of expansion waves at the test section by assuming the end wall of the driver section is moved to be at a different location along the driver section. The Δt values can be calculated at a different location when the end wall of the driver section is assumed to be adjusted at that particular location.

2.7.4 FINDING RATE OF AREA CHANGE IN DRIVER SECTION

As the driver insert area change and the pressure variation in the test section are coupled together, to determine the correlation, a convergent shock tube model is used. Alpher and White [25] put forward a generalized theory that can be used to determine pressure variation in P_5 and the area change in the driver section. This theory considers the convergent shock tube (see Figure 2.11) as a model to establish the correlation between area change and pressure variation.

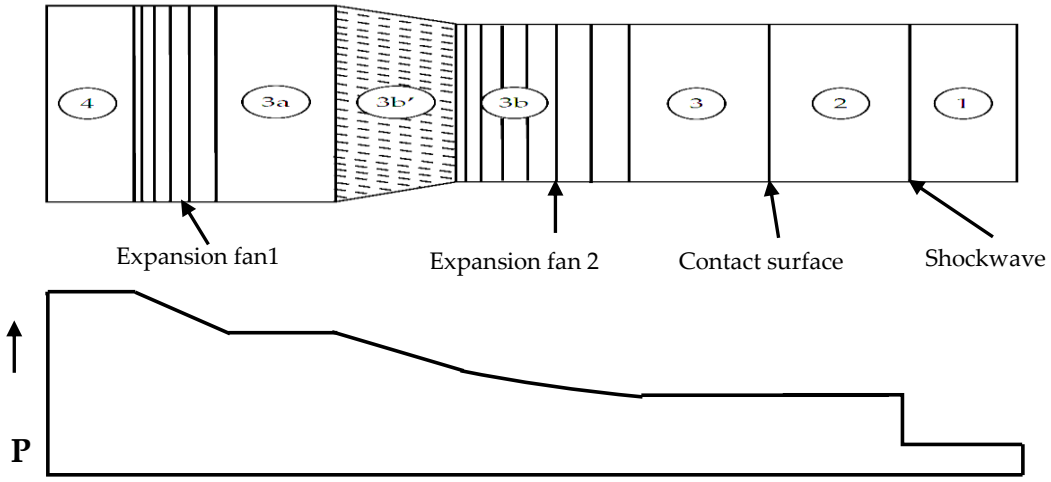

***Figure 2.11**. Schematic diagram of the shock tube with convergent type geometry at the diaphragm section. The dashed lines in the diaphragm section denote a convergent-divergent geometry with the minimum area at 3b`. The bottom figure represents the corresponding pressure distribution along the shock tube.*

In the convergent shock tube, the driver section has a larger cross-sectional area than that of the driven section. The convergent type of shock tube consists of three parts namely driver section (cross-sectional area A_4), driven section (cross-sectional area A_1), and convergent type nozzle in the middle of the driver and driven section.

The tailoring condition for convergent shock tube mainly depends on two processes: (1) the unsteady expansion of high–pressure driver gas present in region 4 into region 3 through expansion fans and a convergent and (2) the

condition required for tailoring mode at the interface between the region 3 and region 2 (see Figure 2.11). The expansion of the driver gas happening from region 4 to region 3 is highly influenced by the cross-sectional area change as mentioned by Alpher and White [25]. The initial unsteady expansion of a driver gas will result in a decrease in pressure through an expansion fan 1. The transition section which connects the two states and 3a and 3b has three possibilities: (a) if it connects equal areas i.e driver and driven sections have the same cross-sectional area, the state's 3*a*, and 3b coalesce and represents the state at the diaphragm location. (b) If the transition section is monotonically convergent, the convergent flow in the state 3b may be either subsonic or sonic and state 3 has uniform flow with $M_3 \leq 1$ or unsteady supersonic expansion to state 3 with $M_3 > 1$. (c) If transition section is a convergent-divergent type, it has a subsonic or supersonic nozzle between states 3*a* and 3b. In the case of supersonic flow at state 3b, it may be subjected to a further unsteady expansion to state 3. The relation between the area-Mach number is well established previously which connects state M_{3a} to state M_{3b} depending upon the flow whether it is subsonic or sonic. The relation is valid if the flow is isentropic, where γ is the specific heat ratio and $\beta = (\gamma + 1) / (\gamma - 1)$.

$$\left\{ \begin{array}{l} \frac{A_4}{A_1} = \frac{M_{3b}}{M_{3a}} \left[\frac{2+(\gamma_4-1)M_{3a}{}^2}{2+(\gamma_4-1)M_{3b}{}^2} \right]^{\beta_4/2} \\ \\ M_{3a} < 1,\ M_{3b} \leq 1 \end{array} \right. \qquad \text{-------- 2. 6}$$

In addition to the area-Mach equation, Alpher and White have provided a relation between incident shock Mack number M_s, to M_3, M_{3a}, and M_{3b} which is given by an equation. The quantity 'g' is called an equivalence factor as defined by Resler et al. [24]

$$\left\{ M_3 = \frac{1}{\frac{a_1 a_4}{u_2 a_1} g^{(\gamma_4-1)/2\gamma_4} - \frac{(\gamma_4-1)}{2}} \right. \qquad \text{---------- 2.7}$$

$$M_s > 1$$

Where

$$\frac{a_1}{u_2} = \frac{\gamma_1+1}{2}\frac{M_s}{{M_s}^2-1}$$

$$\frac{a_4}{a_1} = \sqrt{\frac{\gamma_4}{\gamma_1}\frac{Mw_1}{Mw_4}\frac{T_4}{T_1}} \qquad (T_4=T_1)$$

$$g = \left\{\sqrt{\frac{2+(\gamma_4-1){M_{3a}}^2}{2+(\gamma_4-1){M_{3b}}^2}}\left[\frac{2+(\gamma_4-1)M_{3a}}{2+(\gamma_4-1)M_{3b}}\right]\right\}^{2\gamma_4/(\gamma_4-1)} \qquad \text{------2. 8}$$

Where M_w, T, and a represent the molecular weight, temperature, and speed of sound of a gaseous medium respectively.

However, the cold flow downstream of state 3b can be either supersonic or subsonic in state 3. For supersonic cold flow, $M_3 \geq 1$, another expansion fan 2 appears between the state 3b` and state 3 for which $M_{3b`}=1$(or $M_{3b}=1$). For subsonic cold flow in state 3, the transition section is a subsonic nozzle that follows the condition that $M_{3b} = M_3$, $P_{3b} = P_3$, and $a_{3b} = a_3$. In this case, there is no expansion fan 2 and the conditions in state 3 are like that of a throat. If the driver and driven gas compositions and initial parameters (x_i) are known, the molecular weight and specific heat ratio of the mixture can be calculated using the following relation,

$$M_w = \sum x_i M_{wi} \qquad \text{-------- 2. 9}$$

$$\gamma = \frac{\Sigma\frac{x_i\gamma_i}{\gamma_i-1}}{\left(\Sigma i\frac{x_i\gamma_i}{\gamma_i-1}-1\right)} \qquad \text{------- 2. 10}$$

Therefore, there are four unknowns in the above three independent equations: M_s, M_{3b}, M_{3a}, and M_3. Another equation required for the matching condition for tailored contact surface between states 2 and 3, is presented by Nishida et al. [28]

$$u_2 = a_3\frac{(a_4-1)(p_{52}-1)}{\sqrt{(1+\beta_4)(1+\beta_4 p_{52})}} \qquad \text{-------- 2. 11}$$

Here u_2 denotes the velocity of the gas in state 2 measured in shock fixed coordinates and P_{52} denotes the ratio of pressure change across the reflected shock,

$P_{52} = P_5/P_2$. At the interface between state 2 and state 3, u_2 can be replaced by u_3. Hence above relation can be written as:

$$M_3 = \frac{u_3}{a_3} = \frac{(a_4-1)(p_{52}-1)}{\sqrt{(1+\beta_4)(1+\beta_4 p_{52})}} \qquad \text{------- 2. 12}$$

where $$p_{52} = \frac{M_S^2(3\gamma_1-1)-2(\gamma_1-1)}{M_S^2(\gamma_1-1)+2} \qquad \text{-------- 2. 13}$$

Using an initial condition of a convergent shock tube operating in the tailored driver and driven gas, the four unknown variables (M_s, M_{3b}, M_{3a}, and M_3) can be fully characterized if the solution to equations 2.10 to 2.13 can exist.

To optimize the design for driver insert is mostly dependent upon the desired reflected shock temperature (T_5) and driven section length. The reflected shock temperature is depending upon four different parameters such as the composition of tailored condition required, starting location of driver insert, the length of the insert required for area change, and the distance between starting and ending locations of the area change. The final driver insert design is derived empirically from observed pressure variation (dP_5^*/dt) with its relation to Δt and X_{dist} and between A_4/A_1 and $\Delta P_5/P_5$. In the present study, we have optimized the driver insert design for the two different cases.

2.7.5 WHEN BOTH DRIVER AND DRIVEN SECTIONS ARE AT AN INITIAL TEMPERATURE OF 300 K

The targeted reflected shock temperature (T_5) to be achieved is 1261 K, which is calculated from normal shock relation produced by an incident shock wave of Mach number Ms = 2.2336 when both the driver and driven sections area at an initial temperature of 300 K. The rate of change of non-ideal pressure rise in P_5 is found to be 0.07207 /ms for 1.11 ms. (see Figure 2.9)

The one-dimensional code WiSTL [27] was used to calculate Δt at different locations of the driver section (see Figure 2.12).

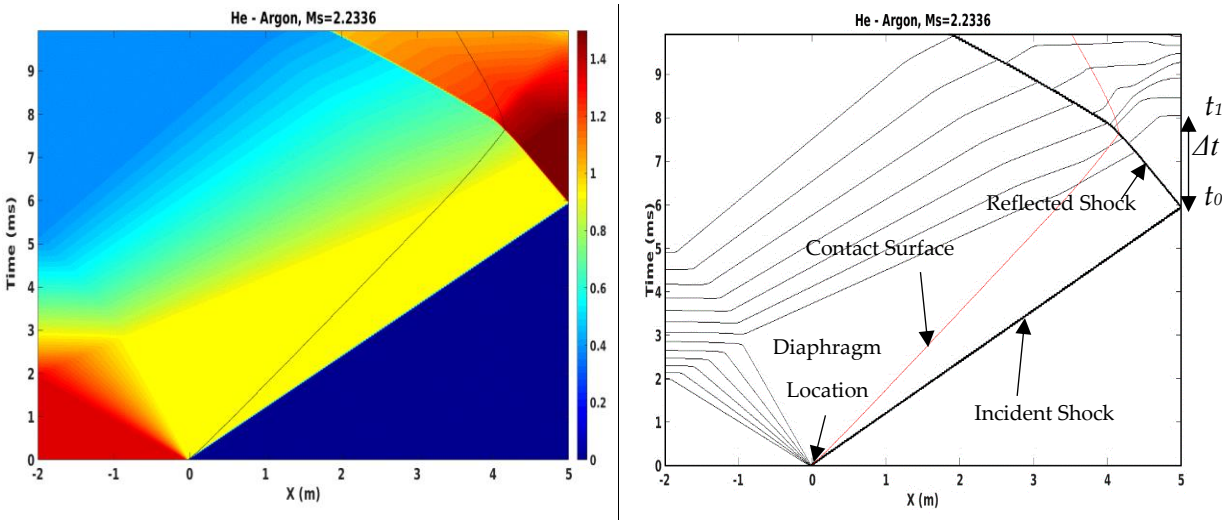

***Figure 2.12**. The color plot (left) and contour plot (right) of the X-t wave diagram generated for the case where the incident shock Mach Number Ms=2.2336 corresponding to temperature T_5=1261 K*

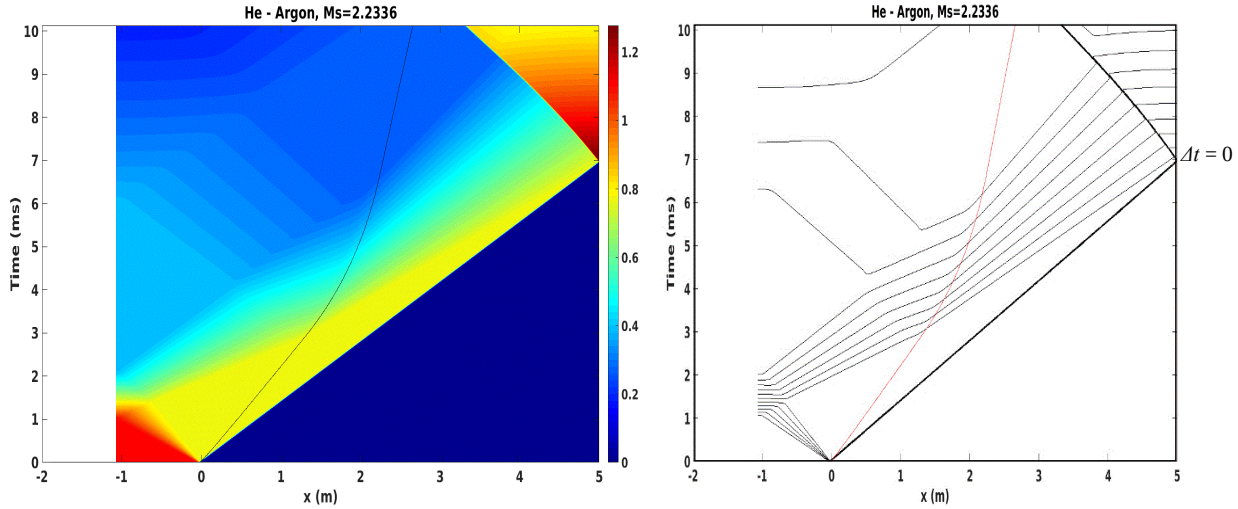

***Figure 2.13**. The color plot (left) and contour plot (right) of the X-t wave diagram generated for the limiting case where the time interval Δt = 0. The location of the driver area changes X_{dist} = -1.0695 m from the diaphragm location which corresponds to shock Mach number Ms = 2.2336 and reflected shock temperature T_5=1261 K.*

Following to same procedure, the Δt values can be calculated at the different X_{dist} locations of the driver section. Figure 2.13 shows that in order to follow the pressure immediately after as reflected shock wave reaches to end wall of the test section, i.e. $\Delta t=0$, the starting position of the driver insert, should be located at X_{dist}= -1.0695 m. It showed that if there is an obstacle placed at a distance X_{dist} = -1.0695 m from the diaphragm location in the driver section, the expansion fan reaches at test section immediately after the passage of the reflected shock wave.

The pressure rise in P_5, in this case, was experimentally determined which varies almost linearly with time having a value of dP_5*/dt= 7.207 % /ms, as shown in Figure 2.9. After 2 ms, the arrival of the expansion wave reflected from the driver end wall effectively ending the nominal test time. The starting and ending location of the area change generated by the driver insert are denoted as X_{dist}^1 and X_{dist}^2 respectively. In this case, X_{dist}^1 = -1.0695 m and X_{dist}^2 = -1.7518 m, X_{dist}^1 denotes the starting location of an insert for which the time delay is zero ($\Delta t = 0$) and X_{dist}^2 denotes the location of an insert corresponding to a delay of 1.11 ms. Figure 2.14 represents the plot of X_{dist} versus time.

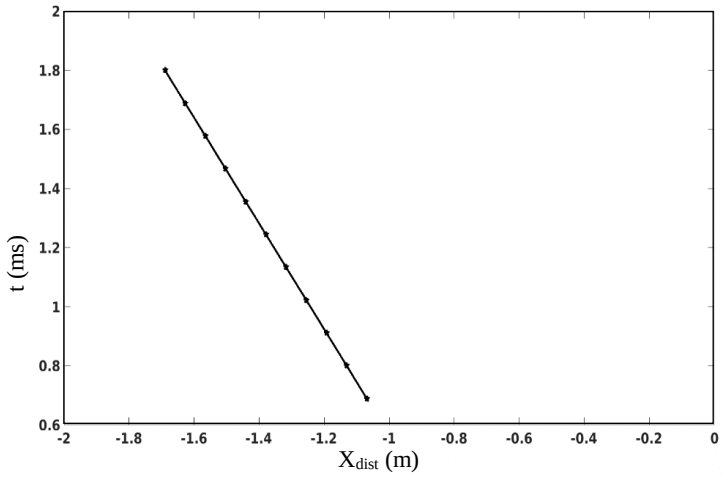

***Figure 2.14**. X_{dist}- t plot calculated for case 1 where incident shock Mach number Ms = 2.2336 and reflected shock temperature T_5=1261*

Table 2.1. Summary of A_4/A_1, Δx, time t, % $\Delta P_5/ P_5$, and corresponding diameter of insert required to cancel non-ideal P_5.

Sr no.	A_4/A_1	x (in m) from diaphragm location	Time t (μs)	% $\Delta P_5/P_5$	Diameter of insert needed
1		-1.0695	690	0	
2	0.9810	-1.131	801	0.8	7.38
3	0.9624	-1.2553	912	1.6	10.39
4	0.9444	-1.3175	1023	2.4	12.63
5	0.9269	-1.3795	1134	3.2	14.49
6	0.9098	-1.4416	1245	4.0	16.09
7	0.8933	-1.5036	1356	4.8	17.50
8	0.8772	-1.5656	1467	5.6	18.78
9	0.8615	-1.6277	1578	6.4	19.94
10	0.8462	-1.6897	1689	7.2	21.02
11	0.8310	-1.7518	1800	8.0	22.03

Using Alpher and White's theory, we can calculate A_4/A_1 for different $\Delta P_5/P_5$ values corresponding to different time steps which are tabulated in Table 2.1. Figure 2.15 represents the relationship between A_4/A_1 and X_{dist} curve for the driver section for the above case.

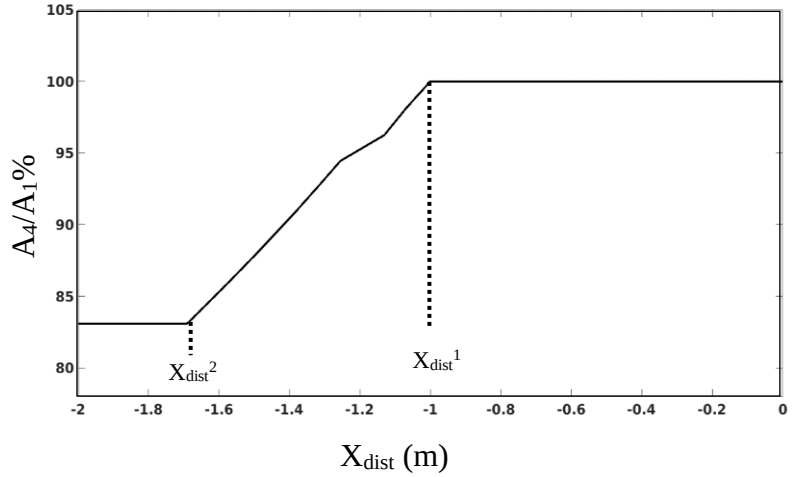

***Figure 2.15**. The relationship between A_4/A_1 and X_{dist} curve for the driver section for the above case. The diaphragm location is at X_{dist} = 0 and the driver end wall location is at X_{dist} = -2.0 m.*

Although driver inserts modeled by Dumitescu [23] and Hanson [21] predict a change in the area (A_4/A_1) which is continuous, it is difficult to fabricate a cone-shaped driver insert for each desired reaction condition. In addition to that calculated A_4/A_1 and X_{dist} (see Figure 2.15) might require some future adjustments to reduce the influence of non-ideal effects on P_5. To overcome this, we have used the step size driver insert which is more reliable to fabricate. The calculated A_4/A_1 as a function of X_{dist} from the experimental data can remove the non-ideal pressure rise completely. Following Figure 2.16 shows the highly uniform pressure trace obtained using the driver insert method (see Figure 2.17) compared to a pressure that is obtained without a driver insert.

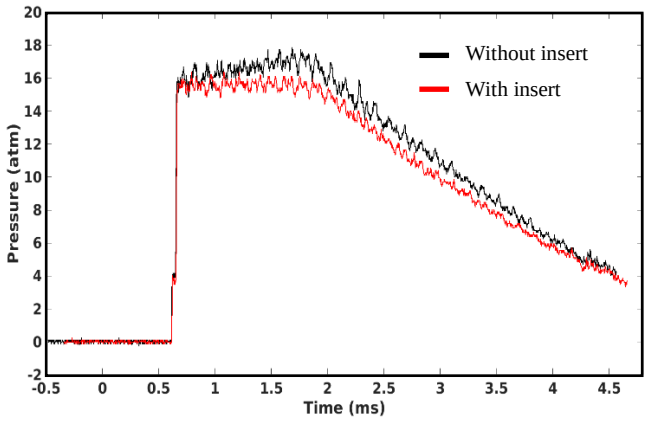

***Figure 2.16**. Highly uniform pressure trace obtained when driver insert is incorporated in the driver section.*

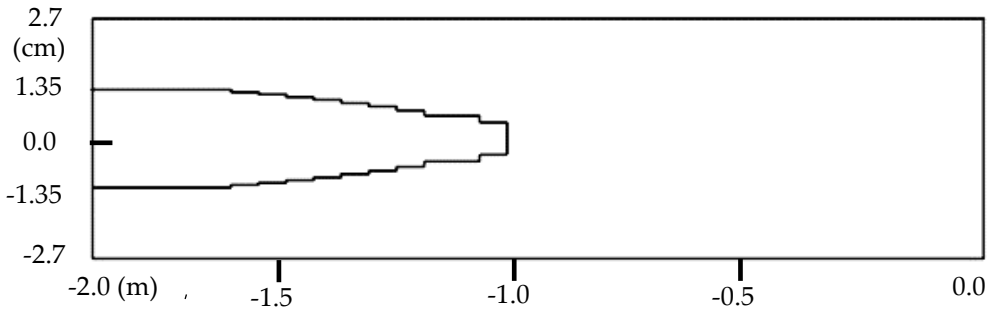

Figure 2.17*. The plot of modified driver section with step size insert in a shock tube to reduce the non-ideal pressure rise behind the reflected shock wave.*

2.7.6 WHEN DRIVER SECTION AT TEMPERATURE OF 300 K AND DRIVEN SECTION AT TEMPERATURE OF 353 K

The targeted reflected shock temperature T_5 to be achieved is 1503 K, which is calculated from normal shock relation produced by an incident shock wave of Mach number Ms = 2.24877 when the driver section is at an initial temperature of 300 K whereas driven sections are heated to the temperature of 353 K. The rate of change of non-ideal pressure rise in P_5 is found to be 0.13922 /ms for 1.10 ms. Figure 2.18 represents the pressure variation behind the reflected shock wave.

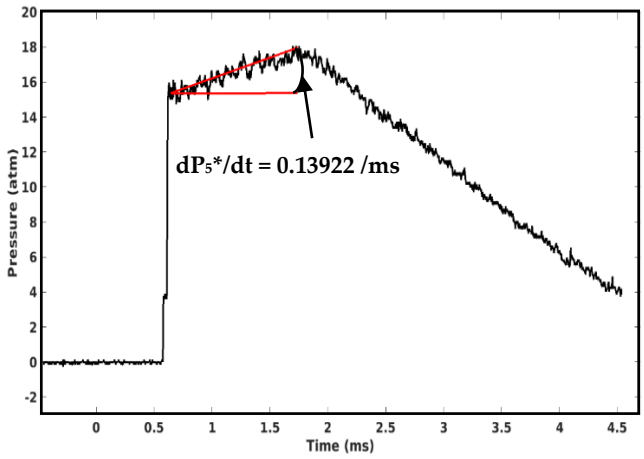

Figure 2.18. *A non-ideal pressure-rise of 0.13922 /ms for 1.10 ms occurs in a 54 mm inner diameter shock tube of uniform cross-sectional area for both driver and driven sections. T_5 = 1503 K and P_5 = 15.41 atm when the driver section is at an initial temperature of 300 K whereas the driven section is heated to 353 K*

The one-dimensional code WiSTL [27] was used to calculate Δt at different locations of the driver section (see Figure 2.19)

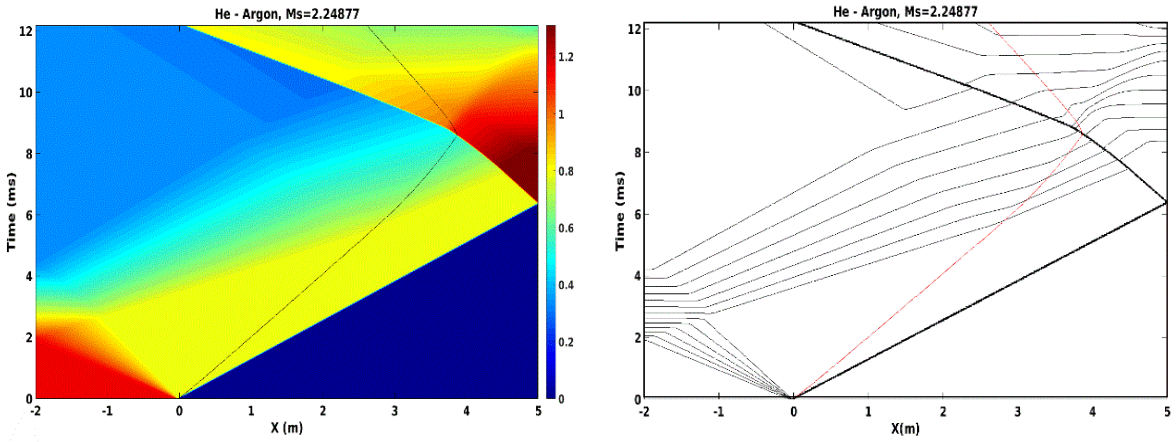

Figure 2.19. *The color plot (left) and contour plot (right) of the X-t wave diagram generated for the case where the incident shock Mach number Ms = 2.24877 corresponding to temperature* T_5 *= 1503 K*

The Δt values can be calculated at the different X_{dist} locations of the driver section. The computed Δt values for X_{dist} = -0.9 m are presented in Figure 2.20.

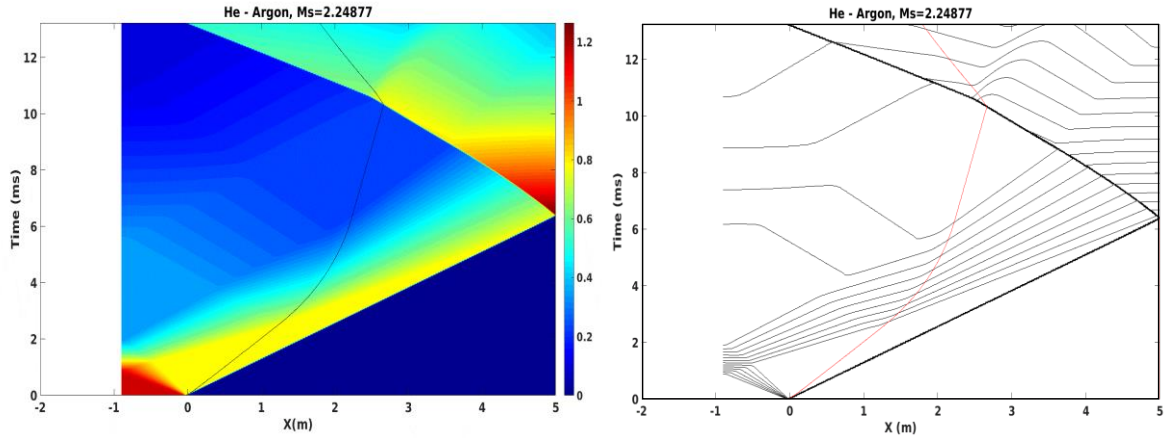

Figure 2.20. *The color plot (left) and contour plot (right) of the X-t wave diagram generated for the limiting case where the time interval* $\Delta t = 0$*. The location of the driver area changes* X_{dist} *= -0.9 m from the diaphragm location which correspond to shock Mach number Ms = 2.24877 and reflected shock temperature* T_5 *= 1503K*

To follow pressure immediately after, as reflected shock wave reaches to end wall of the test section, i.e. $\Delta t=0$, the starting position of the driver insert, should be located at X_{dist}= -0.9 m. Hence if an obstacle is placed at distance X_{dist}= -

0.9 m from the diaphragm location in the driver section, the expansion fan reaches at test section immediately after the passage of the reflected shock wave.

The pressure rise in P_5 is determined from experimental data which varies almost linearly with time having a value of $dP5^*/dt$= 13.922 %/ms, as shown in Figure 2.18. Following the same procedure, the distances X_{dist}^1 and X_{dist}^2 are being calculated. In this case, X_{dist}^1 = -0.9 m and X_{dist}^2 = -1.7518 m, X_{dist}^1 denotes the starting location of an insert for which the time delay is zero ($\Delta t = 0$) and X_{dist}^2 denotes the location of an insert corresponding to the time delay of 1.11 ms. Also, using calculated A_4/A_1 for different $\Delta P_5/P_5$ values corresponding to different time instances, the required diameter of an insert is computed. It has been observed that the calculated geometry for the driver insert requires some future adjustments to reduce the influence caused by non-ideal effects. It can be achieved by successive modification in the final design of the driver insert which is done empirically. Figure 2.21 represents the schematic of the final design of the insert employed to the driver section to a non-ideal pressure rise in P_5. Hence highly uniform pressure profile is obtained using the driver insert method (see Figure 2.22).

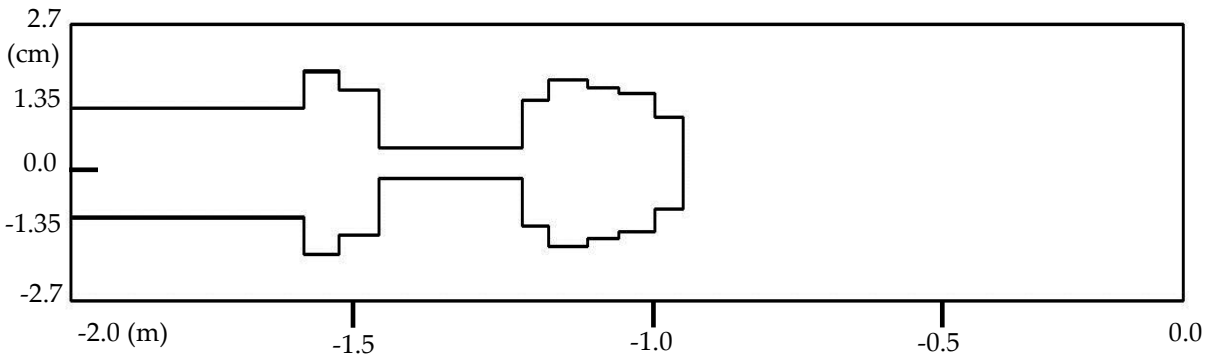

Figure 2.21. *Schematic plot of modified driver section with step size insert in a shock tube to reduce the non-ideal pressure rise behind the reflected shock wave.*

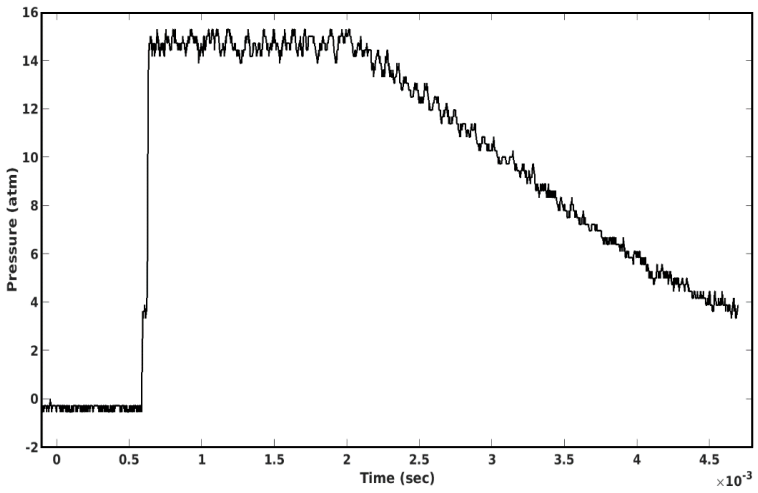

Figure 2.22. *Highly uniform pressure trace obtained when driver insert is incorporated in the driver section.*

2.8 OUTLINE

We outline the following procedure to design the driver insert for the previous example case:

1. Decide on the desired conditions: reflected shock temperature (T_5), reflected shock pressure (P_5), helium driver gas, and driven gas argon.
2. Establish the time duration over which the pressure rises to be compensated for desired conditions and divide it into several steps.
3. Find out the starting location (X_{dist}^1) and ending location (X_{dist}^2) of the area change and calculate the distance (X_{dist}) corresponding to each time step (t_i) from starting location X_{dist}^1 till ending location of the area change (X_{dist}^2).
4. Determine the non-ideal pressure rise from the experimental pressure profile ($\Delta P_5/P_5$) at each time step (t_i).
5. To determine the starting location of the tip of the driver insert for the area change using the shock tube driven section length as a basis parameter (L = 5.0 m, for which $\Delta t = 0$) $X_{dist}^1 = -1.0695$ m.

6. Estimate the A_4/A_1 for corresponding $\Delta P_5/P_5$ and compute the diameter for the driver insert required for each step.

2.9 INSTRUMENTATION

The CST-3 is equipped with PCB piezoelectric transducers (Model no.27403) for pressure measurement. Two PCB transducers are mounted over shock tube at a distance of 450 mm away from each other to measure the shock velocity. One of the PCB transducers is mounted very close to the end wall (5 mm away) of the driven section for the measurement of reflected shock pressure. These pressure transducers are mounted in such a way that they are flush with the inner surface of the shock tube. The output from two PCB transducers are connected to the signal conditioner which in turn is connected to a digital storage oscilloscope to record the time. An acquisition rate of 2 μs is obtained using the PCB piezoelectric transducer. A digital storage oscilloscope (Tektronix, TDS-2014B/100MHz/1GS/s), with a 4-channel 8-bit analog to digital converter was connected to PCB transducers and used to record pressure profile across the shock front. The oscilloscope was triggered by the outcome from the PCB transducer which was triggered by the primary shock wave. The reflected shock pressure can be measured accurately using the initial pressure and sensitivity of the PCB transducer. Also, the output recorded using an oscilloscope is used to calculate the shock velocity. Another type of pressure sensor (IRA) with a low acquisition rate was used to measure the equilibrated pressure in the shock tube. IRA pressure sensors that are used to measure P_1 and P_4 have different working ranges and least count. The working range for the P_1 sensor is 0-1500 mm Hg with an accuracy of ±1 mm Hg whereas the P_4 sensor has a working range of 0-60 bar with an accuracy of ±0.1 bar.

One of the techniques used with shock tube for the measurement of ignition delay times at high temperatures is emission spectroscopy. With the shock tube coupled with a photomultiplier tube, it is possible to measure the emission from CH, OH, and C2 that are triggered by ignition. Ignition delay can also be measured by pressure profile history. One of the PCB transducers is mounted very near to end wall of the driven section to measure the ignition delay. Also, one of the optical ports facilitates the measurement of CH emission. The monochromator was used to record CH emission at 431.5 nm. This port is interfaced to a vacuum monochromator (Acton VM 502), which consists of a concave grating with a groove density of 1200 groove/mm. The monochromator has a photomultiplier tube (DA-780-VUV) which has a range of 200 nm to 600 nm. The monochromator covers a wavelength range of 30 nm to 600 nm. The wavelength can be adjusted by rotating the concave grating to a proper configuration using the motor. Also, the intensity of incoming light, as well as outgoing light, can be adjusted using the entrance slit and exit slit respectively. The output from PMT was recorded using a digital storage oscilloscope.

2.9.1 GAS CHROMATOGRAPHY

In gas chromatography, the mobile phase is a carrier gas such as helium or nitrogen whereas the stationary phase is a microscopic layer of liquid or polymer on an inert solid support, inside the glass or metal tubing called a column. Gas chromatographs (Agilent 7890A, 7890 B) have been used to identify different analysts present in the post-shock mixture. The gas chromatograph consists of three major parts namely injector, oven, and detector. The sample is injected through the injector and passed through the column with the help of carrier gas. Generally, the temperature of the inlet is maintained higher than that of the boiling

point of the analyst so that the compound under consideration is completely vaporized. A liquid sample can be injected directly into the injector with the help of a microsyringe whereas the gas sample is introduced into the injector using six-port pneumatic valves. Two ports of the valve are connected to the controllable loop (capacity of 1 ml), two ports are used as inlet and outlet for carrier gas whereas the remaining two ports are for the inlet and outlet of the sample. When the valve is turned on the sample present in the loop will be permitted to flow through the column with a carrier gas. The carrier gas flow will be maintained irrespective of valve position carrying the introduced sample through the column components into the detector.

The oven is the most important part of the gas chromatograph within which column is located. The separation of different analysts present in the sample is highly dependent upon the length of the column, type of column, and column material. Thus, when the sample is passed through the column, the individual analyst gets adsorbed and desorbed at different rates. Thus, after time interval t, analysts will be located at a different position in the column. The process of adsorption and desorption continues throughout the column enabling the analyst to elute at different time intervals. The time taken for each analyst to travel the distance between the injector side of the column and the exit of the column is referred to as the retention time of that analyst. The exit of the column is connected to the detector for the identification of the analyst both qualitatively and quantitatively. The retention time of the particular analyst will be affected by the flow rate of the carrier gas and oven temperature. Hence, it is required to optimize suitable oven temperature and flow rate to separate the given sample into its original components.

Two capillary columns namely HP-5 cross-linked 5% PH siloxane 30 m long (with inner diameter 0.32 mm) and HP-PLOT-Q of length 30 m (with inner diameter 0.15 mm) were fitted in GC-FID. HP-5 column was used for separation of high molecular mass compounds (typically greater than C_5) whereas HP-PLOT-Q was specially designed for separation of low molecular mass compounds. Using a capillary column of small diameter, peak width can be reduced effectively with a lowering in retention time. GC-FID is equipped with capillary flow technology and flow in both columns is controlled by dean-switch. HP-5 column is used as a primary column whereas HP-PLOT-Q and retention column (a non-polar column) are being used as secondary columns. Inlets of secondary columns are connected to the dean switch whereas another end opens in flame ionization detectors. When the dean switch is off the flow in the HP-PLOT-Q column is restricted and it allows the flow in the retention column only. A HP-5 column of length 30 m long (with i.d. 0.25 mm) is installed in GC-MS. The above-mentioned columns can be operated at a working temperature of 250-350 ^{0}C. Maintaining the column at maximum working temperature reduces its lifetime. Thus, the oven temperature was always maintained at an optimum temperature to utilize the column for a longer time.

The mass selective detector (MSD) equipped with gas chromatography is used for the identification of the different analytes. In principle, a mass-selective detection system means the simple mass spectrometry (MS) system. For the present investigation, MS (Agilent 5895C) is interfaced with GC (Agilent 7890A) having a quadrupole mass analyzer. The MS mainly consists of an ion source, a mass analyzer, and a detector. Another type of detector called a flame ionization detector has been used for compound identification. The gas chromatograph

(Agilent 7890 B) is equipped with dual flame ionization detectors. It consists of a jet, a collector, and a body and insulator plate. The hydrogen and oxygen combustion of the sample will generate the ions and thereby altering the potential difference between the collector plate and the insulator plate. The change in the output current is directly proportional to the concentration of the analyst eluting at the detector and of the column and sensitivity of the detector to it. To avoid condensation of the elutant FID was maintained at a temperature of 200 ^{0}C.

2.10 POST-SHOCK MIXTURE

A stainless-steel hollow cylinder (Swagelok) with a capacity of 1000 ml has been used to collect post-shock mixture into it and used for further analysis. The cylinder is fitted with a ¼ " valve (Swagelok needle valve) for admission of gas into the cylinder. The cylinder is evacuated using a turbo-molecular pump which pumps down to 10^{-8} mbar before sample analysis. It is also assured that no traces of impurity are present inside the cylinder, this can be done by using argon gas only. Using suitable arrangement coupled to the cylinder, post-shock mixture were collected into the cylinder which is further used for gas chromatographic analysis. The same cylinder can be used for the calibration of standard samples. For calibration of the sample, the cylinder is fitted with IRA pressure transducers for pressure measurement.

2.11 SENSITIVITY OF FID

The output signal from FID and MS will be recorded as pico-Amperes (pA) and arbitrary units (a.u) versus retention time, respectively. The magnitude of the area under a peak representing a particular compound in a mixture mainly depends on the concentration of the compound as well as the sensitivity of the

detector towards that compound. To find an actual concentration of a particular compound at a given reaction condition, the sensitivity of a detector towards the particular compound must be known. Usually, the sensitivity of a detector depends upon many factors such as the number of C-C bonds, number of C-H bonds, aromaticity, etc. present in a compound.

The sample cylinder (capacity of 1000 ml) was used for the preparation of the standard sample to calculate the sensitivity of the detector. The cylinder is checked for any impurity present inside it by means of loading argon only. The sample cylinder is pumped down to 10^{-8} mbar of pressure using a turbo-molecular pump. A standard sample of 10-12 mm Hg was then loaded into it and diluted with argon. The total pressure of the mixture within the cylinder is maintained approximately 100 times that of sample pressure. The mixture was allowed to mix uniformly for two hours and then injected into FID. The area under the peak corresponding to the given mole fraction of the sample is calculated. The sample cylinder then pumps down to 600 mm Hg and diluted with argon to a total pressure of 1200 mm Hg. Similarly, the area under the peak, as well as the corresponding mole fraction of the sample, was calculated. This procedure is repeated until the area under the peak becomes nearly zero. A plot of the area under the peak versus mole fraction of the sample is fitted linearly. The slope gives the sensitivity factor of the detector for a particular sample which will be further used to calculate the concentration of the sample. Figure 2.23 represents the calibration curves for the different molecules used in the present study and corresponding sensitivity factors are tabulated in Table 2. 2.

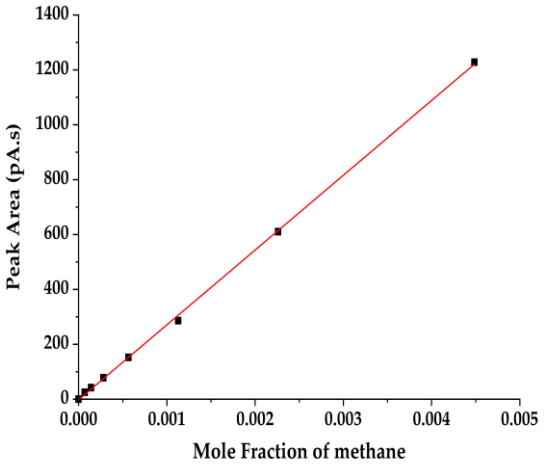
Peak Area (pA.s)
Mole Fraction of methane

(A)

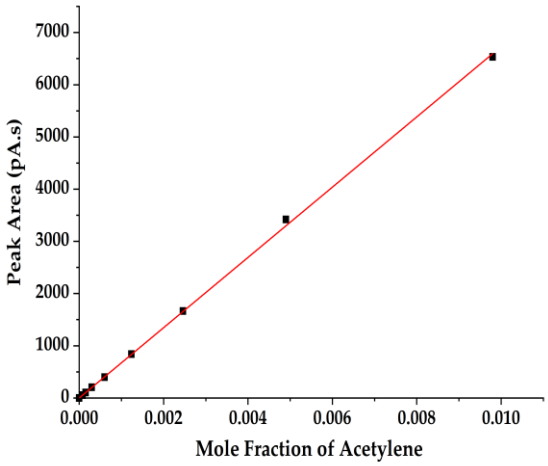
Peak Area (pA.s)
Mole Fraction of Acetylene

(B)

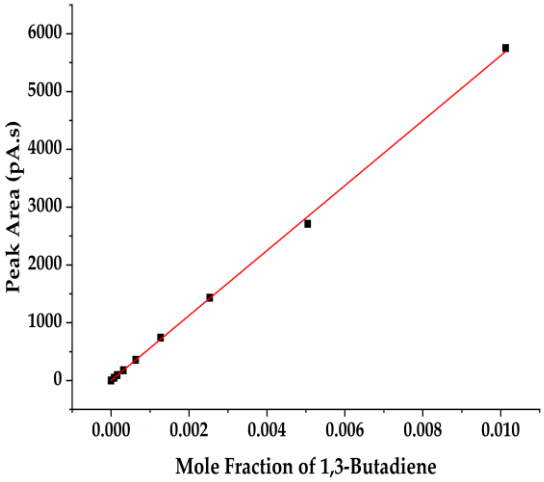
Peak Area (pA.s)
Mole Fraction of 1,3-Butadiene

(C)

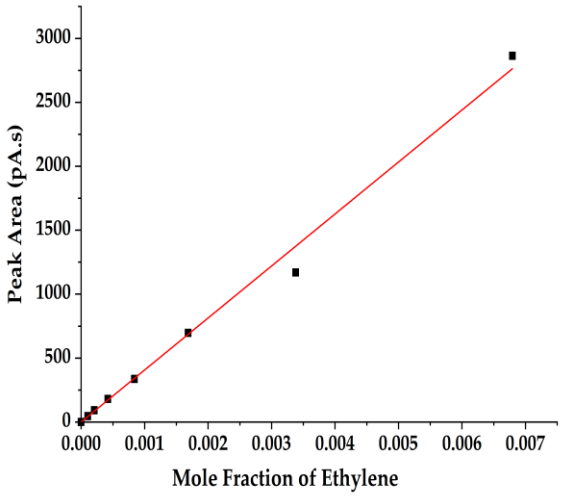
Peak Area (pA.s)
Mole Fraction of Ethylene

(D)

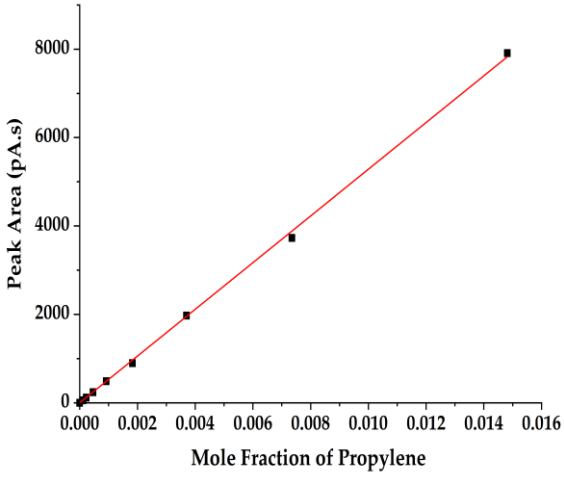
Peak Area (pA.s)
Mole Fraction of Propylene

(E)

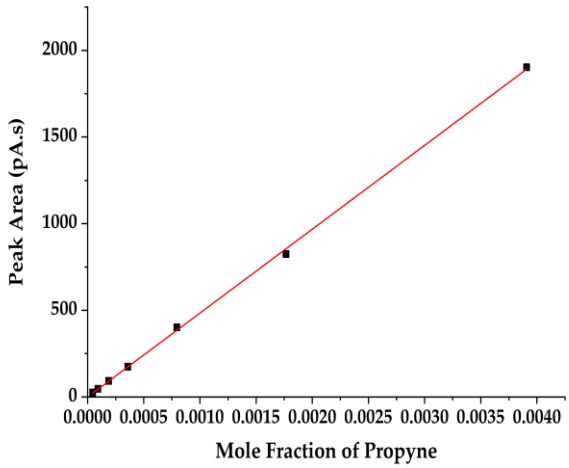
Peak Area (pA.s)
Mole Fraction of Propyne

(F)

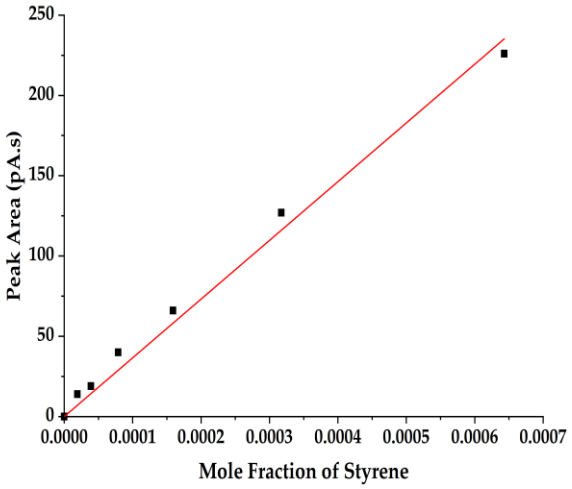
Peak Area (pA.s)
Mole Fraction of Styrene

(G)

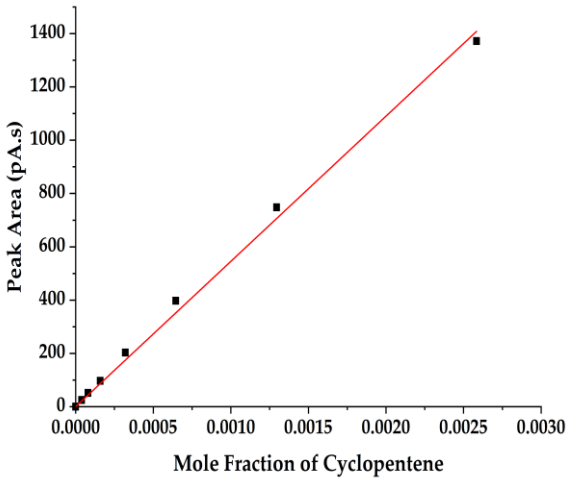
Peak Area (pA.s)
Mole Fraction of Cyclopentene

(H)

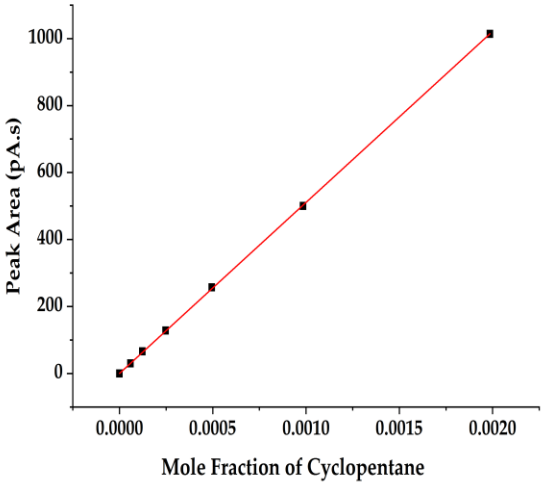
Peak Area (pA.s)
Mole Fraction of Cyclopentane

(I)

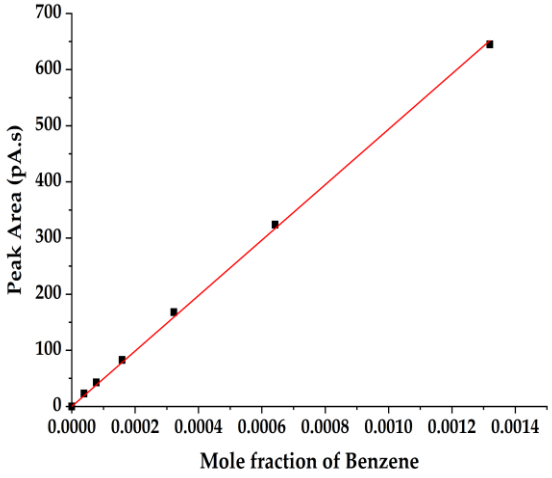
Peak Area (pA.s)
Mole fraction of Benzene

(J)

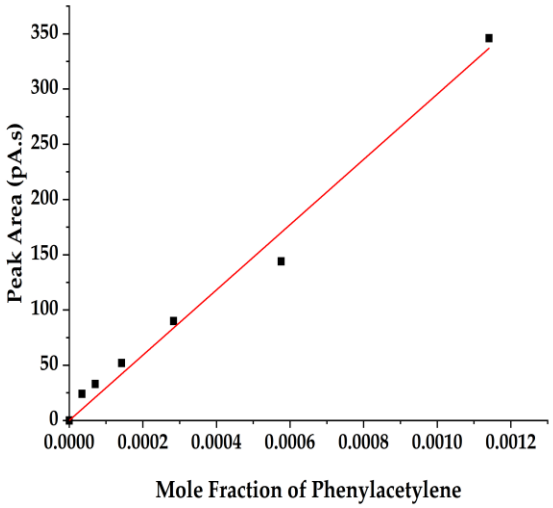
Peak Area (pA.s)
Mole Fraction of Phenylacetylene

(K)

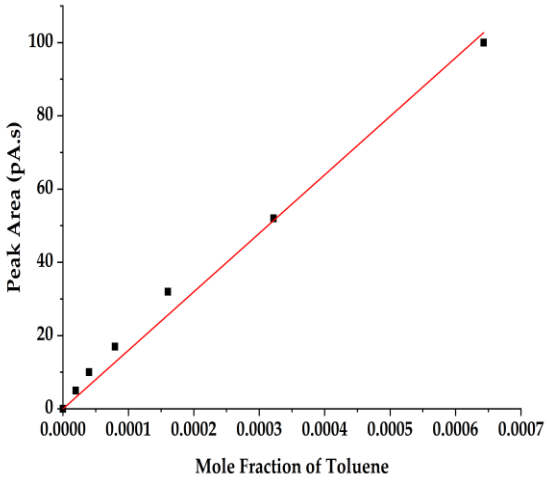
Peak Area (pA.s)
Mole Fraction of Toluene

(L)

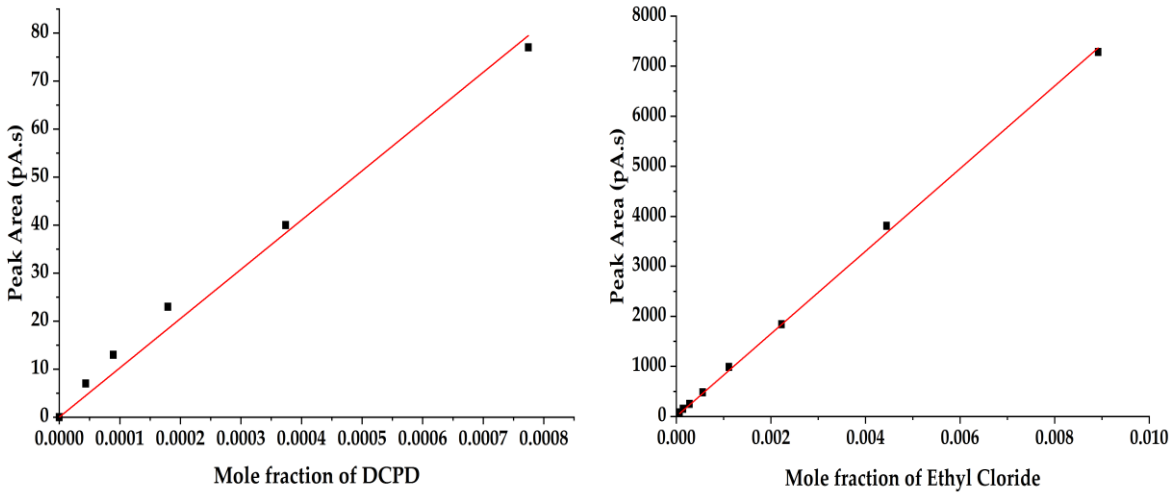

(M) **(N)**

***Figure* 2.23.** *Calibration curves for different molecules: (A) Methane (B) Acetylene (C) 1,3-Butadiene (D) Ethylene (E) Propylene (F) Propyne (G) Styrene (H) Cyclopentene (I) Cyclopentane (J) Benzene (K) Phenyl Acetylene (l) Toluene (M) Dicyclopentadiene (N) Ethyl Chloride*

Table 2.2: Summary of the Sensitivity factor for the molecules.

Sr no	Species	Sensitivity Factor
1	Methane	271968
2	Ethylene	411997
3	Acetylene	456800
4	Propylene	528287
5	Propyne	483893
6	1,3-Butadiene	544344
7	Vinyl Acetylene	562092
8	Cyclopentadiene	589510
9	Benzene	493798
10	Toluene	457491
11	Styrene	399925
12	Phenyl Acetylene	301907
13	Dicyclopentadiene	235740
14	Ethyl Chloride	825487

2.12 CHEMICAL THERMOMETRY

It is important to calculate reflected shock temperature (i.e. T_5) accurately to obtain reliable kinetic and mechanistic chemical data using a shock tube. The accurate measurement of reflected shock temperature has been achieved by a

popularly known technique called a Chemical thermometric method. This technique can be of two types: internal or external chemical thermometry. In the former case, the reflected shock temperature is determined by following the progression of a standard reaction with a known rate constant, which is investigated together with the reaction of interest. In the external standard method, experiments with the sample and standard at various temperatures are carried out independently.

Tsang [28] investigated the influence of non-ideal effects on the reflected shock temperature that led to the development of internal chemical thermometry. This can be done by carrying out the decomposition of the chemical thermometer and the reactant of interest simultaneously under similar reaction conditions. The average temperature that is obtained accurately reflects the average temperature experienced by the reagent and minimizes the variations inherent from experiment to experiment and deviations from ideal conditions. Hence the error computed in the reported rate coefficient for the decomposition of the internal standard determines the accuracy in the estimated temperature. The following expression is used to calculate the reflected shock temperature with the use of an internal standard.

$$T_5 = {}^{(E/R)}\Big/\left[ln\left(-\frac{1}{A\times t}ln(1-\chi)\right)\right] \qquad \text{---------- 2.14}$$

Where t is the reaction dwell time, E, A, and χ are the activation energy and pre-exponential factor and the extent of the standard reaction respectively.

The extent of the standard reaction is defined as

$$\chi = \frac{[product]_t}{\{[product]_t + [internal\ standard]_t\}} \qquad \text{---------- 2.15}$$

However, neither the internal standard nor its product of decomposition should react with the reagent under investigation or any of its products. As the chemical kinetics experiments at elevated temperature and pressure using shock tube involve a complex mixture of radicals and stable species, interference with an internal standard is highly probable. Hence modified method known as "external chemical thermometry" is used to calibrate the reflected shock temperature. The temperature computed from normal shock relation (R-H equation) and calculated from equation 2.13 are plotted which is shown in Figure 2.25. The least-square fitting to the resulting plot is used to determine the T_5 for all the experiments. The commonly used external chemical standard for chemical thermometry is listed in Table 2.3.

Table 2.3. List of chemical standards mainly used for chemical thermometry.

Sr no.	Chemical Standard: Reaction	Rate Expression k_{exp} (sec^{-1})	Temperature Range (K)	References
1	Cyclopropane carbonitrile: c-C_3H_5CN -> $CH_3CH{=}CHCN$ c-C_3H_5CN -> $CH_2{=}CHCH_2CN$	$10^{14.58}$ exp(-57.80/RT) $4.84\times10^{14.0}$ exp(-63.39/RT)	900 – 1040 950 – 1300	29-30
2	Cyclohexene: c-C_6H_{10} -> C_4H_6 + C_2H_4	$10^{13.84}$ exp(-57.80/RT)	960 - 1100	**32, 33**
3	Ethyl chloride: CH_3CH_2Cl -> C_2H_4 + HCl	$10^{14.85}$ exp(-74.05/RT)	1150 - 1350	**20, 31**
4	1,1,1-trifluoroethane: CH_3CF_3 -> $CH_2{=}CF_2$ + HF	5.75×10^{46} $T^{-9.341}$ exp(-47.073K/T)	1000 - 1600	**34-36**

It is noted that one can use more than one chemical thermometer for the same experiment to cover the desired temperature range.

2.13 CALIBRATION OF CST3 USING ETHYL CHLORIDE

We have calibrated the Chemical Shock Tube (CST-3) present in our laboratory as it is modified with some advances. The thermal decomposition of

ethyl chloride (external standard) was carried out behind the reflected shock wave at varying P_4/P_1 conditions to achieve the desired temperature (T_5). The experiments were performed in the temperature ($T_{5\,(Ms)}$) ranging from 960 K -1190 K and pressure ($P_{5\,(expt)}$) ranging from 9 – 14 atm, while reaction time ranges from 1180 – 1420 μs. In the present study, it has been observed that for the given temperature range HCl elimination pathway was found to be the only thermal decomposition pathway for ethyl chloride.

$$CH_3CH_2Cl \rightarrow C_2H_4 + HCl \qquad \text{----------2.16}$$

The product (ethylene) and the reactant (chloroethane) have been identified using Gas Chromatography (Model: Agilent 7890B with dual FIDs) equipped with an HP5 column installed for it. The corresponding concentration can be calculated using calibrations of a standard sample of ethyl chloride and ethylene in GC have been performed separately. The chromatograph is shown in Figure 2.24 identifying the species present in the post-shock mixture.

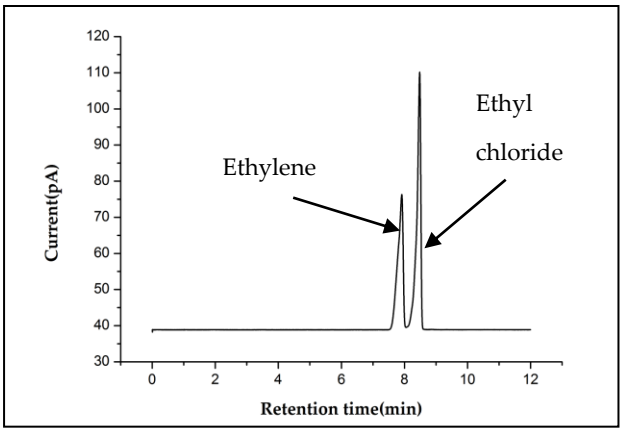

Figure 2.24. *Gas Chromatogram showing the separation of Ethyl Chloride and ethylene in GC during thermal decomposition of chloroethane at temperature ($T_{5\,(kin)}$) of 1054 K.*

The experimental temperature for the reaction can be calculated by using the experimental rate constant values in the Arrhenius equation reported for the

same reaction given by Tschuikow-Roux et al. for the temperature range of 960 – 1100 K. The effect of temperature on the HCl elimination product is summarized in Table 2. It has been observed that the rate of HCl elimination increases with increasing the temperature for the given temperature range.

$$k_{expt}\ (sec^{-1}) = 10\ 13.84 \pm 0.20 \exp\ [-(57.8 \pm 1.0\ kcal/mol) / RT] \qquad \text{-----2.17}$$

$$T_{expt} = (-57.8 \pm 1.0\ kcal/mol) / R \times ([2.303 \times (13.84 \pm 0.20)] - \ln k_{expt}) \qquad \text{------2.18}$$

The experimental $T_{5(kin)}$ are plotted against the $T_{5(Ms)}$ obtained with the incident shock Mach number using normal shock relation. The actual experimental temperature T_5 can be calculated using the least square fitting of the data shown in Figure 2.25. The correlation between $T_{5(kin)}$ and $T_{5(Ms)}$ within the experimental range of temperature is found to be:

$$T_{5(kin)} = [0.8102 \times T_{5(Ms)}] + 163.09 \qquad (R^2 = 0.9933) \qquad \text{------2.19}$$

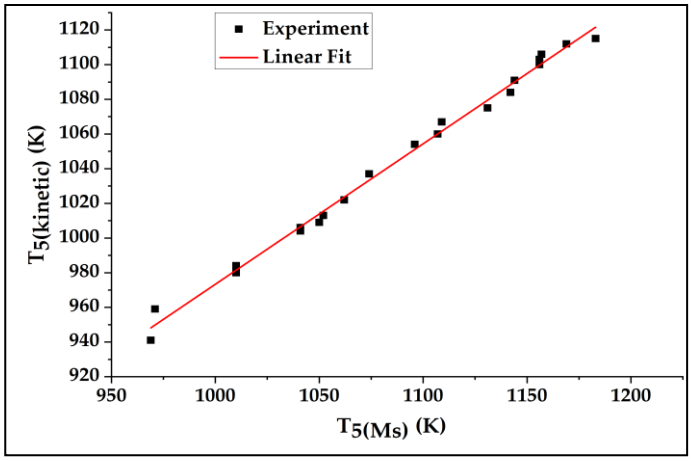

Figure 2.25. *The plot of Experimental $T_{5(kin)}$ Vs $T_{5(Ms)}$ (R-H) showing their correlation within the temperature range of 960-1190 K.*

Table 2.4: Summary of the experimental result on pyrolysis of chloroethane for T_5 calibration

Sr no.	Dwell time (μs)	$T_{5(Ms)}$ (K)	$T_{5(kin)}$ (K)	$[EtCl]_t/[EtCl]_0$	$[C_2H_4]_t/[EtCl]_0$	$P_{5(expt)}$ (atm)
1	1270	969	941.9	0.996865311	0.003134689	11.3
2	1230	971	959.7	0.994621491	0.005378509	10.4
3	1400	1010	980.2	0.98850034	0.01149966	11.7
4	1250	1010	984.9	0.98818795	0.01181205	9.9
5	1240	1041	1006.5	0.978031819	0.021968181	9.9
6	1320	1041	1004.2	0.978104057	0.021895943	11.3
7	1300	1050	1009.9	0.97464941	0.02535059	10.3
8	1390	1052	1013.4	0.970100471	0.029899529	10.5
9	1180	1062	1022.9	0.966932498	0.033067502	10.6
10	1240	1074	1037.4	0.948757104	0.051242896	13.2
11	1270	1096	1054.3	0.919070411	0.080929589	11.2
12	1330	1107	1060.2	0.901930458	0.098069542	9.8
13	1410	1109	1067.4	0.87656224	0.12343776	10.1
14	1380	1131	1075.6	0.853321406	0.146678594	10.6
15	1300	1142	1084.1	0.831352537	0.168647463	12.2
16	1290	1144	1091.3	0.80338808	0.19661192	13.3
17	1260	1156	1100.2	0.767111913	0.232888087	11.4
18	1330	1156	1103.5	0.738343289	0.261656711	11.3
19	1320	1157	1106.7	0.722683489	0.277316511	12.2
20	1350	1169	1112.1	0.685668071	0.314331929	10.9
21	1420	1183	1115.8	0.648798275	0.351201725	9.9

It has been observed from the above plot that the calculated temperature, $T_{5(Ms)}$, overestimates the actual temperature, $T_{5(kin)}$, and the difference increases with increasing the temperature. The reflected shock temperature, $T_{5(Ms)}$, calculated using the incident shock Mach number and that obtained from the measurement of the extent of ethyl chloride decomposition, $T_{5(kin)}$, is differed by ~ 2.8-6.0% in the calibrated range of temperature. This discrepancy observed in calculating temperature (between two temperatures) is due to non-idealities caused behind

reflected shock wave region which does not account for T_5 calculation using R-H relation.

2.14 THEORETICAL CALCULATION

Ab-initio calculations are important to locate the transition state as well as to obtain the corresponding potential energy surface involve in the decomposition of the molecule under investigation. Many methods are reported in the literature, each method has its merit and demerits. For the present investigation, calculations (including reactant, intermediates, and product) were performed at density functional level using the B3LYP method (Becke's Three Parameter Hybrid method with the LYP Correlation Functional of Lee, Yang, and Parr) with the 6-311+G(2d,p) basis set. Geometry optimization, calculated at this level of theory for obtaining the position of the nucleus of a given molecule at a minimum of the potential energy surface. The vibrational frequencies calculated using this level of theory have been used for the characterization of stationary points and moment of inertia computation. However, the transition state (saddle point) was confirmed by the presence of one negative eigenvalue in the hessian. The vibrational motion corresponding to the imaginary frequency is considered to be the reaction coordinate responsible for the conversion from reactant to transition state. Using the calculated vibrational frequencies for the reactant and the transition state, zero point correction to the barrier has been calculated. The vibrational frequencies are scaled by a factor of 0.9692 which are used to calculate TST rate parameters. Intrinsic reaction coordinate (IRC) calculation is performed to confirm the transition state that connects the reactant and product on the potential energy surface. The energetics along the reaction pathway is calculated using single point calculation at a higher level of theory performed at CCSD(T)/6-311+G(2d,p). All

the calculations were carried out using Gaussian 09 program [37]. The theoretical rate constant was calculate using the equation.

$$k = l\frac{k_B T}{h}\frac{Q_{\#}}{Q_R}\, exp\left[\frac{-E_0}{RT}\right] \qquad \ldots\ldots\ldots 2.20$$

Here $Q_{\#}$ and Q_R are the partition functions for transition state and reactant respectively. T represents the reflected shock temperature, E_0 is the zero-point barrier for the reaction, k_B and h are the Boltzmann and Planck constants, l is the reaction degeneracy factor. The activation energy (E_a) and pre-exponential factor were then estimated using the thermodynamic formulation of TST.

$$k = le\frac{k_B T}{h}\exp\left[\frac{\Delta S^{\#}}{R}\right] exp\left[\frac{-E_a}{RT}\right] \qquad \ldots\ldots\ldots\ldots 2.21$$

Here $\Delta S^{\#}$ is the entropy of activation calculated using the partition functions of reactant and transition state.

2.15 CONCLUSION

The shock tube is incorporated with an insert in the driver section to eliminate the non-ideal pressure rise behind the reflected shock wave region. Using Dumitescue's idea and methodology followed by Hanson, we have developed an algorithm to design the driver insert. Hence, with the proper design of an insert, it is possible to eliminate the non-ideal pressure rise and highly uniform pressure is achieved. An example of two different cases is presented here. In the first case, both the driver section and driven section remain at room temperature whereas in the other case, the temperature of the driven section is maintained at 353 K. Thereafter temperature (T_5) calibration study of a chemical shock tube (CST-3) was performed using ethyl chloride as an external standard.

2.16 REFERENCES

1. A. G. Gaydon and I. R. Hurle, The Shock Tube in High-Temperature Chemical Physics, 1963.
3. P. Vielle, C. R. Acad. Sci. Paris, 129, 1899, 1288.
3. S. Janardhanraj, Ph. D. Thesis, Investigation on Supersonic Flow in Miniature Shock Tubes, June 2015.
4. https://en.wikipedia.org/wiki/File:Supersonic_Bullet_Shadowgraph.jpg.
5. R. Backer, Zeitschrift für Physik , 8, 1922, 321-334.
6. R. L. Belford, and R. A. Strehlow, Annual Review of Physical Chemistry 20, 1969, 247-259.
7. A. Lifshitz, in Handbook of Shock Waves edited by A. Lifshitz, G. Ben-Dor, O. Igra, and T. Elperin, Academic Press, New York. 2001.
8. S. H. Bauer, Annual Review of Physical Chemistry, 16, 1965, 245-258.
9. Y. Hidaka, T. Higashihara, N. Ninomiya, H. Oshita, and H. Kawano, Journal of Physical Chemistry, 97, 1993, 10977-10984.
10. Y. Hidaka, T. Nakamura, H. Tanaka, A. Jinno, H. Kawano, and T. Higashihara, International Journal of Chemical Kinetics, 24, 1992, 761-777.
11. A. Lifshitz, M. Frenklach, and A. Burcat, Journal of Physical Chemistry, 80, 1976, 2437-2448.
12. M. B. Colket, and D. J. Seery, Proc. 25th Int. Symp. on Combustion, 1994, 883-896.
13. A. Laskin, and A. Lifshitz, Proceedings of 26th International Symposium on Combustion, 1997, 669-678.
14. A. Lifshitz, Y. Cohen, M. Braun-Unkhoff, and P. Frank, Proceedings of 26th International Symposium on Combustion, 1997, 659-667.

15. G. Porter, Proceedings of the Royal Society A (London) 200, 1950, 284-296.
16. M. I. Christie, R. G. W. Norrish, and G. Porter, Proceedings of the Royal Society A (London) 216, 1952, 152-164.
17. A. Declemy, and C. Rulliere, Review of Scientific Instrument, 57, 1986, 2733-2746.
18. G. Porter, Discussion on Faraday Society, 33, 1962, 198-209.
19. A. Lifshitz, S. H. Bauer, E. L. Resler, Journal of Chemical Physics, 38, 1963, 2056-2068.
20. E. Tschuikow-Roux, J. M. Simmie, and W. J. Quiring, Astonamica Acta 15, 1970, 511-527.
21. E. L. Petersen, and R. K. Hanson, Shock Waves 10, 2001, 405-420.
22. Z. Hong, G. A. Pang, S. S. Vasu, D. F. Davidson, and R. K. Hanson, Shock Waves 19, 2009, 113–123.
23. L. Z. Dumitrescu, Physics of Fluids 15, 1972, 207–209.
24. E. L. Resler, S. C. Lin, and A. Kantrowitz, Journal of Applied Physics, 23, 1952, 1390-1402.
25. R. A. Alpher, and D. R. White, Journal of Fluid Mechanics, 3, 1958, 457–470.
26. D. R. White, Journal of Fluid Mechanics 4, 1958, 585–599.
27. http://silver.neep.wisc.edu/~shock/tools/xt.html. Accessed August 2016.
28. W. Tsang, and A. Lifshitz, Annual Review of Physical Chemistry, 41, 1990, 559–599.
29. A. Lifshitz, C. Tamburu, A. Suslensky and F. Dubnikova, Journal of Physical Chemistry A, 110, 2006, 11677–11683.

30. A. Lifshitz, I. Shweky, J. H. Kiefer, and S. S. Sidhu, In Shock Waves, Proceedings of the 18th International Symposium on Shock Waves, Sendia, Japan (1991); K. Takayama Ed.; Springer-Verlag: Berlin, 1992, 825-829.

31. B. Rajakumar, K. P. J. Reddy and E. Arunan, Journal of Physical Chemistry A, 106, 2002, 8366–8373.

32. R. S. Tranter, R. Sivaramakrishnan, N. Srinivasan, and K. Brezinsky, International Journal of Chemical Kinetics, 33, 2001, 722–731.

33. I. Stranic, D. F. Davidson, and R. K. Hanson, Chemical Physics Letter, 584, 2013, 18-29.

34. A. Lifshitz, C. Tamburu, A. Suslensky and F. Dubnikova, Jornal of Physical Chemistry A, 110, 2006, 11677–11683.

34. W. Tsang, and A. Lifshitz, International Journal of Chemical Kinetics, 30, 1998, 621–628.

35. R. Sivaramakrishnan, R. S. Tranter, and K. Brezinsky, Journal of Physical Chemistry, 110, 2006, 9388–9399.

36. M. Akira, Y. Kenji, and S. Hiroumi, Journal of Physical Chemistry A, 118, 2014, 11688–11695.

37. Gaussian 09, Revision A.02, M. J. Frisch, G. W. Trucks, H. B. Schlegel, G. E. Scuseria, M. A. Robb, J. R. Cheeseman, G. Scalmani, V. Barone, B. Mennucci, G. A. Petersson, H. Nakatsuji, M. Caricato, X. Li, H. P. Hratchian, A. F. Izmaylov, J. Bloino, G. Zheng, J. L. Sonnenberg, M. Hada, M. Ehara, K. Toyota, R. Fukuda, J. Hasegawa, M. Ishida, T. Nakajima, Y. Honda, O. Kitao, H. Nakai, T. Vreven, J. A. Montgomery, Jr., J. E. Peralta, F. Ogliaro, M. Bearpark, J. J. Heyd, E. Brothers, K. N. Kudin, V. N. Staroverov, R. Kobayashi, J. Normand, K. Raghavachari, A. Rendell, J. C. Burant, S. S.

Iyengar, J. Tomasi, M. Cossi, N. Rega, J. M. Millam, M. Klene, J. E. Knox, J. B. Cross, V. Bakken, C. Adamo, J. Jaramillo, R. Gomperts, R. E. Stratmann, O. Yazyev, A. J. Austin, R. Cammi, C. Pomelli, J. W. Ochterski, R. L. Martin, K. Morokuma, V. G. Zakrzewski, G. A. Voth, P. Salvador, J. J. Dannenberg, S. Dapprich, A. D. Daniels, O. Farkas, J. B. Foresman, J. V. Ortiz, J. Cioslowski, and D. J. Fox, Gaussian, Inc., Wallingford CT, 2009.

3

PYROLYSIS OF DICYCLOPENTADIENE: EXPERIMENTAL, COMPUTATIONAL AND MODELING STUDIED

CHAPTER OVERVIEW

This chapter discusses experimental investigations on DCPD carried out in a modified shock tube. The shock tube has been incorporated with a driver insert to cancel out non-ideal pressure rise behind the reflected shock wave. The experiments were performed behind the reflected shock wave in the temperature range of 1250-1550 K and pressure range of 13-16 atm. Thereupon the kinetic modeling carried out to simulate the concentration of different observed products are enumerated.

3.1. INTRODUCTION

Understanding the combustion chemistry of the hydrocarbon fuel and the process of soot formation in the high-temperature gaseous environment is one of the growing areas of research and major work is being carried out to understand these processes. In particular, polycyclic aromatic hydrocarbon (PAHs) [1-3], which are considered combustion-generated pollutants and their role in the formation of soot is of greater interest due to its adverse effect on the environment. However, the process of formation of PAHs in the combustion process is initiated through many species as potential precursors such as methyl, propargyl, and cyclopentadienyl radical. Most importantly, the cyclopentadienyl radical (CPDyl) [4] which is formed in the high-temperature gaseous environment is considered to be one of the most abundant radicals present in the flame. It is of great interest due to its peculiar properties such as high reactivity and toxicity. It is considered to be a starting point of many reaction pathways leading to the formation of polycyclic aromatic hydrocarbons (PAHs) due to the presence of multiple reaction sites, the tendency to undergo self-recombination, etc. Qualitatively there is a large agreement that the chemistry of CPDyl radical plays a significant role in the formation of naphthalene and phenanthrene. The kinetics of the reaction between two CPDyl radicals has been the subject of several investigations since it was proposed by Melius et al. [5] that it can be one of the major production pathways for naphthalene. To study the importance of CPDyl moieties in PAH formation, Mulholland and co-workers [6] investigated CPDyl-PAH growth experimentally in a laminar flow reactor. The radical-molecule recombination reaction for PAH formation and high molecular mass compounds have been studied by Violi and co-workers [7]. They have explained the formation of PAH and higher molecular

mass compounds in the flame using a sequence of radical-molecule reactions between aromatic compounds with six π-electrons and compounds containing conjugated double bonds.

Previous studies of cyclopentadiene (CPD) decomposition by Burcat et al. [8] were performed in a single pulse shock tube for the temperature range 1080-1550 K, the observed products were acetylene, ethylene, methane, allene, propyne, butadiene, propylene, and benzene. Colket [9] performed a shock tube study on CPD pyrolysis and found for the reaction $c\text{-}C_5H_6 = H + c\text{-}C_5H_5$; $k = 2\times10^{15} \exp(-81000/RT)s^{-1}$ in the temperature range of 1100-2000 K and pressure range of 10-13 atm. Butler [10] and Bruisma [11] have carried out experiments in a flow reactor. According to Butler [10], CPDyl radical undergoes ring opening and follows a transition to straight chain aliphatic chemistry which is well inferred. Geem et al. [12] performed the CPD pyrolysis in a tubular continuous-flow reactor under high and low nitrogen dilution covering the temperature range 873 - 1123 K. Benzene, indene, methyl-indenes, and naphthalene were major products observed during CPD pyrolysis.

Kinetics of kerosene-based hydrocarbon fuel such as JP-10 ($C_{10}H_{16}$) [13-16] which is currently used as aviation fuel have been well established. Dicyclopentadiene ($C_{10}H_{12}$) which is a homodimer of the cyclopentadiene (C_5H_6) can be obtained by dehydrogenation of jet fuel (JP-10) by reaction 1.

$$C_{10}H_{16} \rightarrow C_{10}H_{12} + 2\,H_2 \qquad \text{.....(1)}$$

Over the past decades, dicyclopentadiene (DCPD), a homodimer of CPD, has been researched for many reasons in combustion for various purposes such as fuel, binder, etc. The binder performs a dual function of binding fuel and oxidizer as well imparting enough mechanical strength to the solid propellant grain. Presently

hydroxyl-terminated polybutadiene (HTPB) [17] is the most versatile binder used in the solid propellant due to its peculiar properties. HTPB is generally cured by diisocyanates (such as tolylene diisocyanate) to form a polyurethane network. However, this reaction is highly influenced by the presence of moisture which leads to degradation in the properties of the propellant. DCPD is also capable of forming a highly crossed-linked polymeric structural network through ring opening metathesis polymerization (ROMP) [18]. The ROMP reaction of DCPD is highly exothermic due to the release of strain energy through the opening of the norbornyl ring. Relevant thermodynamic properties of the HTPB and DCPD fuels are summarized in Table 3.1.

Table 3.1: Thermodynamic properties of HTPB and DCPD fuels.

Sr. no	Fuel	Density g/cc	Decomposition Temperature (K)	ΔH_f (kcal/mol)
1	HTPB	0.92	887	-5.1
2	DCPD	0.98	932	-50.6

In addition, DCPD has achieved considerable attention due to its peculiar properties with its application in industry. In particular, the ROMP of DCPD is of great importance due to its high polymerization rate, and its ability to impart thermal, chemical, and mechanical stability to its polymer through the ring opening mechanism of the norbornyl ring. The TCPD and higher oligocyclopentadiene [19] formed through successive Diel-Alder reactions, used in the preparation of optical-grade material due to their attractive properties such as low fluorescence, high transference. A polydicyclopentadiene (PDCPD) formed by polymerization of DCPD, a polymer is well known for its versatile use in the preparation of INPs, thermochromic composites, thick and thin film polymer-dispersed liquid crystal material, etc.

To our knowledge, there is no study available on the thermal decomposition of DCPD in the literature. We have performed the thermal decomposition of DCPD in a modified shock tube. A shock tube is incorporated with an insert in the driver section of the shock tube to cancel out the non-ideal rise in pressure behind the reflected shock wave region. DCPD pyrolysis has effectively become CPD pyrolysis for which prior results on experiment and computation are available. However, fewer studies are available on computational work for the formation of toluene, styrene, and phenylacetylene.

3.2 EXPERIMENTAL SECTION

A chemical shock tube-3 (CST3) which is operated in a single pulse shock tube (SPST) mode, is made up of high-purity stainless steel (SS-304 grade) and has an inner diameter of 54 mm, was used to carry out the thermal decomposition of DCPD. The detailed chemical shock tube (CST-3) is described in chapter 2. The driven section is coupled with a turbo molecular pump (Edward turbo-molecular pump TIC model) to achieve a high vacuum. By using a turbo molecular pump an ultimate pressure of 10^{-7} mbar can be achieved with an hour of pumping. The driver section is evacuated using a diffusion pump down to 10^{-5} mbar with an hour of pumping. Helium (purity 99.9996%) is used as a high-pressure driver gas whereas argon (purity 99.9993%) is used as a low-pressure driven gas. A shock wave is generated by the bursting of the metal diaphragm which separates the two sections. Theoretical reflected shock temperature (T_5) and pressure (P_5) were calculated from initial conditions (T_1, P_1, and M_s) using normal shock relation. The initial pressures in the driven section (generally termed as P_1) is measured using IRA pressure transducer (starting range 0 to 1 bar) whereas the pressure in the driver section (generally termed as P_4) is measured using a pressure transducer

which has a range of 0 to 60 bar. The incident shock speed is measured using three high-frequency piezoelectric pressure transducers (PCB) mounted over the last 0.9 meters of the shock tube, the last one 5 mm away from the end wall of the driven section. A Digital storage oscilloscope with 4 channels, 8-bit, Analog to Digital Converter (ADC) is used to record the PCB output voltage which is further converted into pressure using the sensitivity of the PCB sensor. A typical signal recorded using an oscilloscope is represented in Figure 3.1.

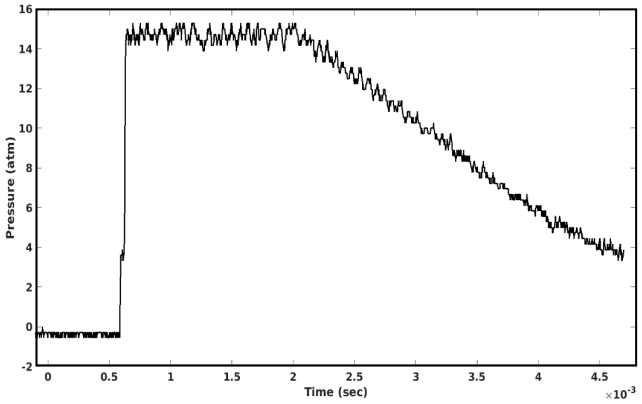

Figure 3.1. *A typical pressure trace recorded using an oscilloscope during the pyrolysis of DCPD at a temperature (T_5) of 1514 K.*

DCPD obtained from Sigma Aldrich which has a purity of greater than 99.0% was used to carry out the experimental investigation. Initial experiments showed that the sample when entrained to the test section of the shock tube, will get condensed on the wall and slowly vaporize after the passage of the incident shock wave. To eliminate the condensation problem the driven section is heated to the temperature of 353 K. A mixture of 0.35% DCPD was seeded with argon gas and premixed in a mixing tank (capacity of 9 Lt) which is also maintained at a temperature of 353 K and was fed into the evacuated test section of the shock tube and subjected to the reflected shock wave. A gas chromatograph (GC-7890 B Agilent) equipped with dual FID (flame ionization detector) was used to analyze

the post-shock mixture. The two capillary columns namely HP-5 (Cross-linked 5% PH siloxane, 30 m × 320 μm × 0.25 μm) and HP-PLOT-Q column (a bonded polystyrene-divinylbenzene, 30 m × 320 μm × 20 μm) have been used in qualitative and quantitative analysis of product molecules in GC. Nitrogen (purity 99.9996 %) has been used as carrier gas and its flow rate was maintained at 3.1 ml/min.

3.3 RESULT AND DISCUSSION

The thermal decomposition experiments on DCPD were carried out in a modified shock tube incorporated with a driver insert. The experimental investigation on DCPD was performed behind the reflected shock wave region in the temperature range 1200-1550 K, and pressure range of 13-26 atm. The observed reaction time in the present study was in the range of 1.430 - 1.890 ms. The experimental reflected shock temperature is computed by calibrating a chemical shock tube (CST3) using ethyl chloride as an external standard. The correlation used in the calculation of the reflected shock temperature is given by equation 3.1.

$$T_{5(kin)} = [0.8102 \times T_{5(Ms)}] + 163.09 \qquad (R^2 = 0.9933) \qquad \text{…….3.1}$$

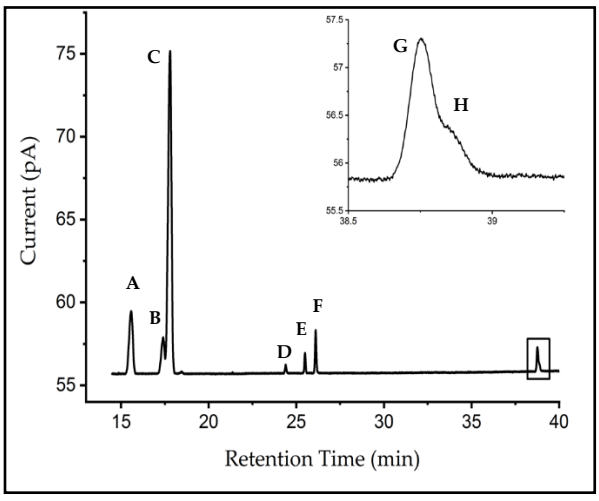

(1)

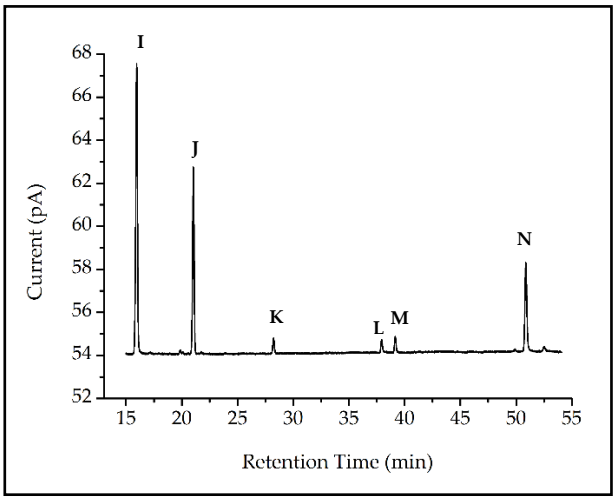

(2)

Figure 3.2. *A typical gas chromatogram obtained (1) from FID1 (2) from FID2 during pyrolysis of DCPD at a temperature of 1462 K. The different products observed are (A)Methane (B)Ethylene (C)Acetylene (D)Propylene (E)Allene (F)Propyne (G)1,3-Butadiene (H)Vinyl Acetylene (I)Cyclopentadiene (J)Benzene (K)Toluene (L)Styrene (M)Phenyl Acetylene and (N)DCPD.*

The major products observed during pyrolysis are methane, acetylene, cyclopentadiene, and benzene whereas the minor products include ethylene, propylene, propyne, allene, 1,3-butadiene, vinyl acetylene, toluene, styrene, and phenylacetylene. A typical gas-chromatogram obtained during pyrolysis of DCPD at a temperature of 1462 K is presented in Figure 3.2. As seen in the gas chromatogram some peaks overlap with others and are not resolved properly (see Figure 3.2(1)), we use the de-convolution procedure to resolve these peaks. The de-convolution is carried out using equation 3.2 to obtain the concentration of the product molecules corresponding to the peak.

$$y = y_0 + \frac{A}{w\sqrt{\frac{\pi}{2}}} e^{\frac{-2(x-x_c)^2}{w^2}} \qquad \ldots\ldots 3.2$$

Where y_o: the value of the baseline, x_c: x-ordinate of the center of the peak, A: peak area under the curve, and w: full width half maximum.

The peaks in the GC were identified and calibrated using a standard sample except for two; allene and cyclopentadiene. Standard samples for these could not be procured. Cyclopentadiene was identified using the mass spectrum. Since the post-shock mixture will be further diluted by helium (driver gas) one needs to find the amount of initial reactant concentration to which it is diluted.

To our observation, it has been found that the primary shock temperature (T_2) is enough for the decomposition of DCPD to CPD. This can be explained by calculating the equilibrium constant for reaction 2.

$$C_{10}H_{12} \rightarrow \text{cy-}C_5H_6 + \text{cy-}C_5H_6 \quad \ldots\ldots(2)$$

The equilibrium constant for the above reaction is calculated using the following expression given by

$$\Delta G^0 = -RT\ lnK \quad \ldots\ldots 3.3$$

Where K is the equilibrium constant for reaction 2. We have calculated the equilibrium constant in the temperature range 300-860 K and found that a very less amount of DCPD remains in this temperature range. For this temperature range equilibrium constant is varied from 10^{-07} to 10^{+04}.

Since we have observed the appearance of a DCPD peak in the gas-chromatogram, its presence in the post-shock mixture might arise due to desorption of the DCPD from the wall of the shock tube or recombination of two CPD monomer into DCPD. But in the case of the recombination of two CPDs to form DCPD will take hours which is not practical. So, the only source for the presence of DCPD in the post-shock mixture mainly arises due to desorption. Hence, it is difficult to find the initial concentration of the DCPD from the gas-chromatogram. To overcome this problem, we used the rate constant for the forward reaction of the decomposition of DCPD which is expressed using the following relation [19]:

$$k = 5.248 \times 10^{10} exp\left(\frac{-38479}{RT}\right) \ \text{sec}^{-1} \quad \ldots.3.4$$

Using the above rate expression, rate constants were calculated at different temperatures from the above relation as well as reaction conditions (T_5 and dwell time τ) and the concentrations of the products calculated from gas-chromatogram used to estimate the initial reactant concentration. However, it is important to ensure that all the reactants and products formed have been recovered. Hence the experimental conditions were chosen to minimize condensation of the reactant on

the wall. Equation 3.4 has been used to obtain the initial concentration of the reactant as the uniformity and the extent of initial reactant concentration dilution were not known accurately. For the temperature range 1281 K to 1532 K, the normalized mole fraction of DCPD ($[DCPD]_t/[DCPD]_0$) is varied from 2.98×10^{-10} to 8.76×10^{-141}.

As the DCPD is fully consumed during the reaction, the presence of the DCPD in the gas chromatogram is mainly due to its desorption from the wall of the shock tube. We consider the CPD concentration as the initial concentration for the decomposition of the DCPD behind the reflected shock region. We use the carbon balance method to calculate the initial CPD concentration. It is summarised in Table 3.2.

$$5 \times [CPD]_0 = 5 \times [CPD]_t + [methane]_t + 2 \times [ethene]_t + 2 \times [acetylene]_t + 3 \times [propylene]_t + 3 \times [allene]_t + 3 \times [propyne]_t + 4 \times [vinyl\ acetylene]_t + 4 \times [1,3\text{-}Butadiene]_t + 6 \times [benzene]_t + 7 \times [toluene]_t + 8 \times [styrene]_t + 8 \times [phenyl\ acetylene]_t$$

Table 3.2: Summary of the experimental conditions and normalized mole fraction of the observed products obtained in pyrolysis experiments of DCPD.

Sr no	Dwell Time	Temp T_5	Pressure P_5	$\frac{[CH_4]}{[CPD]_0}$	$\frac{[C_2H_4]}{[CPD]_0}$	$\frac{[C_2H_2]}{[CPD]_0}$	$\frac{[C_3H_6]}{[CPD]_0}$	$\frac{[C_3H_4(A)]}{[CPD]_0}$	$\frac{[C_3H_4(P)]}{[CPD]_0}$	$\frac{[C_4H_4]}{[CPD]_0}$
	µs	K	atm							
1	1530	1281	16.0	0.0254	0.0064	0.0277	0.0037	0.0028	0.0037	0.0014
2	1580	1294	13.9	0.0446	0.0103	0.0420	0.0051	0.0038	0.0051	0.0028
3	1550	1294	15.3	0.0372	0.0095	0.0406	0.0045	0.0033	0.0045	0.0026
4	1550	1308	15.0	0.0424	0.0126	0.0443	0.0058	0.0046	0.0058	0.0036
5	1520	1308	13.9	0.0708	0.0153	0.1283	0.0063	0.0071	0.0063	0.0040
6	1630	1336	13.8	0.0829	0.0193	0.1475	0.0067	0.0091	0.0067	0.0047
7	1680	1336	13.1	0.0889	0.0284	0.1250	0.0076	0.0086	0.0076	0.0051
8	1610	1336	13.8	0.0930	0.0253	0.1338	0.0072	0.0094	0.0072	0.0047
9	1560	1350	14.1	0.1030	0.0346	0.1490	0.0073	0.0109	0.0073	0.0064
10	1540	1365	14.3	0.1654	0.0455	0.2718	0.0081	0.0152	0.0081	0.0070
11	1610	1365	13.9	0.1708	0.0490	0.4342	0.0077	0.0131	0.0077	0.0070
12	1610	1366	14.3	0.1418	0.0440	0.2445	0.0081	0.0119	0.0081	0.0070

13	1730	1366	13.9	0.1690	0.0491	0.3539	0.0074	0.0125	0.0074	0.0074
14	1660	1380	14.1	0.1929	0.0576	0.3327	0.0086	0.0163	0.0086	0.0068
15	1600	1380	14.6	0.1951	0.0618	0.3506	0.0084	0.0162	0.0084	0.0070
16	1610	1396	15.5	0.1956	0.0576	0.5429	0.0074	0.0156	0.0074	0.0074
17	1610	1396	13.8	0.1795	0.0567	0.5449	0.0070	0.0173	0.0070	0.0077
18	1620	1396	14.2	0.2193	0.0646	0.5311	0.0085	0.0152	0.0085	0.0077
19	1600	1412	14.1	0.2334	0.0715	0.6343	0.0072	0.0156	0.0072	0.0076
20	1600	1412	14.3	0.2401	0.0738	0.6503	0.0071	0.0146	0.0071	0.0070
21	1800	1428	15.3	0.2623	0.0816	0.8443	0.0064	0.0131	0.0064	0.0066
22	1580	1445	15.1	0.2982	0.0893	0.9419	0.0046	0.0103	0.0046	0.0055
23	1810	1445	16.0	0.2936	0.0868	0.9610	0.0043	0.0103	0.0043	0.0056
24	1760	1461	19.7	0.3356	0.0955	0.8809	0.0030	0.0107	0.0030	0.0058
25	1800	1462	14.9	0.3086	0.0836	0.9955	0.0041	0.0097	0.0041	0.0055
26	1740	1479	16.6	0.2952	0.0801	1.0288	0.0029	0.0081	0.0029	0.0046
27	1810	1497	14.8	0.2439	0.0697	1.2112	0.0023	0.0074	0.0023	0.0040
28	1870	1514	23.1	0.2642	0.0637	1.3897	0.0023	0.0059	0.0023	0.0028
29	1890	1532	15.6	0.2502	0.0530	1.4729	0	0.0055	0	0.0023

Sr no	**Dwell Time**	**Temp T_5**	**Pressure P_5**	$\frac{[C_4H_6]}{[CPD]_0}$	$\frac{[CPD]_t}{[CPD]_0}$	$\frac{[C_6H_6]}{[CPD]_0}$	$\frac{[C_7H_8]}{[CPD]_0}$	$\frac{[C_8H_6]}{[CPD]_0}$	$\frac{[C_8H_8]}{[CPD]_0}$
	μs	K	atm						
1	1530	1281	16.0	0.0040	0.9527	0.0149	0	0	0
2	1580	1294	13.9	0.0057	0.9216	0.0220	0.0053	0	0.0035
3	1550	1294	15.3	0.0061	0.9317	0.0191	0.0043	0	0
4	1550	1308	15.0	0.0074	0.9103	0.0246	0.0071	0	0.0067
5	1520	1308	13.9	0.0091	0.8268	0.0524	0.0117	0	0.0065
6	1630	1336	13.8	0.0106	0.7762	0.0623	0.0159	0.0189	0.0095
7	1680	1336	13.1	0.0088	0.7606	0.0766	0.0208	0.0217	0.0082
8	1610	1336	13.8	0.0114	0.7685	0.0660	0.0173	0.0209	0.0106
9	1560	1350	14.1	0.0134	0.7166	0.0890	0.0227	0.0270	0.0088
10	1540	1365	14.3	0.0146	0.5758	0.1268	0.0317	0.0331	0.0176
11	1610	1365	13.9	0.0156	0.5173	0.1175	0.0278	0.0364	0.0211
12	1610	1366	14.3	0.0148	0.5933	0.1269	0.0323	0.0316	0.0238
13	1730	1366	13.9	0.0155	0.5349	0.1300	0.0270	0.0345	0.0252
14	1660	1380	14.1	0.0163	0.4823	0.1679	0.0334	0.0382	0.0195
15	1600	1380	14.6	0.0146	0.4752	0.1663	0.0322	0.0371	0.0217
16	1610	1396	15.5	0.0160	0.3975	0.1601	0.0330	0.0388	0.0304
17	1610	1396	13.8	0.0169	0.3970	0.1590	0.0325	0.0398	0.0349
18	1620	1396	14.2	0.0163	0.3895	0.1600	0.0349	0.0375	0.0364
19	1600	1412	14.1	0.0163	0.2986	0.1931	0.0340	0.0367	0.0435
20	1600	1412	14.3	0.0163	0.2875	0.1971	0.0358	0.0342	0.0422
21	1800	1428	15.3	0.0161	0.1806	0.2157	0.0317	0.0329	0.0504

22	1580	1445	15.1	0.0117	0.0958	0.2609	0.0304	0.0251	0.0510
23	1810	1445	16.0	0.0125	0.0947	0.2549	0.0308	0.0273	0.0513
24	1760	1461	19.7	0.0119	0.0883	0.2769	0.0285	0.0261	0.0551
25	1800	1462	14.9	0.0129	0.1079	0.2285	0.0280	0.0243	0.0599
26	1740	1479	16.6	0.0106	0.0819	0.2489	0.0244	0.0231	0.0644
27	1810	1497	14.8	0.0092	0.0626	0.2227	0.0176	0.0189	0.0685
28	1870	1514	23.1	0.0079	0.0338	0.2072	0.0130	0	0.0656
29	1890	1532	15.6	0.0065	0.0297	0.1898	0.0120	0	0.0697

Here, CH_4 – Methane, C_2H_2 – Acetylene, C_2H_4 – Ethylene, C_3H_6 – Propylene, C_3H_4(A) – Allene, C_3H_4(P) – Propyne, C_4H_4 – Vinyl Acetylene, C_4H_6 – 1,3-Butadiene, CPD – Cyclopentadiene, C_6H_6 – Benzene, C_7H_8 – Toluene, C_8H_8 – Styrene, C_8H_6 – Phenylacetylene.

3.4 THEORETICAL OBSERVATIONS

Ab-initio theoretical calculations were performed to find out the minimum energy pathway that could lead to the formation of observed experimental products. Transition states were optimized to find the energy barrier involved in the reaction. The theoretical rate constant was calculated using equation 3.5.

$$k = l\frac{k_B T}{h} \times \frac{Q_{\#}}{Q_R} exp\left[\frac{-E_a}{RT}\right] \qquad \text{…….3.5}$$

Here, $Q_{\#}$ and Q_R correspond to partition functions for the reactant and activated complex, respectively. T represents the reflected shock temperature, E_a is the activation energy, k_B and h are the Boltzmann and Planck constants, l is the reaction degeneracy factor. Partition functions were calculated using the vibrational frequencies (scaled by a factor 0.9692) and rotational constants at the B3LYP/6-311+G(2d,p) level of theory.

The following section describes the details decomposition pathway of DCPD. The primary decomposition pathway involves the decomposition of

DCPD to form cyclopentadiene (CPD). The secondary channel consists of the CPD decomposition followed by recombination reaction which leads to different products will also be discussed.

The geometries and frequencies of the reactant, transition states, and products in the system were performed at the density functional level using the B3LYP method (Becke's Three Parameter Hybrid method with the LYP Correlation Functional of Lee, Yang, and Parr) with the 6-311+G(2d,p) basis set. The vibrational frequencies computed at this level of theory have been used for the characterization of stationary points, zero-point energy, and moment of inertia calculations. The vibrational frequencies are scaled by a factor of 0.9692 which are used to calculate TST rate parameters. The frequency calculation also allows the zero-point energy (ZPE) correction to be obtained. Transition states (TS) geometries are identified by the presence of only one imaginary frequency in the normal mode analysis. In the transition structure geometry, the movement of atoms in the imaginary frequency mode can be displayed to see if the atoms are moving in the right direction towards reactant and product. Moreover, IRC (Intrinsic Reaction Coordinate) calculations were carried out to confirm that the transition state was found to connect the reactant and product of the reaction step. All the calculations were done using the Gaussian 09 program [39].

3.5 DCPD DECOMPOSITION PATHWAYS

3.5.1 REACTION PATHWAYS FOR THE DCPD DECOMPOSITION (DCPD → CPD)

The experimental observation showed that at lower temperatures CPD is the predominant product formed during the thermal decomposition of DCPD. The formation of the CPD at low temperature indicates that DCPD easily undergoes

C-C bond cleavage between the bridge carbon atoms representing the primary decomposition channel. Hence the primary decomposition channel consists of the dissociation of DCPD into two monomer cyclopentadiene (CPD). It is represented by the reaction (R2). The reverse reaction is similar to Diel-Alder's reaction, a reaction between a conjugated diene and a substituted alkene commonly termed the dienophile. The potential energy surface for the DCPD decomposition leading to CPD is represented in the following Figure 3.3 [52]. The energy barrier for the DCPD decomposition to CPD is found to be 40.2 kcal/mol. The details about the reaction pathway for DCPD decomposition to cyclopentadiene are discussed in *Chapter 4*.

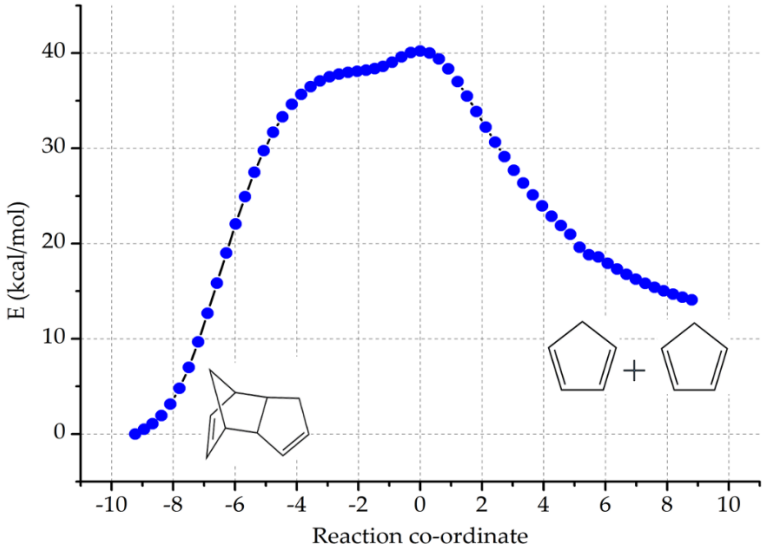

Figure 3.3. *Potential energy diagram for the DCPD decomposition to cyclopentadiene.*

3.5.2 REACTION PATHWAYS FOR CYCLOPENTADIENE DECOMPOSITION ($CY\text{-}C_5H_6 \rightarrow C_3H_4(P) + C_2H_2$)

The potential energy surface of cyclopentadiene and its decomposition products (i.e acetylene and propyne) is characterized using the ab-initio quantum mechanical approach shown in Figure 3.4 [21]. The decomposition pathway for cyclopentadiene is analogous to the decomposition reaction of pyrrole which leads

to the formation of propyne and HCN [21]. The reaction pathway for cyclopentadiene decomposition proceeds via the formation of cyclic carbene intermediate I1 by 1,5-sigmatropic shift. The energy barrier for this conversion is found to be 70.8 kcal/mol and the stability of I1 relative to the parent cyclopentadiene molecule is 60.0 kcal/mol. However, the next two saddle points (TS2 and TS3) are substantially higher at 82.2 and 101.3 kcal/mol respectively. Thus, the third barrier associated with the sigmatropic shift (TS3) will limit the overall reaction rate. The value of angle <H11C4C2 is 126.3^0 to 54.1^0 for the CPD and TS1 respectively. The value of the same at I1 is 29.4^0. The allenic intermediate I2 is significantly more stable relative to intermediate I1 by 31.2 kcal/mol. The C1-C2 bond length varies from 1.543 A^0 to 2.031 A^0 while going from I1 to TS2. The value of the same at I2 is 3.921 A^0. The C3-C5 bond length varies from 1.478 A^0 to 2.012 A^0 while going from I2 to TS3.

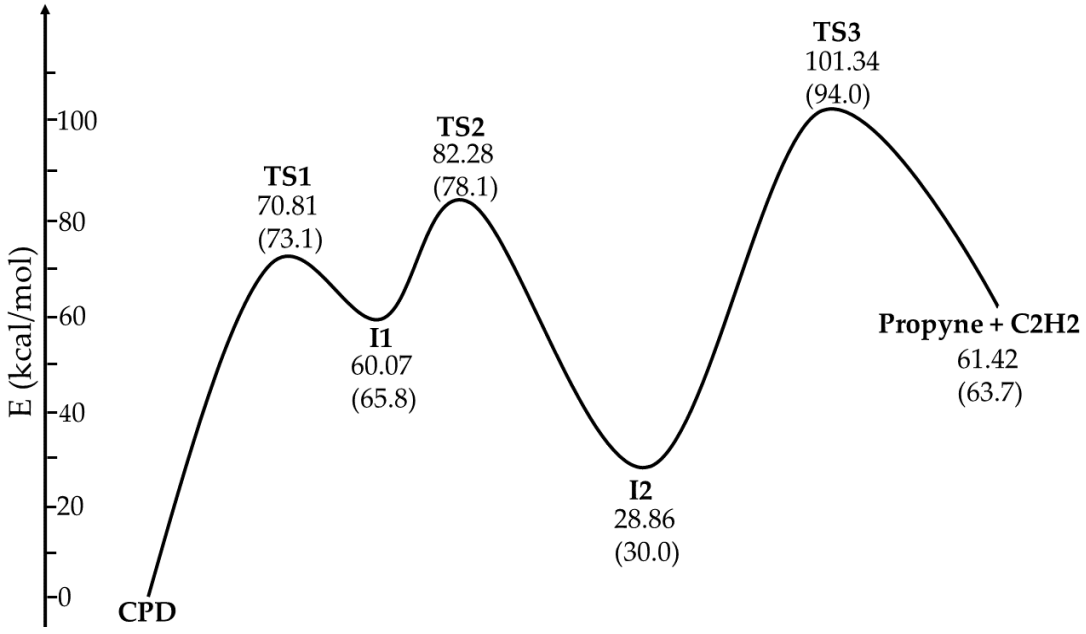

Figure 3.4. *Potential energy diagram for the cy-C_5H_6 decomposition reaction ZPE corrected energies (in kcal/mol) are given as calculated at the CCSD(T)/ 6-311+G(2d,p) level. The numbers in parenthesis are taken from the study by Mackie et al [21].*

The structures for reactant, intermediate, and product involved in the decomposition are given below:

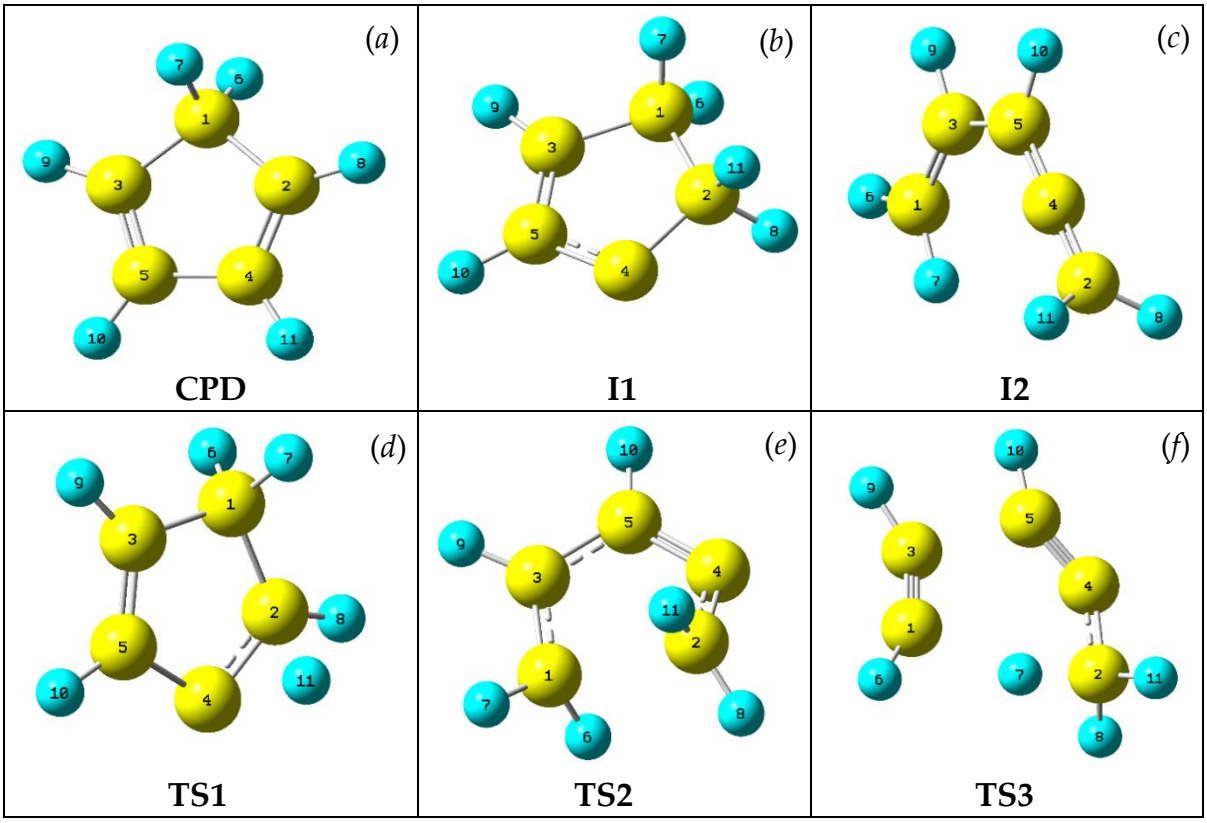

Figure 3.5. *Structures of (a)CPD (b)I1 (c)I2 (d)TS1 (e)TS2 and (f)TS3 optimised at B3LYP/6-311+G(2d,p) level of theory.*

3.5.3 REACTION PATHWAYS FOR CYCLOPENTADIENYL DECOMPOSITION (CY-C_5H_6 → C_3H_3 + C_2H_2)

The reaction path for the decomposition of cyclopentadienyl radical to acetylene and propargyl radicals was produced by optimization of structural parameters for the reactant, products, transition states, and intermediates. The dissociation of the cyclopentadienyl radical to acetylene and propargyl radical occurs in a multiple-step as shown in Figure 3.5. The first step of the dissociation involves the 1,2- hydrogen atom shift forming 1,3-cyclopentadienyl radical, which is termed as 2a. The energy barrier for this conversion is found to be 62.0 kcal/mol

at the CCSD (T)/aug-cc-pVDZ level. The value of angle <H8C3C1 is varying from 126.2^0 to 55.7^0 while going from 1a to TS1. The value of the same at 2a is 27.4^0. Intermediate 2a which undergoes ring opening to form acyclic intermediates depends on which bond of 2a is being broken, leading to the formation of either 1,3,4-pentatrienyl radical referred as 3a, or 1-pentene-4-ynyl radical referred to as 6a. At this point reaction path is split into two, which eventually leads to C_3H_3 + C_2H_2. The detailed discussion presenting the two pathways is labeled as (1) and (2).

In pathway (1), the formation of 6a results from the cleavage of the C4-C5 bond. The same can be formed by the addition of acetylene to the CH_2 site of propargyl. This reaction has an energy barrier of 43.1 kcal/mol. The transition structure for this conversion is referred to as TS6. The value of the C4-C5 bond length varies from 1.482 A^0 to 2.344 A^0 while going from 2a to TS6. The value of the same at 6a is 3.712 A^0. The intermediate 6a undergoes C1-C2 bond cleavage leading to the formation of C_3H_3 and acetylene. The energy barrier for this conversion is found to be 29.4 kcal/mol. The value for the C1-C2 bond length at 6a and TS7 is 1.512 A^0 and 2.172 A^0 respectively.

In pathway (2), the formation of 3a (similar to the addition of acetylene to the CH site of propargyl) results from the cleavage of the C1-C2 bond which undergoes subsequent isomerization leading to 4a via 3a. The energy barrier for the conversion of 3a to 4a is found to be 42.9 kcal/mol. The transition state TS5 exhibits free rotation about the forming C-C bond; we assume that 4a and 5a can be directly formed. The analysis shows that the three diastereomers namely 3a, 4a, and 5a have approximately the same energies, and the energy barrier for internal

rotation or *cis-trans* isomerization are of the order 2 kcal/mol at the CCSD (T)/aug-cc-pVDZ level of theory.

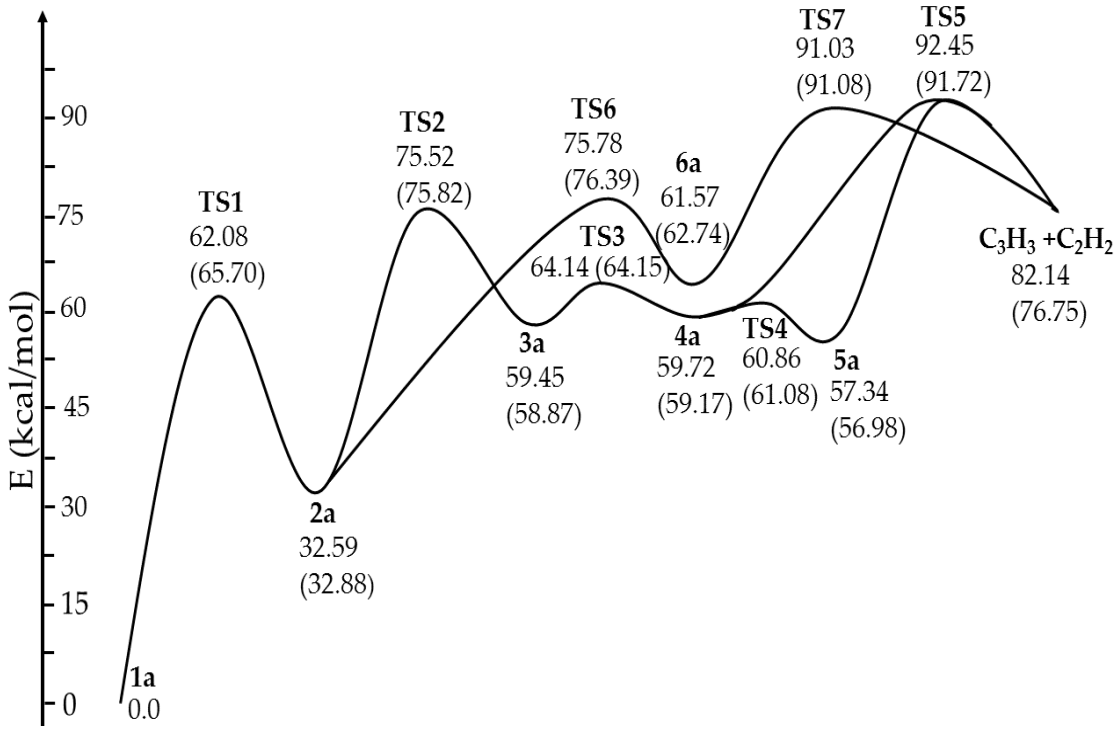

Figure 3.6. *Potential energy diagram for the cy-C_5H_5 radical decomposition reaction ZPE corrected energies (in kcal/mol) are given as calculated at the CCSD (T)/aug-cc-pVDZ level. The number in parenthesis is taken from the study by Lin et al [22].*

The structures for reactant, intermediate, and product involved in the decomposition are given below:

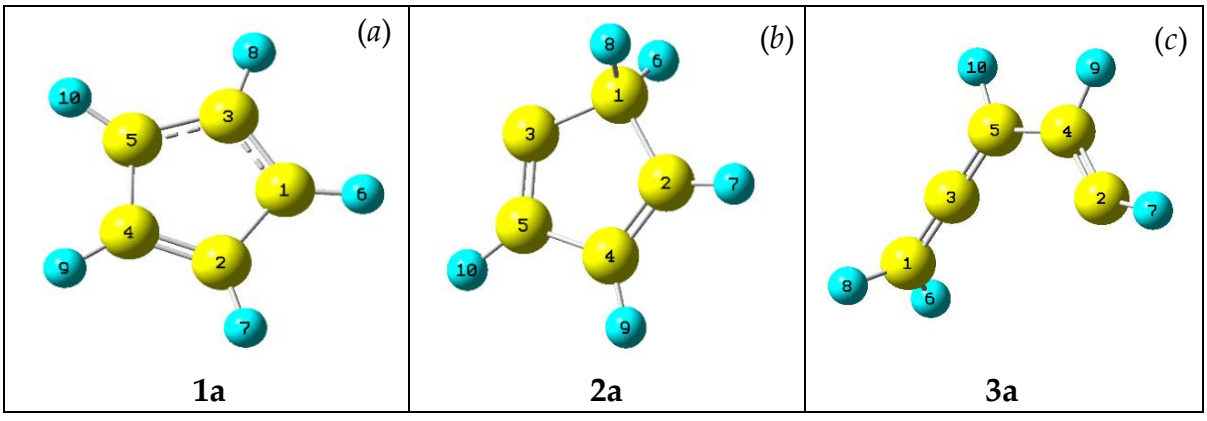

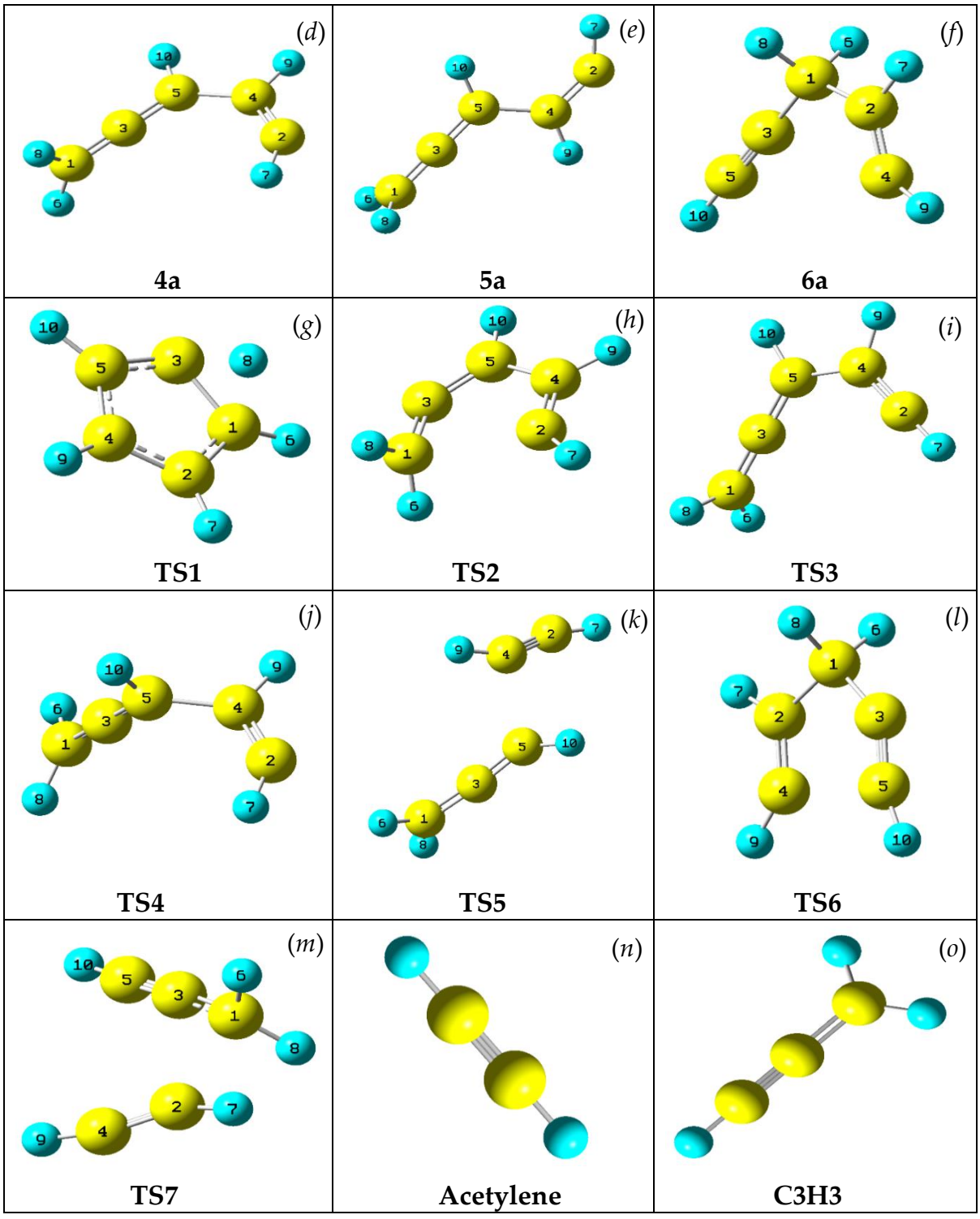

Figure 3.7. *Structures of (a)1a (b)2a (c)3a (d)4a (e)5a (f)6a (g)TS1 (h)TS2 (i)TS3 (j)TS4 (k)TS5 (l)TS6 (m)TS7 (n)Acetylene and (o)C3H3 optimised at B3LYP/6-311+G(2d,p) level of theory.*

3.5.4 REACTION PATHWAY FOR BENZENE FORMATION CY-C_5H_5 + CY-C_5H_6 → C_6H_6 + C_4H_4

The reaction pathways for the formation of benzene by the addition of CPDyl radical to CPD are well established in the study by Violi et al. [7] using B3LYP/6-31G(d,p) level calculations. To compare the feasibility of the different reaction pathways, in addition to the reaction pathway reported by Violi et al. [7] we have investigated the pathway for benzene formation. Figure 3.6 reports the various steps for the pathways which eventually lead to benzene. The corresponding potential energy surface diagram for the formation of benzene is shown in Figure 3.7. The addition of CPDyl radical to Π-bond of CPD leads to the formation of bridged intermediate I. The dihedral angle between H12C7C6H11 was found to be 64.5^0 whereas the dihedral angle between H17C3C2H19 was found to be 117.5^0. The molecule-radical dimer I undergo β-scission of the C-C bond. The value of the C2-C3 bond length varies from 1.564 A^0 to 2.262 A^0 while going from I to TS1d. The intermediate I undergoes the opening of one of the five-membered rings to form the intermediate 1d. The energy barrier for this conversion is found to be 44.4 kcal/mol. The intermediate 1d undergo ring expansion to a six-membered ring via 2d which is a three-membered ring closure. The value of the bond angle <C10C2C6 at TS2d and 2d is found to be 116.0^0 and 57.9^0 respectively. The energy barrier for the conversion of 1d → 2d and 2d → 3d is found to be 18.7 and 19.1 kcal/mol respectively. The six-membered ring intermediate 3d undergoes C-C bond β-scission leading to the formation of benzene and butadienyl radical. The barrier for this conversion is found to be 30.3 kcal/mol. The value of the C1-C2 bond length varies from 1.523 A^0 to 2.192 A^0 while going from 3d to TS3d.

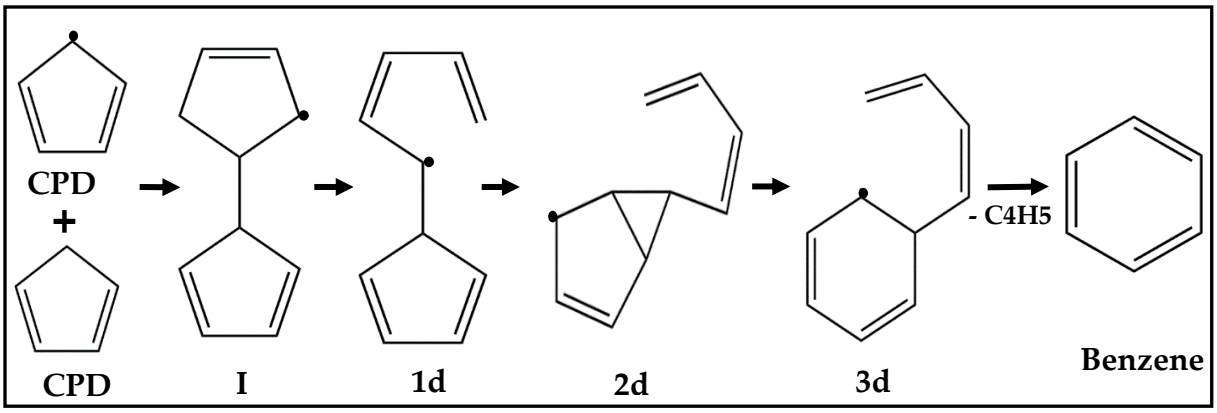

Figure 3.8. *C-C bond β-scission pathway to Benzene formation.*

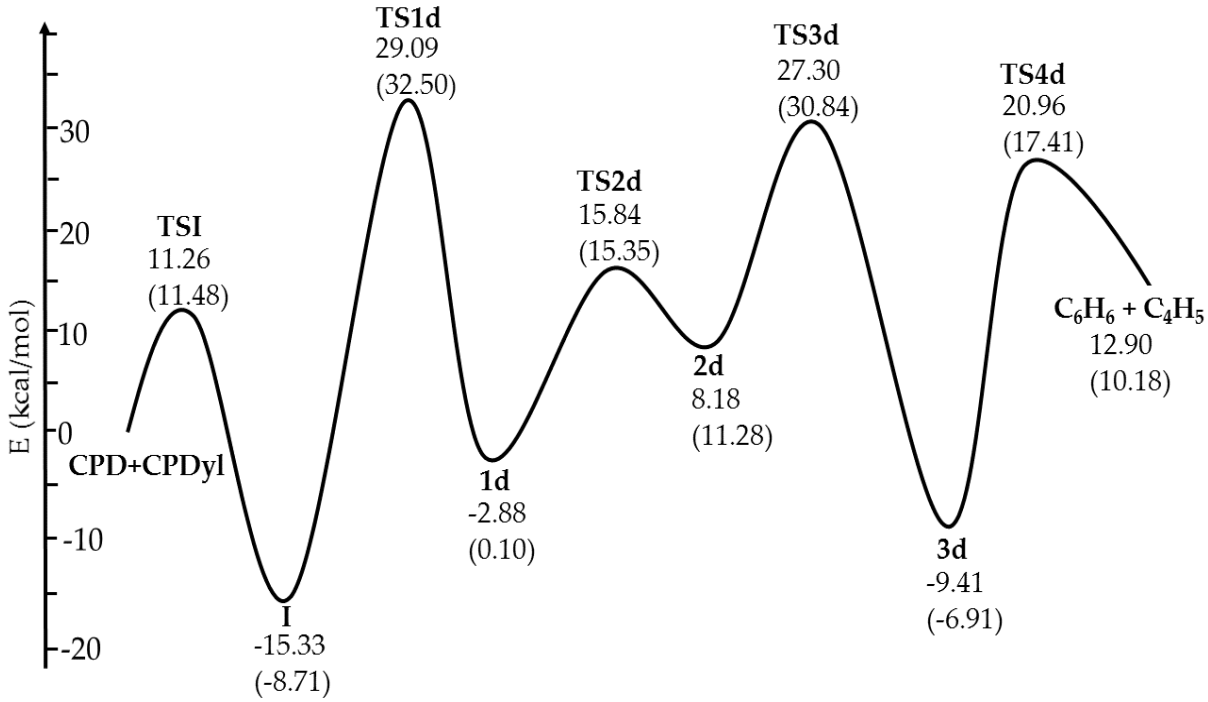

Figure 3.9. *Potential energy diagram for the formation of Benzene. The ZPE corrected energies (in kcal/mol) are given as calculated at the CCSD (T)/aug-cc-pVDZ level. The number in parenthesis is taken from the study by Violi et al [7].*

The structures for reactant, intermediate, and product involved in the decomposition are given below:

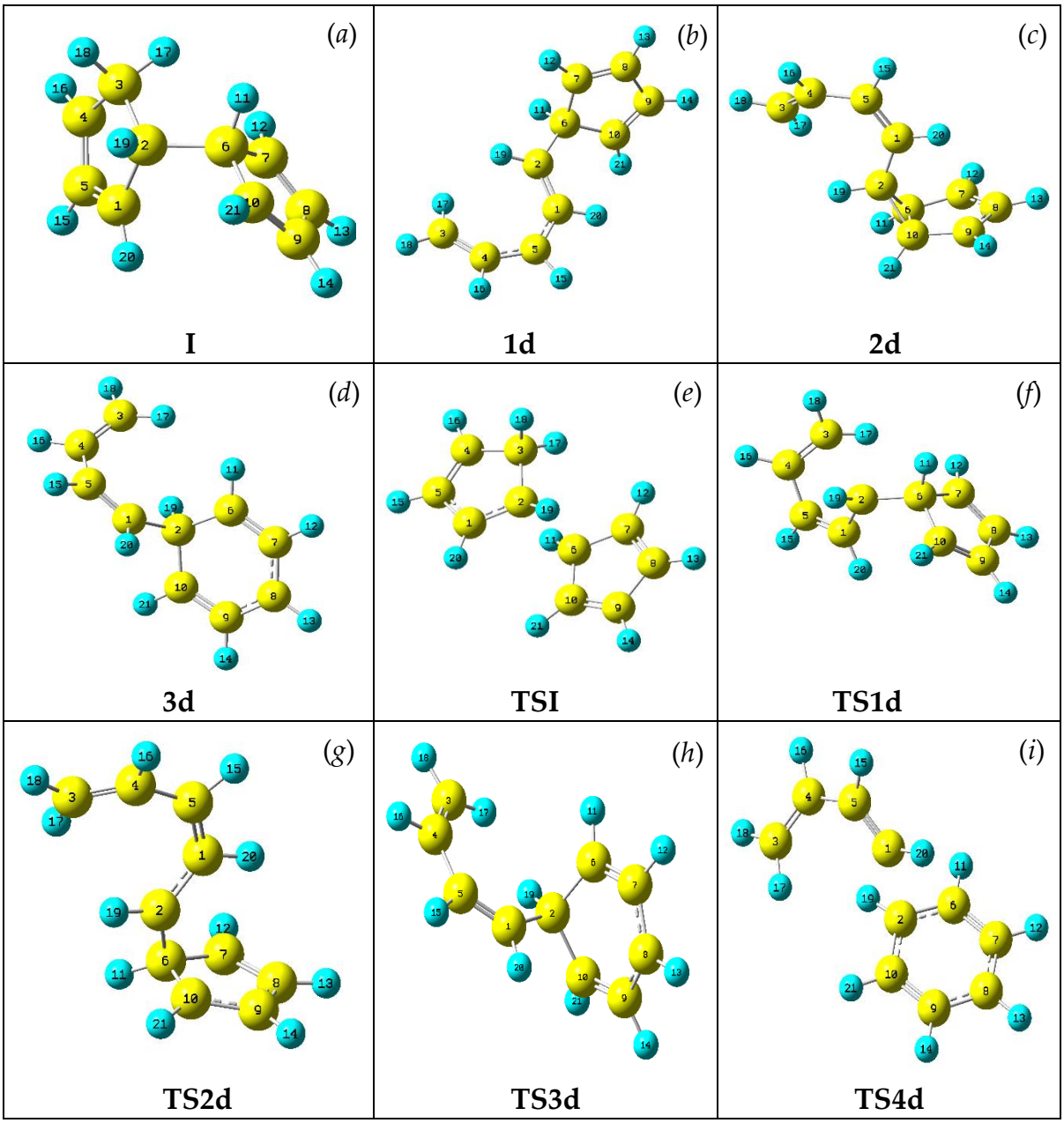

Figure 3.10. *Structures of (a)I (b)1d (c)2d (d)3d (e)TSI (f)TS1d (g)TS2d (h)TS3d and (i)TS4d optimised at B3LYP/6-311+G(2d,p) level of theory.*

3.5.5 REACTION PATHWAY FOR TOLUENE FORMATION (CY-C_5H_6 + C_2H_3 → C_7H_8 + H)

The various steps for the pathways which eventually lead to toluene are depicted in Figure 3.8. The corresponding potential energy surface diagram for the

formation of toluene is shown in Figure 3.9. The reaction begins with the addition of C_2H_3 radical to the CPD ring leading to the formation of intermediate 1f. The energy barrier for this conversion is found to be 6.4 kcal/mol. The value of the C7-C8 bond length varies from 1.503 A^0 to 2.332 A^0 while going from TS1 to 1f. The intermediate 1f undergoes ring expansion via 2f through a three-membered cyclic ring structure. The energy barrier for the conversion 1f → 2f is found to be 16.0 kcal/mol. The value of the bond angle <C1C7C8 at TS2 and 2f is found to be 78.6^0 and 59.2^0 respectively. The cyclic structure 2f undergoes H-transfer from C8 to C9 which leads to the formation of the intermediate 3f. The energy barrier for this conversion 2f → 3f is 51.9 kcal/mol. The ring-opening of 3f forms the intermediate 4f. The value of the bond angle <C1C7C8 at TS4 is found to be 87.7^0. The energy barrier for this conversion 3f → 4f is 14.5 kcal/mol. The intermediate 4f leads to the formation of toluene by removal of H. The energy barrier for this conversion is found to be 30.8 kcal/mol. The value of C2-H14 bond length varies from 1.102 A^0 to 1.873 A^0 while going from 4f to TS5.

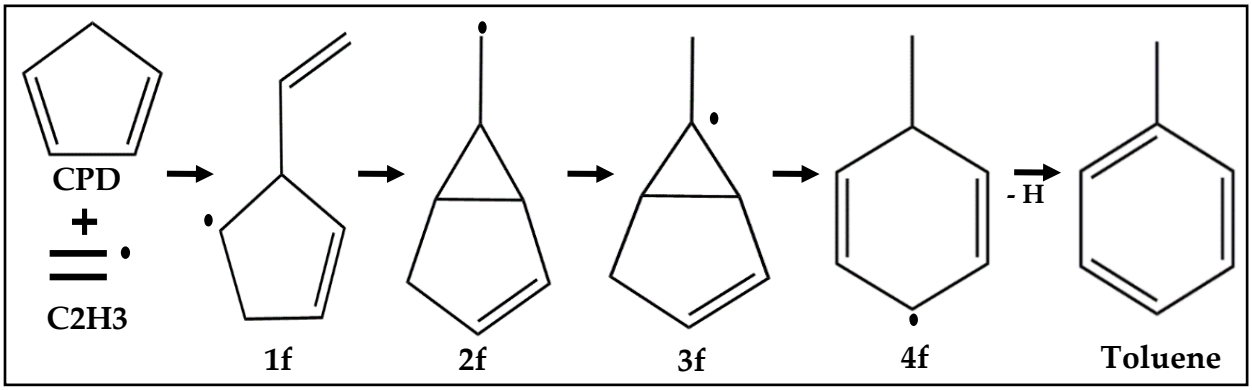

Figure 3.11. *Intramolecular addition pathway to Toluene formation.*

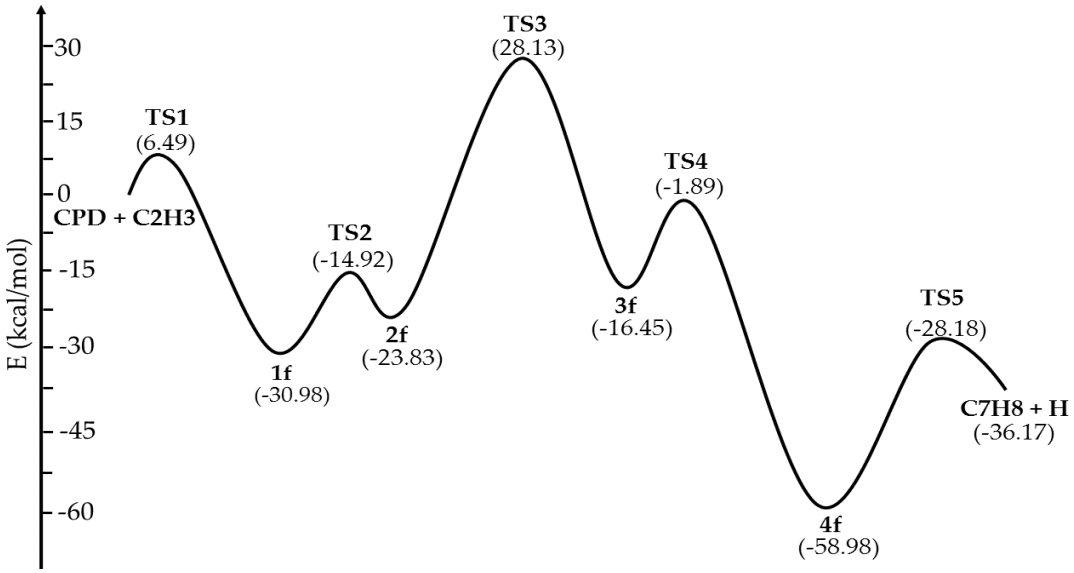

Figure 3.12. *Potential energy diagram for the formation of Toluene. ZPE corrected energies (in kcal/mol) are given as calculated at the CCSD (T)/aug-cc-pVDZ level.*

The structures for reactant, intermediate, and product involved in the decomposition are given below:

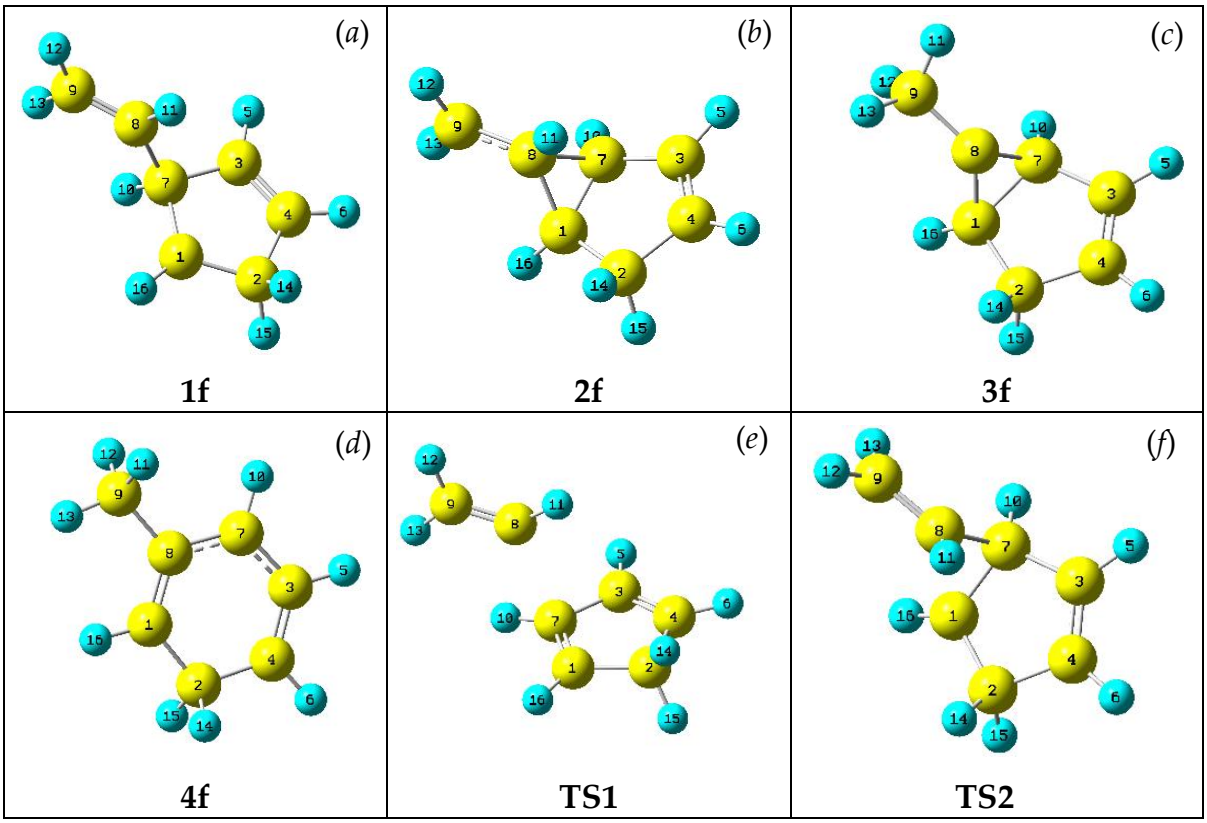

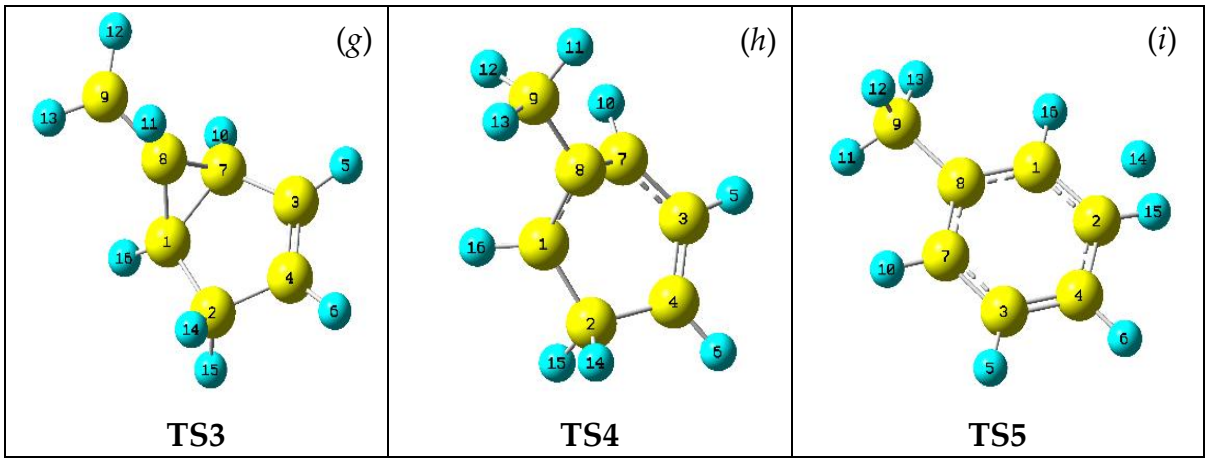

Figure 3.13 *Structures of (a)1f (b)2f (c)3f (d)4f (e)TS1 (f)TS2 (g)TS3 (h)TS4 and (i)TS5 optimised at B3LYP/6-311+G(2d,p) level of theory.*

3.5.6 REACTION PATHWAY FOR STYRENE FORMATION (CY-C_5H_5 + C_3H_5 → C_8H_8 + H + H)

The different steps involved in the formation of styrene are depicted in Figure 3.10. The corresponding potential energy surface diagram for the formation of styrene is shown in Figure 3.11. The reaction begins with the combination of C_3H_5 radical to CPDyl leading to the formation of the intermediate 1g. The H-atom abstraction from the intermediate 1g leading to the formation of intermediate 2g. The energy barrier for the conversion 1g → 2g is found to be 7.6 kcal/mol. The value of the C10-H18 bond length varies from 1.095 A^0 to 1.215 A^0 while going from 1g to TS1. The intermediate 2g undergo ring expansion via 3g through a three-membered cyclic ring structure. The value of the bond angle <C2C1C10 at TS2 and 3g is found to be 77.9^0 and 60.8^0 respectively. The energy barrier for the conversion 2g → 3g is found to be 16.0 kcal/mol. The intermediate 4g is formed by a ring opening of 3g. The energy barrier for this conversion 3g → 4g is found to be 19.7 kcal/mol. The intermediate 4g leads to the formation of styrene by removal of H. The energy barrier for this conversion is found to be 27.7 kcal/mol. The value of

the C10-H11 bond length varies from 1.107 A^0 to 1.798 A^0 while going from 4g to TS4.

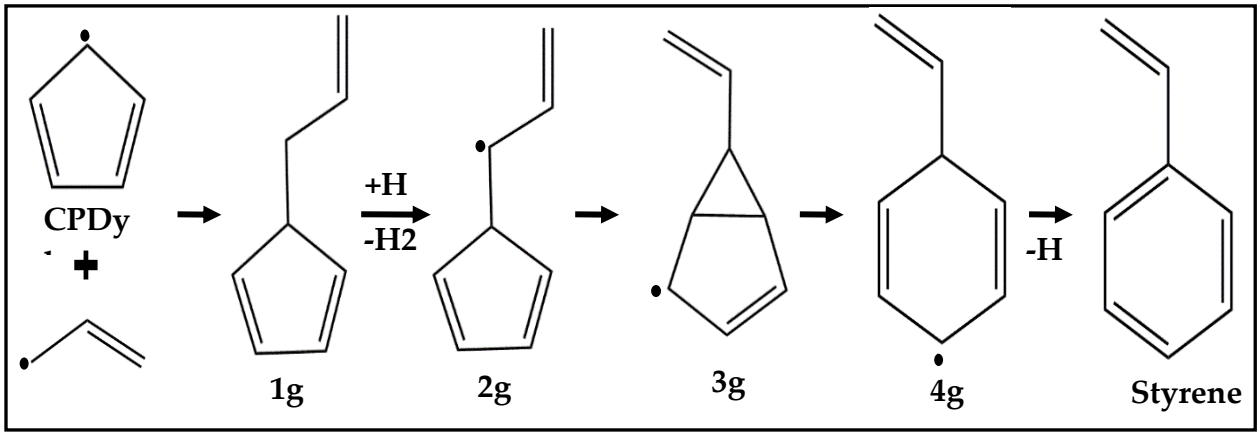

Figure 3.14. *Intramolecular addition pathway to Styrene formation.*

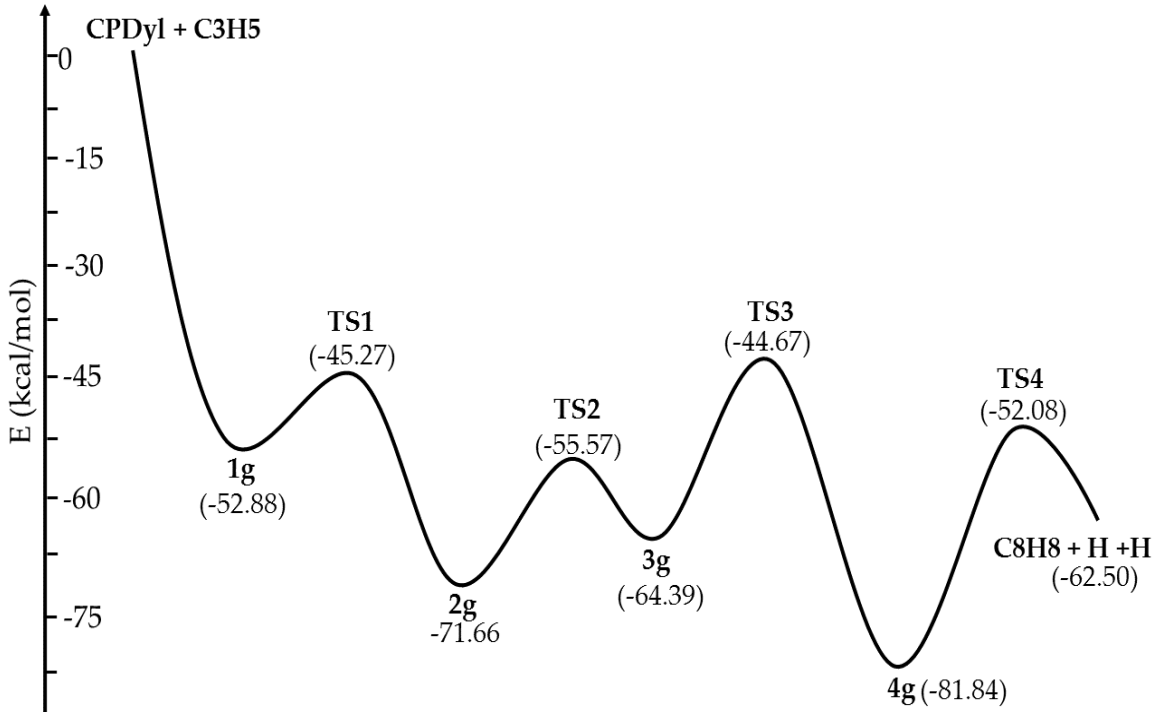

Figure 3.15. *Potential energy diagram for the formation of the Styrene. ZPE corrected energies (in kcal/mol) are given as calculated at the CCSD (T)/aug-cc-pVDZ level.*

The structures for reactant, intermediate, and product involved in the decomposition are given below:

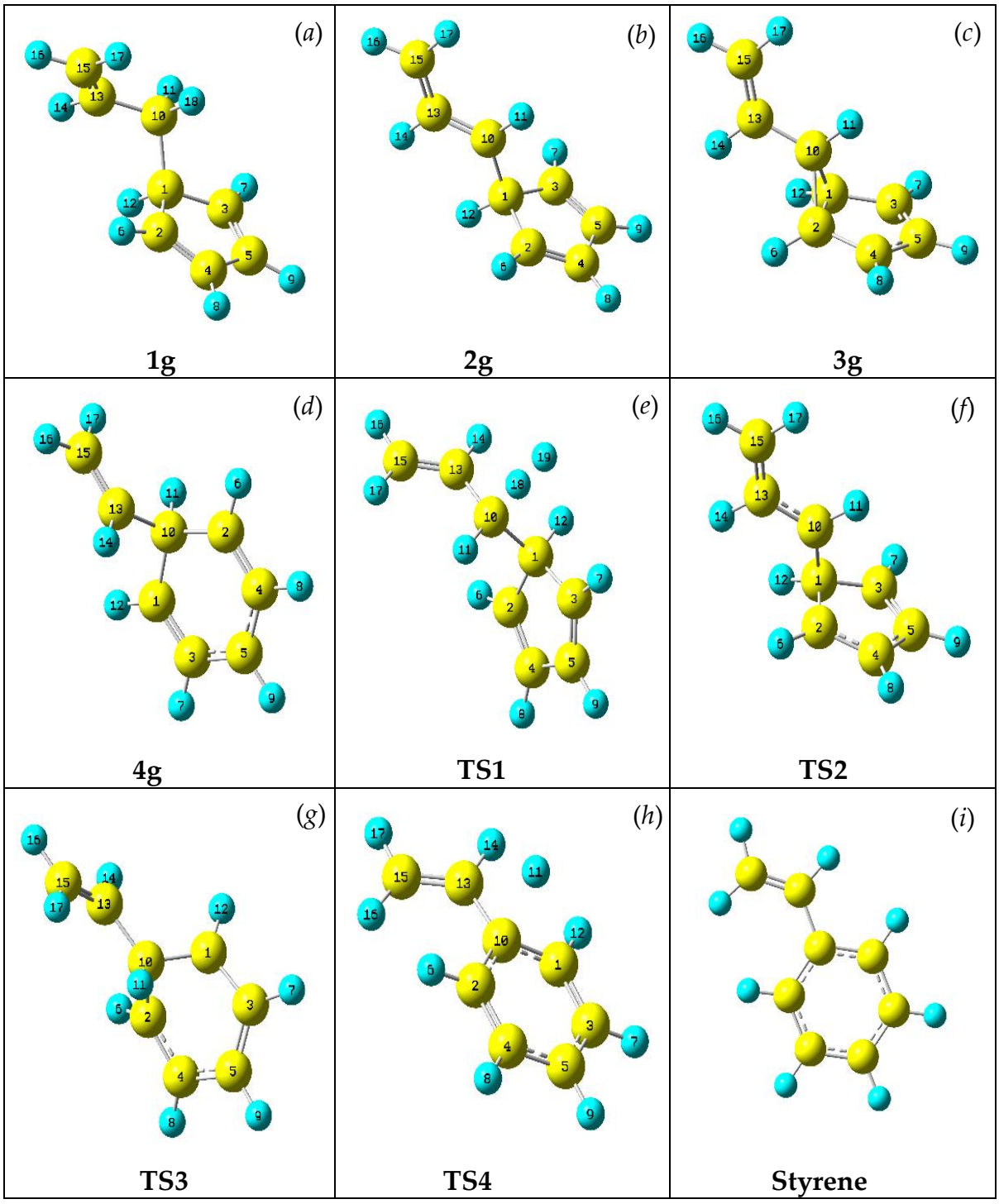

Figure 3.16. *Structures of (a)1g (b)2g (c)3g (d)4g (e)TS1 (f)TS2 (g)TS3 (h)TS4 and (i)Styrene optimised at B3LYP/6-311+G(2d,p) level of theory.*

3.5.7 REACTION PATHWAY FOR PHENYLACETYLENE FORMATION (CY-C_5H_5 + C_3H_3 → C_8H_6 + H + H)

The various steps for the pathways which eventually lead to phenyl acetylene are depicted in Figure 3.12. The corresponding potential energy surface diagram for the formation of phenylacetylene is shown in Figure 3.13. The reaction begins with the combination of C_3H_3 radical to CPDyl leading to the formation of the intermediate 1m. The H-atom abstraction from the intermediate 1m leads to the formation of intermediate 2m. The energy barrier for the conversion 1m → 2m is found to be 7.5 kcal/mol. The value of C11-H16 bond length varies from 1.091 A^0 to 1.243 A^0 while going from 1m to TS1. The intermediate 2m undergoes ring expansion via 3m through a three-membered cyclic ring structure. The value of the bond angles <C3C1C11 at TS2 and 3m are found to be 79.0^0 and 60.8^0 respectively. The energy barrier for the conversion 2m → 3m is found to be 13.3 kcal/mol. The intermediate 4m is formed by a ring-opening of 3m. The energy barrier for this conversion 3m → 4m is found to be 20.3 kcal/mol. The intermediate 4m leads to the formation of phenylacetylene by the removal of H. The energy barrier for this conversion is found to be 29.2 kcal/mol. The value of C11-H15 bond length varies from 1.106 A^0 to 1.771 A^0 while going from 4m to TS4.

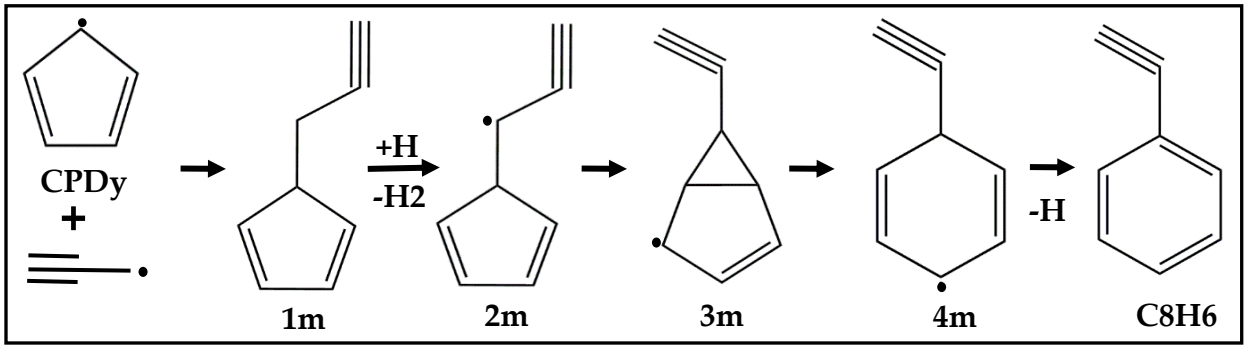

Figure 3.17. *Intramolecular addition pathway to Phenyl Acetylene formation.*

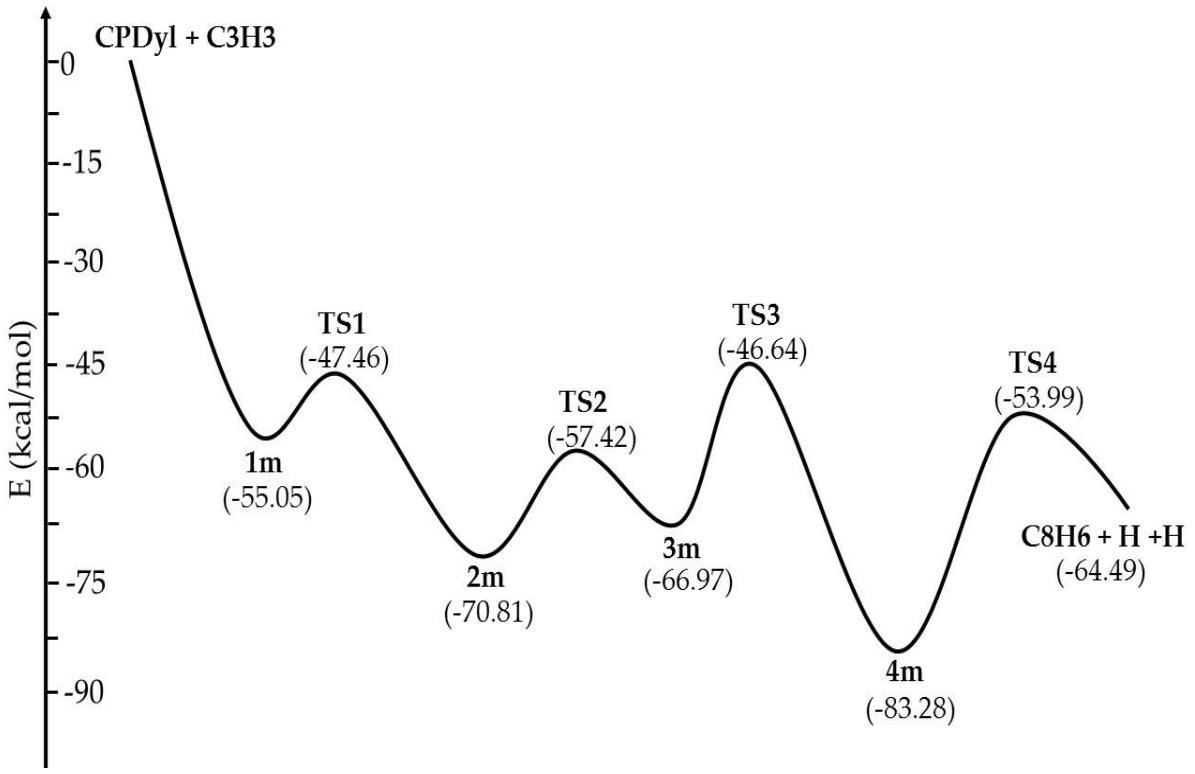

Figure 3.18. *Potential energy diagram for the formation of the Phenyl Acetylene. ZPE corrected energies (in kcal/mol) are given as calculated at the CCSD (T)/aug-cc-pVDZ level.*

The structures for reactant, intermediate, and product involved in the decomposition are given below:

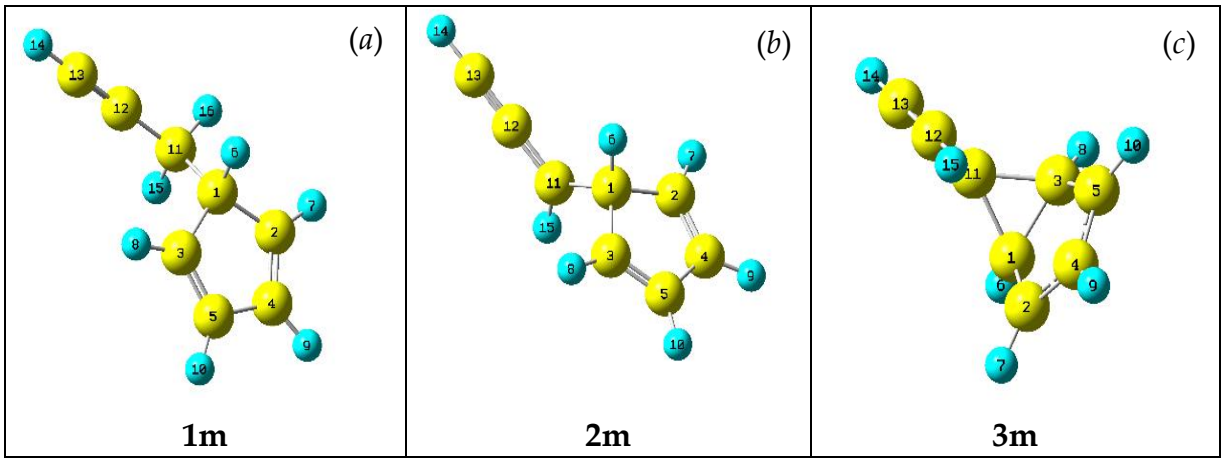

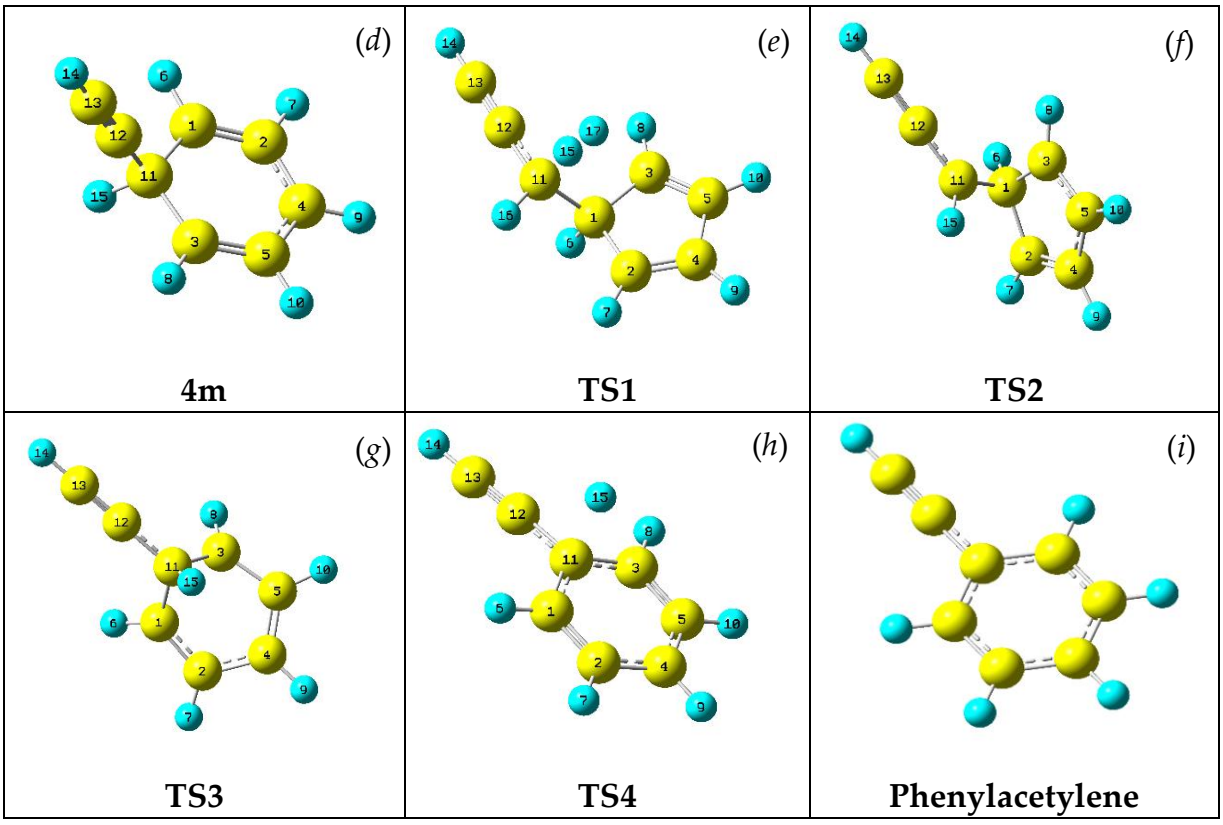

Figure 3.19. *Structures of (a)1m (b)2m (c)3m (d)4m (e)TS1 (f)TS2 (g)TS3 (h)TS4 and (i)Phenylacetylene optimised at B3LYP/6-311+G(2d,p) level of theory.*

3.6. KINETIC MECHANISM

The kinetic program CHMKIN [51] was used to perform the simulation. The CHEMKIN input included the kinetic parameter (k and E_a) and thermodynamic polynomial for all participating species in the reaction in addition to temperature, pressure, and concentration of reactant. Since a mechanism for pyrolysis of the cyclopentadiene [9] does exist in the literature we used this model as a starting point in the present investigation. With the help of the experimental and theoretical results presented above, a mechanism consisting of 82 reactions and 35 species has been derived for the DCPD thermal decomposition. After simulating the mechanism, at reaction conditions, it was continued at 300 K and 2 atm for 2 ms. This has been done to take into account radical reactions which can further

continue until all radicals are consumed. The result of computer modeling using the proposed mechanism is shown in Figure 3.14. It can be seen that the agreement between experiment and computation is fairly good.

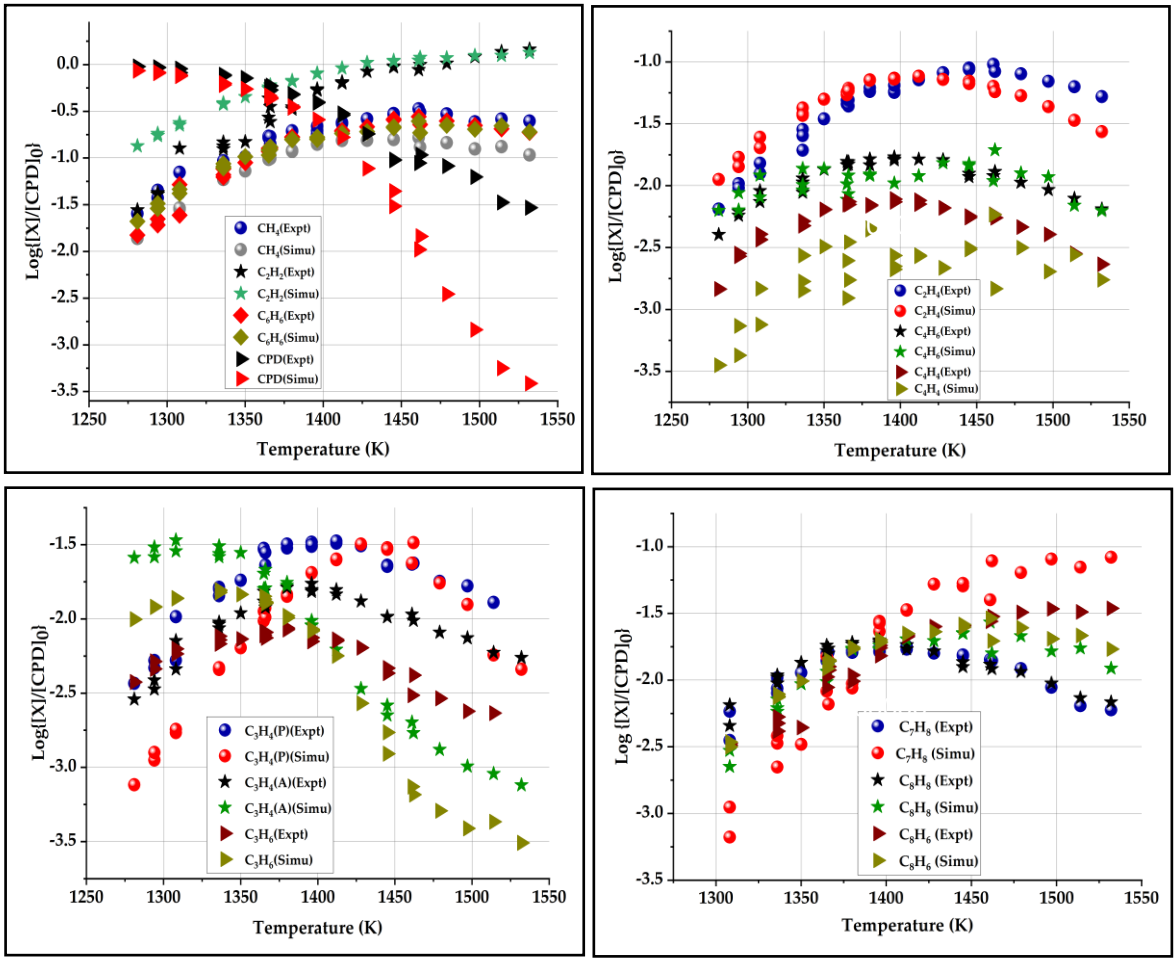

Figure 3.20. *Concentration profile of different product molecules obtained in the thermal decomposition of DCPD.*

DCPD is completely consumed in the reaction leaving behind the cyclopentadiene as a primary decomposition product. The cyclopentadiene can undergo decomposition by spontaneous loss of hydrogen atom generating cyclopentadienyl radical. Three cyclopentadienyl radicals formation are possible: 2,4-cyclopentadiene-1yl, 1,3-cyclopentadiene-1yl, and 1,3-cyclopentadiene-2yl. As 2,4-cyclopentadiene-1yl (symmetry C_{2v}) radical is easier to produce since the C-H

bond dissociation energy for the doubly bonded carbon is higher than the primary carbon atom. Therefore only the first possibility has been taken into account to construct the kinetic model.

$$cy\text{-}C_5H_6 = cy\text{-}C_5H_5 + H \quad \text{.....(3)}$$

The rate constant for reaction (3) that fits best for our study is $k = 2.0\times10^{15}$ exp [-81000/RT] s^{-1}. The proposed model predicts the concentration profile of cyclopentadiene fairly well till temperature 1450 K beyond which it shows a disagreement to observed concentration. This can be explained by the fact that more cyclopentadiene is consumed at high temperatures. The cyclopentadienyl radical undergoes a ring-opening process which is found to be a key step in the proposed mechanism that leads to linear products. Reaction (4) is found to be one of the most important reactions at high temperatures.

$$cy\text{-}C_5H_5 = L\text{-}C_5H_5 \quad \text{.....(4)}$$

The decomposition of the $L\text{-}C_5H_5$ radical results in the formation of acetylene and propargyl radical which is discussed in section 3.5.2. The combination of propargyl radical producing benzene is found to be the primary route for benzene formation.

$$C_3H_3 + C_3H_3 = C_6H_5 + H \quad \text{.....(5)}$$

The reaction of cyclopentadiene with methyl, vinyl, propargyl, allyl, butadienyl, and phenyl radicals are found to be the next important step in the mechanism. In particular, reaction (6) is of high importance in CPD decomposition, acetylene, and propyne formation (section 3.5.1).

$$cy\text{-}C_5H_6 + C_3H_3 = cy\text{-}C_5H_5 + C_3H_4(P) \quad \text{.....(6)}$$

Sensitivity analysis confirms that the reaction (7) of cyclopentadiene with methyl radical is of high importance.

$$cy\text{-}C_5H_6 + CH_3 = cy\text{-}C_5H_5 + CH_4 \quad \text{.....(7)}$$

Figure 3.14 represents that the temperatures above 1450 K, cyclopentadiene shows a large deviation from the observed concentration. The reaction (7) reported by Dean [23] had to be changed to fit our experimental values. This can be done by changing the value of preexponential factor and activation energy or both. We increased the preexponential factor for the reaction (7) from 3.11E+11 to 9.90E+13 to fit the concentration profile for methane. The reactions (8) and (9) are of key importance at low as well as high temperatures for the formation of ethylene, allene, propyne, and propylene.

$$AC_3H_5 + AC_3H_5 = C_6H_{10} \quad \text{.....(8)}$$

$$C_6H_{10} = C_4H_6 + C_2H_4 \quad \text{.....(9)}$$

$$AC_3H_5 + H = C_3H_6 \quad \text{.....(10)}$$

The reaction (10) is of primary importance for the formation of propylene. We increased the preexponential factor for the reaction (10) from 1.88E+26 to 7.88E+26 to fit the experimental values for propylene concentration. The reaction (11) of phenyl radical with methyl radical is also of high importance in cyclopentadiene decomposition. At low temperatures, it is found that the model slightly overpredicted benzene production which in turn affects the toluene production. We increased the preexponential factor for the reaction (11) from 1.07E+65 to 4.60E+66 to fit the experimental value for toluene. The n factor of the reaction was the same as the literature value of -15.64.

$$C_6H_5 + CH_3 = A1CH_3 \quad \text{.....(11)}$$

The preexponential factor for the reaction (12) was slightly reduced from 5.00E+08 to 1.00E+08 to fit the experimental value for allene.

$$C_3H_4(A) + H = C_3H_3 + H_2 \quad \text{.....(12)}$$

The reaction (13) is of high importance at low as well as high temperatures. The addition of vinyl radical to acetylene can produce high yields of vinyl acetylene

and H-atom. The high concentrations of acetylene observed during pyrolysis suggested that the addition of C_2H_3 to C_2H_2 may be the major step in the formation of aromatics. We increased the preexponential factor for the reaction (14) from 5.50E+12 to 9.80E+14 to fit the experimental value for vinylacetylene.

$$C_2H_2 + C_2H_3 = C_4H_4 + H \quad \text{……(13)}$$

$$C_2H_2 + C_2H_2 = C_4H_4 \quad \text{……(14)}$$

Table 3.3: Reaction mechanism used to explain the thermal decomposition of DCPD

Sr no.	Reaction	A	n	E_a (cal/mol)	Ref
R1	$cy\text{-}C_5H_6 = cy\text{-}C_5H_5 + H$	2.00E+15	0.0	81000	9
R2	$cy\text{-}C_5H_5 = L\text{-}C_5H_5$	5.00E+13	0.0	33300	8
R3	$C_3H_3 + C_3H_3 = C_6H_5 + H$	2.00E+12	0.0	3000	8
R4	$cy\text{-}C_5H_5 + AC_3H_5 = cy\text{-}C_5H_6 + C_3H_4(A)$	1.00E+13	0.0	0	23
R5	$C_3H_3 + C_2H_2 = L\text{-}C_5H_5$	5.00E+12	0.0	0	8
R6	$AC_3H_5 + AC_3H_5 = C_6H_{10}$	5.00E+13	0.0	0	8
R7	$C_6H_{10} = C_4H_6 + C_2H_4$	1.00E+12	0.0	24000	8
R8	$AC_3H_5 + AC_3H_5 = C_3H_6 + C_3H_4(A)$	1.00E+12	0.0	0.0	23
R9	$cy\text{-}C_5H_7 = cy\text{-}C_5H_6 + H$	1.02E+58	-13.1	60160	23
R10	$AC_3H_5 + C_2H_2 = cy\text{-}C_5H_6 + H$	2.95E+32	-5.8	25730	23
R11	$cy\text{-}C_5H_7 = C_5H_7(l)$	1.52E+58	-13.1	60660	23
R12	$AC_3H_5 + C_2H_2 = cy\text{-}C_5H_7$	3.42E+52	-12.2	27980	23
R13	$AC_3H_5 + C_2H_2 = C_5H_7(l)$	8.38E+30	-6.2	12870	23
R14	$C_2H_2 + C_2H_2 = C_4H_3 + H$	1.00E+13	0.0	45000	24
R15	$C_3H_6 + H = AC_3H_5 + H_2$	5.01E+12	0.0	1500	24
R16	$CH_4 + H = CH_3 + H_2$	2.20E+04	3.0	8754	5
R17	$C_4H_3 + C_2H_2 = C_6H_5$	2.80E+03	2.9	1400	25
R18	$C_3H_7 = CH_3 + C_2H_4$	3.00E+15	0.0	32960	26
R19	$C_3H_7 = C_3H_6 + H$	1.25E+14	0.0	37000	27

R20	$C_6H_6 + H = C_6H_5 + H_2$	3.00E+07	2.0	5000	24
R21	$C_2H_4 + H = C_2H_3 + H_2$	1.32E+06	2.53	12240	26
R22	$C_4H_6 = C_2H_3 + C_2H_3$	3.98E+19	-1.0	98150	23
R23	$cy\text{-}C_5H_6 + C_6H_5 = cy\text{-}C_5H_5 + C_6H_6$	3.10E+11	0.0	5500	8
R24	$cy\text{-}C_5H_6 + C_2H_3 = cy\text{-}C_5H_5 + C_2H_4$	6.00E+12	0.0	0	27
R25	$cy\text{-}C_5H_6 + C_3H_3 = cy\text{-}C_5H_5 + C_3H_4(A)$	1.10E+11	0.0	5500	8
R26	$cy\text{-}C_5H_6 + AC_3H_5 = cy\text{-}C_5H_5 + C_3H_6$	1.10E+11	0.0	5500	8
R27	$H + C_2H_2(+M) = C_2H_3(+M)$	5.60E+12	0.0	2400	8
R28	$CH_3 + H(+M) = CH_4(+M)$	1.24E+14	0.0	0	28
R29	$C_2H_3 + H(+M) = C_2H_4(+M)$	3.88E+13	0.2	0	8
R30	$C_3H_3 + H (+M) = C_3H_4(A) (+M)$	3.00E+13	0.0	0	29
R31	$C_3H_3 + H (+M) = C_3H_4(P) (+M)$	3.00E+13	0.0	0	30
R32	$C_2H_4 + CH_3 = C_2H_3 + CH_4$	6.62E+00	3.70	9504	8
R33	$A1C_2H_2\text{-}N + H = A1C_2H_3$	1.80E+14	0.0	0	23
R34	$C_3H_6 + H = C_2H_4 + CH_3$	7.23E+12	0.0	1302	9
R35	$C_2H_5 + H = C_2H_4 + H_2$	1.25E+14	0.0	8003	9
R36	$C_2H_5 + CH_3 = C_2H_4 + CH_4$	9.00E+13	0.0	0	30
R37	$C_2H_3 + C_2H_2 = C_4H_4 + H$	4.60E+16	-1.25	8404	30
R38	$C_2H_4 + C_2H = C_4H_4 + H$	1.20E+13	0.0	0	26
R39	$C_2H_3 + C_2H = C_4H_4$	2.12E+60	-13.45	27550	31
R40	$AC_3H_5 + C_2H_3 = C_3H_4(A) + C_2H_4$	1.00E+12	0.0	0	32
R41	$AC_3H_5 + H = C_3H_4(A) + H_2$	5.00E+13	0.0	0	32
R42	$C_3H_6 = C_2H_2 + CH_4$	2.50E+12	0.0	70034	5
R43	$C_3H_6 + CH_3 = AC_3H_5 + CH_4$	2.22E+00	3.50	5678	5
R44	$C_3H_4(P) + C_2H_3 = C_3H_3 + C_2H_4$	1.00E+12	0.0	7700	32
R45	$C_2H_2 + CH_3 = C_2H + CH_4$	1.81E+11	0.0	17297	34
R46	$C_2H_4 + M = C_2H_2 + H_2 + M$	2.60E+17	0.0	79327	32
R47	$C_2H_3 + C_2H_4 = C_4H_6 + H$	5.00E+11	0.0	7307	48
R48	$C_4H_6 = C_4H_4 + H_2$	2.50E+15	0.0	94700	48
R49	$C_4H_5 + H = C_4H_4 + H_2$	1.50E+13	0.0	0	8

R50	$C_4H_6 = C_4H_5 + H$	8.50E+54	-11.78	127507	30
R51	$C_6H_6 + CH_3 = C_6H_5 + CH_4$	7.32E+12	0.0	18920	30
R52	$A1CH_3 + CH_3 = A1CH_2 + CH_4$	3.16E+11	0.0	9504	36
R53	$AC_3H_5 + CH_3 = C_3H_4(A) + CH_4$	3.02E+12	-0.32	131	8
R54	$C_6H_5 + CH_3 = A1CH_2 + H$	4.44E+33	-5.45	24290	32
R55	$C_6H_5 + C_2H = A1C_2H$	2.54E+17	-1.489	1542	34
R56	$A1C_2H_2\text{-}N = A1C_2H + H$	1.30E+41	-8.65	11005	31
R57	$C_6H_6 + C_2H = A1C_2H + H$	5.00E+13	0.0	0	36
R58	$A1CH_2 + H = A1CH_3$	2.59E+14	0.0	0	37
R59	$C_6H_5 + C_4H_6 = A1C_2H_3 + C_2H_3$	3.20E+11	0.0	1900.0	37
R60	$C_6H_6 + C_2H_3 = A1C_2H_3 + H$	0.80E+12	0	6400	38
R61	$C_6H_5 + C_2H_3 = A1C_2H_3$	3.90E+38	-7.63	12901	39
R62	$C_6H_6 + SCH_2 = A1CH_3$	1.20E+14	0.0	0	40
R63	$C_6H_5 + C_2H_2 = A1C_2H_2\text{-}N$	9.90E+41	-9.26	15700	30
R64	$A1CH_2 + SCH_2 = A1C_2H_3 + H$	2.40E+14	0.0	0	41
R65	$cy\text{-}C_5H_6 + C_4H_5 = cy\text{-}C_5H_5 + C_4H_6$	1.20E-01	4.0	0	42
R66	$C_2H + CH_3 = C_3H_4(P)$	8.00E+13	0.0	0	46
R67	$C_4H_5 + C_3H_4(P) = A1CH_3 + H$	3.16E+11	0.0	3699	44
R68	$C_3H_4(A) + CH_3 = C_3H_3 + CH_4$	9.30E+13	0.0	7700	49
R69	$C_3H_4(P) + CH_3 = C_3H_3 + CH_4$	9.80E+13	0.0	7700	49
R70	$C_4H_5 + C_3H_4(A) = A1CH_3 + H$	2.00E+11	0.0	3699	44
R71	$C_3H_3 + SCH_2 = C_4H_4 + H$	5.00E+13	0.0	0	44
R72	$C_6H_6 + C_2H_3 = C_6H_5 + C_2H_4$	6.00E+11	0.0	12978	43
R73	$C_4H_6 + CH_3 = C_4H_5 + CH_4$	4.00E+14	0.0	22801	45
R74	$C_3H_3 + TCH_2 = C_4H_4 + H$	2.00E+13	0.0	0	38
R75	$C_2H_2 + CH_3 = AC_3H_5$	1.90E+45	-9.4	35410	8
R76	$C_6H_5 + C_2H_4 = A1C_2H_3 + H$	2.50E+12	0.0	6199	45
R77	$C_3H_3 + CH_3 = C_4H_6$	5.00E+12	0.0	0	43
Rate Modified					

R78	$AC_3H_5 + H = C_3H_6$	7.88E+26 (1.88E+26)	-3.6	5470	5
R79	$C_3H_4(A) + H = C_3H_3 + H_2$	1.00E+08 (5.00E+08)	2.0	5000	25
R80	$cy\text{-}C_5H_6 + CH_3 = cy\text{-}C_5H_5 + CH_4$	9.90E+13 (3.11E+11)	0.0	5500	23
R81	$C_2H_2 + C_2H_2 = C_4H_4$	9.80E+14 (5.50E+12)	0.0	36962	47
R82	$C_6H_5 + CH_3 = A1CH_3$	4.60E+66 (1.07E+65)	-15.64	22719	48

3.7 CONCLUSION

Thermal decomposition experiments on DCPD were performed behind the reflected shock wave in the temperature range of 1250-1550 K and pressure range of 13-16 atm using a modified shock tube. The major products observed during pyrolysis are methane, acetylene, cyclopentadiene, and benzene whereas the minor products include ethylene, propylene, propyne, allene, 1,3-butadiene, vinyl acetylene, toluene, styrene, and phenylacetylene. Whereas benzene, indene, methyl-indenes, and naphthalene are major species formed during cyclopentadiene pyrolysis [12]. However, we have not observed naphthalene, indene, and methyl-indenes during DCPD pyrolysis for given conditions. As DCPD is expected to fully decompose into CPD in T_2 (incident shock temperature), the formation of CPD monomer is the first step in the decomposition of DCPD. A kinetic mechanism consisting of 82 reactions and 35 species has been derived for the DCPD thermal decomposition based upon the experimental and theoretical results. The mechanism fairly replicated the formation of observed product concentration. We hope that this work will help in deriving the oxidation mechanism.

3.8 REFERENCES

1. W. Tsang and A. Lifshitz, Annual Review of Physical Chemistry, 41, 1990, 559–599.
2. R. Sivaramakrishnan, R. S. Tranter, and K. Brezinsky, Journal of Physical Chemistry, 110, 2006, 9388–9399.
3. M. H. Back, Canadian Journal of Chemistry, 49, 13, 1971, 2199-2204.
4. M. R. Djokic, K. M. Van Geem, C. Cavallotti, A. Frassoldati, E. Ranzi, G. B. Marin, Combustion and Flame, 161, 2014, 2739–2751.
5. C. F. Melius, M. E. Colvin, N. M. Marinov, W. J. Pit, and S. M. Senkan, International Symposium on Combustion, 26, 1, 1996, 685-692.
6. D. H. Kim, J. A. Mulholland, D. Wang, and A. Violi, Journal of Physical Chemistry A, 114,. 47, 2010, 12411-12421.
7. D. Wang, A. Violi, D. H. Kim, and J. A. Mullholland, Journal of Physical Chemistry A, 110, 2006, 4719-4725.
8. A. Burcat, and M. Dvinyaninov, International Journal of Chemical Kinetics 29, 1997, 505 – 514.
9. M. B. Colket, Eastern States Section of Combustion Institute annual meeting, Orlando, 1990, Paper 1.
10. R. G. Butler, MSc. Thesis, Princeton University, 1992.
11. O. S. L. Bruisma, P. J. J. Tromp, H. J. J. de Sauvage Nolting and J. A. Moulijn, Fuel, 67, 1988, 334-348.
12. Marko R. Djokic, Kevin M. Van Geem, Carlo Cavallotti, Alessio Frassoldati, Eliseo Ranzi, and Guy B. Marin, Combustion and Flame, 161, 2014, 2739–2751

13. P. N. Rao and D. Kunzru, Journal of Analytical and Applied Pyrolysis, 76, 2006, 154-160.

14. S. Nakra, R. J Green, and S. L Anderson, Combustion and Flame, 144, 4, 2006, 662-674.

15. K. Chenoweth, A. C. T. van Duin, S. Dasgupta, and W. A. Goddard III, Journal of Physical Chemistry A, 113, 2009, 1740-1746.

16. S. R. Smith and A. S. Gordon, Journal of Physical Chemistry, 65, 7, 1961, 1124-1128.

17. S. Reshmi, E. Arunan, and C. P. Reghunadhan Nair, Industrial Engineering & Chemical Research, 53, 2014, 16612−16620.

18. J. D. Rule, J. S. Moore, Macromolecules, 35, 2002, 7878-7882.

19. H. I. Palmova, J. Kosek, J. SchoKngut, M. Marek, K. Stepahnek, Chemical Engineering Science, 56, 2001, 927-935.

20. W. C. Herndon, C. R. Grayson, and J. M. Manion, Journal of Organic Chemistry, 32, 3, 1967, 526–529.

21. G. B. Bacskay, and J. C. Mackie, Physical Chemistry Chemical Physics, 3, 2001, 2467-2473.

22. L. V. Moskaleva, and M. C. Lin, Journal of Computational Chemistry, 21, 6, 2000, 415–425.

23. A. M. Dean, Journal of Physical Chemistry, 94, 1990, 1432-1439.

24. C. K. Westbrook, W. J. Pitz, M. M. Thornton, and P. C. Malte, Combustion and Flame, 72, 1988, 45-59.

25. A. J. Miller, and C. F. Melius, Combustion and Flame, 91, 1, 1992, 21-39.

26. V. D. Knyazev and K. V. Popov, Journal of Physical Chemistry A, 119, 2015, 7418−7429.

27. W. Tsang, and R. F. Hampson, Journal of Physical and Chemical Reference Data 15, 1986, 1087.
28. R. G. Butler, and I. Glassman, Proceedings of the Combustion Institute 32, 2009, 395–402.
29. V. V. Kislov, and A. M. Mebel, Journal of Physical Chemistry, 111, 38, 2007, 9533-9546.
30. H. Wang, and M. Frenklach, Combustion and Flame, 110, 1–2, 1997, 173-221.
31. H. Wang, and M. Frenklach, Combustion and Flame, 96, 1–2, 1994, 163-170.
32. H. Richter, and J. B. Howard, Physical Chemistry Chemical Physics, 4, 2002, 2038-2055.
33. P. Dagaut, J. C. Boettner, and M. Cathonnet, Combustion Science and Technology, 71, 1990, 1-13.
34. H. Y. Zhang, and J. T. Mckinnon, Combustion Science and Technology, 107, 1995, 4-6.
35. C. Cavallotti, D. Polino, A. Frassoldati, and E. Ranzi, Journal of Physical Chemistry A, 116, 2012, 3313−3324.
36. J. L. Emdee, K. Brezinsky, and I. Glassman, Journal of Physical Chemistry 96, 1992, 2151-2161.
37. S, M, Saunders, D. L. Baulch, K. M. Cooke, M. J. Pilling, and P. I. Smurthwaite, International Journal of Chemical Kinetics, 26, 1, 1994, 113-130.
38. A. Fahr, and S. E. Stein, International Symposium on Combustion, 22, 1, 1989, 1023-1029.

39. S. J. Harris, A. M. Weiner, and R. J. Blint, Combustion and Flame, 72, 1, 1988, 91-109.

40. T. Böhland, K. Héberger, F. Temps, and H. Wagner, Berichte der Bunsengesellschaft für physikalische Chemie, 93, 1, 1989, 80-87.

41. R. P. Lindstedt, and J. C. Maurice, Combustion Science, and Technology, 120, 1996, 1-6.

42. X. Zhong and J. W. Bozzelli, Journal of Physical Chemistry A, 102, 20, 1998, 3537-3555.

43. I. Ziegler, R. Fournet, P. M. Marquaire, Journal of Analytical and Applied Pyrolysis, 73, 2005, 231–247.

44. R. D. Kern, H. J. Singh, and C. H. Wu, International Journal of Chemical Kinetics, 20, 9, 1988, 731-747.

45. Y. Hidaka, T. Higashihara, N. Ninomiya, H. Oshita, and H. Kawano, Journal of Physical Chemistry, 97, 1993, 10977-10983.

46. J. A. Mulholland, L. Mingming and D. H. Kim, Proceedings of the Combustion Institute, 28, 2000, 2593–2599.

47. R. P. Durán, V. T. Amorebieta, and A. J. Colussi, International Journal of Chemical Kinetics, 21, 9, 1989, 847-858.

48. H. Richter, T. G. Benish, O. A. Mazyar, W. H. Green, and J. B. Howard, Proceedings of the Combustion Institute, 28, 2000, 2609–2618.

49. A. Laskin, H. Wang, and C. K. Law, International Journal of Chemical Kinetics, 32, 10, 2000, 589-614.

50. Gaussian 09, Revision A.02, M. J. Frisch, G. W. Trucks, H. B. Schlegel, G. E. Scuseria, M. A. Robb, J. R. Cheeseman, G. Scalmani, V. Barone, B. Mennucci, G. A. Petersson, H. Nakatsuji, M. Caricato, X. Li, H. P. Hratchian, A. F.

Izmaylov, J. Bloino, G. Zheng, J. L. Sonnenberg, M. Hada, M. Ehara, K. Toyota, R. Fukuda, J. Hasegawa, M. Ishida, T. Nakajima, Y. Honda, O. Kitao, H. Nakai, T. Vreven, J. A. Montgomery, Jr., J. E. Peralta, F. Ogliaro, M. Bearpark, J. J. Heyd, E. Brothers, K. N. Kudin, V. N. Staroverov, R. Kobayashi, J. Normand, K. Raghavachari, A. Rendell, J. C. Burant, S. S. Iyengar, J. Tomasi, M. Cossi, N. Rega, J. M. Millam, M. Klene, J. E. Knox, J. B. Cross, V. Bakken, C. Adamo, J. Jaramillo, R. Gomperts, R. E. Stratmann, O. Yazyev, A. J. Austin, R. Cammi, C. Pomelli, J. W. Ochterski, R. L. Martin, K. Morokuma, V. G. Zakrzewski, G. A. Voth, P. Salvador, J. J. Dannenberg, S. Dapprich, A. D. Daniels, O. Farkas, J. B. Foresman, J. V. Ortiz, J. Cioslowski, and D. J. Fox, Gaussian, Inc., Wallingford CT, 2009.

51. J. Kee, F. M. Rupley, and J. A. Miller, Chemkin-II A Fortran Chemical Kinetics Package for Analysis of Gas-Phase Chemical Kinetics. Sandia Report SAND 89-8009B. U.C-706, 1992.

52. Z. Xiong, Z. Mi, and X. Zhang, Reaction Kinetics and Catalysis Letters, 85, 2005, 89-98.

4

QTAIM ANALYSIS ON DISSOCIATION REACTION OF DICYCLOPENTADIENE

CHAPTER OVERVIEW

This chapter forms the theoretical background for the dissociation reaction of dicyclopentadiene to cyclopentadiene conversion. Quantum theory of Atoms in Molecules (QTAIM) which is based upon electron density topology provides insight into the reaction. AIM analysis along the reaction coordinate was carried out which provides information about bond breaking and bond making phenomenon occurring during chemical transformation. In addition, AIM analysis was used to identify the various types of non-covalent interactions and their strength.

4.1 INTRODUCTION

Dicyclopentadiene ($C_{10}H_{12}$), a homodimer of cyclopentadiene (cy-C_5H_6), a molecule that has attracted greater interest in the high-temperature gaseous environment such as combustion, flame, etc. A cyclopentadienyl radical (cy-C_5H_5) [1], produced during the combustion of hydrocarbons leads to the formation of polycyclic aromatic hydrocarbons (PAHs) [2-5] and soot. The process of formation of PAHs and their growth remains a major subject of investigation due to their adverse effect on health and the environment [6]. DCPD has received considerable attention for ROMP (ring opening metathesis polymerization) in solid propellant due to its high polymerization rate, and its ability to provide thermal, chemical, and mechanical stability to its polymer [7-8]. The polymerization process is initiated via the opening of a strained norbornyl double bond which forms a linear polymer whereas the opening of a less reactive cyclopentene ring leading to the formation of the cross-linked polymer. The hydrogenation of DCPD gives TH (endo-tetrahydridodicyclopentadiene) dimer [9], which has been used as a fuel in liquid rocket propellant for missiles and jet propellant (JP-10, $C_{10}H_{16}$, currently used as an aviation fuel).

We have performed experimental investigations on the thermal decomposition of DCPD using a modified shock tube incorporated with a driver insert. The experimental observations showed that the primary decomposition channel consists of the formation of cyclopentadiene. The dissociation reaction is initiated by the breaking of the one C-C bond between bridge carbon atoms. This reaction is called retro Diel Alder's reaction, a [4+2] cycloaddition between a conjugated diene and a substituted alkene commonly called a dienophile. Ab-

initio calculation was performed to locate the transition state for this dissociation reaction.

The quantum theory of atoms in molecules (QTAIM), which is based upon the electron density topology was used to characterize the bond breaking and bond formation process. Heard et al. [10], used the electron densities of transition state geometries to differentiate the HX (X= F, OH, Cl, Br) elimination reactions of halohydrocarbons and halohydroalcohols. It is noted that for HF and HOH elimination, bond paths are present between each of the four atoms involved in transition state geometry. Hence neither C-X nor C-H bonds have been broken in the transition state geometry and the ring critical point is closer to the bond critical point of the C-X bond than to that of the C-H bond. However, for HCl and HBr elimination, the bond path does not exist between the carbon atom and the X (Cl and Br) atom in the transition state geometry. Hence C-X bond is fully broken with the formation of the HX bond. In the present study, we seek to understand the dissociation reaction of DCPD by using the molecular graphs and integrated atomic charges on the important atoms in reactant and transition state geometries to determine the order in which bonds break.

It could be expected that both C-C bonds between bridge carbon atoms are more elongated in the transition state geometry due to molecular symmetry. But, one of the C-C bonds between bridge carbon atoms remains intact in the transition state and it is characterized by the presence of a bond critical point (bcp). We would not expect the formation of a new C-C bond between C2 and C8 atoms which leads to the formation of the cage-like structure characterized by the presence of a cage critical point (ccp) in transition state geometry.

Also, QTAIM is used to understand and quantify the various types of interactions and their behavior as a function of the separation and relative orientation of the molecule. The properties such as electron density (ρ), its Laplacian ($\nabla^2\rho$) and kinetic energy density are correlated with the interaction energy in van der Waal and hydrogen-bonded complexes [11-12]. Accurately describing non-covalent interactions such as van der Waals interactions (vdW), steric clashes (SC), and hydrogen bonds (HBs), including their spatial characteristic, is a key step in the process of decomposing the complex balance of chemical forces. To visualize non-covalent interactions, Yang et al. [13] have put forward a new approach based on the analysis of electron densities and their reduced gradients, s(***r***). The electron density and reduced gradient are used in creating a Non-covalent index (NCI) plot and it has been widely used in the analysis of various interactions. For example, Morrison and Siddick [14] used NCI results to distinguish the various interactions for $(BH_3NH_3)_4$ complex in the gas phase and crystalline tetramer. The crystalline tetramer is stabilized by van der Waal's interactions whereas the gas-phase tetramer gives rise to highly negative interaction energy which is dominated by strong interactions. In the present study, this approach was chosen to highlight the non-covalent interactions in a low electron density regime.

4.2 QUANTUM THEORY OF ATOMS IN MOLECULES (QTAIM)

The physical properties attributed to atoms or functional groups within a molecule are transferable from one molecule to another and played a key role in the development of chemical kinetics. The Quantum theory of atoms in a molecule (QTAIM), developed by Professor Richard Bader and his coworkers [15-20], depends upon quantum observables such as electron density topology ρ(r).

QTAIM is a generalization of quantum mechanics as applied to open systems. It provides a framework that fulfills the gap between physics on one side and experimental chemistry on another side. It enables us to study the properties of the atoms or functional groups within a molecule which determines the chemical behavior and reactivity [21-22].

The electron density is bound by attractive forces of the nuclei with a substantial local maximum at the position of each nucleus. A critical point (CP) in the electron density is a point in space at which the first derivative of the electron density vanishes i.e.:

$$\nabla\rho(r) = i\frac{d\rho}{dx} + j\frac{d\rho}{dy} + k\frac{d\rho}{dz} = 0 \ \text{(at CP)} \qquad \ldots\ldots\ldots\ldots\ldots 4.1$$

The gradient of ρ(r) at a point in the space represents a vector pointing in a direction in which ρ(r) will have the greatest rate of increase with a magnitude equal to the rate of increase in that direction. The topology of electron density is characterized by maxima and minima in a space which can be differentiated by second-order derivatives, the elements of the tensor $\nabla\nabla\rho$. These give nine second-order derivatives that can be arranged in the matrix form called as "Hessian matrix" when calculated at a critical point located at r_c is represented as:

$$A(r_c) = \begin{bmatrix} \frac{\partial^2\rho}{\partial x^2} & \frac{\partial^2\rho}{\partial x\partial y} & \frac{\partial^2\rho}{\partial x\partial z} \\ \frac{\partial^2\rho}{\partial y\partial x} & \frac{\partial^2\rho}{\partial y^2} & \frac{\partial^2\rho}{\partial y\partial z} \\ \frac{\partial^2\rho}{\partial z\partial x} & \frac{\partial^2\rho}{\partial z\partial y} & \frac{\partial^2\rho}{\partial z^2} \end{bmatrix}_{r=r_c} \qquad \ldots\ldots\ldots\ldots 4.2$$

When the Hessian matrix is diagonalized (equivalent to the rotation of the coordinate system), it superimposes the principle curvature axes of critical point

to that of new axes. Hence, the transformation $\mathbf{U^{-1}AU=\Lambda}$ **(U** is the unitary matrix**)**, transform the Hessian matrix into its diagonal form which can be written as:

$$\Lambda = \begin{bmatrix} \frac{\partial^2\rho}{\partial x'^2} & 0 & 0 \\ 0 & \frac{\partial^2\rho}{\partial y'^2} & 0 \\ 0 & 0 & \frac{\partial^2\rho}{\partial z'^2} \end{bmatrix}_{r'=r_c} = \begin{bmatrix} \lambda_1 & 0 & 0 \\ 0 & \lambda_2 & 0 \\ 0 & 0 & \lambda_3 \end{bmatrix} \qquad \text{……..4.3}$$

in which λ_i are the curvatures of the electron density with respect to new principle axes. The trace of Hessian matrix which is invariant to rotations of the coordinate system is known as Laplacian of the density, represented by

$$\nabla^2\rho(r) = \nabla.\nabla\rho(r) = \frac{\partial^2\rho(r)}{\partial x'^2} + \frac{\partial^2\rho(r)}{\partial y'^2} + \frac{\partial^2\rho(r)}{\partial z'^2} = \boldsymbol{\lambda_1 + \lambda_2 + \lambda_3} \qquad \text{……..4.4}$$

Critical points are classified according to their rank (ω) and signature (σ) and represented by (ω,σ). Rank with ω < 3 signifies that the critical points vanish or bifurcate with a small perturbation in electron density caused by nuclear motion. Hence, a critical point (with a rank less than three) is unstable and not found in equilibrium charge distributions whereas CP is found when ω = 3. The signature of the Hessian matrix which is the algebraic sum of the signs of the curvatures (each of three curvatures contributes ±1) defines the maxima or minima. There are four types of CPs having three non-zero eigenvalues:

- (3,-3) represents three negative curvatures: ρ is a local maximum.
- (3,-1)correspond to two negative curvatures: ρ is a maximum in a plane defined by the corresponding two eigenvectors and minimum along the third axis perpendicular to it.
- (3,+1) denotes the presence of two positive curvatures: ρ is a minimum in the plane corresponding two eigenvectors and maximum along the third axis perpendicular to it.

- (3,+3) represents three positive curvatures: ρ is a local minimum.

Each type of critical point described above is a characteristic element of the chemical structure and classified as (3,-3) *nuclear critical point* (NCP) ; (3,-1) *bond critical point* (BCP); (3,+1) *ring critical point* (RCP); (3,+3) *cage critical point* (CCP).

The different type of critical points exists in a molecule or crystal follow the following relationship:

$$n_{NCP} - n_{BCP} + n_{RCP} - n_{CCP} = \begin{cases} 1, & isolated\ molecule \\ 0, & infinite\ crystal \end{cases} \quad \ldots\ldots\ldots 4.5$$

Where 'n' corresponds to the number of subscribed types of the critical point. The first equality is known as the Poincare-Hopf relation which is applicable for isolated finite systems like a molecule whereas the second equality is known as the Morse equation which applies to infinite periodic lattices. The violation of the above equation implies that a critical point has been missed; on the other hand, the satisfaction of this equation does not imply its consistency and completeness of the characteristic set (set of n_{NCP}, n_{BCP}, n_{RCP}, n_{CCP}).

The presence of a ring critical point will always be appearing in the interior of the ring of chemically bonded atoms [10]. When such rings are so connected in a manner that encloses an interstitial cavity, it will form a cage critical point in the enclosed space. As Bader [10] stated in 1990: "*While it is mathematically possible for a cage to be bounded by only two ring surfaces, the minimum number found in an actual molecule so far is three, as in bicycle [1.1.1] pentane, for example*", a statement reiterated in 2000. We have reported an actual molecular system in which the cage critical point (CCP) is enclosed by two ring surfaces. Such CCP arises in the dissociation reaction of dicyclopentadiene ($C_{10}H_{12}$) forming cyclopentadiene (c-C_5H_6).

4.3 NON-COVALENT INTERACTION ANALYSIS

The non-covalent interaction provides the relevant information based upon distance-dependent contact without consideration of the hydrogen atom. It uses the electron density and its derivative to analyze a wide range of non-covalent interactions which can be used as a tool to a chemist's arsenal [23-24]. The reduced electron density $s(\boldsymbol{r})$, obtained from density and its first-order derivative is a key quantity that can be used to characterize the deviation from the homogeneous electron distribution. Equation 4.6 is called as NCI index. NCI index is based upon the 2D plot of reduced electron density $s(r)$ and the electron density $\rho(\boldsymbol{r})$ [25]

$$s(\boldsymbol{r}) = \frac{|\nabla\rho(r)|}{(2(3\pi^2))^{1/3}\rho(r)^{4/3}} \qquad \text{.....4.6}$$

Although small values of a reduced density gradient and density localization enable us to provide the identification of the weak interaction, however, a specific type of interaction cannot be obtained from the values of density. The region associated with low density is mainly related to weak molecular interactions e.g. van-der Waal's interaction, whereas the region associated with the high value of electron density is related to strong molecular interactions [21]. To identify the types of non-covalent interaction, the sign of the Laplacian of the density, $\nabla^2\rho(\boldsymbol{r})$, is used as a key quantity to distinguish between different types of interactions. Generally, the Laplacian of the system can be decomposed into a sum of three components along the mutually perpendicular principal axes of maximal variation. These three components correspond to the three eigenvalues λ_i of the Hessian matrix (second derivative of electron density for which $\nabla^2\rho = \lambda_1 + \lambda_2 + \lambda_3$). In the case of non-covalent interactions, the interatomic region between the bonded atoms is dominated by positive contribution and the resultant Laplacian is positive. In the case of bonding interactions, such as

hydrogen bond where the accumulation of electron density is perpendicular to the bond can be characterized using the negative sign of λ_2. On the other hand, for non-bonded interactions such as steric repulsion, produce density depletion, etc. the value of λ_2 is positive ($\lambda_2 > 0$, $\lambda_3 > 0$ and λ_1 can be either positive or negative). Therefore one can use the sign of λ_2 as a tool to distinguish between bonded and non-bonded interactions.

As there are several studies [26-27] available in the literature on λ_2 in different bonding molecular systems and deviation(accumulation/depletion) in the electron density are rationalized in terms of the attractive or repulsive interaction. In the case of non-covalent interactions, the characteristic feature of electron density and its derivatives appear clearly if the density is constructed from something as simple as the sum of electron density. It has been observed that a large shift contributing to smaller density value corresponds to nonbonded overlap which induces greater stability to the molecular system. Hence low electron density and a small value of reduced density gradient are the characteristic features of the non-covalent interactions.

4.4 COMPUTATIONAL DETAILS

The ab-initio calculations on the decomposition reaction of DCPD to CPD were performed with the Gaussian 09 suite of programs. Geometry optimizations of reactant, product, and TS were carried out at the B3LYP/6-311+G(2d,p) level of theory, a method that gave reliable geometries for the determination of rate constants. The zero-point energy calculated at this level of theory was used for energy correction. The transition state geometry was initially characterized by consideration of the imaginary frequency and has been verified which connects fully bound geometries from reactant to product by IRC calculation (see Figure

3.3). The energetics along the reaction pathway is calculated using single point calculation at CCSD(T)/6-311+G(2d,p) level of theory. The barrier height for this reaction is found to be 40.2 kcal/mol calculated at this level of theory with zero-point correction. As the DCPD molecule is symmetric, we performed the transition state calculations by interchanging the atoms but could not find the different transition states.

The quantum theory of atoms in a molecule (QTAIM) which depends upon the electron density topology was applied to find the bond paths and the corresponding critical point associated with them. The QTAIM calculations were performed with the use of the AIMALL program. The complete search of the bond, ring, and cage critical points has been carried out for each bound geometry to verify the Poincare-Hopf relationship.

In the present study, we approached to map and analyze the non-covalent interactions for the dissociation reaction of dicyclopentadiene to cyclopentadiene. The atoms in the molecules help to visualize the covalent bond for the molecular geometry calculated along the reaction coordinate. Also, the properties associated with the reduced density gradient are investigated in depth using the web-published code NCIPLOT by Yang et al. [23] at Duke University. The reduced density gradient will have a very large positive value in the region far from the molecule whereas these values approaching zero for the regions of non-covalent interactions.

4.5 RESULT AND DISCUSSION

The molecular geometry for the reactant, product, and transition state involved in the conversion of DCPD to CPD is represented in Figures 4.1, 4.2, and 4.3 respectively, in the form of a molecular graph and the corresponding gradient

vector plot. The DCPD exhibit two types of the double bond in which one is of norbornene-type whereas the other is cyclopentene type. In the reactant geometry, there exist the bond paths between the bridge carbon atoms (between C3-C6 and C4-C5) which are represented in Figure 4.1. Also, it is characterized by the presence of ring critical points in the interior of the two cyclopentadiene rings. However, the bonding between two cyclopentadiene rings through bridge carbon atoms leads to the formation of a closed ring structure which is characterized by the presence of another ring critical point. As the reaction progresses a cage critical point (ccp) appears in the interior of rings formed by three rings.

In the transition state geometry, there is significant cleavage of the bond between C4-C5 also a new bond between C2-C8 starts forming which is represented in Figure 4.2. It has been observed that the bond present between C3-C6 is still intact in the transition state geometry. The appearance of a new bond between C2-C8 would result in the formation of additional two ring critical paths enclosed by a cage critical point. The first ring critical point arises in the ring formed by the atoms (C3, C4, C5, C6, and C10), which is closer to the bond critical point of the C4-C5 bond. Another ring critical point appears in the interior of the ring formed by the atoms (C1, C2, C4, C5, C8, and C9) which is in the vicinity of the cage critical point. The third ring critical point exists in the ring formed by atoms (C2, C3, C6, C7, and C8) which is closer to the bond critical point of the C2-C8 bond. In the near product geometry, it has been seen that a new bond appears between C1-C9 whereas there is significant cleavage of the bond between C3-C6 (see Figure 4.3). The variation in atomic charges correspond to different atoms in the reactant, transition state, and near product state is summarized in Table 4.1.

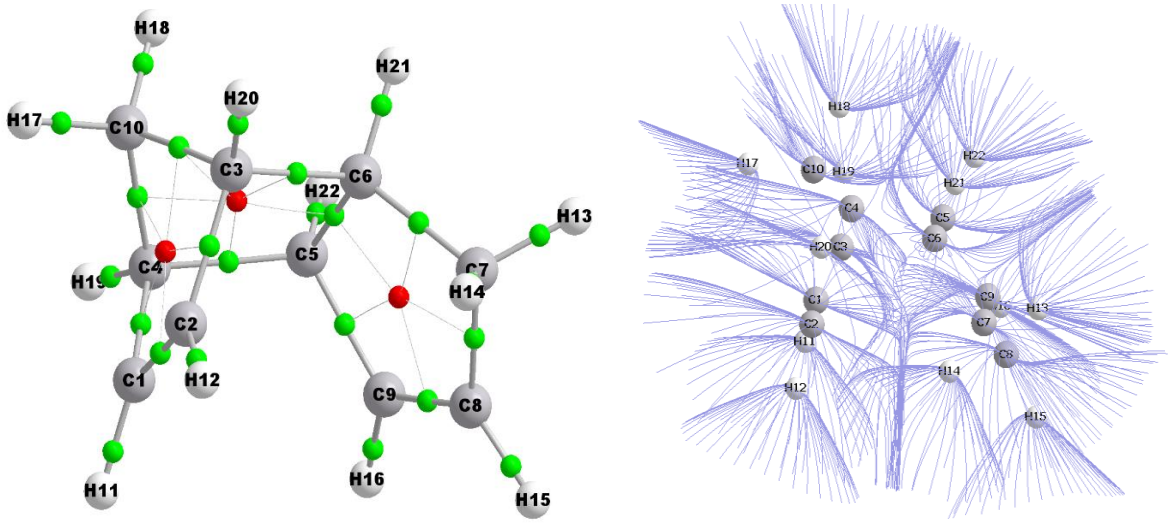

Figure 4.1. *The geometry of DCPD as a molecular graph and the corresponding gradient vector plot showing interatomic surface.*

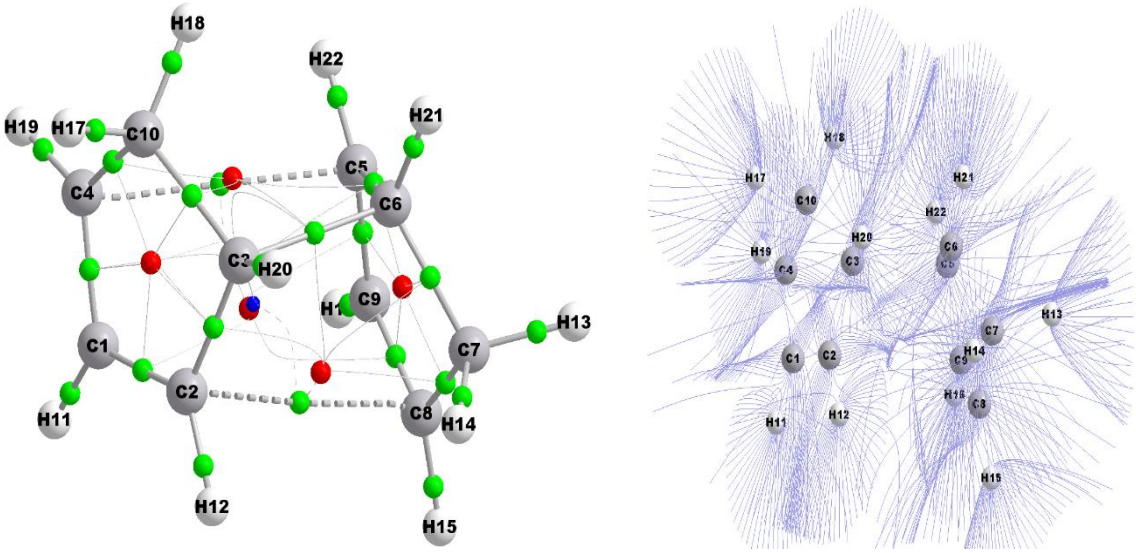

Figure 4.2. *The geometry of transition state as a molecular graph and the corresponding gradient vector plot showing interatomic surface.*

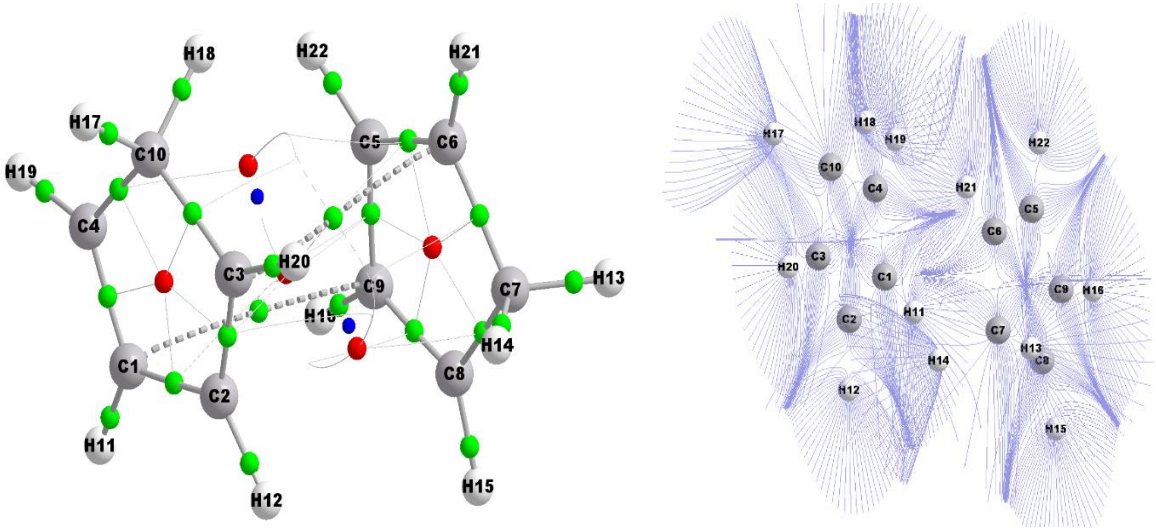

Figure 4.3. *The geometry of near product as a molecular graph and the corresponding gradient vector plot showing interatomic surface.*

Table 4.1: QTAIM Atomic Charges (Q) for Atoms in dissociation reaction of DCPD

Atom	Q (reactant)	Q (TS)	Q(near product)
C1	-0.0615	-0.0252	-0.0413
C2	-0.0692	-0.0663	-0.0394
C3 (eliminating)	+0.0250	-0.0123	-0.0575
C4 (eliminating)	+0.0187	-0.0795	-0.0626
C5 (eliminating)	+0.0182	-0.0667	-0.0392
C6 (eliminating)	+0.0244	-0.0129	-0.0572
C7	+0.0120	+0.0155	-0.0110
C8	-0.0535	-0.0788	-0.0630
C9	-0.0565	-0.0253	-0.0414
C10	+0.0129	+0.0163	-0.0109
H11 (bonded to C1)	+0.0363	+0.0344	+0.0350
H12 (bonded to C2)	+0.0330	+0.0364	+0.0332
H13 (bonded to C7)	+0.0045	+0.0249	+0.0373
H14 (bonded to C7)	+0.0003	+0.0112	+0.0386

H15 (bonded to C8)	+0.0268	+0.0361	+0.0351
H16 (bonded to C9)	+0.0247	+0.0344	+0.0349
H17 (bonded to C10)	+0.0073	+0.0251	+0.0375
H18 (bonded to C10)	-0.0091	+0.0110	+0.0386
H19 (bonded to C4)	+0.0045	+0.0362	+0.0350
H20 (bonded to C3)	+0.0018	+0.0244	+0.0335
H21 (bonded to C6)	-0.0032	+0.0244	+0.0334
H22 (bonded to C5)	+0.0022	+0.0366	+0.0331

In distorting the ground state geometry of dicyclopentadiene to the transition state geometry, few atoms undergo a noticeable change in partial atomic charge. The carbon atoms undergoing bond-breaking gain a significant amount of electron density going from reactant to transition state. In the case of the C3 carbon atom, it has an atomic charge of +0.0250 in the ground state, -0.0123 in the transition state. Similarly, for C4, C5 and C6 carbon atoms, the values of atomic charges in the ground state are +0.0187, +0.0182, +0.0244 whereas in the transition state geometry the values changes to -0.0795, -0.0667, -0.0129 respectively. The other significant change in the atomic charges is with the hydrogen atoms (H18 and H21) bonded to carbon atoms (C10, C6) losing a considerable amount of electron density while going from reactant to transition state. For hydrogen atoms, H18 and H21, the values of atomic charges in the ground state are -0.0091 and -0.0032 whereas for transition state geometry these values are +0.0110 and +0.0244 respectively.

There is a large transfer of electron density onto the carbon atoms (C4 and C5) in the transition state geometry, an increase in charge from +0.0187 to -0.0795 for C4 and +0.0182 to -0.0667 for C5. This suggests that the bond between C4 and C5 bond is likely to break first which can be identified in transition state geometry.

However, there is a little change in electron density on to carbon atoms C3 and C6 which can be characterized by a small change in atomic charges. This suggests that the bond between C3 and C6 will remain intact in transition state geometry.

There is a decrease in electron density on carbon atom C1 which goes from atomic charge -0.0615 to -0.0252 in the transition state geometry. In the case of C9, the atomic charge decreases from -0.0565 to -0.0253. For the remaining (C2, C7, C8, C10) carbon atoms there is not much change in electron density in the transition state geometry. The hydrogen atoms (H13 and H14) bonded to a carbon atom (C7) gain a significant amount of electron density which goes from atomic charge +0.0045 to +0.0249 for hydrogen atom H13 and +0.0003 to +0.0112 for hydrogen atom H14 respectively. Similarly, a hydrogen atom bonded to a carbon atom (C10) gains a considerable amount of electron density which goes from atomic charge +0.0073 to +0.0251 for the hydrogen atom (H17) and -0.0091 to +0.0110 for the hydrogen atom (H18).

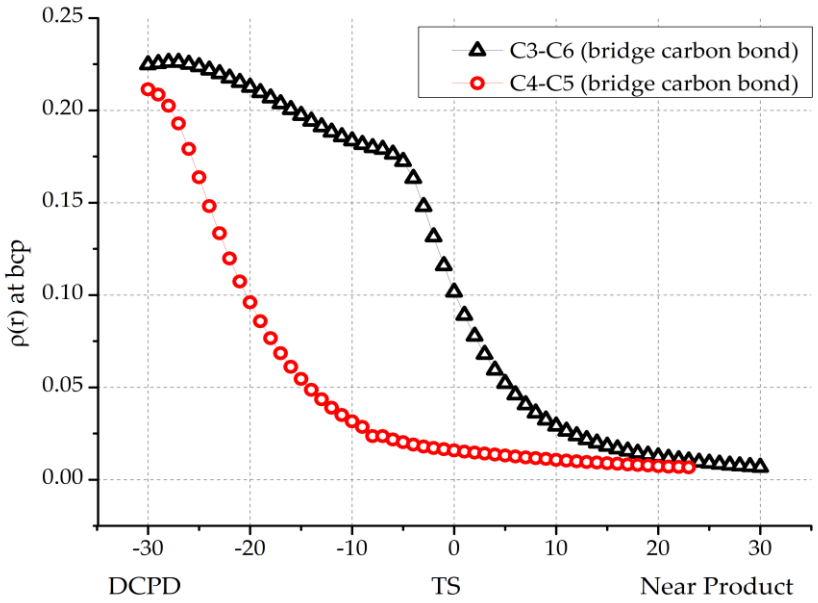

Figure 4.4 (a). *A plot of variation in electron density ρ(r) at the bond critical point (bcp) along the reaction coordinate.*

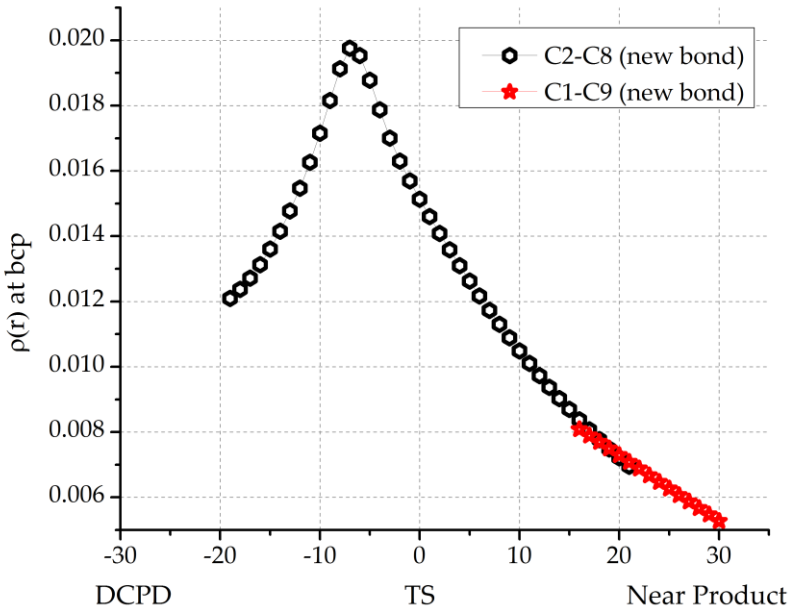

Figure 4.4 (b). *A plot of variation in electron density ρ(r) at the bond critical point (bcp) along the reaction coordinate.*

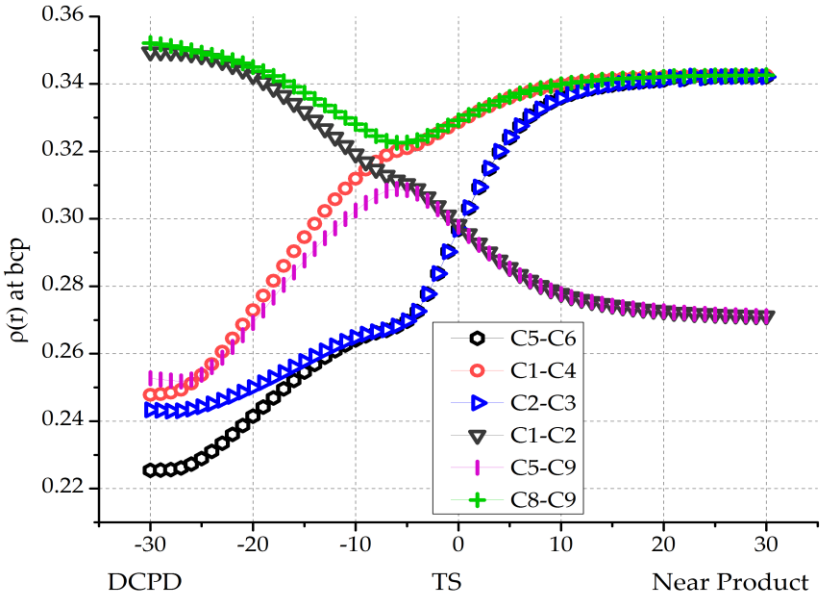

Figure 4.4 (c). *A plot of variation in electron density ρ(r) at the bond critical point (bcp) along the reaction coordinate.*

It is clear from Figure 4.4 (a) that the electron density at the bond critical point of the C4-C5 bond decreases exponentially while going from reactant to

transition state whereas the electron density at the bond critical point of C3-C6 bond decreases slowly from reactant to transition state and further decreases exponentially going towards the product. This suggests that the C3-C6 bond is still intact in a transition state whereas the C4-C5 bond is likely to break first. The appearance of new bonds C2-C8 and C1-C9 (see Figure 4.4 (b)) is characterized by a small value of electron density at the bond critical point suggest that the cleavage between bridge carbon atoms C4 and C5 has occurred with the formation of new bond C2-C8 whereas the breaking of the bond between carbon atoms C3 and C6 proceeds via formation of new bond C1-C9. Also, the value of electron density at the bond critical point of the C1-C2 bond decreases due to the migration of electron density on the C1-C4 and C2-C3 (see Figure 4.4 (c)). As a result it leads in the formation of double bonds between C1-C4 and C2-C3. Also, there is a migration of electron density from the carbon atoms C3 and C4 to the carbon atom C5 and C6 respectively (C3-C6 and C4-C5 bonds are undergoing break), the value of electron density at the bond critical point of C5-C6 increases resulting in the formation of a double bond between C5-C6. The electron density value at the bond critical point of the C5-C9 bond increases slowly from the value of 0.2527 to 0.3085 and thereafter decreases to a value of 0.2711 while going from reactant to near product geometry. Also, the electron density value at the bond critical point of the C8-C9 decreases slowly from the value of 0.3521 to 0.3225 and thereafter increases to a value of 0.3426 while going from reactant to near product geometry. Hence, there is no significant change in the the electron density value at the bond critical point of the C8-C9 bond.

To investigate the non-covalent interaction associated with small values of the reduced density gradient, we plotted the s versus ρ (see Figure 4.6 (a1), (b1),

(c1)). The reactant geometry (4.6 (a1)) represents the fundamental pattern of intramolecular interaction. The top left-side points correspond to the exponentially decreasing electron density region far from nuclei whereas the right-side points (electron density value greater than 0.21 and s=0) correspond to the covalent bond. Also, this plot exhibits a new feature that the spike corresponds to the low value of electron density, and gradient density is a characteristic feature of non-covalent interaction. The results are similar in the case of transition state geometry the only difference is being the covalent bonds are located at a higher value of electron density (ρ = 0.24). The presence of spikes in the low-density region with a low-density gradient value corresponds to the non-covalent interaction. In the case of near product geometry, the value of electron density for the covalent bond lies at ρ = 0.25.

This is illustrated in Figure 4.6 (a2, b2, and c2). It represents a plot of a reduced density gradient and a sign of (λ_2) multiplied by $\rho(r)$ correspond to the reactant, transition state, and near product geometry.

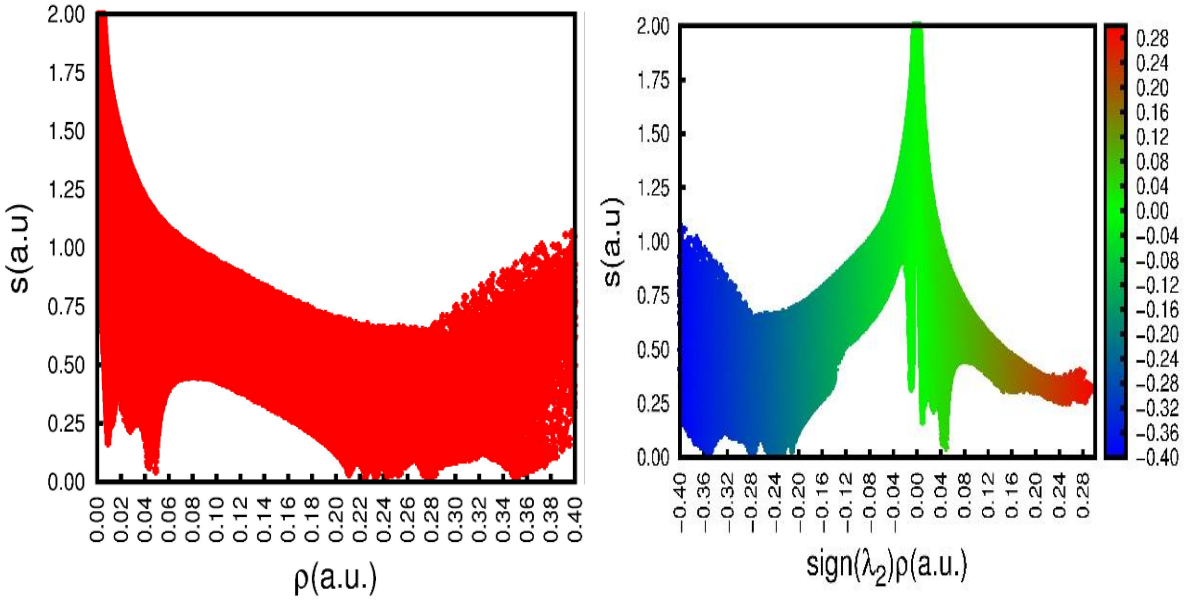

(a1) (a2)

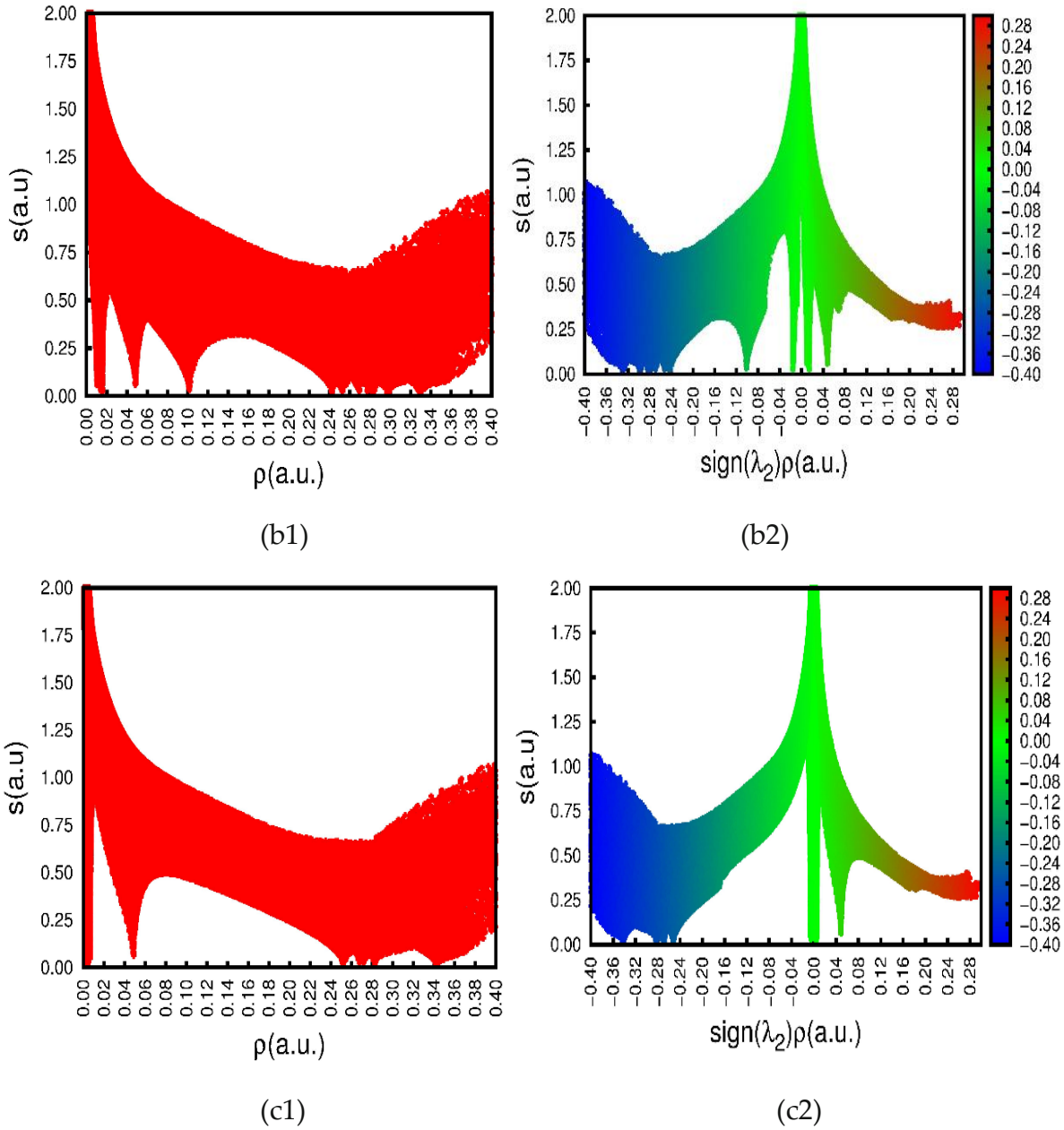

Figure 4.5. *The plot of the electron density and its reduced density gradient for (a1) DCPD (b1) TS (c1) near the product. The plot of the reduced density gradient versus the electron density ρ(r) multiplied by the sign of the second Hessian eigenvalue (a2) DCPD (b2) TS (c2) near the product.*

In the reactant geometry, there appears a spike on the sign of $(\lambda_2)\rho$ near zero which corresponds to the low-density gradient with a slightly positive value of λ_2.

This low density with low-density gradient spike for the molecular geometry with a slightly positive value shows a signature of weak interaction. This shows an indicative signature of very weak van der Waals interactions. For the large negative value of the sign of $(\lambda_2)\rho$, it represents the signature of attractive interactions (such as dipole-dipole or hydrogen bond). In case of a large and positive value of sign of $(\lambda_2)\rho$, the interaction is nonbonding. In the transition state geometry, two spikes present very near zero on both sides indicate very weak, van der Waals interactions. The spike located at negative (-0.10) value of sign of $(\lambda_2)\rho$, shows attractive interaction whereas the spike at slightly positive value sign of $(\lambda_2)\rho$, shows non-bonding interaction. In the case of near product geometry, a spike with a positive value sign of $(\lambda_2)\rho$, represents the nonbonding interaction.

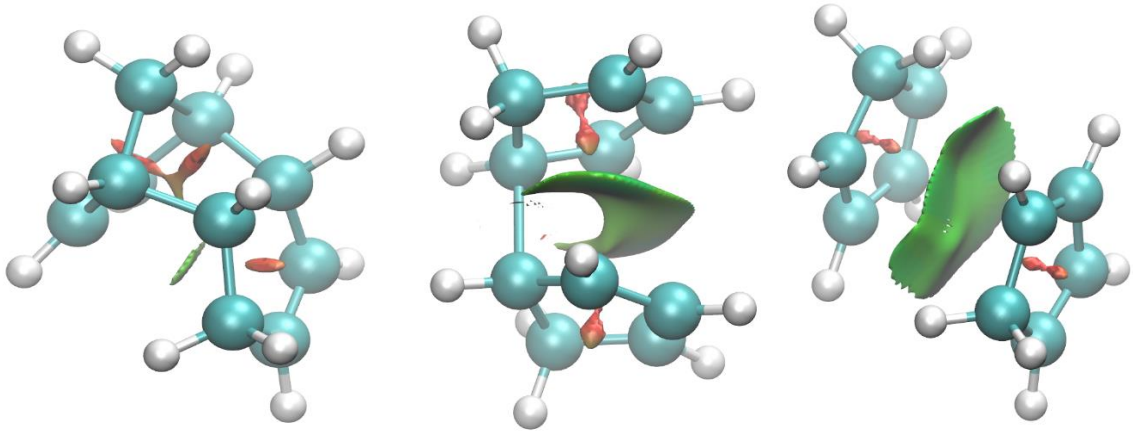

Figure 4.6. *Gradient isosurfaces for DCPD, transition state, and near product geometry.*

Figure 4.7 represents the low-density gradient isosurfaces for the DCPD, transition state, and near product geometry which corresponds to the constraint of low electron density. We choose the electron density cutoff of 0.06 ($\rho < 0.05$) since it covers the interaction region of non-bonded atoms. Also, the corresponding isovalue of the reduced density gradient is used as a diagnostic tool for non-covalent interaction. It is important to select the appropriate bound for

electron density and corresponding reduced density gradient which isolates the low electron density and reduced density gradient peak for the molecular system of interest. The location of the appearing peak is sensitive to many factors such as the level of theory used to obtain electron density, interaction strength, and type of atoms involved in the interaction. The gradient isosurfaces are represented in color according to the corresponding value of the sign, which signifies the extent of the interaction strength. The large, negative value of the sign (λ_2) is an indicative sign of attractive interaction whereas the positive value of λ_2 represents the nonbonding interaction. The values near zero are indicative of very weak interactions such as van der Waals interactions. The reduced density gradient isosurfaces provide rich information about the non-covalent interactions. In the case of the reactant geometry, the isosurfaces represented at the center of the ring signify the steric repulsion between the bridge carbon atoms whereas the isosurfaces lie in between the norbornene ring and cyclopentene ring shows repulsive interaction. For the transition state geometry, there is a region of non-covalent interaction at the center of two cyclopentadiene rings. This is another type of interaction where Π-stacking is expected. In the case of the near product geometry, the isosurfaces are similar to the transition state geometry.

4.6 CONCLUSION

In conclusion, the quantum theory of atoms in molecule (QTAIM) is used as a tool for studying the dissociation reaction of dicyclopentadiene to cyclopentadiene. AIM study shows that the dissociation is initiated by breaking on 1 C-C bond first and even at the TS only one of the two bridging bonds are broken. The electron density analysis along the reaction coordinate provides detailed information about the bond breaking and bond making process. At the

transition state, one of the C-C bonds between bridge carbon atoms is more elongated while the other C-C bond remains intact. Hence, none of the C-C bonds is broken in the transition state. Also, a new C-C bond is formed at the transition state characterized by a bond critical point that forms a cage-like structure. In addition, AIM analysis was used to identify various types of non-covalent interactions. Non-covalent interactions are highly nonlocal and characterized as low-density gradient isosurfaces with a low value of electron density. The sign of the λ_2 (second Hessian eigenvalue) is the key quantity to identify the types of interactions and strength will be determined from the value of density on the region of non-covalent interaction. This approach provides a detailed picture of various kinds of interactions such as van der Waal's interaction, hydrogen bonds, steric clashes, etc. DCPD shows the nonbonding interactions correspond to the positive value of sign of $(\lambda_2)\rho$. The transition state exhibit attractive as well as non-bonding interactions correspond to the negative and positive value of sign of $(\lambda_2)\rho$ respectively. Whereas near product geometry shows the nonbonding interactions correspond to a positive value sign of $(\lambda_2)\rho$. For DCPD, gradient isosurfaces represented at the center of the ring signify the steric repulsion between the bridge carbon atoms whereas the isosurfaces present in between the norbornene ring and cyclopentene ring shows repulsive interaction. For the transition state, isosurfaces show a region of non-covalent interaction at the center of two cyclopentadiene rings where Π-stacking is expected. In the case of the near product geometry, the isosurfaces are similar to the transition state geometry.

4.7 REFERENCES

1. C. F. Melius, M. E. Colvin, N. M. Marinov, W. J. Pit, and S. M. Senkan, International Symposium on Combustion, 26, 1, 1996, 685-692.
2. W. Tsang and A. Lifshitz, Annual Review of Physical Chemistry, 41, 1990, 559–599.
3. R. Sivaramakrishnan, R. S. Tranter, and K. Brezinsky, Journal of Physical Chemistry, 110, 2006, 9388–9399.
4. M. H. Back, Canadian Journal of Chemistry, 49, 13, 1971, 2199-2204.
5. M. R. Djokic, K. M. Van Geem, C. Cavallotti, A. Frassoldati, E. Ranzi, G. B. Marin, Combustion and Flame, 161, 2014, 2739–2751.
6. D. H. Kim, J. A. Mulholland, D. Wang, and A. Violi, Journal of Physical Chemistry A, 114, 47, 2010, 12411-12425.
7. J. D. Rule, J. S. Moore, Macromolecules, 35, 2002, 7878-7882.
8. S. Reshmi, E. Arunan, and C. P. Reghunadhan Nair, Industrial Engineering & Chemical Research, 53, 2014, 16612−16620.
9. G. Liu, Z. Mi, Li Wang, X. Zhang, and S. Zhang, Industrial Engineering & Chemical Research, 45, 2006, 8807-8814.
10. C. L. Parworth, M. K. Tucker, B. E. Holmes, and G. L. Heard, Journal of Physical Chemistry A, 115, 2011, 13133–13138
11. E. Espinosa, M. Souhassou, H. Lachekar, and C. Lecomte, Acta Crystallographica Section B, 55, 1999, 563-576.
12. S. J. Grabowski, Journal of Physical Chemistry A, 105, 2001, 10739-10748.
13. J. Contreras-García, E. R. Johnson, S. Keinan, R. Chaudret, J. P. Piquemal, D. N. Beratan, and W. Yang, Journal of Chemical Theory and Computation 7, 2011, 625–632.

14. C. A. Morrison, and M. M. Siddick, Angewandte Chemie International Edition England, 116, 2004, 4884-4893.

15. R. F. W. Bader, Atoms in Molecules - A Quantum Theory, Oxford University Press, Oxford, 1990. ISBN: 0198558651

16. R. F. W. Bader, P. L. A. Popelier and T. A. Keith, Angewandte Chemie, International Edition in English, 33, 1994, 620-632.

17. R. F. W. Bader, Physical Review B, 49, 1994, 13348-13359.

18. P. L. A. Popelier and R. F. W. Bader, Journal of Physical Chemistry, 98, 1994, 4473-4482.

19. R. F. W. Bader and T. A. Keith, Journal of Chemical Physics, 99, 1993, 3683-3694.

20. T. A. Keith and R. F. W. Bader, Journal of Chemical Physics, 99, 1993, 3669-3676.

21. C. Chang and R. F. W. Bader, Journal of Physical Chemistry, 96, 1992, 1654-1668.

22. K. B. Wiberg, R. F. W. Bader, and C. D. H. Lau, Journal of American Chemical Society, 109, 1987, 985-998.

23. E. R. Johnson, S. Keinan, P. Mori-Sanchez, J. Contreras-Garcıa, A. J. Cohen, and Weitao Yang, Journal of American Chemical Socicty, 132, 2010, 6498–6506

24. D. R. Salahub, and R. P. Messmer, Journal of Chemical Physics, 64, 1994, 2039- 2048.

25. S. Liu, C. Ruspic, P. Mukhopadhyay, S. Chakrabarti, P. Y. Zavalij, and L. J. Isaacs, American Chemical Society, 127, 2005, 15959-15968.

26. T. B. Richardson, S. de Gala, R. H. Crabtree, and P. E. M. Siegbahn, Journal of American Chemical Society, 117, 1995, 12875-12883.

27. M. P. Brown, and R.W. Heseltine, Chemical Communication (London) 23, 1968, 1551-1559.

5

MEASUREMENT OF IGNITION DELAY TIMES OF DICYCLOPENTADIENE

CHAPTER OVERVIEW

This chapter discusses the measurement of ignition delay of dicyclopentadiene in a modified chemical shock tube (CST3). The ignition delay measurement were carried out for three different equivalent ratios 0.5, 1, and 1.5 when the 0.5 % of DCPD was seeded with argon. Furthermore, a detailed kinetic mechanism was developed for a detailed understanding of the elementary steps involved. In addition, a comparison was made between the calculated and experimental observed ignition delays.

5.1 INTRODUCTION

The shock tube is one of the well-characterized thermal reactors to carry out ignition delay (typically less than 2 ms) measurement study on fuel [1]. Initially, the experiments of ignition delay time measurement were carried out to compare the efficiencies of various fuels [2]. Later, ignition delay can be used as an important parameter for designing the combustor of supersonic vehicles such as SCAMJET, RAMJET, etc. [3]. Researchers across the world are using the shock tube for ignition delay times measurement of the fuel which will help to derive a kinetic mechanism for further understanding of the fuel oxidation process [4-8]. In particular, ignition delay measurement studies on kerosene-based hydrocarbon fuel are being carried out with its application in understanding the extent of heat sink for thermal protecting system (TPS) [9]. Initially, the spectroscopic technique adapted for measurement of ignition delay times was limited to CH emission, measured at 431.5 nm. With the advances in technology sink with spectroscopy, it is possible to measure other species including OH, H, and C_2 for the determination of ignition delay.

The ignition delay of the fuel can be defined as the time delay between the moment of providing heat (energy) to the fuel and the onset of the ignition process. However, the definition of ignition delay time varies depending upon the starting point of ignition hence the experimental definition of ignition delay time is not unique. The variation in the measurement of ignition delay mainly depends upon the methods being used for measurement such as pressure rise due to the ignition of the fuel, ignition delay measurement based upon absorption and emission of the species under consideration. In the case of the shock tube, the arrival of the incident shock wave to the end wall of the driven section is considered to be the

starting point of the ignition process. The ignition delay time in the range of 100 μsec to 2 ms could be measured in our shock tube. A typical pressure trace obtained in the ignition of DCPD is shown in Figure 5.1. At higher temperatures, the pressure rise due to ignition of the fuel is abrupt and the ignition delay can be defined easily as the difference between the arrival of the reflected shock wave and the onset of the ignition. However, at lower temperatures the pressure rise due to ignition of the fuel is gradual and the definition of the ignition delay is not consistent. Ignition delay, using the emission signal can also be defined as the time difference between the arrival of reflected shock and the time at which radical (CH/OH) just start coming characterized by the appearance of its emission spectrum. As shown in Figure 5.2 the value of ignition delay, ID can be defined as the time difference between the arrival of reflected shock wave and the time taken for CH or OH species to reach their peak concentration [9].

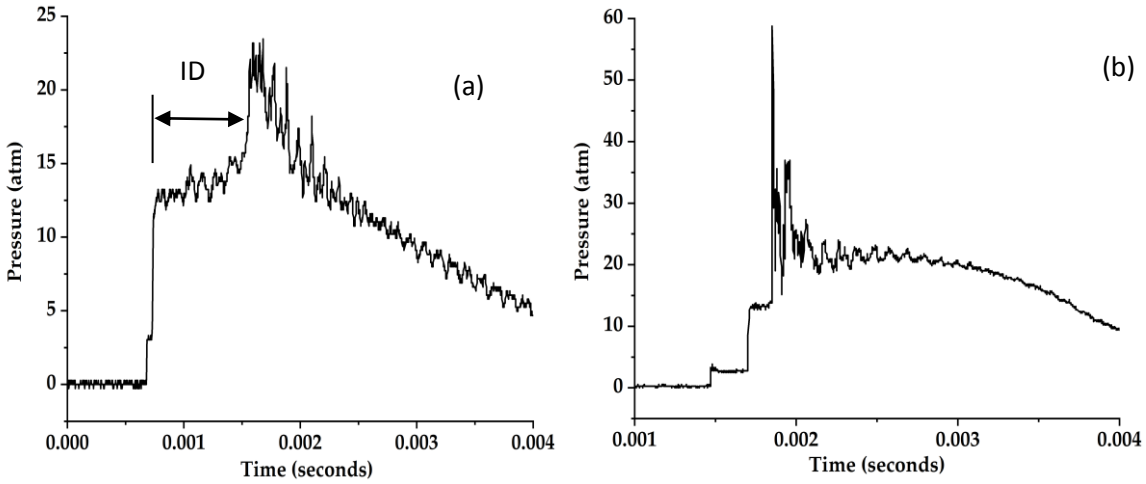

Figure 5.1: *Typical pressure trace obtained in the ignition delay times measurement of DCPD (a) Pressure trace obtained in ignition delay times measurement at low temperature where pressure rise is gradual due to combustion. (b) Pressure trace obtained in ignition delay times measurement at high temperature where pressure rise is abrupt due to combustion.*

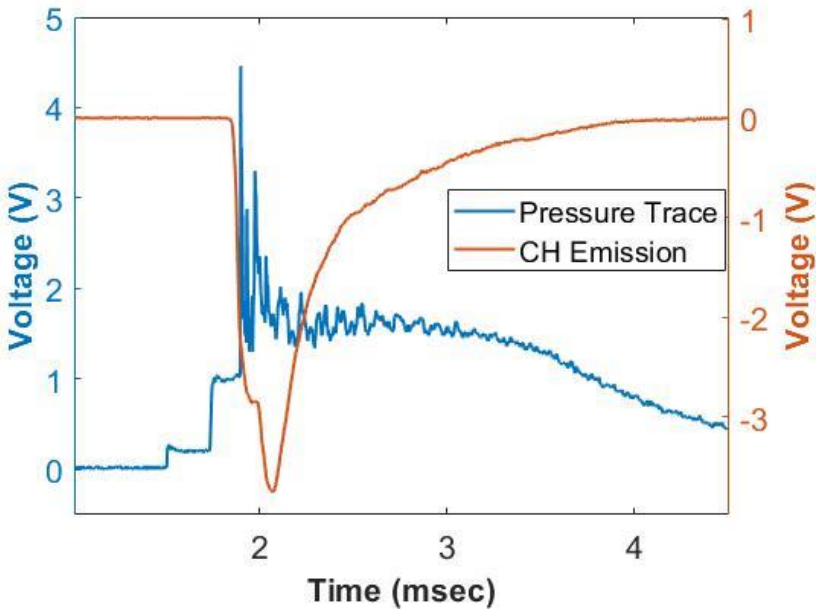

Figure 5.2: *Typical pressure trace obtained in the ignition delay times measurement of DCPD.*

The kinetics of JP-10 (exo-tetrahydro dicyclopentadiene $C_{10}H_{16}$), a kerosene-based hydrocarbon that is currently used as aviation fuel has been well established. JP-10 (an endothermic fuel) [10] has been of great interest in the area of combustion due to its high volumetric density compared to other kerosene-based hydrocarbon fuels. This is being used as a propellant in missiles, supersonic-combustion ramjets, etc. As JP-10 is a single component fuel, the detailed kinetic mechanism for pyrolysis and oxidation study becomes simpler. Previously, many studies have been reported to investigate the oxidation of JP-10 [11-12]. The major disadvantage of JP-10 is its slow oxidation kinetics i.e. the ignition delay times measurement in the oxidation of JP-10 is large. Dicyclopentadiene ($C_{10}H_{12}$) which is a homodimer of the cyclopentadiene (C_5H_6) can be obtained by dehydrogenation of jet fuel (JP-10). Relevant thermodynamic properties of the JP-10 and DCPD fuels are summarized in Table 5.1.

Table 5.1: Thermodynamic properties of JP-10 and DCPD fuels

Sr. no	Fuel	Density g/cc	ΔH_f (kcal/mol)
1	JP-10	0.94	10.3
2	DCPD	0.98	-50.6

Over the past decades, dicyclopentadiene (DCPD), has been researched for use as a potential binder in the composite solid propellant formulation. The binder of a composite solid propellant is very important in defining the mechanical, combustion, and ballistic characteristics of a propellant. The binder provides stability to the composite and good mechanical properties (binding fuel and oxidizer) to the solid propellant grain. Currently, in all composite solid propellants, polymers perform the important role of the binder for the oxidizer, metallic fuel, and other additives. Hydroxyl-terminated polybutadiene (HTPB) is the most versatile binder which is commonly used in the composite solid propellant. However, the curing of HTPB with diisocyanates (tolylene diisocyanate or isophorone diisocyanate) is highly influenced by the presence of moisture which leads to degradation in the properties of the propellant. In addition, the high reactivity of the isocyanate group limits the pot life of the propellant. Also, the incompatibility of isocyanates with energetic oxidizers such as ammonium dinitramide (ADN) and hydrazinium nitroformate (HNF) requires finding new cure methodologies for processing high energy propellants using HTPB as a binder [13]. DCPD is capable of undergoing ring opening metathesis polymerization (ROMP) to form a highly crossed linked polymeric structural network that imparts good mechanical strength [14]. The relevant thermodynamic properties of HTPB and DCPD are found in Table 3.1.

This study involved a detailed investigation of the ignition delay of DCPD to address the above problem. For the derivation of the oxidation mechanism of the fuel, it is necessary to have prior knowledge about the pyrolysis of the fuel. The DCPD oxidation mechanism has been derived using pyrolysis of DCPD which was discussed in chapter 3. To our knowledge, no literature is available on the oxidation mechanism of dicyclopentadiene.

Equation 5.1 shows the correlation between the ignition delay and the temperature which can be used to calculate the activation barrier for ignition of fuel at a particular equivalence ratio.

$$\tau = A.e^{\frac{E_a}{RT}} \qquad \ldots\ldots 5.1$$

Here, τ = Ignition delay of the fuel

T = Reflected shock temperature

A = Pre-exponential factor

E_a = Ignition activation energy barrier

5.2 EXPERIMENTAL SETUP

Chemical shock tube 3 (CST-3) has been used to carry out ignition delay times measurement of dicyclopentadiene. The schematic diagram and details of CST-3 used for the present investigation have been described in chapter 2. Details of the experimental setup and its calibration are also described in chapter 2. Before each run, the test section of the shock tube was pumped down to 10^{-7} mbar. A separate tank of a capacity of 9 lit was maintained at a temperature of 353 K which is used to prepare DCPD, oxygen, and argon mixture in different equivalence ratios. The premixed mixture was then fed to the test section of the shock tube. The temperature of the test section was also maintained at 353 K to prevent the condensation of the sample on the wall. A typical experimental signal recorded

using a digital storage oscilloscope is presented in Figure 5.2. The Figure represents the measurement of ignition delay obtained using CH emission as well as recorded using pressure signal. The ignition delay from the pressure signal was measured using a PCB sensor located 5 mm away from the end wall of the driven section.

DCPD obtained from Sigma Aldrich (purity > 99.0%) was used to carry out the experimental study. The premix mixture of DCPD seeded with argon was used for the measurement of the ignition delay of DCPD. Ignition delay of DCPD was performed for three equivalent ratios namely 0.5, 1, and 1.5. Each set of experiments (ϕ = 0.5, 1, and 1.5) was performed at the same concentration of DCPD. The mole fraction of DCPD and O_2 used in each set of experiments is summarized in Table 5.2.

Table 5.2: Mole fraction of DCPD and O_2.

Sr. no	Equivalence ratio	Mole fraction of DCPD	Mole fraction of O_2
1	Φ= 0.5	0.005053	0.129787
2	Φ=1.0	0.007142	0.092857
3	Φ=1.5	0.008347	0.072285

5.3 RESULT AND DISCUSSION

The ignition delay experiments for DCPD/O_2/Ar were carried out for the temperature ranging from 1192 K to 1490 K. The observed pressure was in the range of 12.8 - 21.8 atm. In the above-mentioned conditions, the ignition delay of the DCPD was found to vary from 64 to 1230 μs. One of the pressure signals obtained in stoichiometric DCPD/O_2/Ar experiments is shown in Figure 5.2. The result of ignition delay on DCPD has been summarized in Table 5.3.

Table 5.3: Experimental data for ignition delay of DCPD

Equivalence ratio ϕ = 0.5				Equivalence ratio ϕ = 1.0				Equivalence ratio ϕ = 1.5			
Sr no.	T_5 (K)	P_5 (atm)	τ (μs)	Sr no.	T_5 (K)	P_5 (atm)	τ (μs)	Sr no.	T_5 (K)	P_5 (atm)	τ (μs)
1	1192	21.2	1230	1	1241	14.7	1110	1	1258	14.2	1180
2	1205	21.8	1080	2	1254	14.7	970	2	1269	14.1	1170
3	1205	12.8	1040	3	1260	13.3	1280	3	1280	14.2	1030
4	1229	13.0	756	4	1267	16.2	860	4	1293	13.4	820
5	1241	13.2	704	5	1267	15.6	920	5	1329	13.9	716
6	1254	13.0	610	6	1280	15.0	816	6	1368	18.4	580
7	1254	13.4	432	7	1294	15.9	770	7	1368	14.7	510
8	1267	14.0	504	8	1294	15.0	632	8	1368	14.7	480
9	1280	16.8	380	9	1294	15.3	710	9	1381	14.4	470
10	1294	14.4	380	10	1336	16.3	408	10	1395	15.8	370
11	1307	14.9	320	11	1336	15.7	400	11	1422	15.7	272
12	1307	14.3	308	12	1350	18.0	310	12	1437	14.3	280
13	1321	17.1	240	13	1380	17.5	276	13	1437	19.8	220
14	1321	15.5	244	14	1396	18.3	212	14	1482	20.7	90
15	1321	17.3	192	15	1411	18.1	180				
16	1336	17.4	236	16	1444	18.5	160				
17	1336	18.5	252	17	1444	19.2	136				
18	1336	16.5	232								
19	1336	16.2	220								
20	1336	17.1	244								
21	1350	18.4	208								
22	1350	18.5	224								
23	1396	18.9	120								
24	1411	18.7	96								
25	1427	18.8	96								
26	1444	20.0	74								
27	1461	21.4	64								

It has been found that for a particular equivalence ratio, with an increase in reflected shock temperature ignition delay decreases which is shown in Figure 5.3. Also, it is clear that the ignition delay increases with an increase in the concentration of DCPD and decreases with an increase in the concentration of oxygen. A plot showing the variation of ignition delay with temperature for three different equivalence ratios is presented in Figure 5.3. The data plotted were

linearly fitted to obtain A and E_a which is represented in equation 5.1. The pre-exponential factor and activation energy corresponding to the different equivalence ratios are summarized in Table 5.4. When it is compared with JP-10, the activation energy was found to be 36.92 kcal/mol by Harish et al. [15] in the temperature range 1300-1675 K and pressure range 15-20 atm. The activation energy of JP-10 by Davidson et al. [16] was found to be 54.0 kcal/mol in the temperature range of 1200-1700 K for a pressure range of 1-9 atm.

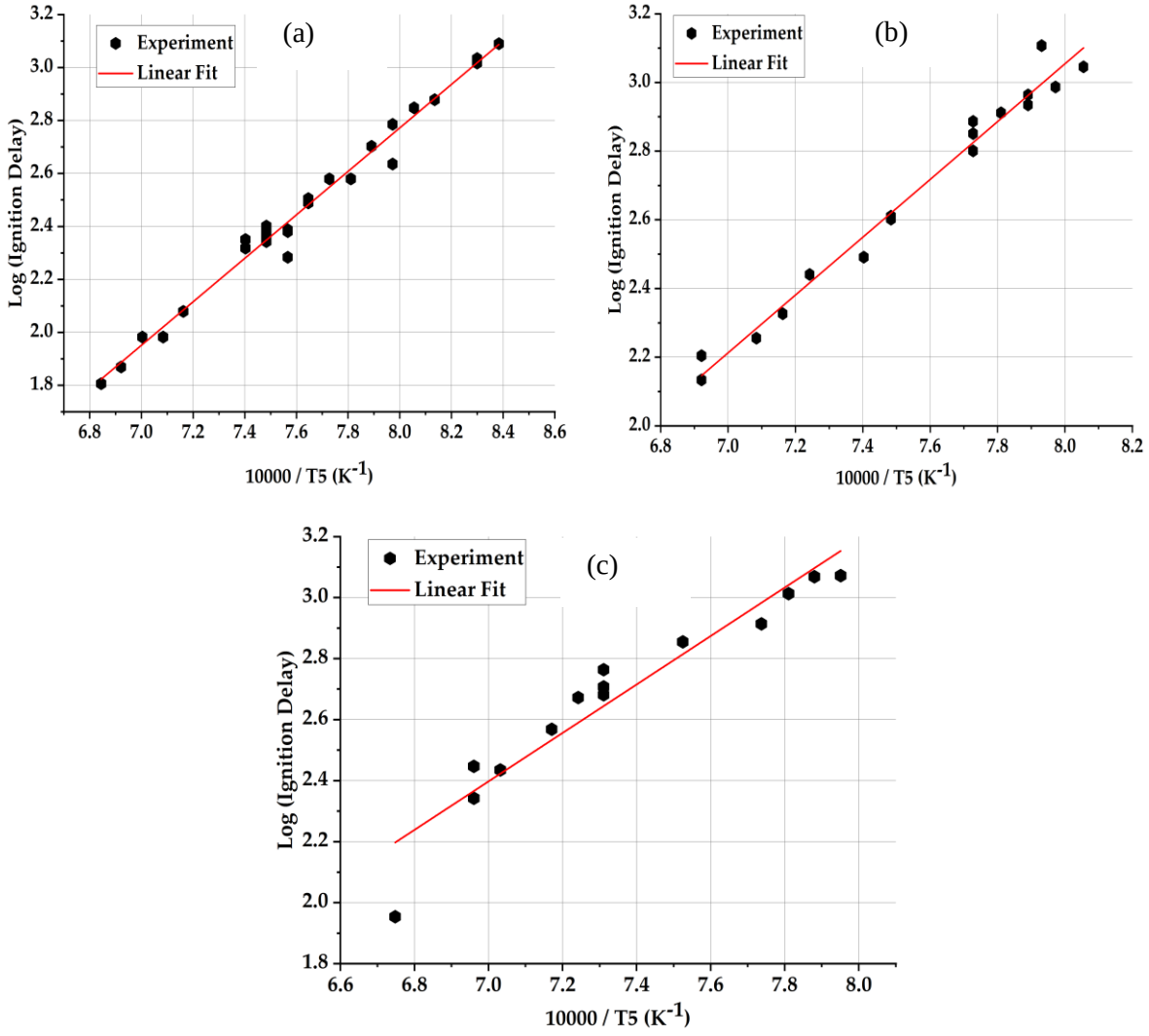

Figure 5.3: *Plot showing the variation of ignition delay of DCPD with temperature (a) ϕ = 0.5 (b) ϕ = 1.0 (c) ϕ = 1.5*

Table 5.4: Activation Energy and Pre-exponential factor for DCPD and JP-10.

Sr no	Fuel	Equivalence ratio	A (sec)	E_a (kcal/mol)	References
1	DCPD	Φ = 0.5	$10^{-7.28\pm0.14}$	38.51±0.87	Present work
2	DCPD	Φ = 1.0	$10^{-8.47\pm0.11}$	37.58±0.62	Present work
3	DCPD	Φ = 1.5	$10^{-8.74\pm0.18}$	36.34±1.10	Present work
4	JP-10	Φ = 1.0	$10^{-16.61\pm0.32}$	36.92±1.80	15
5	JP-10	Φ = 1.0	$10^{-15.54}$	54.00	16

5.4 OXIDATION MECHANISM

DCPD can be used as a fuel and there is a need for an oxidation mechanism to explain the observed experimental ignition delay. As discussed earlier, the oxidation mechanism for DCPD at high temperature and high pressure does not exist in the literature. The ignition delay times are usually used to derive the oxidation mechanism. To derive the oxidation mechanism of DCPD, we used the kinetic model for the oxidation of cyclopentadiene derived by Butler as an initial step, knowing that a very little amount of DCPD remains after passing the incident shock wave. The original kinetic model developed by Butler et al. [17] consists of 719 reactions with 153 species. We refine this kinetic model to fit the observed ignition delay and eliminated all the reactions involving naphthyl radical ($C_{10}H_7$) as we have not observed the naphthalene as a product during the pyrolysis of DCPD.

The constant volume method available in the closed homogeneous reactor model in CHEMKIN was used to simulate the mechanism. The entire mechanism given in Table 5.5 was simulated for each temperature and pressure given in Table 5.3. We have used 153 species and 651 reactions in the kinetic mechanism. In the oxidation mechanism, for the reaction, cy-C_5H_6 = cy-C_5H_5 +H, we used the rate expression k = 1.10 x 10^{15} exp (-77023/RT) [18] which gave a satisfactory result

whereas in the case of pyrolysis we used the expression k = 2.0 x 10^{15} exp (-81000/RT) [19]. The kinetics of the reactions of cyclopentadienyl radical with H, OH, HO_2, O, and O_2 are well established in the study by Zhong and Bozzelli [27]. They computed pressure-dependent rate constants for each channel using bimolecular quantum Rice Ramsperger Kassel, QRRK, for k(E) with a modified strong collision approach for falloff. Robinson and Lindstedt [29] studied the reactions of cyclopentadienyl radical with OH, HO_2, O, and O_2.

Butler et al [30] carried out CPD oxidation in a plug flow reactor. The addition of an O atom to the double bond of CPD is exothermic and producing a potentially large number of products. It leads to the formation of CO and either 1,3-butadiene or 3-methyl cyclopropene. 3-methyl cyclopropane is unstable under reaction conditions and has not been detected as an oxidative product. The addition reaction of the H atom to CPD results in stabilization of adduct followed by ring-opening or fragmentation leading to the formation of acetylene (C_2H_2) and allyl radical (C_3H_5). The recombination of two CPDs leads to the formation of 1,2-dihydro naphthalene or phenyl-C_4H_5. The oxidation results showed the reaction between CPD and CPDyl radicals occurs via 19 different pathways producing 1,2-dihydro naphthyl, indene, and methyl, or benzene and n-C_4H_5 radical. Methyl addition to CPD yields chemically activated 5-methyl cyclopentadiene which isomerizes to 1- or 2-methyl cyclopentadiene. 1- or 2-methyl cyclopentadiene forms early in the combustion environment and subsequently decompose whereas benzene continues to grow in the reaction. The reaction of O atom with CPDyl radical leading to the formation of C_5H_5O (expoxidyl) intermediate which can easily form 2,4-cyclopentadienoxy radical. The ring-opening of 2,4-cyclopentadienoxy (c-C_5H_5O) radical via β-scission plays a key role to form linear

products. The oxidation of CPDyl radical leads to the formation of either CO and a C_4 (or two C2's), or acetylene and a propenal-3-yl radical. Although cyclopentadienone (CPDone) has been assumed to be an important intermediate formed, it has not been observed in the combustion environment. During the oxidation of CPD, the concentration of benzene increases than those seen during pyrolysis of CPD. The concentrations of methyl cyclopentadienes, 1,3-butadiene, vinyl acetylene, C_3, and C_2 were observed considerably higher than those in pyrolysis experiments. The higher methyl concentration observed in oxidation under lean conditions resulting in a slight increase in benzene concentration which is an unusual result observed for nominal pyrolysis products. The relative concentrations of propenal (C_2H_3CHO) decrease with increasing initial concentration.

Table 5.5: Proposed Oxidation Mechanism for DCPD

Sr no.	Reaction	A	n	E*a*	Reference
R1	$C_{10}H_{12}$=cy-C_5H_6 + cy-C_5H_6	3.36E+19	-1.2	38654	28
R2	C_9H_7+O=C_9H_7O	1.00E+13	0.0	0	20
R3	C_9H_8+OH=C_9H_7+H_2O	3.43E+09	1.2	-447	20
R4	C_9H_8+H=C_9H_7+H_2	2.19E+08	1.8	3011	20
R5	C_9H_8+O=C_9H_7+OH	1.81E+13	0.0	3081	20
R6	C_9H_8+HO_2=C_9H_7+H_2O_2	1.99E+12	0.0	11705	20
R7	C_9H_7+H=C_9H_8	1.00E+14	0.0	0	20
R8	A1C_2H_2-N+H=A1C_2H_3	2.00E+13	0.0	0	20
R9	A1C_2H_2-N=A1C_2H+H	1.30E+41	-8.7	11005	20
R10	A1+C_2H_2=A1C_2H_2-N	7.00E+38	-8.0	3921	20
R11	$C_6H_4C_2H$+H=A1C_2H	4.20E+11	0.5	-72	20
R12	A1C_2H+OH=$C_6H_4C_2H$+H_2O	2.10E+13	0.0	0	20
R13	A1C_2H+OH=A1H+HCCO	1.00E+13	0.0	0	20
R14	A1C_2H+H=$C_6H_4C_2H$+H_2	5.00E+13	-0.5	1500	20
R15	A1C_2H+H=A1+C_2H_2	2.50E+14	-0.5	1500	20
R17	A1C_2H_5=A1CH_2+CH_3	2.00E+15	0.0	72735	20

R18	$A1C_2H_5+H=A1C_2H_3+H_2+H$	8.00E+13	0.0	8239	20
R19	$A1C_2H_5+OH=A1C_2H_3+H_2O+H$	8.43E+12	0.0	2584	20
R20	$A1C_2H_5+O_2=A1C_2H_3+HO_2+H$	2.00E+14	0.0	41420	20
R21	$A1CH_3+O=OA1CH_3+H$	1.63E+13	0.0	3149	20
R22	$OA1CH_3+H=HOA1CH_3$	2.50E +14	0.0	0	20
R23	$OA1CH_3=A1H+H+CO$	2.51E+11	0.0	43921	20
R24	$HOA1CH_3+OH=OA1CH_3+H2O$	6.00E+12	0.0	0	20
R25	$HOA1CH_3+H=OA1CH_3+H2$	1.15E+14	0.0	12406	20
R26	$HOA1CH_3+H=A1CH_3+OH$	2.21E+13	0.0	7913	20
R27	$HOA1CH3+H=A1OH+CH_3$	1.20E+13	0.0	5150	20
R28	$A1CH_2+H=A1CH_3$	1.80E+14	0.0	0	20
R29	$A1CH_3+H=A1CH_2+H_2$	1.20E+14	0.0	8239	20
R30	$A1CH_3+H=A1H+CH_3$	1.20E+13	0.0	5150	20
R31	$A1CH_3+OH=A1CH_2+H_2O$	1.26E+13	0.0	2584	20
R32	$A1CH_3+CH_3=A1CH_2+CH_4$	3.16E+11	0.0	9504	20
R33	$A1CH_3+A1=A1H+A1CH_2$	2.10E+12	0.0	4402	20
R34	$A1CH_2+A1OH=A1CH_3+A1O$	1.05E+11	0.0	9504	20
R35	$A1CH_2+A1CHO=A1CH_3+A1CO$	2.77E+03	2.8	5775	20
R36	$A1CH_3=A1+CH_3$	1.40E+16	0.0	99848	20
R37	$A1CH_2+OH=A1CH_2OH$	6.00E+13	0.0	0	20
R38	$A1CH_2OH+H=A1CHO+H_2+H$	8.00E+13	0.0	8239	20
R39	$A1CH_2OH+H=A1H+CH_2OH$	1.20E+13	0.0	5150	20
R40	$A1CH_2OH+OH=A1CHO+H_2O+H$	8.43E+12	0.0	2584	20
R41	$A1CH_2OH+O_2=A1CHO+HO_2+H$	2.00E+14	0.0	41420	20
R42	$A1CH_2OH+A1=A1CHO+A1H+H$	1.40E+12	0.0	4402	20
R43	$A1CH_2+O=A1CHO+H$	2.50E+14	0.0	0	20
R44	$A1CH_2+O=A1+CH_2O$	8.00E+13	0.0	0	20
R45	$A1CH_2+HO_2=>A1+CH_2O+OH$	8.00E+13	0.0	0	20
R46	$A1CHO+H=A1CO+H_2$	5.00E+13	0.0	4930	20
R47	$A1CHO+H=A1H+CHO$	1.20E+13	0.0	5150	20
R48	$A1CHO+O=A1CO+OH$	9.04E+12	0.0	3079	20
R49	$A1CHO+OH=A1CO+H_2O$	1.71E+09	1.2	-447	20
R50	$A1CHO+O_2=A1CO+HO_2$	1.02E+13	0.0	38969	20
R51	$A1CHO+CH_3=A1CO+CH_4$	2.77E+03	2.8	5775	20
R52	$A1CHO+A1=A1CO+A1H$	7.01E+11	0.0	4402	20

R53	A1CO=A1+CO	3.98E+14	0.0	29414	20
R54	A1OH+H=A1H+OH	2.21E+13	0.0	7913	20
R55	A1OH+H=A1O+H_2	1.15E+14	0.0	12406	20
R56	A1OH+O=A1O+OH	2.81E+13	0.0	7355	20
R57	A1OH+OH=A1O+H_2O	6.00E+12	0.0	0	20
R58	A1OH+C_2H_3=A1O+C_2H_4	6.00E+12	0.0	0	20
R59	A1OH+C_4H_5-N=A1O+C_4H_6	6.00E+12	0.0	0	20
R60	A1O+cy-C_5H_6=A1OH+cy-C_5H_5	3.16E+11	0.0	8003	20
R61	A1OH+A1=A1H+A1O	4.91E+12	0.0	4402	20
R62	A1O+H=A1OH	2.50E+14	0.0	0	21
R63	A1H+O=A1O+H	2.78E+13	0.0	4912	21
R64	A1+O_2=A1O+O	2.09E+12	0.0	7473	21
R65	A1O=cy-C_5H_5+CO	2.51E+11	0.0	43923	21
R66	A1H+H=A1+H_2	2.50E+14	0.0	16007	21
R67	A1H+OH=A1+H_2O	2.11E+13	0.0	4572	21
R68	A1H+O_2=A1+HO_2	6.30E+13	0.0	60029	21
R69	A1+H=A1H	2.20E+14	0.0	0	21
R70	cy-C_5H_6+O=cy-C_5H_5+OH	1.81E+13	0.0	3081	21
R71	cy-C_5H_6+OH=cy-C_5H_5+H_2O	3.43E+09	1.2	-447	21
R72	cy-C_5H_6+HO_2=cy-C_5H_5+H_2O_2	1.99E+12	0.0	11665	21
R73	C_5H_4OH=C_5H_4O+H	2.10E+13	0.0	48023	21
R74	C_5H_4O=>C_2H_2+C_2H_2+CO	1.00E+15	0.0	78038	21
R75	HOA1CH_3+A1CH_2=OA1CH_3+A1CH_3	1.05E+11	0.0	9504	21
R76	A1CH_2OH+A1CH_2=A1CHO+A1CH_3+H	2.11E+11	0.0	9504	21
R77	C_2H_3CHO+cy-C_5H_5=C_2H_3CO+cy-C_5H_6	7.11E+11	0.0	18058	21
R78	C_2H_3CHO+cy-C_5H_5=CHCHCHO+cy-C_5H_6	3.56E+11	0.0	26863	21
R79	A1C_4H_5+cy-C_5H_5=$C_6H_4C_4H_5$+cy-C_5H_6	3.56E+11	0.0	28664	21
R80	A1C_4H_5+cy-C_5H_5=A1C_4H_4-4+cy-C_5H_6	3.56E+11	0.0	28664	21
R81	A1C_2H_3+cy-C_5H_5=A1C_2H_2-I+cy-C_5H_6	1.78E+11	0.0	19959	21
R82	A1C_2H_3+cy-C_5H_5=A1C_2H_2-N+cy-C_5H_6	3.56E+11	0.0	26863	21
R83	A1C_2H_3+cy-C_5H_5=$C_6H_4C_2H_3$+cy-C_5H_6	3.56E+11	0.0	26863	21
R84	$C_5H_5CH_3$-1+OH=$C_5H_4CH_3$+H_2O	2.36E+13	0.0	-800	21
R85	$C_5H_5CH_3$-1+cy-C_5H_5=$C_5H_4CH_3$+cy-C_5H_6	1.42E+12	0.0	18058	21
R86	C_4H_5-I+cy-C_5H_6=C_4H_6-12+cy-C_5H_5	1.21E+12	0.0	7503	21
R87	$C_5H_5CH_3$-2+OH=$C_5H_4CH_3$+H_2O	2.36E+13	0.0	-800	21

R88	$C_5H_5CH_3$-2+cy-C_5H_5=$C_5H_4CH_3$+cy-C_5H_6	1.42E+12	0.0	18058	21
R89	$C_5H_5CH_3$-5+OH=$C_5H_4CH_3$+H_2O	1.18E+13	0.0	-800	21
R90	$C_5H_5CH_3$-5+cy-C_5H_5=$C_5H_4CH_3$+cy-C_5H_6	7.11E+12	0.0	18058	21
R91	C_5H_6O-2+O=>CO_2+C_2H_4+C_2H_2	3.00E+13	0.0	0	21
R92	C_5H_6O-2+cy-C_5H_5=C_5H_5O-13+cy-C_5H_6	3.56E+11	0.0	18659	21
R93	C_5H_6O-2+cy-C_5H_5=C_5H_5O-14+cy-C_5H_6	3.56E+11	0.0	19959	21
R94	C_5H_6O-3+cy-C_5H_5=C_5H_5O-13+cy-C_5H_6	7.11E+11	0.0	18659	21
R95	C_4H_6-1+cy-C_5H_5=C_4H_5-121+cy-C_5H_6	3.56E+11	0.0	18659	21
R96	C_4H_6-12+cy-C_5H_5=C_4H_5-121+cy-C_5H_6	1.78E+11	0.0	18659	21
R97	C_4H_6-12+cy-C_5H_5=C_4H_5-123+cy-C_5H_6	3.56E+11	0.0	18659	21
R98	C_4H_6-2+cy-C_5H_5=C_4H_5-123+cy-C_5H_6	1.07E+12	0.0	18659	21
R99	A1C_4H_5+H=A1H+C_4H_5-N	1.20E+13	0.0	5150	21
R100	A1C_4H_5+H=A1C_4H_4-4+H_2	3.17E+13	0.0	14807	21
R101	A1C_4H_5+H=$C_6H_4C_4H_5$+H_2	3.17E+13	0.0	14807	21
R102	A1C_4H_5+OH=A1C_4H_4-4+H_2O	5.90E+12	0.0	8003	21
R103	A1C_4H_5+OH=$C_6H_4C_4H_5$+H_2O	5.90E+12	0.0	8003	21
R104	A1C_4H_4-4=A1C_2H_2-N+C_2H_2	4.00E+13	0.0	39519	21
R105	A1C_4H_4-4=$C_6H_4C_4H_5$	2.19E+13	0.0	15807	21
R106	C_9H_{10}+H=C_9H_9+H_2	9.35E+13	0.0	7903	21
R107	C_9H_{10}+OH=C_9H_9+H_2O	1.77E+13	0.0	1100	21
R108	C_9H_{10}+cy-C_5H_5=C_9H_9+cy-C_5H_6	1.07E+12	0.0	19909	21
R109	C_9H_9=C_9H_8+H	2.40E+13	0.0	45432	21
R110	C_9H_8O=>A1C_2H_3+CO	8.00E+15	0.0	73846	21
R111	C_9H_8O+O=>CO_2+A1C_2H_3	3.00E+13	0.0	0	21
R112	C_9H_7O=$C_6H_4C_2H_3$+CO	2.51E+11	0.0	43923	21
R113	C_9H_8+O=C_9H_8O	8.73E+13	0.0	0	21
R114	C_9H_8+O_2=C_9H_7+HO_2	1.40E+12	0.0	25402	21
R115	C_9H_8+cy-C_5H_5=C_9H_7+cy-C_5H_6	1.42E+12	0.0	18058	21
R116	cy-C_5H_6+cy-C_5H_5=>C_9H_8+CH_3	9.63E+13	1.6	59556	21
R117	C_9H_7+O=$C_6H_4C_2H_3$+CO	1.00E+14	0.0	0	21
R118	A1C_2H_3+H=A1C_2H_2-I+H_2	2.00E+07	2.0	6002	21
R119	A1C_2H_3+H=A1C_2H_2-N+H_2	3.36E-07	6.0	1692	21
R120	A1C_2H_3+H=$C_6H_4C_2H_3$+H_2	2.40E+15	0.0	16007	21
R121	A1C_2H_3+OH=A1C_2H_2-I+H_2O	1.00E+07	2.0	2000	21
R122	A1C_2H_3+OH=A1C_2H_2-N+H_2O	5.90E+12	0.0	8003	21

R123	A1C$_2$H$_2$-I+O$_2$=A1CHO+CHO	1.09E+23	-3.3	3893	21
R124	A1C$_2$H$_2$-I+O$_2$=A1C$_2$H+HO$_2$	5.19E+15	-1.3	3311	21
R125	A1C$_2$H$_3$+O=>C$_8$H$_6$O+H+H	2.78E+13	0.0	4912	21
R126	C$_8$H$_6$O+O=>A1+CHO+CO	5.00E+13	0.0	0	21
R127	A1CH$_3$+cy-C$_5$H$_5$=A1CH$_2$+cy-C$_5$H$_6$	2.13E+12	0.0	18058	21
R128	A1CH$_3$+O$_2$=A1CH$_2$+HO$_2$	2.00E+12	0.0	40809	21
R129	A1CH$_2$+HO$_2$=>A1CHO+OH+H	5.00E+12	0.0	0	21
R130	A1H+H=C$_6$H$_7$	8.18E+57	-13.2	26312	21
R131	C$_6$H$_7$=C$_5$H$_4$CH$_3$	5.00E+12	0.0	38118	21
R132	A1O+CH$_3$=C$_5$H$_5$CH$_3$-5+CO	2.05E+75	-18.3	38899	21
R133	A1+cy-C$_5$H$_6$=A1H+cy-C$_5$H$_5$	3.10E+11	0.0	5502	21
R134	A1H+H=C$_5$H$_4$CH$_3$	5.22E+28	-4.3	28814	21
R135	C$_5$H$_5$CH$_3$-5=C$_5$H$_5$CH$_3$-1	6.99E+10	0.0	19879	22
R136	C$_5$H$_5$CH$_3$-1=C$_5$H$_5$CH$_3$-2	2.56E+14	0.0	55727	22
R137	C$_5$H$_5$CH$_3$-1+H=C$_5$H$_4$CH$_3$+H$_2$	1.27E+14	0.0	6002	22
R138	C$_5$H$_5$CH$_3$-1+H=cy-C$_5$H$_6$+CH$_3$	1.20E+13	0.0	5150	22
R139	C$_5$H$_5$CH$_3$-1=C$_5$H$_4$CH$_3$+H	1.40E+15	0.0	77377	22
R140	C$_5$H$_5$CH$_3$-2=C$_5$H$_4$CH$_3$+H	1.40E+15	0.0	75807	22
R141	C$_5$H$_5$CH$_3$-2+H=C$_5$H$_4$CH$_3$+H$_2$	1.27E+14	0.0	6002	22
R142	C$_5$H$_5$CH$_3$-2+H=cy-C$_5$H$_6$+CH$_3$	1.20E+13	0.0	5150	22
R143	C$_5$H$_5$CH$_3$-5=cy-C$_5$H$_5$+CH$_3$	1.00E+16	0.0	67533	22
R144	C$_5$H$_5$CH$_3$-5=C$_5$H$_4$CH$_3$+H	7.00E+14	0.0	71885	24
R145	C$_5$H$_5$CH$_3$-5+H=C$_5$H$_4$CH$_3$+H$_2$	6.34E+14	0.0	6002	22
R146	C$_5$H$_4$CH$_3$+H=cy-C$_5$H$_5$+CH$_3$	8.00E+13	0.0	0	22
R147	C$_5$H$_6$O-2=>C$_2$H$_4$+C$_2$H$_2$+CO	8.81E+16	0.0	78098	22
R148	C$_5$H$_6$O-2=C$_5$H$_5$O-13+H	1.40E+15	0.0	82240	24
R149	C$_5$H$_6$O-2=C$_5$H$_5$O-14+H	1.40E+15	0.0	87242	24
R150	C$_5$H$_6$O-2+H=C$_5$H$_5$O-13+H$_2$	3.17E+13	0.0	6603	22
R151	C$_5$H$_6$O-2+H=C$_5$H$_5$O-14+H$_2$	3.17E+13	0.0	7903	22
R152	C$_5$H$_6$O-2+OH=C$_5$H$_5$O-13+H$_2$O	5.90E+12	0.0	-200	22
R153	C$_5$H$_6$O-2+OH=C$_5$H$_5$O-14+H$_2$O	5.90E+12	0.0	1100	22
R154	C$_5$H$_6$O-3=C$_4$H$_6$+CO	3.30E+14	0.0	51255	25
R155	C$_5$H$_5$O-14=C$_5$H$_5$O-13	3.51E+12	0.0	24211	22
R156	C$_5$H$_5$O-24=C$_5$H$_5$O-13	3.51E+12	0.0	24211	22
R157	C$_5$H$_5$O-13=C$_5$H$_4$O+H	1.20E+13	0.0	60679	22

R158	C_5H_5O-13=C_4H_5CO	2.00E+13	0.0	28133	22
R159	C_5H_5O-14=C_5H_4O+H	1.20E+13	0.0	55677	22
R160	C_5H_5O-14=VINCOC_2H_2	4.00E+13	0.0	43351	22
R161	VINCOC_2H_2=C_2H_3CO+C_2H_2	4.00E+13	0.0	21680	22
R162	C_5H_5O-24=C_4H_4CHO	2.00E+13	0.0	14337	22
R163	C_5H_5O-24=C_5H_4O+H	6.00E+12	0.0	18679	22
R164	cy-C_5H_6+O2=C_5H_5O-24+OH	4.00E+06	0.0	0	22
R165	cy-C_5H_6=cy-C_5H_5+H	1.10E+15	0.0	77023	22
R166	cy-C_5H_6+H=cy-C_5H_5+H2	5.42E+12	0.3	3766	22
R167	cy-C_5H_6+O=C_5H_6O-2	1.09E+13	0.0	0	22
R168	cy-C_5H_6+O=C_5H_6O-3	1.09E+13	0.0	0	22
R169	cy-C_5H_6+O=C_2H_3CHO+C_2H_2	1.09E+13	0.0	0	22
R170	cy-C_5H_6+O_2=cy-C_5H_5+HO_2	1.40E+12	0.0	28373	22
R171	cy-C_5H_5+OH=C_5H_4OH+H	5.00E+11	0.0	0	22
R172	cy-C_5H_5+O=C_5H_5O-24	3.50E+13	0.0	0	22
R173	cy-C_5H_5+O=CHCHCHO+C_2H_2	3.50E+13	0.0	0	22
R174	cy-C_5H_5+HO_2=C_5H_5O-24+OH	5.00E+12	0.0	0	22
R175	C_5H_4O+O=>CO_2+C_2H_2+C_2H_2	3.00E+13	0.0	0	22
R176	C_4H_5CO=C_4H_5-N+CO	4.00E+13	0.0	37538	22
R177	C_4H_4CHO=CHCHCHO+C_2H_2	4.00E+13	0.0	41410	22
R178	C_4H_4CHO=C_4H_5CO	1.09E+12	0.0	7003	22
R179	C_2H_3+C_2H_2=C_4H_5-N	2.51E+05	1.9	2103	22
R180	C_4H_3-N=C_2H_2+C_2H	3.16E+14	0.0	57228	22
R181	C_3H_5-N=C_2H_2+CH_3	1.26E+13	0.0	33416	22
R182	C_4H_6-12=C_4H_6	1.50E+13	0.0	67733	22
R183	C_4H_5-N=C_4H_5-I	8.43E+12	0.0	34917	22
R184	C_4H_5-I+cy-C_5H_6=C_4H_6+cy-C_5H_5	1.21E+12	0.0	7503	22
R185	C_4H_5-N+cy-C_5H_6=C_4H_6+cy-C_5H_5	7.98E+11	0.0	6703	22
R186	C_3H_5-A+cy-C_5H_6=C_3H_6+cy-C_5H_5	1.42E+12	0.0	18058	22
R187	C_3H_3+cy-C_5H_6=C_3H_4-A+cy-C_5H_5	1.10E+11	0.0	5502	22
R188	C_3H_3+cy-C_5H_6=C_3H_4-P+cy-C_5H_5	1.10E+11	0.0	5502	22
R189	C_2H_5+cy-C_5H_6=C_2H_6+cy-C_5H_5	1.36E+12	0.0	9704	22
R190	C_2H_3+cy-C_5H_6=cy-C_5H_5+C_2H_4	2.00E+12	0.0	7003	22
R191	CH_3+cy-C_5H_6=cy-C_5H_5+CH_4	3.11E+11	0.0	5502	22
R192	CHO+cy-C_5H_6=CH_2O+cy-C_5H_5	7.47E+12	0.0	15007	22

R193	C_4H_6-2+H=C_4H_5-123+H_2	9.51E+13	0.0	6603	22
R194	C_4H_6-2+OH=C_4H_5-123+H_2O	1.77E+13	0.0	-200	22
R195	C_2H_3O-C=CH_3CO	8.50E+14	0.0	14006	22
R196	C_2H_3O-C=CH_2CHO	1.00E+14	0.0	14006	22
R197	C_2H_3O-C=CH_2CO+H	1.60E+13	0.0	35017	22
R198	C_4H_{10}+C_3H_5-A=C_4H_9-1+C_3H_6	7.94E+11	0.0	20510	22
R199	C_4H_{10}+C_3H_5-A=C_4H_9-2+C_3H_6	3.16E+11	0.0	16408	22
R200	C_4H_8-1+C_3H_5-A=C_4H_7-I+C_3H_6	7.90E+10	0.0	12406	22
R201	C_4H_5-123+OH=C_4H_4-123+H_2O	1.00E+13	0.0	0	22
R202	C_4H_5-123+C_4H_5-123=CH_3A1CH_2+H	3.00E+12	0.0	0	22
R203	C_4H_5-121+C_4H_5-121=CH_3A1CH_2+H	3.00E+12	0.0	0	22
R204	C_3H_6+OH+O_2=CH_3CHO+CH_2O+OH	3.00E+10	0.0	-8284	22
R205	C_4H_{10}=C_2H_5+C_2H_5	2.00E+16	0.0	81339	22
R206	C_4H_10=C_3H_7-N+CH_3	1.74E+17	0.0	85741	24
R207	C_4H_{10}=C_4H_9-1+H	1.00E+14	0.0	100049	24
R208	C_4H_{10}= C_4H_9-2+H	1.00E+14	0.0	100049	24
R209	C_4H_{10}+O_2= C_4H_9-1+HO_2	2.50E+13	0.0	49024	24
R210	C_4H_{10}+O_2= C_4H_9-2+HO_2	4.00E+13	0.0	47623	24
R211	C_4H_{10}+CH_3= C_4H_9-1+CH_4	2.19E+11	0.0	11405	24
R212	C_4H_{10}+CH_3= C_4H_9-2+CH_4	2.19E+11	0.0	9604	24
R213	C_4H_{10}+H= C_4H_9-1+H_2	5.63E+07	2.0	7703	24
R214	C_4H_{10}+H= C_4H_9-2+H_2	1.76E+07	2.0	5002	24
R215	C_4H_{10}+OH= C_4H_9-1+H_2O	4.13E+07	1.7	753	24
R216	C_4H_{10}+OH= C_4H_9-2+H_2O	7.23E+07	1.6	-247	24
R217	C_4H_{10}+O= C_4H_9-1+OH	1.13E+14	0.0	7853	24
R218	C_4H_{10}+O= C_4H_9-2+OH	5.62E+13	0.0	5202	24
R219	C_4H_{10}+HO_2= C_4H_9-1+H_2O_2	1.70E+13	0.0	20470	24
R220	C_4H_{10}+HO_2= C_4H_9-2+H_2O_2	1.12E+13	0.0	17708	24
R221	C_4H_9-2=C_3H_6+CH_3	2.00E+14	0.0	33216	21
R222	C_4H_9-2=C_4H_8-1+H	2.00E+13	0.0	40419	21
R223	C_4H_9-2=C_4H_8-2+H	5.01E+12	0.0	37918	21
R224	C_4H_9-1=C_2H_5+C_2H_4	2.50E+13	0.0	28814	21
R225	C_4H_9-1=C_4H_8-1+H	1.26E+13	0.0	38618	21
R226	C_4H_8-1=C_2H_3+C_2H_5	1.00E+19	-1.0	96817	21
R227	C_4H_8-1=H+C_4H_7-I	4.11E+18	-1.0	97397	21

R228	C_4H_8-1+CH_3= C_4H_7-I+CH_4	1.00E+11	0.0	7303	21
R229	C_4H_8-1+H= C_4H_7-I+H_2	5.00E+13	0.0	3901	21
R230	C_4H_8-1+O=C_3H_7-N+CHO	1.80E+05	2.5	-1029	21
R231	C_4H_8-1+O=C_2H_3CHO+CH_3+H	9.67E+04	2.5	-1029	21
R232	C_4H_8-1+OH=C_4H_7-I+H_2O	2.25E+13	0.0	2218	21
R233	C_4H_8-1+O_2=C_4H_7-I+HO_2	4.00E+12	0.0	33216	21
R234	C_4H_8-2=H+C_4H_7-I	4.11E+18	-1.0	97397	21
R235	C_4H_8-2+CH_3=C_4H_7-I+CH_4	1.00E+11	0.0	8204	21
R236	C_4H_8-2+H=C_4H_7-I+H_2	5.00E+13	0.0	3801	21
R237	C_4H_8-2+O=C_3H_7-I+CHO	2.79E+06	2.1	-1775	21
R238	C_4H_8-2+OH=C_4H_7-I+H_2O	3.90E+13	0.0	2218	21
R239	C_4H_8-2+O=CH_3CO+C_2H_5	1.53E+07	1.9	-1476	21
R240	C_4H_8-2+O=CH_3+CH_3CHCO+H	8.22E+06	1.9	-1476	21
R241	C_4H_8-2+O_2=C_4H_7-I+HO_2	8.00E+13	0.0	37418	21
R242	C_4H_7-I=C_4H_6+H	1.00E+14	0.0	55026	21
R243	C_4H_7-I+OH=C_4H_6+H_2O	1.00E+14	0.0	0	21
R244	C_4H_7-I+CH_3=C_4H_6+CH_4	8.00E+12	0.0	0	21
R245	C_4H_7-I+C_3H_5-A=C_3H_6+C_4H_6	6.31E+12	0.0	0	21
R246	C_4H_7-I+O_2=C_4H_6+HO_2	1.00E+09	0.0	0	21
R247	C_4H_7-I+H=C_4H_6+H_2	3.16E+13	0.0	0	21
R248	C_4H_6+OH=C_4H_5-N+H_2O	2.00E+07	2.0	5002	21
R249	C_4H_6+OH=C_4H_5-I+H_2O	2.00E+07	2.0	2000	21
R250	C_4H_6+O=CHO+C_3H_5-A	6.02E+08	1.4	-858	24
R251	C_4H_6+O=CH_2CHO+C_2H_3	1.00E+12	0.0	0	24
R252	C_4H_6+H=C_4H_5-N+H_2	3.00E+07	2.0	13006	24
R253	C_4H_6+H= C_4H_5-I+H_2	3.00E+07	2.0	6002	24
R254	C_4H_6-1+OH= C_4H_5-121+H_2O	1.00E+07	2.0	2000	24
R255	C_4H_6-1+H=C_2H_5+C_2H_2	1.00E+14	0.0	3001	24
R256	C_4H_6-12+OH= C_4H_5-I+H_2O	2.00E+07	2.0	1000	24
R257	C_4H_6-12+OH= C_4H_5-123+H_2O	1.00E+07	2.0	2000	24
R258	C_4H_6-12+OH= C_4H_5-121+H_2O	2.00E+07	2.0	2501	24
R259	C_4H_6-12+H= C_4H_5-I+H_2	5.00E+07	2.0	5002	24
R260	C_4H_6-12+H= C_4H_5-123+H_2	1.05E+07	2.0	6002	24
R261	C_4H_6-12+H= C_4H_5-121+H_2	3.00E+07	2.0	6503	23
R262	C_4H_6-12+H=CH_3+C_3H_4-A	2.00E+13	0.0	2000	23

R263	C_4H_5-121+H=CH_3+C_3H_3	1.00E+14	0.0	0	23
R264	C_4H_5-121+O_2=CH_3CHCO+CHO	4.16E+10	0.0	2511	23
R265	C_4H_5-121+OH=C_4H_4+H_2O	3.00E+13	0.0	0	23
R266	C_4H_5-I+H=CH_3+C_3H_3	1.00E+14	0.0	0	23
R267	C_4H_5-I+H=C_4H_5-123+H	3.00E+13	0.0	0	23
R268	C_4H_5-I+C_2H_2=A1H+H	3.00E+11	0.0	14907	23
R269	C_4H_5-123+H=CH_3+C_3H_3	1.00E+14	0.0	0	23
R270	C_4H_5-123+O_2=CH_3CO+CH_2CO	4.16E+10	0.0	2511	23
R271	C_4H_5-123+H=C_4H_4-123+H_2	1.00E+14	0.0	8003	23
R272	C_4H_5-N+H=C_4H_5-I+H	1.00E+14	0.0	0	23
R273	C_4H_5-N+OH=C_4H_4+H_2O	2.00E+07	2.0	1000	23
R274	C_4H_5-N+H=C_4H_4+H_2	3.00E+07	2.0	1000	23
R275	C_4H_5-N+C_2H_2=A1H+H	1.60E+16	-1.3	5402	23
R276	C_4H_5-N+O_2=CHCHCHO+CH_2O	1.00E+12	0.0	0	23
R277	C_4H_5-N+O_2=C_4H_4+HO_2	1.00E+07	2.0	10004	23
R278	C_4H_5-123+C_3H_3=A1CH_2+H	3.00E+12	0.0	0	23
R279	C_4H_5-121+C_3H_3=A1CH_2+H	3.00E+12	0.0	0	23
R280	C_4H_4-123+OH=C_4H_3-I+H_2O	2.00E+07	2.0	2000	23
R281	C_4H_4-123+H=C_4H_3-I+H_2	3.00E+07	2.0	6002	23
R282	C_4H_4+OH=C_4H_3-N+H_2O	7.50E+06	2.0	5002	23
R283	C_4H_4+H=C_4H_3-N+H_2	2.00E+07	2.0	15007	23
R284	C_4H_4+OH=C_4H_3-I+H_2O	1.00E+07	2.0	2000	23
R285	C_4H_4+H=C_4H_3-I+H_2	3.00E+07	2.0	5002	23
R286	C_4H_3-N+C_2H_2=A1	2.80E+03	2.9	1400	23
R287	C_4H_3-N+H=C_4H_3-I+H	1.00E+14	0.0	0	23
R288	C_4H_3-N+O_2=C_2HCHO+CHO	3.00E+12	0.0	0	23
R289	C_4H_3-I+O_2=CH_2CO+HCCO	1.00E+12	0.0	0	23
R290	C_4H_3-I+OH=C_4H_2+H_2O	3.00E+13	0.0	0	23
R291	C_4H_3-I+O=CH_2CO+C_2H	2.00E+13	0.0	0	23
R292	C_4H_3-I+O=H_2C_4O+H	2.00E+13	0.0	0	23
R293	C_4H_3-I+H=C_4H_2+H_2	5.00E+13	0.0	0	23
R294	C_4H_3-I+CH_2=C_3H_4-A+C_2H	2.00E+13	0.0	0	23
R295	C_4H_3-I+C_2H_2=A1	3.00E+11	0.0	14907	23
R296	C_4H_2+CH_2=C_5H_3+H	1.30E+13	0.0	4328	23
R297	C_4H_2+CH=C_5H_2+H	1.00E+14	0.0	0	23

R298	$C_4H_2+CH_2-S=C_5H_3+H$	3.00E+13	0.0	0	23
R299	$C_4H_2+C_2H=C_6H_2+H$	9.60E+13	0.0	0	23
R300	$C_4H_2+OH=H_2C_4O+H$	6.66E+12	0.0	-410	23
R301	$C_4H_2+O=C_3H_2+CO$	1.20E+12	0.0	0	23
R302	$H_2C_4O+H=C_2H_2+HCCO$	5.00E+13	0.0	3001	23
R303	$H_2C_4O+OH=CH_2CO+HCCO$	1.00E+07	2.0	2000	23
R304	$C_3H_8+O_2=C_3H_7-I+HO_2$	4.00E+13	0.0	48633	23
R305	$C_3H_8+O_2=C_3H_7-N+HO_2$	4.00E+13	0.0	51385	23
R306	$C_3H_8+HO_2=C_3H_7-N+H_2O_2$	4.76E+04	2.5	16500	23
R307	$C_3H_8+HO_2=C_3H_7-I+H_2O_2$	9.64E+03	2.6	13915	23
R308	$C_3H_8+OH=C_3H_7-N+H_2O$	3.16E+07	1.8	934	23
R309	$C_3H_8+OH=C_3H_7-I+H_2O$	7.08E+06	1.9	-159	23
R310	$C_3H_8+O=C_3H_7-N+OH$	3.73E+06	2.4	5506	23
R311	$C_3H_8+O=C_3H_7-I+OH$	5.48E+05	2.5	3140	23
R312	$C_3H_8+H=C_3H_7-I+H_2$	1.30E+06	2.4	4473	23
R313	$C_3H_8+H=C_3H_7-N+H_2$	1.33E+06	2.5	6759	23
R314	$C_3H_8+CH_3=C_3H_7-N+CH_4$	9.04E-01	3.6	7156	23
R315	$C_3H_8+CH_3=C_3H_7-I+CH_4$	1.51E+00	3.5	5482	23
R316	$C_3H_8+C_2H_3=C_3H_7-I+C_2H_4$	1.00E+03	3.1	8834	23
R317	$C_3H_8+C_2H_3=C_3H_7-N+C_2H_4$	6.00E+02	3.3	10505	23
R318	$C_3H_8+C_2H_5=C_3H_7-I+C_2H_6$	1.51E+00	3.5	7473	23
R319	$C_3H_8+C_2H_5=C_3H_7-N+C_2H_6$	9.03E-01	3.6	9144	23
R320	$C_3H_8+C_3H_5-A=C_3H_6+C_3H_7-N$	2.35E+02	3.3	19851	23
R321	$C_3H_8+C_3H_5-A=C_3H_6+C_3H_7-I$	7.83E+01	3.3	18177	23
R322	$C_3H_7-N+O_2=C_3H_6+HO_2$	3.58E+09	0.0	-3533	23
R323	$C_3H_7-I+O_2=C_3H_6+HO_2$	6.10E+20	-2.9	7913	23
R324	$C_3H_7-I+H=C_2H_5+CH_3$	5.00E+13	0.0	0	23
R325	$C_3H_7-N+H=C_2H_5+CH_3$	1.00E+14	0.0	0	23
R326	$C_3H_6=C_3H_5-N+H$	7.58E+14	0.0	101349	23
R327	$C_3H_6=C_3H_5-S+H$	1.45E+15	0.0	98108	23
R328	$C_3H_6=C_2H_2+CH_4$	2.50E+12	0.0	70034	23
R329	$C_3H_6=C_3H_4-A+H_2$	3.00E+13	0.0	80039	23
R330	$C_3H_6+HO_2=C_3H_5-A+H_2O_2$	9.64E+03	2.6	13916	23
R331	$C_3H_6+OH=C_3H_5-A+H_2O$	3.12E+06	2.0	-298	23
R332	$C_3H_6+OH=C_3H_5-S+H_2O$	1.11E+06	2.0	1451	23

R333	$C_3H_6+OH=C_3H_5-N+H_2O$	2.11E+06	2.0	2779	23
R334	$C_3H_6+O=CH_3CHCO+H+H$	5.01E+07	1.8	76	23
R335	$C_3H_6+O=C_2H_5+CHO$	1.58E+07	1.8	-1216	23
R336	$C_3H_6+O=C_3H_5-A+OH$	5.24E+11	0.7	5886	23
R337	$C_3H_6+O=C_3H_5-N+OH$	1.20E+11	0.7	8963	23
R338	$C_3H_6+O=C_3H_5-S+OH$	6.03E+10	0.7	7635	23
R339	$C_3H_6+H=C_2H_4+CH_3$	7.23E+12	0.0	1302	23
R340	$C_3H_6+H=C_3H_5-A+H_2$	1.73E+05	2.5	2493	23
R341	$C_3H_6+H=C_3H_5-S+H_2$	4.09E+05	2.5	9798	23
R342	$C_3H_6+H=C_3H_5-N+H_2$	8.04E+05	2.5	12290	23
R343	$C_3H_6+O_2=C_3H_5-N+HO_2$	2.00E+13	0.0	47623	23
R344	$C_3H_6+O_2=C_3H_5-S+HO_2$	2.00E+13	0.0	44021	23
R345	$C_3H_6+O_2=C_3H_5-A+HO_2$	2.29E+12	0.0	39219	23
R346	$C_3H_6+CH_3=C_3H_5-A+CH_4$	2.22E+00	3.5	5677	23
R347	$C_3H_6+CH_3=C_3H_5-S+CH_4$	8.43E-01	3.5	11661	23
R348	$C_3H_6+CH_3=C_3H_5-N+CH_4$	1.35E+00	3.5	12854	23
R349	$C_3H_6+CHO=C_3H_5-A+CH_2O$	1.08E+07	1.9	17018	23
R350	$CH_3CHCO+OH=C_2H_3CO+H_2O$	4.00E+06	2.0	0	23
R351	$CH_3CHCO+O=C_2H_3CO+OH$	7.60E+08	1.5	8504	23
R352	$CH_3CHCO+H=C_2H_3CO+H_2$	2.00E+05	2.5	2501	23
R353	$CH_3CHCO+H=C_2H_5+CO$	2.00E+13	0.0	2000	23
R354	$CH_3CHCO+O=CH_3+CHO+CO$	3.00E+07	2.0	0	23
R355	$C_2H_3CHO+OH=C_2H_3CO+H_2O$	1.00E+13	0.0	0	23
R356	$C_2H_3CHO+O=C_2H_3CO+OH$	7.24E+12	0.0	1970	23
R357	$C_2H_3CHO+O=CH_2CO+CHO+H$	5.01E+07	1.8	76	23
R358	$C_2H_3CHO+H=C_2H_3CO+H_2$	3.98E+13	0.0	4202	23
R359	$C_2H_3CHO+H=C_2H_4+CHO$	2.00E+13	0.0	3501	23
R360	$C_2H_3CHO+O_2=C_2H_3CO+HO_2$	3.00E+13	0.0	36017	23
R361	$C_2H_3CO=C_2H_3+CO$	1.00E+14	0.0	34016	23
R362	$C_2H_3CO+O=C_2H_3+CO_2$	1.00E+14	0.0	0	23
R363	$C_3H_5-A+O_2=C_2H_3CHO+OH$	1.82E+13	-0.4	22870	23
R364	$C_3H_5-A+O_2=C_3H_4-A+HO_2$	4.99E+15	-1.4	2439	23
R365	$C_3H_5-A+O_2=CH_2CHO+CH_2O$	1.06E+10	0.3	12844	23
R366	$C_3H_5-A+O_2=C_2H_2+CH_2O+OH$	2.78E+25	-4.8	15475	23
R367	$C_3H_5-A+HO_2=C_2H_3CHO+H+OH$	1.00E+13	0.0	0	23

R368	C_3H_5-A+OH=C_3H_4-A+H_2O	1.00E+13	0.0	0	23
R369	C_3H_5-A+H=C_3H_4-A+H_2	5.00E+13	0.0	0	23
R370	C_3H_5-A+H=C_3H_6	1.88E+26	-3.6	5470	23
R371	C_3H_5-A+O=C_2H_3CHO+H	1.81E+14	0.0	0	23
R372	C_3H_5-A+CH_3=C_3H_4-A+CH_4	3.02E+12	-0.3	-131	23
R373	C_3H_5-A+CH_3=C_4H_8-1	1.76E+50	-11.0	18609	23
R374	C_3H_5-A+C_2H_3=cy-C_5H_6+H+H	1.59E+65	-14.0	61655	23
R375	C_3H_5-N+O_2=CH_3CHO+CHO	1.09E+23	-3.3	3893	23
R376	C_3H_5-N+O_2=CH_3CHCO+H+O	1.6E+15	-0.8	3136	23
R377	C_3H_5-N+O=CH_3CHCO+H	1.00E+14	0.0	0	23
R378	C_3H_5-N+H=C_3H_4-P+H_2	2.00E+13	0.0	0	23
R379	C_3H_5-N+OH=C_3H_4-P+H_2O	1.00E+13	0.0	0	23
R380	C_3H_5-N+H=C_3H_5-A+H	1.00E+14	0.0	0	23
R381	C_3H_5-S+H=C_3H_5-A+H	1.00E+14	0.0	0	23
R382	C_3H_5-S+O_2=CH_3CO+CH_2O	1.09E+22	-3.3	3893	23
R383	C_3H_5-S+O=CH_2CO+CH_3	1.00E+14	0.0	0	23
R384	C_3H_5-S+H=C_3H_4-P+H_2	4.00E+13	0.0	0	23
R385	C_3H_5-S+OH=C_3H_4-P+H_2O	2.00E+13	0.0	0	23
R386	C_3H_4-A+H=C_3H_3+H_2	5.00E+07	2.0	5002	23
R387	C_3H_4-A+O=C_2H_4+CO	1.34E+07	1.9	179	23
R388	C_3H_4-A+OH=C_3H_3+H_2O	2.00E+07	2.0	1000	23
R389	C_3H_4-A=C_3H_4-P	2.19E+14	0.0	68134	23
R390	C_3H_4-P+H=C_3H_3+H_2	5.00E+07	2.0	5002	23
R391	C_3H_4-P+O=C_2H_4+CO	1.50E+13	0.0	2103	23
R392	C_3H_4-P+OH=C_3H_3+H_2O	2.00E+07	2.0	1000	23
R393	C_3H_4-P+CH_3=C_3H_3+CH_4	2.22E+00	3.5	5602	23
R394	C_3H_4-P+H=CH_3+C_2H_2	1.00E+14	0.0	4002	23
R395	C_3H_3+O_2=CH_2CO+CHO	3.00E+10	0.0	2869	23
R396	C_3H_3+O=CH_2O+C_2H	2.00E+13	0.0	0	23
R397	C_3H_3+H=C_3H_2+H_2	5.00E+13	0.0	3001	23
R398	C_3H_3+OH=C_3H_2+H_2O	2.00E+13	0.0	0	23
R399	C_3H_3+C_2H_3=cy-C_5H_5+H	9.63E+40	-7.8	28834	23
R400	C_3H_3+CH_3=C_4H_6-12	5.00E+12	0.0	0	23
R401	C_3H_3+CH_3=C_4H_6-1	5.00E+12	0.0	0	23
R402	C_3H_3+CH=C_4H_3-N+H	7.00E+13	0.0	0	23

R403	$C_3H_3+CH=C_4H_3-I+H$	7.00E+13	0.0	0	23
R404	$C_3H_3+C_3H_3=A1+H$	3.00E+12	0.0	0	23
R405	$C_3H_2+O_2=HCCO+CO+H$	5.00E+13	0.0	0	23
R406	$C_3H_2+OH=C_2H_2+CHO$	5.00E+13	0.0	0	23
R407	$CHCHCHO+O_2=CHOCHO+CHO$	3.00E+12	0.0	0	23
R408	$CHCHCHO=C_2H_2+CHO$	1.00E+14	0.0	33016	23
R409	$CHCHCHO+H=C_2H_3CO+H$	1.00E+14	0.0	0	23
R410	$CHCHCHO+OH=C_2HCHO+H_2O$	1.00E+13	0.0	0	23
R411	$CHCHCHO+H=C_2HCHO+H_2$	2.00E+13	0.0	0	23
R412	$C_2HCHO+H=C_2H_2+CHO$	1.00E+14	0.0	3001	23
R413	$C_2HCHO+OH=C_2HCO+H_2O$	1.00E+13	0.0	0	23
R414	$C_2HCHO+H=C_2HCO+H_2$	4.00E+13	0.0	4202	23
R415	$C_2HCO+O_2=CHO+CO+CO$	1.40E+09	1.0	0	23
R416	$C_2HCO+H=C_2H_2+CO$	1.00E+14	0.0	0	23
R417	$C_2H_6+CH_3=C_2H_5+CH_4$	5.50E-01	4.0	8304	23
R418	$C_2H_6+H=C_2H_5+H_2$	5.40E+02	3.5	5212	23
R419	$C_2H_6+O=C_2H_5+OH$	3.00E+07	2.0	5117	23
R420	$C_2H_6+OH=C_2H_5+H_2O$	7.23E+06	2.0	864	23
R421	$C_2H_5+H=C_2H_4+H_2$	1.25E+14	0.0	8003	23
R422	$C_2H_5+H=CH_3+CH_3$	3.00E+13	0.0	0	23
R423	$C_2H_5+H=C_2H_6$	1.00E+14	0.0	0	23
R424	$C_2H_5+OH=C_2H_4+H_2O$	4.00E+13	0.0	0	23
R425	$C_2H_5+O=CH_3+CH_2O$	1.00E+14	0.0	0	23
R426	$C_2H_5+HO_2=CH_3+CH_2O+OH$	3.00E+13	0.0	0	23
R427	$C_2H_5+O_2=C_2H_4+HO_2$	3.00E+20	-2.9	6763	23
R428	$C_2H_4+H=C_2H_3+H_2$	3.36E-07	6.0	1692	23
R429	$C_2H_4+OH=C_2H_3+H_2O$	2.02E+13	0.0	5938	23
R430	$C_2H_4+O=CH_3+CHO$	1.02E+07	1.9	179	23
R431	$C_2H_4+O=CH_2CHO+H$	3.39E+06	1.9	179	23
R432	$C_2H_4+CH_3=C_2H_3+CH_4$	6.62E+00	3.7	9504	23
R433	$C_2H_4+M=C_2H_2+H_2+M$	2.60E+17	0.0	79327	23
R434	$C_2H_4+M=C_2H_3+H+M$	3.80E+17	0.0	98216	23
R435	$C_2H_3+H=C_2H_2+H_2$	4.00E+13	0.0	0	23
R436	$C_2H_3+O=CH_2CO+H$	3.00E+13	0.0	0	23
R437	$C_2H_3+O_2=CH_2O+CHO$	1.09E+23	-3.3	3893	23

R438	$C_2H_3+O_2=CH_2CHO+O$	1.60E+15	-0.8	3136	23
R439	$C_2H_3+O_2=C_2H_2+HO_2$	5.19E+15	-1.3	3311	23
R440	$C_2H_3+OH=C_2H_2+H_2O$	2.00E+13	0.0	0	23
R441	$C_2H_3+C_2H=C_2H_2+C_2H_2$	3.00E+13	0.0	0	23
R442	$C_2H_3+CH=CH_2+C_2H_2$	5.00E+13	0.0	0	23
R443	$C_2H_3+CH_3=C_3H_5\text{-}A+H$	4.73E+02	3.7	5679	23
R444	$C_2H_3+CH_3=C_3H_6$	4.46E+56	-13.0	13871	23
R445	$C_2H_3+CH_3=C_2H_2+CH_4$	2.00E+13	0.0	0	23
R446	$C_2H_3+C_2H_2=C_4H_4+H$	2.00E+12	0.0	5002	23
R447	$C_2H_3+C_2H_4=C_4H_6+H$	5.00E+11	0.0	7307	23
R448	$C_2H_3+C_2H_3=C_4H_5\text{-}I+H$	7.00E+13	0.0	0	23
R449	$C_2H_3+C_2H_3=C_2H_4+C_2H_2$	1.45E+13	0.0	0	23
R450	$C_2H_2+OH=C_2H+H_2O$	3.37E+07	2.0	14006	23
R451	$C_2H_2+OH=HCCOH+H$	5.04E+05	2.3	13506	23
R452	$C_2H_2+OH=CH_2CO+H$	2.18E-04	4.5	-1000	23
R453	$C_2H_2+OH=CH_3+CO$	4.83E-04	4.0	-2000	23
R454	$HCCOH+H=CH_2CO+H$	1.00E+13	0.0	0	23
R455	$C_2H_2+O=CH_2+CO$	6.12E+06	2.0	1900	23
R456	$C_2H_2+O=HCCO+H$	1.43E+07	2.0	1900	23
R457	$C_2H_2+O=C_2H+OH$	3.16E+15	-0.6	15007	23
R458	$C_2H_2+CH_3=C_2H+CH_4$	1.81E+11	0.0	17297	23
R459	$C_2H_2+O_2=HCCO+OH$	2.00E+07	1.5	30114	23
R460	$C_2H_2+M=C_2H+H+M$	4.20E+16	0.0	107052	23
R461	$CH_3CHO+OH=CH_3CO+H_2O$	5.37E+10	0.7	-1110	23
R462	$CH_3CHO+H=CH_3CO+H_2$	4.09E+09	1.2	2401	23
R463	$CH_3CHO+O=CH_3CO+OH$	5.89E+12	0.0	1810	23
R464	$CH_3CHO+HO_2=CH_3CO+H_2O_2$	1.70E+12	0.0	10705	23
R465	$CH_3CHO+O_2=CH_3CO+HO_2$	2.00E+13	0.5	42220	23
R466	$CH_3CHO+CH_3=CH_3CO+CH_4$	2.00E-06	5.6	2465	23
R467	$CH_2CHO+H=CH_2CO+H_2$	4.00E+13	0.0	0	23
R468	$CH_2CHO+O=CH_2O+CHO$	1.00E+14	0.0	0	23
R469	$CH_2CHO+OH=CH_2CO+H_2O$	3.00E+13	0.0	0	23
R470	$CH_2CHO+O_2=CH_2O+CO+OH$	3.00E+13	0.0	0	23
R471	$CH_2CHO+CH_3=>C_2H_5+CO+H$	4.90E+14	-0.5	0	23
R472	$CH_2CHO=CH_2CO+H$	3.95E+38	-7.7	45137	23

R473	$CHOCHO=CO+CO+H_2$	4.07E+42	-8.5	69311	23
R474	$CHOCHO+OH=CHO+CO+H_2O$	1.00E+13	0.0	0	23
R475	CHOCHO+O=CHO+CO+OH	7.24E+12	0.0	0	23
R476	$CHOCHO+H=CH_2O+CHO$	1.00E+12	0.0	0	23
R477	$CHOCHO+HO_2=CHO+CO+H_2O_2$	1.70E+12	0.0	10705	23
R478	$CHOCHO+CH_3=CHO+CO+CH_4$	1.74E+12	0.0	8444	23
R479	$CHOCHO+O_2=CHO+CO+HO_2$	1.00E+14	0.0	37018	23
R480	$CH_2CO+O=CO_2+CH_2$	1.75E+12	0.0	1350	23
R481	$CH_2CO+H=CH_3+CO$	7.00E+12	0.0	3012	23
R482	$CH_2CO+H=HCCO+H_2$	2.00E+14	0.0	8003	23
R483	$CH_2CO+O=HCCO+OH$	1.00E+13	0.0	8003	23
R484	$CH_2CO+OH=HCCO+H_2O$	1.00E+13	0.0	2000	23
R485	$CH_2CO+OH=CH_2OH+CO$	3.73E+12	0.0	-1013	23
R486	$C_2H+H_2=C_2H_2+H$	4.09E+05	2.4	864	23
R487	$C_2H+O=CH+CO$	5.00E+13	0.0	0	23
R488	$C_2H+OH=HCCO+H$	2.00E+13	0.0	0	23
R489	$C_2H+OH=C_2+H_2O$	4.00E+07	2.0	8003	23
R490	$C_2H+O_2=CO+CO+H$	9.04E+12	0.0	-457	23
R491	$C_2H+C_2H_2=C_4H_2+H$	9.64E+13	0.0	0	23
R492	$C_2H+C_2H_4=C_4H_4+H$	1.20E+13	0.0	0	23
R493	$HCCO+C_2H_2=C_3H_3+CO$	1.00E+11	0.0	0	23
R494	$HCCO+H=CH_2\text{-}S+CO$	1.00E+14	0.0	0	23
R495	HCCO+O=H+CO+CO	8.00E+13	0.0	0	23
R496	$HCCO+O=CH+CO_2$	2.95E+13	0.0	1113	23
R497	$HCCO+O_2=CO_2+CO+H$	1.40E+09	1.0	0	23
R498	$HCCO+CH=C_2H_2+CO$	5.00E+13	0.0	0	23
R499	HCCO+HCCO=C_2H_2+CO+CO	1.00E+13	0.0	0	23
R500	$HCCO+OH=C_2O+H_2O$	3.00E+13	0.0	0	23
R501	$C_2O+H=CH+CO$	1.00E+13	0.0	0	23
R502	$C_2O+O=CO+CO$	5.00E+13	0.0	0	23
R503	$C_2O+OH=CO+CO+H$	2.00E+13	0.0	0	23
R504	$C_2O+O_2=CO+CO+O$	2.00E+13	0.0	0	23
R505	$C_2+H_2=C_2H+H$	4.00E+05	2.4	1000	23
R506	$C_2+O_2=CO+CO$	5.00E+13	0.0	0	23
R507	$C_2+OH=C_2O+H$	5.00E+13	0.0	0	23

R508	$CH_4+H=CH_3+H_2$	2.20E+04	3.0	8754	23
R509	$CH_4+OH=CH_3+H_2O$	4.19E+06	2.0	2548	23
R510	$CH_4+O=CH_3+OH$	6.92E+08	1.6	8489	23
R511	$CH_4+HO_2=CH_3+H_2O_2$	1.12E+13	0.0	24652	23
R512	$CH_3+HO_2=CH_3O+OH$	7.00E+12	0.0	0	23
R513	$CH_3+HO_2=CH_4+O_2$	3.00E+12	0.0	0	23
R514	$CH_3+O=CH_2O+H$	8.00E+13	0.0	0	23
R515	$CH_3+O_2=CH_3O+O$	1.45E+13	0.0	29223	23
R516	$CH_3+O_2=CH_2O+OH$	2.51E+11	0.0	14647	23
R517	$CH_3O+H=CH_3+OH$	1.00E+13	0.0	0	23
R518	$CH_2OH+H=CH_3+OH$	1.00E+13	0.0	0	23
R519	$CH_3+OH=CH_2-S+H_2O$	2.65E+13	0.0	2187	23
R520	$CH_3+OH=CH_2+H_2O$	3.00E+06	2.0	2501	23
R521	$CH_3+OH=HCOH+H_2$	5.48E+13	0.0	2982	23
R522	$CH_3+OH=CH_2O+H_2$	2.25E+13	0.0	4302	23
R523	$CH_3+H=CH_2+H_2$	9.00E+13	0.0	15107	23
R524	$CH_3+M=CH+H_2+M$	6.90E+14	0.0	82509	23
R525	$CH_3+M=CH_2+H+M$	1.90E+16	0.0	91455	23
R526	$CH_3OH+OH=CH=OH+H_2O$	2.61E+05	2.2	-1344	23
R527	$CH_3OH+OH=CH_3O+H_2O$	2.62E+06	2.1	916	23
R528	$CH_3OH+O=CH_2OH+OH$	3.88E+05	2.5	3081	23
R529	$CH_3OH+H=CH_2OH+H_2$	1.70E+07	2.1	4870	23
R530	$CH_3OH+H=CH_3O+H_2$	4.24E+06	2.1	4870	23
R531	$CH_3OH+HO_2=CH_2OH+H_2O_2$	9.64E+10	0.0	12584	23
R532	$CH_3O+M=CH_2O+H+M$	5.45E+13	0.0	13503	23
R533	$CH_2OH+M=CH_2O+H+M$	1.00E+14	0.0	25012	23
R534	$CH_3O+H=CH_2O+H_2$	2.00E+13	0.0	0	23
R535	$CH_2OH+H=CH_2O+H_2$	2.00E+13	0.0	0	23
R536	$CH_3O+OH=CH_2O+H_2O$	1.00E+13	0.0	0	23
R537	$CH_2OH+OH=CH_2O+H_2O$	1.00E+13	0.0	0	23
R538	$CH_3O+O=CH_2O+OH$	1.00E+13	0.0	0	23
R539	$CH_2OH+O=CH_2O+OH$	1.00E+13	0.0	0	23
R540	$CH_3O+O_2=CH_2O+HO_2$	6.30E+10	0.0	2601	23
R541	$CH_2OH+O_2=CH_2O+HO_2$	1.57E+15	-1.0	0	23
R542	$HCOH+OH=CHO+H_2O$	2.00E+13	0.0	0	23

R543	HCOH+H=CH_2O+H	2.00E+14	0.0	0	23
R544	HCOH+O=CO_2+H+H	5.00E+13	0.0	0	23
R545	HCOH+O=CO+OH+H	3.00E+13	0.0	0	23
R546	HCOH+O_2=CO_2+H+OH	5.00E+12	0.0	0	23
R547	HCOH+O_2=CO_2+H_2O	3.00E+13	0.0	0	23
R548	CH_2+H=CH+H_2	1.00E+18	-1.6	0	23
R549	CH_2+OH=CH+H_2O	1.13E+07	2.0	3001	23
R550	CH_2+OH=CH_2O+H	2.50E+13	0.0	0	23
R551	CH_2+CO_2=CH_2O+CO	1.10E+11	0.0	1005	23
R552	CH_2+O=CO+H+H	5.00E+13	0.0	0	23
R553	CH_2+O=CO+H_2	3.00E+13	0.0	0	23
R554	CH_2+O_2=CH_2O+O	3.29E+21	-3.3	2869	23
R555	CH_2+O_2=CO_2+H+H	3.29E+21	-3.3	2869	23
R556	CH_2+O_2=CO_2+H_2	1.01E+21	-3.3	1508	23
R557	CH_2+O_2=CO+H_2O	7.28E+19	-2.5	1809	23
R558	CH_2+O_2=CHO+OH	1.29E+20	-3.3	284	23
R559	CH_2+CH_3=C_2H_4+H	4.00E+13	0.0	0	23
R560	CH_2+CH_2=C_2H_2+H+H	4.00E+13	0.0	0	23
R561	CH_2+HCCO=C_2H_3+CO	3.00E+13	0.0	0	23
R562	CH_2+C_2H_2=C_3H_3+H	1.20E+13	0.0	6603	23
R563	CH_2-S+CH_4=CH_3+CH_3	4.00E+13	0.0	0	23
R564	CH_2-S+C_2H_6=CH_3+C_2H_5	1.20E+14	0.0	0	23
R565	CH_2-S+O_2=CO+OH+H	7.00E+13	0.0	0	23
R566	CH_2-S+H_2=CH_3+H	7.00E+13	0.0	0	23
R567	CH_2-S+C_2H_2=C_3H_3+H	1.50E+14	0.0	0	23
R568	CH_2-S+C_2H_4=C_3H_5-A+H	1.30E+14	0.0	0	23
R569	CH_2-S+O=CO+H+H	3.00E+13	0.0	0	23
R570	CH_2-S+OH=CH_2O+H	3.00E+13	0.0	0	23
R571	CH_2-S+H=CH+H_2	3.00E+13	0.0	0	23
R572	CH_2-S+CO_2=CH_2O+CO	3.00E+12	0.0	0	23
R573	CH_2-S+CH_3=C_2H_4+H	2.00E+13	0.0	0	23
R574	CH_2-S+CH_2CO=C_2H_4+CO	1.60E+14	0.0	0	23
R575	CH+O_2=CHO+O	3.30E+13	0.0	0	23
R576	CH+O=CO+H	5.70E+13	0.0	0	23
R577	CH+OH=CHO+H	3.00E+13	0.0	0	23

R578	CH+OH=C+H_2O	4.00+07	2.0	3001	23
R579	CH+CO_2=CHO+CO	3.40+12	0.0	690	23
R580	CH+H=C+H_2	1.50+14	0.0	0	23
R581	CH+H_2O=CH_2O+H	1.17+15	-0.8	0	23
R582	CH+CH_2O=CH_2CO+H	9.46+13	0.0	-515	23
R583	CH+C_2H_2=C_3H_2+H	1.00+14	0.0	0	23
R584	CH+CH_2=C_2H_2+H	4.00+13	0.0	0	23
R585	CH+CH_3=C_2H_3+H	3.00+13	0.0	0	23
R586	CH+CH_4=C_2H_4+H	6.00+13	0.0	0	23
R587	C+O_2=CO+O	2.00+13	0.0	0	23
R588	C+OH=CO+H	5.00+13	0.0	0	23
R589	C+CH_3=C_2H_2+H	5.00+13	0.0	0	23
R590	C+CH_2=C_2H+H	5.00+13	0.0	0	23
R591	CH_2O+OH=CHO+H_2O	3.43+09	1.2	-447	23
R592	CH_2O+H=CHO+H_2	2.19+08	1.8	3001	23
R593	CH_2O+M=CHO+H+M	3.31+16	0.0	81039	23
R594	CH_2O+O=CHO+OH	1.80+13	0.0	3081	23
R959	CHO+OH=H_2O+CO	1.00+14	0.0	0	23
R596	CHO+H=CO+H_2	1.19+13	0.2	0	23
R597	CHO+O=CO+OH	3.00+13	0.0	0	23
R598	CHO+O=CO_2+H	3.00+13	0.0	0	23
R599	CO+OH=CO_2+H	9.42+03	2.2	-2352	23
R600	CO+O+M=CO_2+M	6.17+14	0.0	3001	23
R601	CO+O_2=CO_2+O	2.53+12	0.0	47711	23
R602	CO+HO_2=CO_2+OH	5.80+13	0.0	22945	23
R603	OH+H_2=H+H_2O	2.14+08	1.5	3450	23
R604	O+OH=O_2+H	2.02+14	-0.4	0	23
R605	O+H_2=OH+H	5.06+04	2.7	6293	23
R606	OH+HO_2=H_2O+O_2	2.13+28	-4.8	3501	23
R607	H+HO_2=OH+OH	1.50+14	0.0	1005	23
R608	H+HO_2=H_2+O_2	8.45+11	0.7	1241	23
R609	H+HO_2=O+H_2O	3.01+13	0.0	1721	23
R610	O+HO_2=O_2+OH	3.25+13	0.0	0	23
R611	OH+OH=O+H_2O	3.57+04	2.4	-2113	23
R612	H+H+H_2=H_2+H_2	9.20+16	-0.6	0	23

R613	H+H+H_2O=H_2+H_2O	6.00+19	-1.2	0	23
R614	H_2O_2+H=HO_2+H_2	1.98+06	2.0	2436	23
R615	H_2O_2+H=OH+H_2O	3.07+13	0.0	4219	23
R616	H_2O_2+O=OH+HO_2	9.55+06	2.0	3971	23
R617	H_2O_2+OH=H_2O+HO_2	2.40+00	4.0	-2163	23
R618	O+O+M=O_2+M	1.89+13	0.0	-1788	23
R619	HO_2+HO_2=H_2O_2+O_2	4.20+14	0.0	11987	23
R620	C_4H_5-123(+M)=C_4H_4-123+H(+M)	1.00+13	0.0	56027	23
R621	C_4H_5-121(+M)=C_4H_4+H(+M)	1.00+13	0.0	49024	23
R622	C_4H_5-I(+M)=C_4H_4+H(+M)	1.00+14	0.0	50024	23
R623	C_4H_5-N(+M)=C_4H_4+H(+M)	1.00+14	0.0	37018	23
R624	C_4H_3-I(+M)=C_4H_2+H(+M)	1.00+14	0.0	55026	23
R625	C_4H_3-N(+M)=C_4H_2+H(+M)	1.00+14	0.0	36017	23
R626	C_3H_4-P+H(+M)=C_3H_5-S(+M)	6.50+12	0.0	2001	23
R627	C_3H_4-A+H(+M)=C_3H_5-A(+M)	1.20+11	0.7	3008	23
R628	C_3H_4-A+H(+M)=C_3H_5-S(+M)	8.49+12	0.0	2001	23
R629	CHOCHO(+M)=CH_2O+CO(+M)	4.27+12	0.0	50624	23
R630	CH_3CO(+M)=CH_3+CO(+M)	3.00+12	0.0	16730	23
R631	CH_2CO(+M)=CH_2+CO(+M)	3.00+14	0.0	71014	23
R632	C_3H_8(+M)=C_2H_5+CH_3(+M)	7.90+22	-1.8	88672	23
R633	C_3H_7-N(+M)=C_2H_4+CH_3(+M)	1.23+13	-0.1	30216	23
R634	C_3H_6+H(+M)=C_3H_7-I(+M)	5.70+09	1.2	874	23
R635	C_3H_3+H(+M)=C_3H_4-A(+M)	1.66+15	-0.4	0	23
R636	C_3H_3+H(+M)=C_3H_4-P(+M)	1.66+15	-0.4	0	23
R637	C_2H_4+H(+M)=C_2H_5(+M)	1.08+12	0.5	1822	23
R638	C_2H_2+H(+M)=C_2H_3(+M)	3.11+11	0.6	2590	23
R639	CH_3+CH_3(+M)=C_2H_6(+M)	9.22+16	-1.2	636	23
R640	CH_3+H(+M)=CH_4(+M)	2.14+15	-0.4	0	23
R641	CH_3+OH(+M)=CH_3OH(+M)	5.65+13	0.1	0	23
R642	CH_3OH(+M)=HCOH+H_2(+M)	4.15+16	-0.1	92330	23
R643	CH_2-S+M=CH_2+M	1.00+13	0.0	0	23
R644	CHO+M=H+CO+M	1.86+17	-1.0	17008	23
R645	H+O_2(+M)=HO_2(+M)	4.52+13	0.0	0	23
R646	H+O2(+H_2)=HO_2(+H_2)	4.52+13	0.0	0	23
R647	H+O_2(+H_2O)=HO_2(+H_2O)	4.52+13	0.0	0	23

R648	$H+H+M=H_2+M$	1.00+18	-1.0	0	23
R649	$H+OH+M=H_2O+M$	2.21+22	-2.0	0	23
R650	$H+O+M=OH+M$	4.71+18	-1.0	0	23
R651	$OH+OH(+M)=H_2O_2(+M)$	1.24+14	-0.4	0	23

Units are in cm^3-mole-second, K, cal mol^{-1}

The pyrolytic products continue to form under an oxidative environment along with new products. As expected, incident shock temperature (T_2) dissociates DCPD into a CPD monomer. The CPD undergoes dissociation forming cyclopentadienyl radical and H-atom. The CPD consumes either by H-atom abstraction or by a series of reactions with H, OH, O, O_2 and HO_2. The H-atom abstraction of CPD leading to the formation of CPDyl radical which undergoes ring opening leading to different linear products. It is found that the amount of methane, ethylene, 1,3-butadiene, styrene and vinyl acetylene formed in the oxidation of DCPD is considerably higher than that of pyrolysis. In the oxidation of DCPD, acetylene is formed significantly fewer amounts than that observed in pyrolysis. Also, propyne, allene, propylene, benzene, and toluene concentration are found to be considerably low for oxidation than pyrolysis. The early formation of 1,3-butadiene, acetylene, methane, and ethylene observed during oxidation of DCPD is directly coming from the fragmentation of the C_5 ring. The C_5 ring undergoes fragmentation to form either $C_4 + C_1$ or $C_2 + C_3$. The possible way which explains the benzene formation in the oxidation process is coming from the combination of C_5 and C_1. The oxidation of CPDyl radical leads to the formation of either CO and C_4 (two C_2) or acetylene and propenal-yl radical.

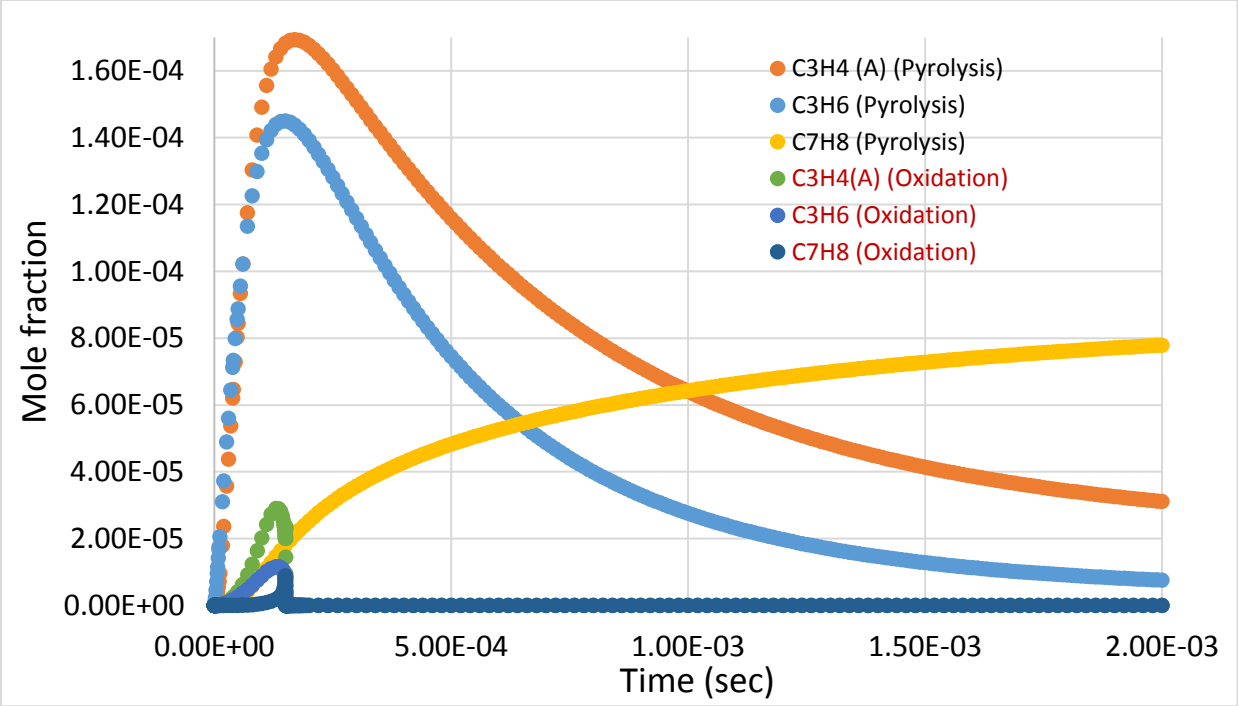

Figure 5.4 (a): *The model prediction for different products formed during oxidation and pyrolysis of DCPD at a temperature of 1445 K.*

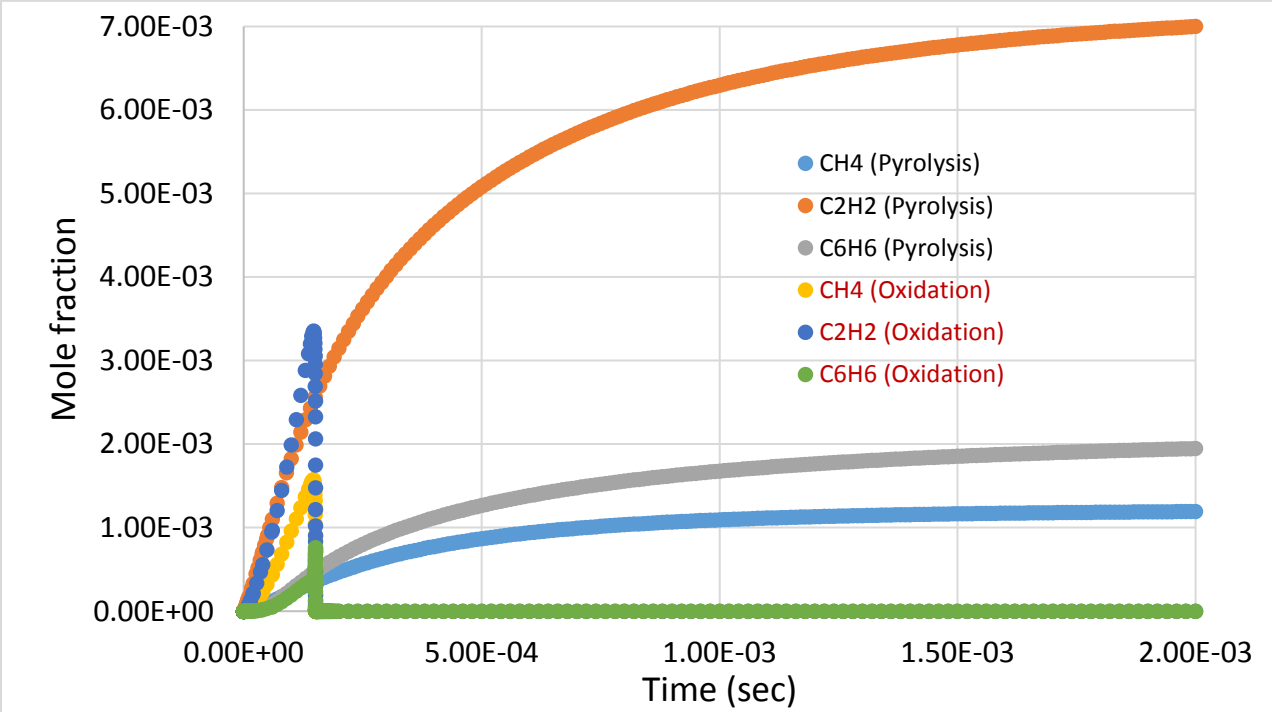

Figure 5.4 (b): *The model prediction for different products formed during oxidation and pyrolysis of DCPD at a temperature of 1445 K.*

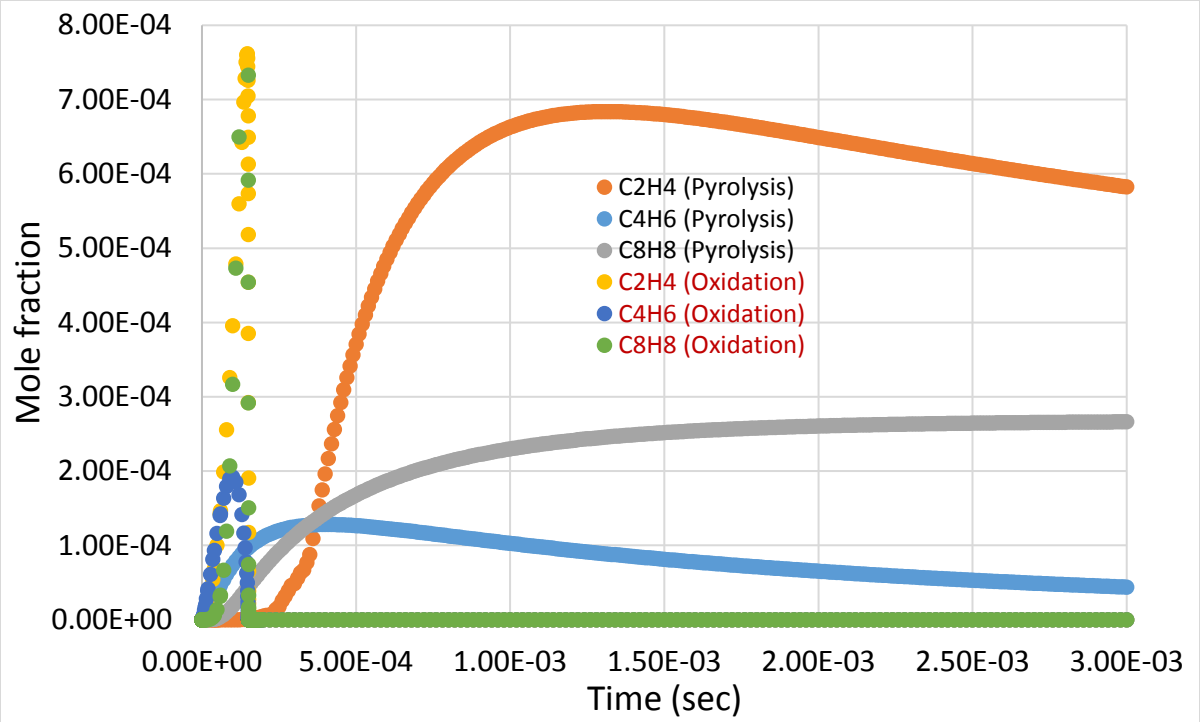

Figure 5.4 (c): *The model prediction for different products formed during oxidation and pyrolysis of DCPD at a temperature of 1445 K.*

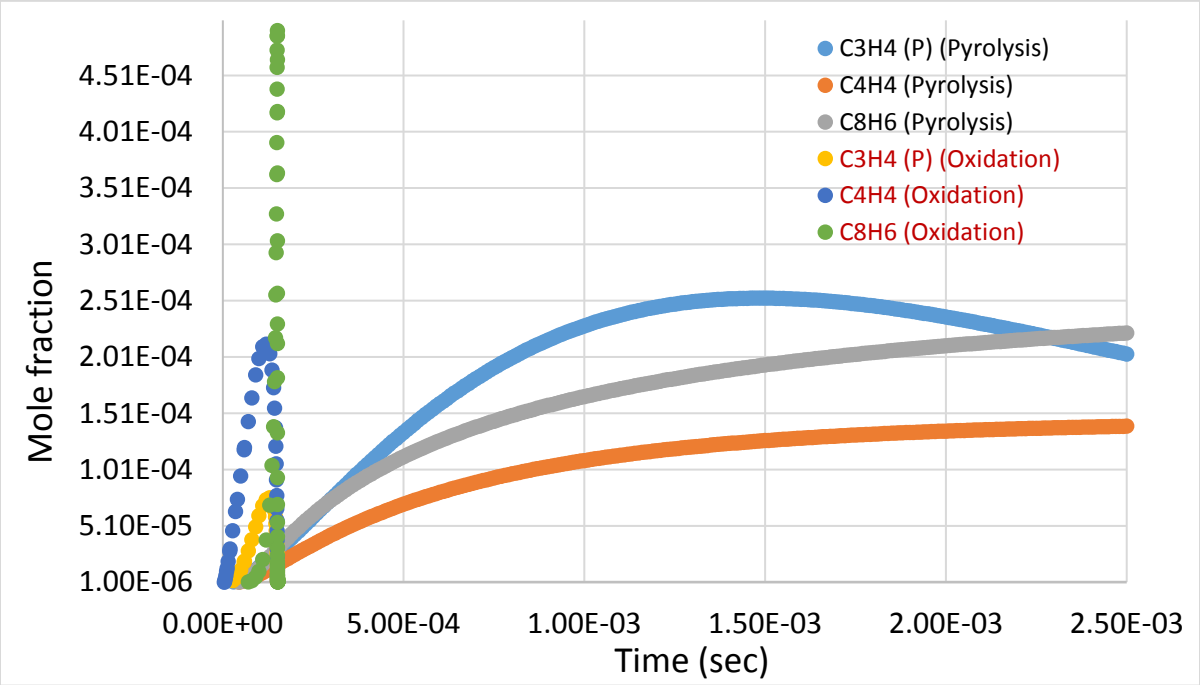

Figure 5.4 (d): *The model prediction for different products formed during oxidation and pyrolysis of DCPD at a temperature of 1445 K.*

A comparison between the observed ignition delay and simulated ignition delay is presented in Figure 5.5. It has been observed that simulated ignition delays are in reasonable agreement with the observed ignition delay for all three equivalent ratios. Figure 5.6 represents the comparison of the ignition delay of JP-10 and DCPD. The activation energy for JP-10 and DCPD oxidation are found to be 37.58 kcal/mol and 36.92 kcal/mol respectively. This clearly shows that DCPD can be used as a fuel due to its high energy density.

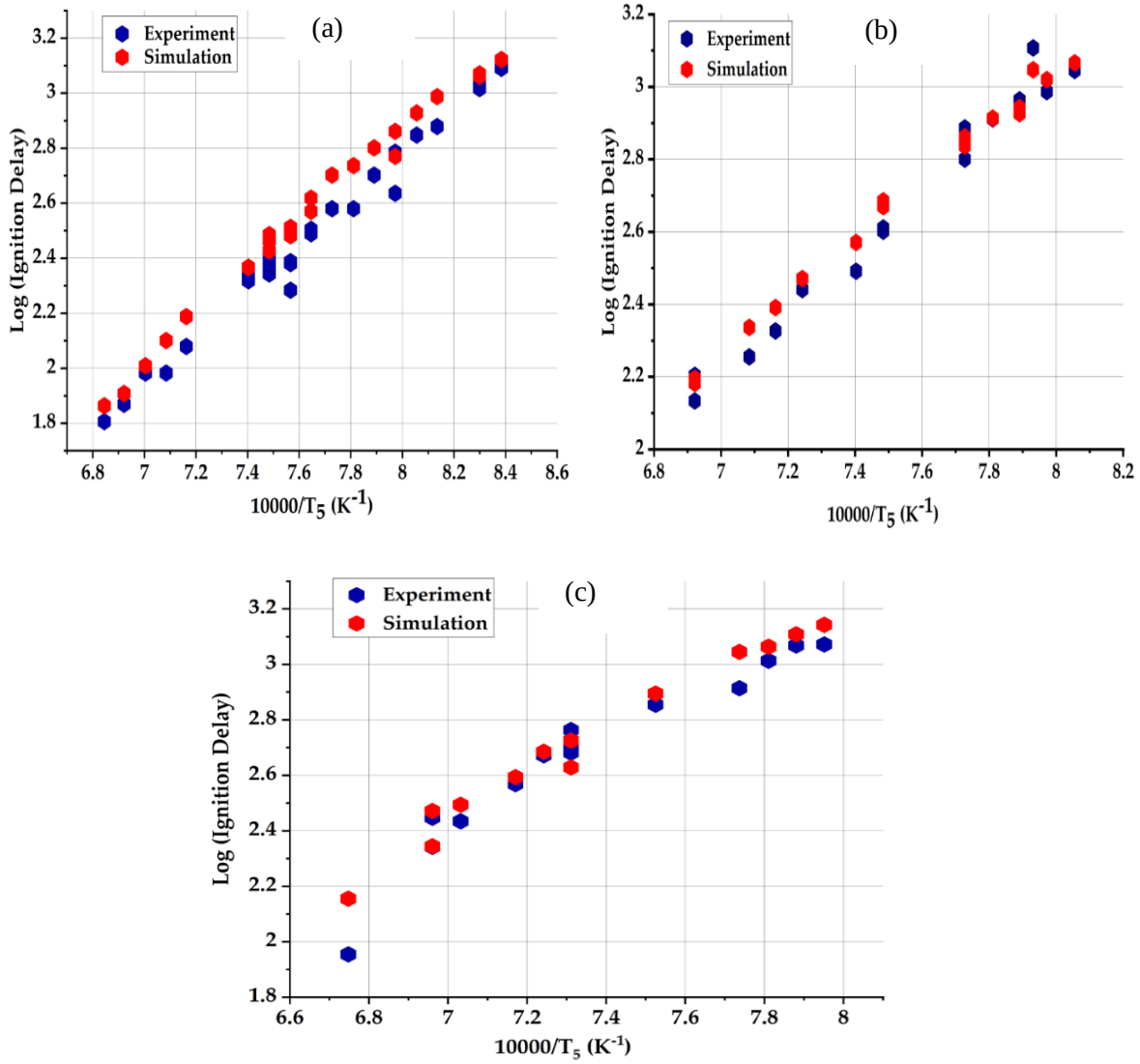

Figure 5.5: *Comparison between the ignition delay obtained using the mechanism and experiments (a) $\phi = 0.5$ (b) $\phi = 1.0$ (c) $\phi = 1.5$.*

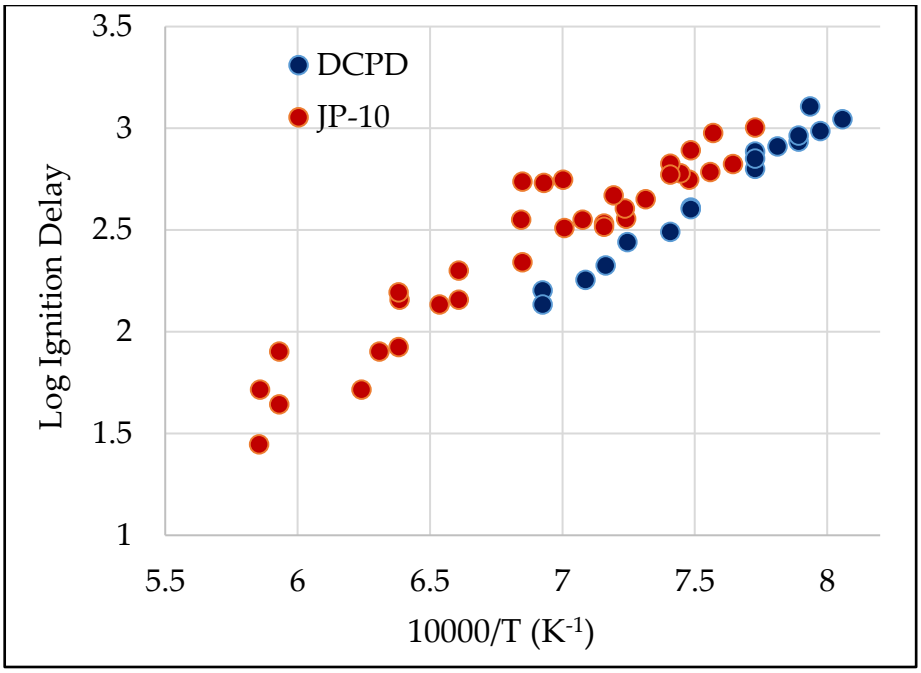

Figure 5.6: *Plot showing the comparison between the ignition delays of DCPD and JP-10 [15] for equivalence ratio 1.*

5.5 CONCLUSION

The ignition delay measurements were carried out in a modified chemical shock tube (CST3) for three different equivalent ratios 0.5, 1, and 1.5. Furthermore, a detailed kinetic mechanism was developed for a better understanding of oxidation mechanism. In addition, a comparison was made between the calculated and observed ignition delay. The mechanism fairly replicated the observed ignition delay. The comparison between ignition delays of DCPD and JP-10 showed that DCPD resembles almost same fuel characteristics than that of JP-10. The activation energy for JP-10 and DCPD oxidation are found to be 37.58 kcal/mol and 36.92 kcal/mol respectively.

The pyrolytic products continue to form under the oxidation environment. DCPD dissociates into CPD due to incident shock temperature (T_2). CPD undergoes dissociation producing cyclopentadienyl radical and H-atom. CPD

continues to consume either by H-abstraction of by other species such as OH, O, O2, HO2 etc. The H-atom abstraction of CPD leads to the formation of CPDyl radical. The kinetic model showed that the early formation of 1,3-butadiene, acetylene, methane, and ethylene observed during oxidation of DCPD is directly coming from the fragmentation of the C_5 ring. CPDyl continue to oxidize to form either CO and C4 (two C2) or acetylene and propenal-yl radical.

5.6 REFERENCES

1. R. D. Hawthorn, and A. C. Nixon, AIAA Journal, 4, 3, 1966, 513- 521.
2. A. Burcat, R. C. Farmer, R. L. Espinoza, and R. A. Matula, Combustion and Flame, 36, 1979, 313-316.
3. D. F. Davidson, D. C. Horning, and R. K. Hanson, 35th AlAA/ ASME/ SAE/ ASEE Joint Propulsion Conference.
4. C. J. Brown and G. O. Thomas, Combustion and Flame, 117, 1999, 861-870.
5. D. F. Davidson and R. K. Hanson, International Journal of Chemical Kinetics, 36, 2004, 510-523.
6. J. Herzler, and C. Naumann, Proceedings of the Combustion Institute, 32, 2009, 213-220.
7. J. Huang, W. K. Bushe, P. G. Hill and S. R. Munshi, International Journal of Chemical Kinetics, 38, 2006, 221-233.
8. H. J. Curran, M. P. Dunphy, J. M. Simmie, C. K. Westbrook, and W. J. Pitz, Twenty-Fourth Symposium (International) on Combustion/ The Combustion Institute, 1992, 769-776.
9. S. M. Anderson, A. Freedman, and C. E. Kolb, Journal of Physical Chemistry, 91, 1987, 6212-6211.
10. S. Nakra, R. J. Green, and S. L Anderson, Combustion and Flame, 144, 4, 2006, 662-674.
11. K. Chenoweth, A. C. T. van Duin, S. Dasgupta, and W. A. Goddard III, Journal of Physical Chemistry A, 113, 2009, 1740-1746.
12. S. R. Smith and A. S. Gordon, Journal of Physical Chemistry, 65, 7, 1961, 1124-1128.

13. S. Reshmi, E. Arunan, and C. P. Reghunadhan Nair, Industrial Engineering & Chemical Research, 53, 2014, 16612−16620.
14. J. D. Rule, J. S. Moore, Macromolecules, 35, 2002, 7878-7882.
15. H. K. Chakravarty, Ph.D Thesis on Thermal Decomposition of Haloethanols and Ignition of JP-10., August 2011.
16. D. F. Davidson, D. C. Horning, J. T. Herbon, and R. K. Hanson, Proceedings of Combustion Institute, 28, 2000, 1687-1696.
17. R.G. Butler, Combustion Chemistry of 1–3 Cyclopentadiene, Ph.D. thesis, Princeton University, Princeton, NJ, 2001.
18. M. B. Colket, L. J. Spaddaccini, Journal of Propulsion and Power, 17, 2001, 315-323.
19. A. Burcat, and M. Dvinyaninov, International Journal of Chemical Kinetics 29, 1997, 505 – 514.
20. H. Pitsch, Proceedings of the Combustion Institute, 26, 1996, 721-728.
21. J. L. Emdee, K. Brezinsky, and I. Glassman, Journal of Physical Chemistry 96, 1992, 2151-2161.
22. E. Ranzi, T. Faravellip, P. Gaffurig, C. Pennattia and A. Sogaro, Combustion Science and Technology 100, 1-6, 1994, 11-28
23. N. M. Marinov, W. J. Pitz, C. K. Westbrook, M. J. Castaldi, and S. M. Senkan, Combustion Science and Technology 116–117, 1996, 211–287.
24. A. M. Dean, Journal of Physical Chemistry, 89, 21, 1985, 4600-4608.
25. W. R. Dolbier jun. and H. M. Frey, Journal of Chemical Society, Perkin Trans. 2, 1974, 1674-1676.
26. A. M. Dean, Journal of Physical Chemistry, Vol. 89, No. 21, 1985, 4600-4608.

27. X. Zhong, and J. W. Bozzelli, Journal of Physical Chemistry A, 102, 1998, 3537–3555.

28. https://rmg.mit.edu

29. R. K. Robinson, and R. P. Lindstedt, Combustion and Flame, 158, 2011, 666–686.

30. R.G. Butler, and I. Glassman, Proceedings of the Combustion Institute 32, 2009, 395–402.

6

CONCLUSION AND FUTURE DIRECTION

CHAPTER OVERVIEW

This chapter presents a comprehensive description of the entire work and emphasizes the salient features of the present work. The concluding remarks are followed by some suggestions regarding future directions of research related to this work.

6.1 THERMAL DECOMPOSITION OF DCPD

Thermal decomposition experiments of DCPD were performed behind the reflected shock wave in the temperature range of 1250-1550 K and pressure range of 13-16 atm using a modified shock tube. The shock tube is incorporated with the step size driver insert to cancel the non-ideal rise in pressure behind the reflected shock wave. The driver insert provides near-ideal behavior for the accurate measurement of chemical kinetic data. The major pyrolytic products observed during thermal decomposition of DCPD are methane, acetylene, cyclopentadiene, and benzene whereas the minor products include ethylene, propylene, propyne, allene, 1,3-butadiene, vinyl acetylene, toluene, styrene, and phenylacetylene. Whereas, naphthalene, indene, methyl-indenes, benzene, and methane are major species formed during cyclopentadiene pyrolysis. However, we have not observed naphthalene, indene, and methyl-indenes during DCPD pyrolysis for given conditions. Although DCPD is expected to fully decompose into CPD in T_2 (incident shock temperature), the appearance of a DCPD peak in the gas chromatogram might arise due to the desorption of DCPD from the wall of the shock tube. The formation of CPD monomer constitutes the primary decomposition channel for DCPD pyrolysis. The CPD has the weakest C-H bond of any common hydrocarbon, its dissociation leading to the formation of cyclopentadienyl radical. The ring-opening of CPDyl radical is an important step for the formation of linear products.

Ab-initio theoretical calculations were performed to explore the minimum energy pathway for decomposition of DCPD which explains the formation of experimentally observed products. These calculations were carried out using the B3LYP/6-311+G(2d,p) level of theory, and single-point energies were calculated

using the CCSD(T)/6-311+G(2d,p) level of theory. A kinetic mechanism consisting of 82 reactions and 35 species has been derived for the DCPD thermal decomposition based upon the experimental and theoretical results. The mechanism fairly replicated the formation of observed product concentration.

6.2 QTAIM ANALYSIS ON DISSOCIATION REACTION OF DCPD

The quantum theory of atoms in molecule (QTAIM) is used as a tool for studying the dissociation reaction of DCPD to CPD. The dissociation reaction of DCPD to CPD is initiated by the breaking of one C-C bond between bridge carbon atoms. The electron density analysis along the reaction coordinate provides detailed information about the bond breaking and bond making process. It could be expected that both C-C bonds are elongated at the transition state due to molecular symmetry. However, we found that one of the C-C bonds between bridge carbon atoms is more elongated while the other C-C bond remains intact. None of the C-C bonds is broken in the transition state. Also, a new C-C bond is formed at the transition state characterized by a bond critical point that forms a cage-like structure. Dissociation reaction of DCPD to CPD is characterized by the presence of a cage critical point (CCP) at the transition state which is unique of its kind. In addition, AIM analysis was used to identify various types of non-covalent interactions. Non-covalent interactions are highly nonlocal and characterized as low-density gradient isosurfaces with a low value of electron density. The sign of the λ_2 (second Hessian eigenvalue) is the key quantity to identify the types of interactions and strength will be determined from the value of density on the region of non-covalent interaction. This approach provides a detailed picture of various kinds of interactions such as van der Waal's interaction, hydrogen bonds,

steric clashes, etc. In the case of DCPD, the NCI result shows an indicative signature of very weak van der Waals interactions which was not seen using AIMALL. The transition state exhibits attractive as well as non-bonding interactions corresponding to the negative and positive value of sign of $(\lambda_2)\rho$ respectively. Whereas near product geometry shows the nonbonding interaction corresponds to a positive value sign of $(\lambda_2)\rho$. The gradient isosurfaces for reactant geometry represent the center of the ring signifying the steric repulsion between the bridge carbon atoms whereas the isosurfaces lie in between the norbornene ring and cyclopentene ring shows repulsive interaction. For the transition state, isosurfaces show a region of non-bonded at the center of two cyclopentadiene rings where Π-stacking is expected. In the case of the near product geometry, the isosurfaces are similar to the transition state geometry.

6.3 MEASUREMENT OF IGNITION DELAY OF DCPD

The measurement of ignition delay of DCPD was performed behind reflected shock wave for three different equivalent ratios 0.5, 1, and 1.5 using a modified shock tube. A kinetic mechanism consisting of 153 species and 651 reactions has been derived for the oxidation of DCPD for better understanding of oxidation mechanism. It is found that the mechanism fairly replicated the observed ignition delay. A comparison between the observed ignition delay and simulated ignition delay shows reasonable agreement with each other for all three equivalent ratios. Also, the comparison between ignition delays of DCPD and JP-10 showed that DCPD resembles almost same fuel characteristics of JP-10. The activation energy for JP-10 and DCPD oxidation are found to be 37.58±0.62 kcal/mol and 36.92±1.80 kcal/mol respectively. This clearly shows that DCPD can be used as a fuel due to its high energy density.

The pyrolytic products continue to form under oxidative environment along with new products. The model prediction analysis for oxidative and pyrolytic products showed the early formation of 1,3-butadiene, acetylene, methane, and ethylene observed during oxidation of DCPD is directly coming from the fragmentation of the C_5 ring. DCPD is decomposed into CPD due to incident shock temperature (T_2). The CPD undergoes dissociation producing CPDyl radical and H-atom. The CPD consume either by H-abstraction or by other species such as O, O_2, OH, HO_2 etc. The H-atom abstraction of CPD leading to the formation of CPDyl radical. CPDyl continues to oxidize to form either CO and C4 (two C2) or acetylene and propenal-yl radical.

6.4 SCOPE OF FURTHER STUDIES AND FUTURE DIRECTION

Although the incorporation of the driver insert provides near-ideal behavior behind the reflected shock wave, the dynamics of the flow in shock tube is not well understood. The computation study has to be done to get details of flow characteristics which could be a subject of investigation. The experimental results on thermal decomposition of DCPD as well as oxidation of DCPD using shock tube are highly reliable. Still, there is more scope for modifying the reported theoretical and kinetic mechanism. With the help of online techniques such as time of flight mass spectrometry (TOF-MS), matrix IR, Laser absorption, and other online detection methods it is possible to measure the concentration profile for different species formed in the thermal decomposition of DCPD. Also, the field of combustion will be explored by studying the kinetics of newer molecules and important pathways leading to the formation of PAHs and soot. The hydrogenation of DCPD gives the saturated derivative $C_{10}H_{16}$ (fuel in military applications), which undergoes acid-catalyzed rearrangement to adamantane

($C_{10}H_{16}$). The adamantane can be described as a fusion of three cyclohexane rings. JP-10 consists of 96.5 wt % exo-tetrahydrodicyclopentadiene ($C_{10}H_{16}$), along with the two isomers of $C_{10}H_{16}$ molecules, endo-tetrahydrodicyclopentadiene, 2.5 wt %, and adamantine, 1.0 wt %.

FREQUENCIES OF MOLECULES, INTERMEDIATES, AND TS

A. DCPD → CPD

Table III.S1: Vibrational frequencies (in cm^{-1}; scaled by a factor 0.9692) of the species/TS computed at B3LYP/6-311+G(2d,p) level of theory.

DCPD			CPD		TS		
140	937.7	1442.1	341.2	2938.1	-157.8	923.8	1437.9
190.9	949.2	1454.2	508.1	3088.3	161.6	933.1	1438.9
317.6	982.6	1582.5	657.8	3098.5	175.4	957.5	1442.0
372.4	1003.2	1621.7	688.9		282.9	960.8	1464.9
448.8	1012.3	2919.7	793.7		352.3	994.2	2893.5
459.9	1051.1	2924.3	795.6		399.2	995.0	2893.8
475.2	1083.8	2935.1	890.4		428.7	1055.6	2975.0
618.1	1095.9	2943.2	893.6		476.3	1064.4	2976.3
659.6	1111.7	2968.2	916.3		592.1	1076.6	2991.2
693.3	1123.7	2995.7	922.2		628.9	1076.9	3002.4
718.6	1144.7	2998.8	938.2		688.1	1108.7	3084.6
746.6	1151.3	3002.5	978.1		695.6	1115.8	3086.2
763.6	1213.5	3060.5	1081.1		695.8	1135.8	3108.1
793.9	1233.6	3082.5	1093.2		722.3	1218.2	3108.4
802.4	1244.4	3085.1	1098.2		769.6	1227.8	3130.4
847.5	1246.3	3108.2	1230.5		783.1	1242.1	3132.6
876.2	1259.8		1281.6		802.6	1265.4	
886.1	1277.1		1358.5		820.0	1267.9	
910.8	1289.2		1372.3		876.4	1314.4	
916.8	1302.8		1497.5		901.6	1315.2	
925.3	1331.9		1581.2		905.4	1405.8	
934.1	1346.2		2919.2		920.1	1418.6	

B. cy-C_5H_6 → C_3H_4(P) + C_2H_2

Table III.S2: Vibrational frequencies (in cm^{-1}; scaled by a factor 0.9692) of the species/TS computed at B3LYP/6-311+G(2d,p) level of theory.

I1	I2	TS1	TS2	TS3
89.9	50.5	-1039.1	-612.5	-700.4
311.9	146.3	344.2	309.6	230.2
568.8	310.3	473.9	455.4	258.8
747.8	382.4	655.3	525.9	339.7
780.9	487.0	767.2	665.3	448.1
784.6	634.5	790.4	727.2	467.7
881.8	691.8	800.0	747.3	506.9
889.6	854.2	880.8	834.9	585.1
903.8	881.1	918.6	861.8	655.3
958.6	882.6	926.3	943.6	668.2
986.2	910.5	957.4	955.4	678.5
1073.2	981.3	963.1	996.0	816.5
1096.5	989.6	1090.9	1037.0	915.1
1117.8	1020.4	1099.3	1046.8	979.4
1142.7	1119.1	1140.6	1066.7	1027.4
1197.4	1299.7	1230.0	1157.4	1046.6
1261.9	1335.2	1273.9	1293.9	1311.7
1344.8	1405.6	1299.1	1364.6	1321.6
1353.8	1432.5	1359.5	1411.7	1419.6
1398.2	1621.2	1379.2	1436.8	1581.1
1492.3	1950.2	1529.8	1475.4	1859.6
2918.4	3009.3	2077.7	2979.1	1949.6
2926.6	3025.8	2922.3	3004.9	2972.9
2936.8	3040.4	2949.9	3049.2	3023.3
2947.8	3051.9	3055.8	3050.4	3206.0

C. cy-C_5H_5 → C_3H_3 + C_2H_2

Table III.S3: Vibrational frequencies (in cm^{-1}; scaled by a factor 0.9692) of the species/TS computed at B3LYP/6-311+G(2d,p) level of theory.

(1a)	(2a)	(3a)	(4a)	(5a)	(6a)	C2H2	C3H3
59.6	301.0	76.3	34.6	115.5	140.2	609.4	341.5

473.4	444.4	146.6	146.8	164.4	144.9	609.4	384.9
507.5	649.2	312.4	310.2	333.0	319.5	719.5	435.6
653.3	763.7	374.5	362.8	363.8	343.7	719.5	601.9
692.9	777.7	493.0	516.2	522.2	571.3	2001.3	670.9
787.3	794.7	611.9	607.6	544.7	574.9	3303.3	1001.3
823.5	877.5	644.3	672.9	661.1	630.9	3401.2	1050.2
847.8	899.0	796.6	840.6	797.4	643.4		1416.1
867.8	906.8	834.3	856.4	860.1	778.9		1937.7
892.3	920.0	854.7	862.6	860.7	797.3		3044.5
934.1	960.2	877.2	873.0	879.6	838.0		3131.0
1002.7	1081.0	894.6	877.3	982.9	927.9		3346.9
1048.2	1084.6	979.7	981.7	1011.8	995.5		
1108.8	1183.2	1111.8	1105.1	1104.9	1201.6		
1183.9	1206.3	1238.0	1235.4	1211.8	1212.1		
1263.0	1300.3	1328.2	1318.3	1309.6	1306.7		
1357.1	1372.1	1429.6	1427.4	1425.4	1415.2		
1403.5	1488.3	1584.8	1575.7	1573.5	1625.7		
1515.7	1577.2	1954.4	1952.5	1951.4	2150.0		
3103.6	2938.6	2933.7	2998.5	3007.9	2914.3		
3105.6	2964.3	3013.0	3010.9	3012.9	2933.0		
3118.3	3086.7	3034.4	3030.8	3037.5	2933.0		
3132.3	3112.2	3079.3	3077.7	3080.1	3148.9		
3139.6	3118.3	3147.8	3142.6	3134.5	3354.8		

Table III.S4: Vibrational frequencies (in cm^{-1}; scaled by a factor 0.9692) of the species/TS computed at B3LYP/6-311+G(2d,p) level of theory.

TS1	**TS2**	**TS3**	**TS4**	**TS5**	**TS6**	**TS7**
-1348.1	-444.1	-665.9	-125.2	-572.6	-466.9	-563.1
526.8	254.0	77.1	182.1	25.4	303.0	51.6
563.5	396.0	147.1	291.8	124.4	312.6	108.0
689.4	504.7	313.2	326.6	234.0	499.0	265.1

693.0	518.6	382.0	510.9	295.9	595.4	330.1
782.3	638.9	524.7	570.3	376.4	626.4	440.9
803.5	665.1	570.6	680.9	454.5	633.4	526.4
825.3	802.7	667.7	808.3	517.1	695.2	526.7
888.0	822.0	786.7	834.0	613.9	796.3	549.7
955.5	834.7	854.1	851.8	674.0	819.8	618.3
1019.1	853.0	869.8	866.6	715.1	900.9	639.5
1057.9	940.2	876.5	942.0	732.8	931.3	724.7
1080.7	968.6	981.0	988.1	764.5	962.2	725.6
1124.8	1069.5	1101.4	1099.3	838.7	1153.2	887.5
1192.2	1175.3	1231.6	1208.4	999.1	1171.7	1007.2
1285.9	1270.1	1321.4	1276.3	1108.1	1256.4	1041.8
1322.2	1416.2	1427.4	1425.8	1423.1	1415.1	1412.3
1386.0	1542.8	1576.5	1590.6	1777.3	1589.3	1794.9
1438.9	1726.1	1953.0	1964.5	1881.2	1904.9	2046.3
2000.0	3002.7	2905.8	2994.8	3033.2	2935.4	3023.8
3092.4	3012.1	3012.0	3019.6	3111.3	2956.2	3103.6
3119.3	3072.2	3030.9	3022.5	3237.5	3014.5	3228.2
3139.5	3100.4	3078.9	3091.2	3249.3	3130.2	3323.1
3142.5	3150.2	3319.3	3132.5	3335.9	3304.9	3352.6

D. cy-C_5H_5 + cy-C_5H_6 → C_6H_6 + C_4H_4 + H

Table III.S5: Vibrational frequencies (in cm^{-1}; scaled by a factor 0.9692) of the species/TS computed at B3LYP/6-311+G(2d,p) level of theory.

I		**1d**		**2d**		**3d**	
50.7	1073.5	47.0	1067.1	53.5	1048.5	44.6	1061.1
84.7	1082.5	62.6	1079.1	96.1	1051.9	63.0	1077.8
110.1	1102.3	79.9	1109.4	100.7	1065.0	104.2	1142.6
201.3	1124.8	138.0	1151.4	195.6	1089.2	153.0	1163.0
285.4	1161.1	190.3	1176.8	211.1	1129.2	200.3	1198.0

342.6	1190.5	282.7	1181.8	345.3	1231.0	326.2	1242.8
428.6	1243.4	312.0	1221.4	349.0	1248.1	337.7	1252.3
531.4	1262.7	352.1	1272.3	361.3	1251.2	381.2	1293.5
561.9	1273.5	368.3	1272.4	431.0	1289.3	447.6	1310.6
616.8	1285.5	520.8	1327.8	528.2	1290.5	531.4	1358.5
653.5	1300.3	548.1	1356.4	604.0	1302.3	573.7	1378.4
676.	1361.5	562.0	1395.8	642.1	1367.0	591.5	1411.4
698.9	1365.5	679.8	1420.2	671.9	1404.1	608.9	1419.6
720.4	1429.8	703.9	1491.3	698.8	1423.1	640.3	1491.8
775.56	1437.9	740.8	1505.8	710.8	1432.7	699.3	1544.9
792.8	1498.8	746.7	1552.6	758.5	1580.5	719.6	1613.5
812.1	1582.9	791.2	1579.8	777.4	1624.8	765.1	1631.4
824.0	2874.0	809.6	2907.9	796.1	3014.6	774.5	2853.3
878.7	2882.4	821.9	3012.1	810.8	3020.4	855.9	3012.8
908.7	2904.7	842.6	3023.7	861.5	3041.6	884.6	3023.6
910.8	2929.2	875.9	3053.5	898.5	3046.0	919.3	3043.6
919.0	3081.5	904.5	3058.3	906.4	3062.4	935.8	3047.3
922.6	3086.7	921.6	3085.7	911.9	3074.0	940.2	3052.9
923.5	3096.0	926.1	3089.4	926.0	3082.8	956.4	3054.8
969.3	3105.0	939.4	3099.6	958.9	3093.5	962.5	3072.5
1001.9	3111.7	965.6	3118.5	994.4	3110.9	975.7	3073.0
1007.6	3116.1	973.5	3123.6	1003.3	3120.6	991.1	3094.7
1037.9	3120.6	988.0	3142.5	1010.4	3124.4	997.6	3121.8
1042.2		1047.1		1030.8		1024.6	

Table III.S6: Vibrational frequencies (in cm^{-1}; scaled by a factor 0.9692) of the species/TS computed at B3LYP/6-311+G(2d,p) level of theory.

TS1d		**TS2d**		**TS3d**		**TS4d**	
-603.5	1070.0	-497.8	1061.8	-672.9	1075.7	-409.1	1020.0
54.9	1079.7	56.9	1069.2	45.8	1099.6	30.4	1054.9
81.7	1112.6	97.8	1115.3	93.9	1132.4	74.9	1137.7
114.7	1131.1	105.0	1136.2	105.2	1165.0	79.0	1145.0

161.5	1161.4	191.6	1223.4	208.6	1222.5	111.7	1158.7
271.1	1179.5	222.1	1227.8	212.4	1249.7	148.2	1233.5
332.3	1203.7	336.0	1265.9	363.0	1270.2	248.0	1278.8
408.6	1272.7	359.2	1287.1	373.1	1297.0	296.1	1291.4
445.3	1291.2	405.7	1301.9	397.3	1357.0	373.8	1341.3
544.1	1343.6	445.4	1315.9	430.0	1360.8	403.2	1407.0
557.8	1357.9	552.2	1379.5	504.1	1370.8	498.9	1446.7
610.2	1386.3	610.8	1407.5	579.1	1405.4	595.2	1459.6
659.4	1481.4	668.9	1443.2	608.2	1427.4	598.6	1532.1
686.7	1494.2	716.1	1458.6	640.6	1501.4	636.7	1548.3
698.5	1539.4	719.5	1479.7	673.2	1613.3	654.1	1576.9
734.6	1580.3	763.6	1592.4	700.7	1638.4	693.9	1624.5
754.4	2863.2	771.5	3014.9	719.3	2962.2	735.3	2925.7
790.0	2996.1	805.1	3020.6	765.4	3017.3	809.1	3027.5
807.1	3018.4	831.2	3029.2	796.2	3025.2	846.0	3041.4
840.8	3021.1	866.8	3048.9	815.9	3040.6	848.8	3060.3
886.3	3054.1	878.5	3053.0	873.2	3043.7	870.8	3066.7
911.2	3072.0	889.5	3096.3	886.2	3061.5	895.8	3072.8
916.3	3087.8	903.1	3110.7	925.4	3063.6	915.6	3082.7
923.6	3095.3	911.3	3114.1	931.2	3074.0	943.3	3084.4
940.3	3097.5	937.5	3123.1	971.5	3079.5	952.4	3091.7
952.2	3117.2	957.7	3133.1	982.0	3101.9	969.2	3098.9
970.8	3122.5	985.7	3140.2	995.5	3121.9	987.4	3121.5
976.2		996.1		999.0		998.9	
1000.7		1029.5		1060.4		1008.0	
1035.1		1054.6		1069.4		1012.3	

E. cy-C_5H_6 + C_2H_3 ---> C_7H_8 + H

Table III.S7: Vibrational frequencies (in cm^{-1}; scaled by a factor 0.9692) of the species/TS computed at B3LYP/6-311+G(2d,p) level of theory.

(1f)		**(2f)**		**(3f)**		**(4f)**		**(TS1)**	
90.9	1104.3	205.6	1118.5	136.9	1153.3	115.1	1160.7	-332.0	1067.7

104.8	1207.4	218.4	1147.8	145.2	1198.3	152.0	1271.3	35.6	1090.8
252.1	1235.6	244.2	1169.3	222.9	1236.1	226.3	1294.5	94.8	1094.6
311.3	1252.8	301.3	1248.4	295.1	1274.4	328.3	1347.1	125.7	1234.9
364.9	1272.2	392.5	1259.6	378.8	1324.9	410.2	1370.7	183.1	1274.4
383.2	1281.0	455.7	1288.1	454.8	1355.3	485.3	1392.9	271.8	1351.2
465.2	1344.5	520.2	1327.6	618.4	1403.8	538.2	1401.9	352.3	1356.3
647.8	1405.1	626.5	1355.9	666.7	1423.3	571.1	1437.7	498.1	1377.9
691.4	1414.3	694.6	1430.2	699.6	1433.7	640.5	1448.7	650.9	1429.8
737.4	1610.2	743.6	1434.0	762.8	1434.7	742.0	1514.8	683.5	1560.1
776.4	1633.4	752.7	1588.5	812.9	1606.7	743.0	1564.2	774.4	1583.2
852.5	2845.0	792.8	2907.8	833.0	2852.2	747.4	2812.1	777.3	2899.1
897.0	2856.9	865.0	2936.9	905.6	2916.6	869.4	2829.2	793.3	2919.2
900.5	2861.9	890.2	3042.0	917.4	2941.4	906.3	2927.9	852.8	2957.5
914.5	3026.1	918.6	3046.7	925.9	2949.2	934.6	2971.9	872.8	3032.1
927.4	3034.1	926.6	3066.0	946.1	2985.3	934.9	3004.2	893.4	3094.4
941.9	3076.4	946.1	3075.8	978.9	3006.5	956.7	3051.2	896.3	3100.2
973.8		962.4	3081.8	996.4	3013.4	1029.2	3052.3	902.0	3102.7
992.8		1016.7	3101.4	1028.5	3073.2	1036.4	3070.3	924.1	3116.0
1014.7		1028.8	3143.4	1055.0	3095.5	1072.4	3080.4	934.3	3122.9
1081.5		1042.8		1077.7		1144.1		971.9	
1097.0		1096.4		1107.7		1146.9		1055.4	

Table III.S8: Vibrational frequencies (in cm^{-1}; scaled by a factor 0.9692) of the species/TS computed at B3LYP/6-311+G(2d,p) level of theory.

(TS2)		**(TS3)**		**(TS4)**		**(TS5)**	
-530.4	1119.0	-1900.6	1103.1	-699.4	1185.6	-725.6	1142.4
193.3	1162.6	165.3	1124.9	124.8	1202.7	50.4	1159.6
224.9	1212.0	193.0	1155.1	171.6	1244.6	197.5	1186.3
256.7	1243.6	289.9	1209.7	258.1	1293.4	277.7	1278.6
387.1	1250.7	320.5	1249.6	296.2	1356.8	329.0	1316.7
452.5	1279.0	401.3	1276.7	391.0	1362.6	364.8	1372.7

499.7	1341.1	473.1	1331.5	449.3	1392.7	426.5	1418.8
665.5	1356.8	634.2	1380.5	577.9	1431.4	490.5	1442.6
699.9	1423.1	676.5	1413.3	658.3	1438.0	510.5	1454.2
706.8	1461.2	713.7	1431.7	697.1	1455.6	614.9	1477.4
729.1	1604.5	732.6	1605.0	756.7	1550.8	674.6	1551.4
785.5	2877.9	769.4	2108.0	796.4	2845.4	741.9	1573.6
850.3	2888.4	809.1	2916.6	855.5	2898.0	773.9	2930.8
878.5	2992.6	845.2	2940.4	876.4	2919.1	846.1	2978.0
890.5	3040.6	903.2	3016.5	891.1	2951.7	869.3	3004.8
918.6	3066.6	918.4	3021.5	905.9	2956.4	949.2	3057.8
934.6	3079.5	946.5	3022.9	947.0	2993.0	967.3	3062.9
942.3	3101.9	973.8	3073.8	1007.2	3018.4	977.4	3072.8
967.0	3127.6	986.0	3095.7	1027.7	3053.0	995.3	3079.5
1030.2	3129.2	1032.4	3129.6	1045.0	3094.8	1012.9	3091.3
1061.3		1049.3		1093.4		1032.0	
1093.4		1064.6		1123.5		1068.4	

F. cy-C_5H_5 + C_3H_5 ---> C_8H_8 + H + H

Table III.S9: Vibrational frequencies (in cm^{-1}; scaled by a factor 0.9692) of the species/TS computed at B3LYP/6-311+G(2d,p) level of theory.

(1g)		**(2g)**		**(3g)**		**(4g)**	
76.2	1080.5	67.2	1116.2	108.5	1052.7	70.6	1139.2
84.6	1108.9	100.7	1151.4	153.8	1108.7	84.1	1162.6
150.7	1176.4	163.1	1167.6	231.9	1174.4	252.3	1224.8
214.6	1195.5	272.6	1175.9	346.6	1233.2	327.1	1249.5
328.7	1262.9	332.9	1246.7	353.3	1248.5	361.0	1280.4
398.2	1280.7	382.8	1271.9	401.7	1282.2	403.8	1309.9
513.1	1287.0	521.4	1318.4	526.5	1287.8	536.5	1358.9
545.6	1298.5	550.9	1356.3	633.0	1303.1	574.2	1401.6
619.5	1363.0	552.1	1447.4	650.3	1363.9	599.4	1411.2
697.5	1411.3	702.9	1472.3	671.1	1413.8	643.9	1492.6

711.5	1436.9	708.5	1494.7	715.9	1412.9	654.9	1545.2
780.2	1500.7	744.8	1580.3	780.4	1617.3	726.1	1633.0
800.7	1584.0	783.0	2903.1	783.5	3019.1	765.9	2823.4
850.7	1648.7	790.7	3018.3	801.4	3036.9	834.6	3026.9
907.0	2878.7	809.6	3042.4	870.4	3053.5	911.7	3039.1
908.7	2914.0	887.0	3047.4	891.1	3060.7	921.3	3053.8
920.2	2968.8	920.3	3089.1	897.1	3069.0	937.0	3055.8
921.0	3015.6	925.5	3099.4	924.3	3092.1	941.2	3073.8
925.4	3030.5	936.5	3118.9	958.2	3110.2	956.8	3074.1
967.6	3087.7	960.5	3123.8	975.6	3118.6	982.0	3094.5
995.2	3097.3	974.1	3134.9	1005.6	3119.7	988.1	3108.9
1013.5	3109.4	983.5		1010.1		999.7	
1020.8	3112.8	1074.9		1028.7		1077.6	
1067.4	3123.3	1079.1		1046.7		1079.0	

Table III.S10: Vibrational frequencies (in cm^{-1}; scaled by a factor 0.9692) of the species/TS computed at B3LYP/6-311+G(2d,p) level of theory.

(TS1)		**(TS2)**		**(TS3)**		**(TS4)**	
-879.7	1079.0	-499.2	1180.1	-676.2	1158.7	-898.8	1159.7
77.0	1080.8	126.0	1222.7	94.3	1232.7	91.8	1178.3
94.8	1110.1	151.2	1261.0	150.2	1270.2	179.9	1262.9
135.3	1165.5	200.8	1265.3	248.9	1289.0	225.8	1296.6
189.5	1197.3	324.8	1295.0	370.0	1358.7	380.0	1320.4
283.3	1236.6	396.0	1316.6	386.2	1359.4	387.7	1407.3
302.9	1276.9	466.7	1377.9	419.8	1371.5	438.6	1434.9
347.9	1284.7	558.2	1416.9	508.2	1423.0	477.7	1466.3
416.3	1298.0	603.1	1473.1	581.1	1502.5	480.3	1536.9
530.4	1306.5	687.1	1531.9	624.0	1646.9	544.4	1570.1
547.4	1358.5	713.1	3017.0	656.6	2944.9	609.8	1636.0
635.3	1372.0	763.8	3021.1	675.5	3022.2	642.8	3041.0
701.4	1421.6	796.6	3040.6	707.6	3035.4	672.6	3047.9

711.2	1498.6	812.6	3088.1	793.4	3063.3	748.0	3063.7
788.9	1583.4	825.3	3094.8	815.3	3066.1	773.9	3069.0
801.4	1629.3	847.4	3113.1	870.8	3075.2	812.3	3078.7
862.5	2885.8	886.9	3122.6	918.0	3078.5	891.7	3087.1
914.0	2978.6	911.0	3127.4	931.3	3103.0	911.2	3093.5
916.0	3022.3	937.7	3141.0	936.5	3114.9	945.5	3123.1
921.4	3034.3	949.1		983.3	1158.7	960.3	1159.7
925.8	3089.8	970.5		994.1	1232.7	975.5	1178.3
935.5	3099.7	1008.9		1001.4	1270.2	994.9	
971.5	3115.2	1038.7		1071.7		1005.7	
988.9	3117.7	1063.5		1098.2		1016.0	
1018.4	3123.1	1067.0		1115.2		1076.2	
1035.3		1115.2		1154.1		1143.5	

G. cy-C_5H_5 + C_3H_3 ---> C_8H_6 + H + H

Table III.S11: Vibrational frequencies (in cm^{-1}; scaled by a factor 0.9692) of the species/TS computed at B3LYP/6-311+G(2d,p) level of theory.

(1m)		**(2m)**		**(3m)**		**(4m)**	
77.2	1156.2	39.5	1177.1	138.7	1129.7	70.6	1226.4
117.6	1188.6	102.0	1177.4	141.3	1236.0	144.2	1234.9
172.3	1265.3	196.5	1271.6	285.8	1248.9	247.7	1306.0
277.0	1280.6	281.1	1345.8	348.8	1287.0	366.5	1355.3
342.8	1299.6	379.0	1355.2	469.0	1304.7	415.5	1409.1
433.6	1362.1	402.6	1492.2	470.2	1364.2	501.3	1494.8
531.5	1430.4	444.3	1579.8	521.0	1423.7	503.5	1550.2
562.5	1502.3	534.0	1941.2	578.2	2115.6	574.1	2134.5
628.0	1584.8	538.2	2928.7	639.1	3051.7	596.6	2785.8
642.3	2140.9	614.9	3059.5	653.3	3076.9	628.7	3059.4
691.7	2902.4	631.9	3091.2	671.9	3084.2	647.9	3061.8
708.9	2932.8	705.6	3101.6	714.7	3095.1	650.4	3085.1
768.2	2964.8	706.1	3121.5	773.7	3113.6	712.6	3085.5

797.3	3088.7	790.0	3126.2	777.7	3122.7	758.2	3098.0
843.9	3098.5	810.2	3346.9	803.2	3354.3	829.5	3353.8
913.7	3113.6	891.4		872.9		917.2	
921.5	3125.1	921.7		901.6		935.2	
926.2	3353.9	925.9		921.5		939.8	
931.8		970.3		987.3		957.0	
968.2		982.1		998.3		989.0	
1016.8		997.1		1014.7		1007.4	
1022.1		1079.8		1035.6		1078.5	
1080.6		1090.1		1049.7		1138.5	
1105.8		1117.7		1056.1		1164.0	

Table III.S12: Vibrational frequencies (in cm^{-1}; scaled by a factor 0.9692) of the species/TS computed at B3LYP/6-311+G(2d,p) level of theory.

(TS1)		**(TS2)**		**(TS3)**		**(TS4)**	
-1177.3	1033.5	-489.1	1126.1	-682.3	1142.1	-981.7	1154.1
73.5	1079.8	119.6	1224.2	139.8	1236.8	132.8	1174.8
117.4	1102.6	139.3	1266.8	143.9	1271.2	152.0	1247.9
155.3	1140.3	263.7	1288.6	301.1	1358.4	319.5	1303.8
241.7	1174.4	409.8	1322.6	383.3	1364.3	379.5	1423.9
286.9	1230.0	434.2	1377.0	473.7	1370.5	445.9	1459.2
299.6	1272.7	475.7	1476.8	481.3	1504.5	449.8	1529.2
429.2	1288.4	497.4	2030.2	496.6	2142.2	501.3	1568.8
452.7	1293.5	550.0	3033.5	579.7	2936.6	518.1	2136.2
533.0	1318.3	643.3	3094.4	629.9	3071.0	547.6	3069.2
587.2	1361.6	688.5	3096.0	641.0	3074.2	609.5	3076.2
612.9	1502.6	710.6	3116.0	649.6	3089.3	611.0	3089.1
639.0	1585.7	725.9	3124.5	671.9	3092.6	661.9	3097.0
689.0	2112.9	792.6	3144.5	709.1	3104.6	662.4	3099.7
708.5	2875.3	806.6	3351.6	790.2	3353.6	727.8	3354.4
779.6	2970.8	830.2		810.7		769.2	

798.2	3091.0	896.0		878.9		809.4	
846.9	3100.8	915.1		930.5		894.0	
920.9	3116.1	949.7		978.6		945.9	
924.9	3127.3	961.0		989.0		962.4	
928.8	3352.6	1017.6		1011.3		977.0	
947.1		1060.2		1073.8		1007.0	
970.9		1068.2		1098.3		1067.6	
1016.8		1085.3		1131.7		1144.2	

APPENDIX A

A. CALCULATION OF ENTHALPY AND ENTROPY FOR MOLECULES

Here we present the procedure for calculation of Enthalpy and Entropy of the molecules at the G3 level of theory. For example, the enthalpy and entropy calculation on dicyclopentadiene is given below. The energy values which is obtained from the Gaussian output file of dicyclopentadiene (DCPD) optimized at the G3 level of theory are summarized in Table A.1.

Table A.1: Parameters at G3 level of theory.

Parameters	Value
ZPE	0.186205
Thermal Correction	0.193483
G3(0K)	-387.903205
G3 Energy	-387.895927
G3 Enthalpy	-387.894983
G3 Free energy	-387.93458
Number of carbon (C)	10
Number of hydrogen (H)	12

The following equation is employed to calculate the enthalpy and entropy of a molecule.

$$\boldsymbol{H_f}(0K) = No.\ of\ Carbon * 169.98 + No.\ of\ Hydrogen * 51.63 - 627.5095 * \{[No.\ of\ Carbon * (-37.827717) + No.\ of\ Hydrogen * (-0.501003)] - G3\ (0K)\}$$

$$\boldsymbol{H_f}(298K) = H_f(0K) + 627.5095 * [Thermal\ correction - ZPE] - [No.\ of\ Carbon * 0.25 + No.\ of\ Hydrogen * 1.01]$$

$\boldsymbol{S}$ (298 K) = {*G3 (Enthalpy) – G3 (Free Energy)*} / 298

The estimated value of enthalpy and entropy for the dicyclopentadiene molecule at the G3 level of theory is tabulated in Table A.2.

Table A.2: Estimated values at G3 level of theory.

Parameters	**Values**
$\boldsymbol{H_f}$(0 K) kcal/mol	51.541294
$\boldsymbol{H_f}$(298 K) kcal/mol	41.488309
$\boldsymbol{S}$ (298 K) kcal/mol	0.08338085
$\boldsymbol{S}$ (298 K) cal/mol	83.38085

CHEMKIN expects the thermodynamic data of any chemical species to be provided in a specific format. The data for any species requires four formatted lines each of length 80 characters. The first line includes the species name, data, the elemental composition of species, phase of species (S, L, or G for solid, liquid, or gas), and the temperature ranges over which polynomial fits the thermodynamic data. The fits to C^0_p/R, H^0/RT, S^0/R, consist of seven coefficients for each of two temperature ranges given by the equations (1)-(3).

$$\frac{C^0_{pk}}{R} = a_{1k} + a_{2k}T_k + a_{3k}\,T_k^2 + a_{4k}\,T_k^3 + a_{5k}\,T_k^4 \qquad \text{……..(1)}$$

$$\frac{H^0_k}{RT_k} = a_{1k} + \frac{a_{2k}}{2}T_k + \frac{a_{3k}}{3}\,T_k^2 + \frac{a_{4k}}{4}\,T_k^3 + \frac{a_{5k}}{5}\,T_k^4 + \frac{a_{6k}}{T_k} \qquad \text{……..(2)}$$

$$\frac{S^0_k}{R} = a_{1k}\ln T_k + a_{2k}T_k + \frac{a_{3k}}{2}\,T_k^2 + \frac{a_{4k}}{3}\,T_k^3 + \frac{a_{5k}}{4}\,T_k^4 + a_{7k} \qquad \text{……..(3)}$$

The second line includes the coefficients a_1, a_2, a_3, a_4, and a_5 as represented in equations (1)-(3) for the upper-temperature interval. The third line includes the coefficients a_6 and a_7 for upper-temperature interval and coefficients a_1, a_2, and a_3 for lower temperature interval. The fourth line includes the coefficients a_4, a_5, a_6, and a_7 for lower temperature intervals.

```
H2               TPIS78H   2               G   200.000  3500.000 1000.000    1
 3.33727920E+00-4.94024731E-05 4.99456778E-07-1.79566394E-10 2.00255376E-14    2
-9.50158922E+02-3.20502331E+00 2.34433112E+00 7.98052075E-03-1.94781510E-05    3
 2.01572094E-08-7.37611761E-12-9.17935173E+02 6.83010238E-01                   4
AR               120186AR  1               G   300.000  5000.000 1000.00     1
 2.50000000e+00 0.00000000e+00 0.00000000e+00 0.00000000e+00 0.00000000e+00    2
-7.45375000e+02 4.36600100e+00 2.50000000e+00 0.00000000e+00 0.00000000e+00    3
 0.00000000e+00 0.00000000e+00-7.45375000e+02 4.36600100e+00                   4
CO               TPIS79C   1O   1   00   00G   200.000  3500.000  1000.000    1
 2.71518561E+00 2.06252743E-03-9.98825771E-07 2.30053008E-10-2.03647716E-14    2
-1.41518724E+04 7.81868772E+00 3.57953347E+00-6.10353680E-04 1.01681433E-06    3
 9.07005884E-10-9.04424499E-13-1.43440860E+04 3.50840928E+00 8.67100000E+03    4
A2CH3            MAR94 C  11H  10    0    0g   300.000  5000.000 1388.000    1
 2.51695452e 01 3.06623666e-02-1.07325255e-05 1.69233411e-09-9.92571012e-14    2
 1.89171186e 03-1.15036002e 02-5.83569401e 00 1.02894702e-01-7.55130040e-05    3
 2.84055718e-08-4.37865877e-12 1.27117089e 04 5.16088842e 01                   4
H2O2             L 7/88H   2O   2   00   00G   200.000  3500.000  1000.000    1
 4.16500285E+00 4.90831694E-03-1.90139225E-06 3.71185986E-10-2.87908305E-14    2
-1.78617877E+04 2.91615662E+00 4.27611269E+00-5.42822417E-04 1.67335701E-05    3
-2.15770813E-08 8.62454363E-12-1.77025821E+04 3.43505074E+00 1.11588350E+04    4
CH2OH            IU2/03C   1H   3O   1   00G   200.000  6000.00               1
 5.09314370E+00 5.94761260E-03-2.06497460E-06 3.23008173E-10-1.88125902E-14    2
-4.03409640E+03-1.84691493E+00 4.47834367E+00-1.35070310E-03 2.78484980E-05    3
-3.64869060E-08 1.47907450E-11-3.50072890E+03 3.30913500E+00-2.04462770E+03    4
CH2O             L 8/88H   2C   1O   1   00G   200.000  3500.000  1000.000    1
 1.76069008E+00 9.20000082E-03-4.42258813E-06 1.00641212E-09-8.83855640E-14    2
-1.39958323E+04 1.36563230E+01 4.79372315E+00-9.90833369E-03 3.73220008E-05    3
-3.79285261E-08 1.31772652E-11-1.43089567E+04 6.02812900E-01 1.00197170E+04    4
A2CO        10/21/97THERC  11H   7O   1    0G   300.000  5000.000 1397.000    1
 2.82275360E+01 2.18350283E-02-7.45407649E-06 1.15760326E-09-6.72316566E-14    2
 9.27445303E+03-1.31016072E+02-5.77988871E+00 1.10378058E-01-9.62307014E-05    3
 4.16616204E-08-7.11931774E-12 1.99992059E+04 4.81074527E+01                   4
A2OH                    C  10H   8O   1    0g   300.000  5000.000 1428.000    1
 1.70545603e 01 2.71399777e-02-8.37556985e-06 1.20806091e-09-6.64265060e-14    2
-1.60606637e 04-5.91338880e 01-8.85357874e 00 1.07649510e-01-1.02973597e-04    3
 5.04843296e-08-9.60093087e-12-9.23181655e 03 7.26290702e 01                   4
A2O              MAR94 C  10H   7O   1    0g   300.000  5000.    1402.        1
 2.73202720e 01 2.06287145e-02-7.07119840e-06 1.10136964e-09-6.41024638e-14    2
 1.22677534e 03-1.24813148e 02-3.96924112e 00 9.54479821e-02-7.37031626e-05    3
 2.72312623e-08-3.85415426e-12 1.16368615e 04 4.21473784e 01                   4
C9H7                    C   9H   7    0    0g   300.000  5000.00  1396.00     1
 1.88496987e 01 2.30750390e-02-7.97012499e-06 1.24573420e-09-7.26203331e-14    2
```

```
 2.15148314e 04-8.07377133e 01-7.55449024e 00 9.17109694e-02-7.78588594e-05    3
 3.40781245e-08-6.00585308e-12 2.99922277e 04 5.86084835e 01                   4
C9H7O      10/29/96     C   9H   7O   1    0G   300.000  5000.000 1404.000    1
 2.51076292E+01 2.01860050E-02-6.96790367E-06 1.09035427E-09-6.36667441E-14    2
 9.65697630E+03-1.12850245E+02-7.61335755E+00 9.84645454E-02-7.66361016E-05    3
 2.83537784E-08-4.00243035E-12 2.05294989E+04 6.17187488E+01                   4
C9H8                    H   8C   9          G   100.000  5000.000 1066.52     1
 1.31709644E+01 3.70449600E-02-1.57693963E-05 3.05357250E-09-2.20724149E-13    2
 1.25770590E+04-4.89660662E+01 1.33565302E+00 4.34084597E-02 2.87604224E-05    3
-5.82106137E-08 2.19760487E-11 1.72641976E+04 1.90333176E+01                   4
A2CH2             MAR94 C  11H   9    0    0g   300.000  5000.000 1389.000    1
 2.66596107e 01 2.69903845e-02-9.49827903e-06 1.50313533e-09-8.83831941e-14    2
 2.10180607e 04-1.22975161e 02-5.51514480e 00 1.06245066e-01-8.57510752e-05    3
 3.55122444e-08-5.98055713e-12 3.18146452e 04 4.84291679e 01                   4
A2H               MAR94 C  10H   8    0    0g   300.000  5000.    1389.       1
 2.26796811e 01 2.56406162e-02-9.01884317e-06 1.42679026e-09-8.38746748e-14    2
 7.15869139e 03-1.04560335e 02-7.22113353e 00 9.86835940e-02-7.85937984e-05    3
 3.21311283e-08-5.35095416e-12 1.72527463e 04 5.49455699e 01                   4
A2CH2OH    2/26/96 THERMC  11H  10O   1    0G   300.000  5000.000 1399.000    1
 2.84083357E+01 2.89997204E-02-9.93572669E-06 1.54515596E-09-8.97786709E-14    2
-1.69654021E+04-1.31390113E+02-6.97361905E+00 1.18422094E-01-9.70187021E-05    3
 4.02326624E-08-6.67149874E-12-5.48856314E+03 5.60097221E+01                   4
A2CHO       10/21/97THERC  11H   8O   1    0G   300.000  5000.000 1397.000    1
 2.86304055E+01 2.41957191E-02-8.29938161E-06 1.29254031E-09-7.52027451E-14    2
-9.81976071E+03-1.33907075E+02-6.98623212E+00 1.15164340E-01-9.75569060E-05    3
 4.11139283E-08-6.85939227E-12 1.58810888E+03 5.43164988E+01                   4
A2                G3B3  C  10H   7O   0N   0G   300.000  3000.000  1000.000    1
 3.22892303E+00 6.31264486E-02-3.80582381E-05 1.08454069E-08-1.18342512E-12    2
 4.78400840E+04 5.82016697E+00-8.02718034E+00 1.02924518E-01-8.34272010E-05    3
 2.72135383E-08-7.24559554E-13 5.01363344E+04 6.08902264E+01 2.10209869E+04    4
A2C2H5                  C  12H  12    0    0g   300.000  5000.000 1393.000    1
 2.89853383e 01 3.39680004e-02-1.17265032e-05 1.83245637e-09-1.06814341e-13    2
-2.18564737e 03-1.33852524e 02-7.57755435e 00 1.23905796e-01-9.74487941e-05    3
 3.94103218e-08-6.46891513e-12 1.00243094e 04 6.08512792e 01                   4
CH4                     H   4C   1          G   100.000  5000.000 1122.23     1
 1.19935714E+00 1.10795591E-02-4.08368048E-06 7.35029002E-10-5.08320954E-14    2
-9.87128311E+03 1.23131908E+01 4.22972997E+00-5.78252757E-03 2.65555822E-05    3
-2.22787788E-08 6.14802144E-12-1.01697842E+04-9.55642789E-01                   4
CH3                     H   3C   1          G   100.000  5000.000  897.45     1
 2.73168098E+00 6.26283482E-03-2.27067791E-06 3.82997768E-10-2.46397213E-14    2
 1.65992930E+04 6.07543412E+00 3.94216057E+00 8.68529507E-04 6.74388827E-06    3
-6.31232639E-09 1.84014903E-12 1.63819882E+04 3.66341380E-01                   4
```

```
C2H               T-5-10H   1C   2          G     200.0    6000.0  1000.0      1
   3.66270248E0  3.82492252E-3   -1.366325E-6  2.1345504E-10-1.23216848E-14    2
    6.7168379E4   3.92205792E0   2.89867676E0  1.32988489E-2 -2.80733327E-5    3
  2.89484755E-8-1.07502351E-11    6.7061605E4   6.18547632E0                   4
SCH2     CH2(S)    31287C   1H   2          G  0300.00   4000.00  1000.00      1
 0.03552888E+02 0.02066788E-01-0.01914116E-05-0.11046733E-09 0.02021349E-12    2
 0.04984975E+06 0.01686570E+02 0.03971265E+02-0.01699088E-02 0.10253689E-05    3
 0.02492550E-07-0.01981266E-10 0.04989367E+06 0.05753207E+00                   4
TCH2     CH2      120186C   1H   2          G  0250.00   4000.00  1000.00      1
 0.03636407E+02 0.01933056E-01-0.01687016E-05-0.10098994E-09 0.01808255E-12    2
 0.04534134E+06 0.02156560E+02 0.03762237E+02 0.11598191E-02 0.02489585E-05    3
 0.08800836E-08-0.07332435E-11 0.04536790E+06 0.01712577E+02                   4
C2H4                    H   4C   2          G   100.000  5000.000  927.06     1
 2.54472224E+00 1.32860402E-02-5.51151894E-06 1.05201468E-09-7.54052185E-14    2
 4.79401342E+03 7.64867124E+00 3.87548501E+00-4.62000433E-03 4.31428284E-05    3
-4.80901191E-08 1.69936397E-11 5.06998884E+03 4.14851741E+00                   4
C2H2                    H   2C   2          G   100.000  5000.000 1039.23     1
 4.96211352E+00 4.76106617E-03-1.76896829E-06 3.32750311E-10-2.41327819E-14    2
 2.55443609E+04-5.97514292E+00 3.09481504E+00 6.81342859E-03 2.68032458E-06    3
-7.27607710E-09 2.95005791E-12 2.62097520E+04 4.43942006E+00                   4
C2H3                    H   3C   2          G   100.000  5000.000  919.90     1
 3.29187317E+00 9.26412900E-03-3.76729932E-06 7.11368830E-10-5.06783092E-14    2
 3.41629826E+04 6.40060856E+00 3.20398636E+00 2.56351617E-03 1.87079542E-05    3
-2.39466080E-08 8.92521495E-12 3.44788323E+04 8.44614106E+00                   4
A1         Ph.D.   82489C   6H   5          g  0300.00   4000.00  1000.00      1
 0.01577589e+03 0.09651109e-01-0.09429416e-05-0.05469111e-08 0.01026522e-11    2
 0.03302698e+06-0.06176280e+03 0.01143557e+01 0.03627325e+00 0.01158286e-04    3
-0.02196965e-06 0.08463556e-10 0.03836054e+06 0.02380117e+03                   4
C6H4C2H           MAR94 C   8H   5    0    0g   300.000  5000.    1396.       1
 1.68316021e 01 1.67689325e-02-5.80036217e-06 9.07204455e-10-5.29017068e-14    2
 5.88280539e 04-6.65053548e 01-5.44701359e 00 8.50347082e-02-8.80141224e-05    3
 4.56991772e-08-9.17878229e-12 6.51138786e 04 4.76781849e 01                   4
A1H               20387C   6H   6          g  0300.00   5000.00  1000.00      1
 0.01291074e+03 0.01723297e+00-0.05024211e-04 0.05893497e-08-0.01947521e-12    2
 0.03664512e+05-0.05002699e+03-0.03138012e+02 0.04723103e+00-0.02962208e-04    3
-0.03262819e-06 0.01718692e-09 0.08890031e+05 0.03657573e+03                   4
HCCO              SRIC91H   1C   2O   1     G  0300.00   4000.00  1000.00      1
 0.56282058E+01 0.40853401E-02-0.15934547E-05 0.28626052E-09-0.19407832E-13    2
 0.19327215E+05-0.39302595E+01 0.22517214E+01 0.17655021E-01-0.23729101E-04    3
 0.17275759E-07-0.50664811E-11 0.20059449E+05 0.12490417E+02                   4
A1C2H5                  C   8H  10    0    0g   300.000  5000.000 1397.000     1
 2.02816724e+01 2.59464082e-02-8.92667064e-06 1.39161163e-09-8.09786280e-14    2
```

```
-6.88695837e+03-8.65892579e+01-5.93600077e+00 8.94618416e-02-6.81230510e-05    3
 2.66103734e-08-4.21398102e-12 1.94317497e+03 5.33309542e+01                    4
OA1CH3              jle C   7H   7O   1    0G   300.000  5000.000 1398.000     1
 2.00333477E+01 1.83142467E-02-6.17265091E-06 9.50353551E-10-5.48634044E-14    2
-7.76864165E+03-8.60606102E+01-3.82920147E+00 7.73376217E-02-6.15929083E-05    3
 2.43728641E-08-3.80779615E-12 2.89377185E+01 4.06647799E+01                    4
CHO               121286H   1C   1O   1     G   300.000  5000.000 1000.00      1
 3.55727100e+00 3.34557300e-03-1.33500600e-06 2.47057300e-10-1.71385100e-14    2
 3.91632400e+03 5.55229900e+00 2.89833000e+00 6.19914700e-03-9.62308400e-06    3
 1.08982500e-08-4.57488500e-12 4.15992200e+03 8.98361400e+00                    4
C2H5                    H   5C   2          G   250.0    5000.0   995.0        1
   4.74777319E0  1.14086285E-2 -3.81375099E-6  5.8746302E-10-3.41128644E-14    2
   1.22404195E4  -1.52590277E0   3.87193994E0 -3.57531865E-4  3.69680741E-5    3
 -4.21755109E-8 1.45890315E-11   1.31715059E4   6.49792536E0                   4
C3H2              121686C   3H   2          G  0300.00   5000.00  1000.00      1
 0.06530853E+02 0.05870316E-01-0.01720776E-04 0.02127498E-08-0.08291910E-13    2
 0.05115213E+06-0.11227278E+02 0.02691077E+02 0.14803664E-01-0.03250551E-04    3
-0.08644363E-07 0.05284877E-10 0.05219072E+06 0.08757391E+02                    4
C3H3                    H   3C   3          G   100.000  5000.000 1285.11      1
 7.03262642E+00 7.99165951E-03-3.00724885E-06 5.29779555E-10-3.57295748E-14    2
 3.80728946E+04-1.20959018E+01 3.02395174E+00 2.04689456E-02-1.75709152E-05    3
 8.08485473E-09-1.50546150E-12 3.91032131E+04 8.24919301E+00                    4
C3H4(P)                 H   4C   3          G   100.000  5000.000 1049.76      1
 5.21780246E+00 1.29652604E-02-5.11733757E-06 9.36294778E-10-6.49492488E-14    2
 1.99033931E+04-4.22359230E+00 3.26735782E+00 1.28611243E-02 5.79984609E-06    3
-1.28355086E-08 4.84343888E-12 2.07281280E+04 7.25866046E+00                    4
C3H6                    H   6C   3          G   100.000  5000.000 1041.31      1
 4.37092735E+00 1.95208711E-02-7.89595077E-06 1.46990979E-09-1.03114596E-13    2
-1.35170831E+02 6.98557970E-01 3.28280698E+00 1.06185816E-02 2.37725065E-05    3
-3.08696856E-08 1.05576140E-11 8.00703489E+02 9.39777944E+00                    4
C3H4(A)                 H   4C   3          G   100.000  5000.000 1011.26      1
 5.13890540E+00 1.35237844E-02-5.53963444E-06 1.04531490E-09-7.41955931E-14    2
 2.05111513E+04-4.64020732E+00 3.33088582E+00 9.74955901E-03 1.62650072E-05    3
AC3H5                   C   3H  5          G   200.000  6000.000 900.00       1
 6.54174678E+00 1.36925550E-02-4.92244313E-06 7.96875582E-10-4.78649400E-14    2
 1.74361074E+04-1.13275428E+01 2.02492271E+00 1.44512591E-02 2.60064995E-05    3
-4.59604518E-08 1.95644481E-11 1.90314366E+04 1.43337431E+01                    4
HOA1CH3            L 6/87C   7H   8O   1    0G   300.000  3000.000 1000         1
 0.15932987E+02 0.27011160E-01-0.99448722E-05 0.16296689E-08-0.98513298E-13    2
-0.23592065E+05-0.59732841E+02 0.42258267E+00 0.45551636E-01 0.32012513E-04    3
-0.81121959E-07 0.37665658E-10-0.18202621E+05 0.26032903E+02-0.15911701E+05    4
A1OH               g 8/00C   6H   6O   1    0G   300.000  3000.000  1000.       1
```

```
 1.41552427E+01 1.99350340E-02-7.18219540E-06 1.16229002E-09-6.97147483E-14    2
-1.81287441E+04-5.17984911E+01-2.90978575E-01 4.08562397E-02 2.42829425E-05    3
-7.14477617E-08 3.46002146E-11-1.34129780E+04 2.68745637E+01-1.15940687E+04    4
A1O                82489C   6H   5O   1     g  0300.00   4000.00  1000.00      1
 0.01822639e+03 0.01003985e+00-0.09915668e-05-0.05672804e-08 0.01068372e-11    2
-0.02620846e+05-0.07361391e+03 0.01107497e+02 0.03956946e+00 0.08497295e-05    3
-0.02436311e-06 0.09650660e-10 0.03159672e+05 0.01973496e+03                   4
A1CHO             G3B3  C   7H   6O   1N   0G   300.000  3000.000  1000.000    1
 1.87355756E+00 5.26231551E-02-3.17644962E-05 9.06403069E-09-9.90306123E-13    2
-7.23603865E+03 1.49787009E+01-3.47171048E+00 6.92891889E-02-4.32603509E-05    3
 3.43871096E-09 4.81010261E-12-6.14558774E+03 4.14094024E+01 1.95577369E+04    4
C3H7                    H   7C   3          G   100.000  5000.000 1022.38      1
 5.36187747E+00 2.04003129E-02-8.01623234E-06 1.45815412E-09-1.00833118E-13    2
 9.19356308E+03-2.52593005E+00 3.00553759E+00 1.66222152E-02 1.65957265E-05    3
-2.70248967E-08 9.90455955E-12 1.03546505E+04 1.22162104E+01                   4
C4H3                    H   3C   4          G   100.000  5000.000 1137.81      1
 9.98403839E+00 8.75496422E-03-4.15972030E-06 9.51539169E-10-7.66574759E-14    2
 6.16957101E+04-2.75559537E+01 2.96070652E+00 1.61928821E-02 8.77945220E-06    3
-1.99564240E-08 7.44538163E-12 6.44107353E+04 1.21419081E+01                   4
C4H6                    H   6C   4          G   100.000  5000.000 1038.81      1
 5.80068848E+00 2.07183206E-02-8.29155354E-06 1.53184957E-09-1.06980234E-13    2
 1.02302878E+04-4.78580896E+00 2.91749601E+00 1.81493504E-02 1.51580330E-05    3
-2.61854962E-08 9.61222301E-12 1.15669393E+04 1.27840774E+01                   4
C4H4                    H   4C   4          G   100.000  5000.000 1019.55      1
 7.03981058E+00 1.39807004E-02-5.53057726E-06 1.01843883E-09-7.11926076E-14    2
 3.15146252E+04-1.17051475E+01 2.86540141E+00 2.03725748E-02-2.43426547E-07    3
-1.20449835E-08 5.48754271E-12 3.28848224E+04 1.10599902E+01                   4
C4H5                    C   4H   5          G   200.000  6000.000 1000.00      1
 8.78608925E+00 1.43145979E-02-5.12056955E-06 8.24782525E-10-4.93158540E-14    2
 3.93421346E+04-2.09424392E+01 2.01421956E+00 2.39714042E-02 6.54022957E-06    3
-2.43797560E-08 1.06094869E-11 4.15680422E+04 1.60855856E+01                   4
cy-C5H5                 H   5C   5          G   100.000  5000.000 1092.67      1
 8.62065764E+00 1.98892433E-02-8.49334961E-06 1.65584192E-09-1.20527648E-13    2
 2.76219773E+04-2.33291317E+01 2.70784308E+00 2.04032443E-02 1.98097712E-05    3
-3.33115711E-08 1.19293809E-11 3.01755993E+04 1.14932144E+01                   4
C5H7(l)                 H   7C   5          G   100.000  5000.000 1057.02      1
 9.36953888E+00 2.43846707E-02-1.02774566E-05 1.96845771E-09-1.41109454E-13    2
 1.99052515E+04-2.36987486E+01 2.30695919E+00 2.78326416E-02 1.78633839E-05    3
-3.66144932E-08 1.39118952E-11 2.26987557E+04 1.69172177E+01                   4
L-C5H5             T 4/94C   5H   5    0    0G   298.150  5000.000 1000.        1
 0.14889675E+02 0.82161004E-02-0.15178062E-05 0.16268184E-09-0.88052708E-14    2
 0.42719249E+05-0.53382883E+02-0.26085299E+01 0.65236909E-01-0.82191379E-04    3
```

```
 0.60364270E-07-0.19071607E-10 0.47360405E+05 0.35504920E+02 0.48866379E+05    4
cy-C5H6                 C   5H   6          G   100.000  5000.000  862.78      1
 5.98167971E+00 2.63449740E-02-1.14897760E-05 2.27740646E-09-1.67934278E-13    2
 1.26240237E+04-1.01256202E+01 1.18293328E+00 1.34341474E-02 7.20822516E-05    3
-1.09529993E-07 4.59153851E-11 1.47606617E+04 1.99008278E+01                   4
 cy-C5H7                 H   7C   5          G   100.000  5000.000  957.48     1
 1.14663923E+01 1.81268519E-02-5.84977406E-06 1.11024079E-09-8.55148315E-14    2
 2.23915783E+04-3.78299999E+01 2.75219728E+00 9.81731723E-03 7.72173585E-05    3
-1.05500079E-07 4.04852825E-11 2.61099578E+04 1.45356101E+01                   4
C4H5-N                  C   4H   5          G   200.000  6000.000 1000.00     1
 8.78608925E+00 1.43145979E-02-5.12056955E-06 8.24782525E-10-4.93158540E-14    2
 3.93421346E+04-2.09424392E+01 2.01421956E+00 2.39714042E-02 6.54022957E-06    3
-2.43797560E-08 1.06094869E-11 4.15680422E+04 1.60855856E+01                   4
C5H5                    H   5C   5          G   100.000  5000.000 1020.18     1
 1.05187786E+01 1.71449110E-02-7.15003969E-06 1.36473315E-09-9.79169714E-14    2
 4.41992829E+04-2.97492151E+01 2.21284106E+00 3.11861518E-02-5.57147035E-07    3
-2.07430343E-08 9.68150977E-12 4.68580264E+04 1.52128814E+01                   4
C5H6              000000N   0H   6O   0C   5G       300      3000    1000     1
 2.30537462E-01 4.09571826E-02-2.41588958E-05 6.79763480E-09-7.36374421E-13    2
 1.43779465E+04 2.02551234E+01-5.13691194E+00 6.06953453E-02-4.60552837E-05    3
 1.28457201E-08 7.41214852E-13 1.53675713E+04 4.61567559E+01                   4
C5H4OH            T 8/99C   5H   5O   1    0G   200.000  6000.000 1000.       1
 1.33741248E+01 1.51996469E-02-5.45685046E-06 8.80944866E-10-5.27493258E-14    2
 2.20358027E+03-4.59569069E+01-1.28398054E+00 4.90298511E-02-1.35844414E-05    3
-2.92983743E-08 1.90820619E-11 6.37364803E+03 3.08073591E+01 8.00114499E+03    4
CH                TPIS79C   1H   1   00   00G   200.000  3500.000  1000.000    1
 2.87846473E+00 9.70913681E-04 1.44445655E-07-1.30687849E-10 1.76079383E-14    2
 7.10124364E+04 5.48497999E+00 3.48981665E+00 3.23835541E-04-1.68899065E-06    3
 3.16217327E-09-1.40609067E-12 7.07972934E+04 2.08401108E+00 8.62500000E+03    4
OH                IU3/03O   1 H  1    0    0G   200.000  6000.00  1000.00     1
 2.83853033E+00 1.10741289E-03-2.94000209E-07 4.20698729E-11-2.42289890E-15    2
 3.69780808E+03 5.84494652E+00 3.99198424E+00-2.40106655E-03 4.61664033E-06    3
-3.87916306E-09 1.36319502E-12 3.36889836E+03-1.03998477E-01 4.48613328E+03    4
O                 L 1/90O   1    0    0    0G   200.000  6000.00  1000.00     1
 2.54363697E+00-2.73162486E-05-4.19029520E-09 4.95481845E-12-4.79553694E-16    2
 2.92260120E+04 4.92229457E+00 3.16826710E+00-3.27931884E-03 6.64306396E-06    3
-6.12806624E-09 2.11265971E-12 2.91222592E+04 2.05193346E+00 2.99687009E+04    4
O2                RUS 89O   2    0    0    0G   200.000  6000.00  1000.00     1
 3.66096065E+00 6.56365811E-04-1.41149627E-07 2.05797935E-11-1.29913436E-15    2
-1.21597718E+03 3.41536279E+00 3.78245636E+00-2.99673416E-03 9.84730201E-06    3
-9.68129509E-09 3.24372837E-12-1.06394356E+03 3.65767573E+00 0.00000000E+00    4
HO2               T 1/09H   1O   2    0    0G   200.000  5000.00  1000.00     1
```

```
 4.17228741E+00 1.88117627E-03-3.46277286E-07 1.94657549E-11 1.76256905E-16    2
 3.10206839E+01 2.95767672E+00 4.30179807E+00-4.74912097E-03 2.11582905E-05    3
-2.42763914E-08 9.29225225E-12 2.64018485E+02 3.71666220E+00 1.47886045E+03    4
H2O               L 5/89H   2O   1    0    0G   200.000  6000.00  1000.00      1
 0.26770389E+01 0.29731816E-02-0.77376889E-06 0.94433514E-10-0.42689991E-14    2
-0.29885894E+05 0.68825500E+01 0.41986352E+01-0.20364017E-02 0.65203416E-05    3
-0.54879269E-08 0.17719680E-11-0.30293726E+05-0.84900901E+00-0.29084817E+05    4
C5H4O             PM3/96C   5H   4O   1    0G   300.000  3000.000              1
 0.10948009E+02 0.17044615E-01-0.71457334E-05 0.14228289E-08-0.11320175E-12    2
 0.19402539E+03-0.36391907E+02-0.33546367E+01 0.55846833E-01-0.41542669E-04    3
 0.90184651E-08 0.21885297E-11 0.42019507E+04 0.37696220E+02                   4
C2H3CHO           USC/07C   3H   4O   1    0G   300.000  5000.000              1
 0.58111868E+01 0.17114256E-01-0.74834161E-05 0.14252249E-08-0.91746841E-13    2
-0.10784054E+05-0.48588004E+01 0.12713498E+01 0.26231054E-01-0.92912305E-05    3
-0.47837272E-08 0.33480543E-11-0.93357344E+04 0.19498077E+02                   4
C2H3CO            MAR94 C   3H   3O   1    0g   300.00   5000.    1391.       1
 9.48105566e 00 7.77714755e-03-2.71155669e-06 4.26495971e-10-2.49722495e-14    2
 3.20858016e 03-2.42916680e 01 7.83370450e-01 2.90353899e-02-2.28846927e-05    3
 9.25645234e-09-1.52213238e-12 6.13409525e 03 2.20858902e 01                   4
A1C4H5     9/25/96 THERMC  10H  10    0    0G   300.000  5000.000 1398.000     1
 2.51177291E+01 2.71079788E-02-9.36415847E-06 1.46361840E-09-8.53182081E-14    2
 1.23688395E+04-1.10413157E+02-6.13672076E+00 1.09990763E-01-9.57033138E-05    3
 4.29399928E-08-7.72933039E-12 2.22598478E+04 5.39819170E+01                   4
C6H4C4H5   11/4/96      C  10H   9    0    0G   300.000  5000.000 1399.000     1
 2.39564235E+01 2.53884729E-02-8.73362025E-06 1.36110279E-09-7.91771494E-14    2
 4.38827792E+04-1.00939448E+02-4.73625698E+00 1.04085961E-01-9.37540000E-05    3
 4.36079149E-08-8.08842763E-12 5.27355971E+04 4.91106797E+01                   4
A1C4H4-4   9/25/96 THERMC  10H   9    0    0G   300.000  5000.000 1398.000     1
 2.49933174E+01 2.47057624E-02-8.54399023E-06 1.33644552E-09-7.79466457E-14    2
 4.24823359E+04-1.07850221E+02-5.20340439E+00 1.06405931E-01-9.54036939E-05    3
 4.38261772E-08-8.02465989E-12 5.18799868E+04 5.04120586E+01                   4
C3H5-S            G3B3  C   3H   5O   0N   0G   300.000  3000.000  1000.000    1
 2.02509360E+00 2.35513249E-02-1.28254556E-05 3.39579222E-09-3.51794724E-13    2
 3.11812042E+04 1.46653302E+01 3.13106581E-01 3.18769663E-02-2.53420013E-05    3
 1.02999073E-08-1.35301854E-12 3.13767683E+04 2.23728832E+01 1.37214139E+04    4
C3H4-P            T 2/90H   4C   3    0    0G   200.000  6000.000              1
 0.60252400E+01 0.11336542E-01-0.40223391E-05 0.64376063E-09-0.38299635E-13    2
 0.19620942E+05-0.86043785E+01 0.26803869E+01 0.15799651E-01 0.25070596E-05    3
-0.13657623E-07 0.66154285E-11 0.20802374E+05 0.98769351E+01 0.22302059E+05    4
CHCHCHO                C   3H   3O   1     g  0300.00   5000.00  1380.00      1
 1.02029457e 01 6.98642466e-03-2.40453423e-06 3.75386729e-10-2.18791232e-14    2
 1.44575591e 04-2.82423192e 01 2.03583477e 00 2.55739847e-02-1.81713324e-05    3
```

```
 6.28551145e-09-8.46222353e-13 1.73077219e 04 1.57368973e 01                   4
A1C2H2-I                C   8H   7    0    0g   300.000  5000.000 2047.000    1
 1.71139518e 01 2.25377917e-02-7.99496419e-06 1.27893717e-09-7.59484848e-14    2
 3.24892099e 04-6.28243270e 01-9.90113676e-01 6.36930626e-02-4.12377605e-05    3
 1.25738717e-08-1.42731738e-12 3.85039514e 04 3.42439436e 01                   4
C6H4C2H3          MAR94 C   8H   7    0    0g   300.000  5000.    1394.       1
 1.74540862e 01 2.22040686e-02-9.33350484e-06 1.73528698e-09-1.13685613e-13    2
 3.87604904e 04-6.90454166e 01-5.18004315e 00 8.45709724e-02-7.57339260e-05    3
 3.38554022e-08-6.01465106e-12 4.55621698e 04 4.89682087e 01                   4
C5H5CH3-1  4/29/96 THERMC   6H   8    0    0G   300.000  5000.000 1397.000    1
 1.57704224E+01 2.00188910E-02-6.88069149E-06 1.07186393E-09-6.23371891E-14    2
 3.44917855E+03-6.33204014E+01-4.67848294E+00 7.17775340E-02-5.80295089E-05    3
 2.43974501E-08-4.16614935E-12 1.01506608E+04 4.50860291E+01                   4
C5H4CH3                 H   7C   6          G   100.000  5000.000  960.13     1
 1.30070389E+01 1.91333167E-02-6.30281776E-06 1.18359139E-09-8.96495674E-14    2
 2.14514482E+04-4.45595826E+01 2.25035592E+00 2.16020882E-02 5.59945424E-05    3
-8.80066605E-08 3.50941532E-11 2.54687908E+04 1.70616625E+01                   4
C4H5-I            H6W/94C   4H   5    0    0G   300.000  3000.000             1
 0.10229092E+02 0.94850138E-02-0.90406445E-07-0.12596100E-08 0.24781468E-12    2
 0.34642812E+05-0.28564529E+02-0.19932900E-01 0.38005672E-01-0.27559450E-04    3
 0.77835551E-08 0.40209383E-12 0.37496223E+05 0.24394241E+02                   4
C4H6-12           A 8/83C   4H   6    0    0G   300.     3000.     1000.0     1
  0.1781557E 02 -0.4257502E-02  0.1051185E-04 -0.4473844E-08  0.5848138E-12    2
  0.1267342E 05 -0.6982662E 02  0.1023467E 01  0.3495919E-01 -0.2200905E-04    3
  0.6942272E-08 -0.7879187E-12  0.1811799E 05  0.1975066E 02  0.1950807E+05    4
C5H5CH3-2  BURCAT T10/94C   6H   8    0    0G   298.150  5000.000 1000.00     1
 0.16399698E+02 0.18988824E-01-0.60996114E-05 0.95861755E-09-0.59364731E-13    2
 0.48834021E+04-0.65341031E+02-0.35829269E+01 0.78077845E-01-0.73143499E-04    3
 0.33645368E-07-0.48086229E-11 0.10447644E+05 0.37418709E+02 0.12267710E+05    4
C5H5CH3-5  FITBOZELLI   C   6H   8    0    0G   300.000  5000.000 1363.000    1
 1.42358779E+01 2.23433609E-02-7.91414849E-06 1.25775234E-09-7.41691900E-14    2
 6.02181337E+03-5.68678735E+01-1.67229500E+00 4.86346771E-02-1.94776538E-05    3
 4.98106965E-10 9.33947219E-13 1.27501719E+04 3.26259083E+01                   4
C4H3-I            AB1-93H   3C   4          G     300.0    3000.0  1000.0     1
    9.0978165E0   9.2207119E-3  -3.3878441E-6  4.9160498E-10  -1.452978E-14    2
    5.6600574E4   -1.9802597E1    2.0830412E0   4.0834274E-2  -6.2159685E-5    3
   5.1679358E-8 -1.7029184E-11    5.8005129E4    1.3617462E1                   4
C5H6O-2    5/15/96      C   5H   6O   1    0G   300.000  5000.000 1377.000    1
 1.46518014E+01 1.71432085E-02-6.08092351E-06 9.67447628E-10-5.70963907E-14    2
-2.16069106E+04-6.13066535E+01-4.38894997E+00 5.70919265E-02-3.59745510E-05    3
 1.01204988E-08-9.42938595E-13-1.45945285E+04 4.24752788E+01                   4
CO2               L 7/88C   1O   2   00   00G   200.000  3500.000  1000.000    1
```

```
 3.85746029E+00 4.41437026E-03-2.21481404E-06 5.23490188E-10-4.72084164E-14    2
-4.87591660E+04 2.27163806E+00 2.35677352E+00 8.98459677E-03-7.12356269E-06    3
 2.45919022E-09-1.43699548E-13-4.83719697E+04 9.90105222E+00 9.36546900E+03    4
C5H5O-13          PM3/96C   5H   5O   1    0G   300.000  3000.000             1
 0.12374012E+02 0.17309485E-01-0.65852723E-05 0.11661907E-08-0.81730223E-13    2
-0.41964380E+04-0.41368584E+02-0.36890411E+00 0.36575675E-01 0.18297369E-04    3
-0.59576148E-07 0.29254717E-10-0.62515869E+02 0.27862198E+02                   4
C5H5O-14          PM3/96C   5H   5O   1    0G   300.000  3000.000             1
 0.13169959E+02 0.15550226E-01-0.51386078E-05 0.65631761E-09-0.16959780E-13    2
-0.19228318E+04-0.45589508E+02 0.11064005E+00 0.33403017E-01 0.26840644E-04    3
-0.69127687E-07 0.32994329E-10 0.23940938E+04 0.25787146E+02                   4
C5H6O-3    5/15/96      C   5H   6O   1    0G   300.000  5000.000 1380.000    1
 1.42902852E+01 1.74573768E-02-6.19160116E-06 9.85023447E-10-5.81338262E-14    2
-1.86118767E+04-5.89348198E+01-6.48602406E+00 6.15484948E-02-3.94723543E-05    3
 1.11895413E-08-1.02537693E-12-1.10534845E+04 5.40563191E+01                   4
C4H6-1            120189C   4H   6          g  0300.00   4000.00  1000.00     1
 0.01200695e+03 0.09576069e-01-0.08995018e-05-0.05369808e-08 0.09934174e-12    2
 0.01729420e+06-0.03802692e+03 0.03726043e+02 0.02053493e+00 0.03021439e-04    3
-0.08131813e-07 0.01095280e-10 0.02048821e+06 0.08538826e+02                   4
C4H5-121               C   4H   5    0    0g   300.000  5000.000 1558.000    1
 1.15707301e 01 1.10521653e-02-3.74679986e-06 5.78988738e-10-3.35056170e-14    2
 3.28916203e 04-3.61427241e 01 3.87375812e 00 2.35292310e-02-7.91954580e-06    3
-1.34382648e-09 9.26833346e-13 3.60697147e 04 7.07337245e 00                   4
C4H5-123           82489C   4H   5          g  0300.00   4000.00  1000.00     1
 0.01156506e+03 0.08030297e-01-0.07649450e-05-0.04476534e-08 0.08313260e-12    2
 0.03256813e+06-0.03014066e+03 0.05068450e+02 0.01571747e+00 0.02968975e-04    3
-0.04990587e-07-0.02984224e-11 0.03518855e+06 0.06791893e+02                   4
C4H6-2            A 8/83C   4H   6    0    0G   300.     3000.     1000.0     1
  9.0338133E+00 8.2124510E-03   7.1753952E-06 -5.8834334E-09  1.0343915E-12    2
  1.4335068E+04 -2.0985762E+01  2.1373338E+00  2.6486229E-02 -9.0568711E-06    3
 -5.5386397E-19 2.1281884E-22   1.5710902E+04  1.3529426E+01  1.7488676E+04    4
A1CO        tHerM       C   7H   5O   1    0g   300.000  5000.000 1392.000    1
 1.75116258e+01 1.62650511e-02-5.65051892e-06 8.86922680e-10-5.18657990e-14    2
 4.67641545e+03-6.70531966e+01-1.56729686e+00 5.99817511e-02-4.29153585e-05    3
 1.48666854e-08-1.98938453e-12 1.12873830e+04 3.55490009e+01                   4
C10H10            MAR94 C  10H  10    0    0g   300.000  5000.    1394.       1
 2.29880333e 01 2.98673083e-02-1.03408159e-05 1.61884929e-09-9.44755534e-14    2
 3.83422928e 03-1.04059080e 02-7.70165798e 00 1.04115841e-01-7.97562323e-05    3
 3.14343302e-08-5.04355723e-12 1.42169008e 04 5.98250716e 01                   4
C10H9             MAR94 C  10H   9    0    0g   300.000  5000.    1392.       1
 2.27884959e 01 2.78271679e-02-9.71214416e-06 1.52855130e-09-8.95351533e-14    2
 1.71260507e 04-1.04051271e 02-7.41682284e 00 1.01265732e-01-7.90577209e-05    3
```

```
 3.17566399e-08-5.19920372e-12 2.73369737e 04 5.71663310e 01                   4
C9H9       2/26/96 THERMC   9H   9    0    0G   300.000  5000.000 1399.000     1
 2.26728087E+01 2.36911196E-02-8.02389316E-06 1.23913095E-09-7.16761559E-14    2
 1.20693162E+04-1.01228503E+02-9.24864062E+00 1.04828177E-01-8.70354537E-05    3
 3.61409728E-08-5.94893666E-12 2.23164040E+04 6.75781563E+01                   4
C9H8O      9/ 3/96 THERMC   9H   8O   1    0G   300.000  5000.000 1392.000     1
 2.19442927E+01 2.54740607E-02-8.78772129E-06 1.37273323E-09-8.00028755E-14    2
-1.79570979E+04-9.45605022E+01-6.01589886E+00 9.32450493E-02-7.19851447E-05    3
 2.83246893E-08-4.50591137E-12-8.54773739E+03 5.46421815E+01                   4
CH2CO             D05/90C   2H   2O   1   00G   200.000  3500.000  1000.000    1
 4.51129732E+00 9.00359745E-03-4.16939635E-06 9.23345882E-10-7.94838201E-14    2
-7.77850000E+03 6.32247205E-01 2.13583630E+00 1.81188721E-02-1.73947474E-05    3
 9.34397568E-09-2.01457615E-12-7.27000000E+03 1.22156480E+01 1.17977430E+04    4
C8H6O             T 1/94C   8H   6O   1    0G   298.150  5000.000  1000.00     1
 0.16260779E+02 0.25251982E-01-0.98113297E-05 0.17473791E-08-0.11720720E-12    2
-0.46522585E+04-0.64478655E+02-0.39760390E+01 0.68789961E-01-0.22095246E-04    3
-0.28325945E-07 0.18870094E-10 0.16310801E+04 0.43193929E+02 0.32608440E+04    4
C6H7              MAR94 C   6H   7    0    0g   300.00   5000.    1378.00      1
 1.62179737e 01 1.76354762e-02-6.10140365e-06 9.55946476e-10-5.58580718e-14    2
 1.64611253e+04-6.76882854e+01-5.92510435e+00 6.58626515e-02-4.35988397e-05    3
 1.28973156e-08-1.26423888e-12 2.43278179e+04 5.21888505e+01                   4
A1CH2OH           T10/06C  7.H  8.O  1.   0.G   300.000  3000.000  1000.      1
 1.51623145E+01 2.69370369E-02-9.80289631E-06 1.59282076E-09-9.57107837E-14    2
-1.88226234E+04-5.47426976E+01 2.85739935E+00 2.38770620E-02 8.40508017E-05    3
-1.33985586E-07 5.69938876E-11-1.37956049E+04 1.73101737E+01-1.13776999E+04    4
C6H5                    H   5C   6          G   100.000  5000.000 1111.42     1
 8.04340231E+00 2.28159936E-02-9.79698517E-06 1.91185936E-09-1.38968232E-13    2
 3.64643943E+04-2.01899408E+01 2.73502012E+00 1.95854895E-02 2.47071596E-05    3
-3.68662381E-08 1.26508293E-11 3.90238646E+04 1.21867178E+01                   4
C6H6                    H   6C   6          G   100.000  5000.000 867.61      1
 6.59144581E+00 2.90304399E-02-1.26939777E-05 2.51919337E-09-1.85875347E-13    2
 6.05022791E+03-1.51888734E+01 1.03727301E+00 1.53133085E-02 7.90087353E-05    3
-1.20186313E-07 5.02249451E-11 8.49403078E+03 1.93474419E+01                   4
C6H10                   H  10C   6          G   100.000  5000.000 1007.85     1
 1.18247614E+01 3.08764588E-02-1.20828589E-05 2.22412529E-09-1.55986303E-13    2
 9.54037185E+02-3.50936615E+01 1.32866272E+00 4.76530656E-02-2.09269242E-08    3
-3.02497071E-08 1.39753941E-11 4.33337047E+03 2.18950124E+01                   4
A1CH2       TROEjpC,1990C   7H   7    0    0g   300.000  5000.000 1392.000     1
 1.77752663e+01 1.88366755e-02-6.58968982e-06 1.03873424e-09-6.09096279e-14    2
 1.65061292e+04-7.37168331e+01-3.82523574e+00 7.22854694e-02-5.81397283e-05    3
 2.40211852e-08-4.03015544e-12 2.37153019e+04 4.12436407e+01                   4
A1C2H                   C   8H   6          G   100.000  5000.000 1024.06      1
```

```
 1.42351344E+01 2.54058423E-02-1.04381414E-05 1.97333909E-09-1.40490294E-13    2
 3.17767101E+04-5.07360860E+01 1.04702485E+00 5.37797899E-02-1.81056194E-05    3
-1.51000969E-08 9.41428169E-12 3.56910783E+04 1.91263927E+01                   4
C2H6              G-8-88H   6C   2          G     200.0    6000.0  1000.0     1
   4.04666411E0  1.53538802E-2 -5.47039485E-6 8.77826544E-10-5.23167531E-14    2
  -1.24473499E4 -9.68698313E-1   4.29142572E0 -5.50154901E-3  5.99438458E-5    3
 -7.08466469E-8 2.68685836E-11  -1.15222056E4   2.66678994E0                   4
C2H3O-C           T 9/92C   2H   3O   1    0G 298.150  3000.000   1000.00     1
 0.48131470E+00 0.20711914E-01-0.12693155E-04 0.34579642E-08-0.35399703E-12    2
 0.15648642E+05 0.34629876E+02 0.10854772E+01 0.12845259E-01 0.24138660E-05    3
-0.44642672E-08-0.29381916E-12 0.15910655E+05 0.33395312E+02 0.16817588E+05    4
C4H10             P11/94C   4H  10    0    0G   300.000  3000.000              1
 0.10526774E+02 0.23590738E-01-0.78522480E-05 0.11448408E-08-0.59827703E-13    2
-0.20479223E+05-0.32198579E+02 0.15685419E+01 0.34652278E-01 0.68168129E-05    3
-0.27995097E-07 0.12307742E-10-0.17129977E+05 0.17908045E+02                   4
C4H9-1            USC/07C   4H   9O   0    0G   300.000  5000.000              1
 0.86822395E+01 0.23691071E-01-0.75948865E-05 0.66427136E-09 0.54845136E-13    2
 0.49644058E+04-0.17891747E+02 0.12087042E+01 0.38297497E-01-0.72660509E-05    3
-0.15428547E-07 0.86859435E-11 0.73221040E+04 0.22169268E+02                   4
C4H9-2            USC/07C   4H   9O   0    0G   300.000  5000.000              1
 0.84981728E+01 0.24689538E-01-0.86487589E-05 0.10779325E-08-0.64340570E-15    2
 0.44288174E+04-0.18441397E+02 0.97527862E+00 0.41613799E-01-0.14467331E-04    3
-0.93852393E-08 0.68797377E-11 0.66688267E+04 0.21277582E+02                   4
C4H7-I    Burcat20008/83C   4H   7    0    0G   300.     3000.    1000.       1
 0.5521420E+01  0.2683684E-01 -0.1286430E-04  0.3088640E-08 -0.3030856E-12     2
 0.1198044E+05 -0.4482447E+01 -0.1080514E+01  0.4638686E-01 -0.3464697E-04     3
 0.1401374E-07 -0.2395040E-11  0.1375538E+05  0.2934466E+02                   4
C4H4-123           82489C   4H   4          g  0300.00   4000.00  1000.00     1
 0.01062083e+03 0.07199370e-01-0.06806234e-05-0.04021185e-08 0.07378498e-12    2
 0.03358798e+06-0.03193583e+03 0.03849007e+02 0.01713169e+00 0.01644270e-04    3
-0.07761590e-07 0.01947860e-10 0.03608372e+06 0.05732121e+02                   4
C5H5O-24          PM3/96C   5H   5O   1    0G   300.000  3000.000              1
 0.73781247E+01 0.25073020E-01-0.11180981E-04 0.22804640E-08-0.17065700E-12    2
 0.18617090E+05-0.15289108E+02-0.28933799E+01 0.50778717E-01-0.26535929E-04    3
-0.42241357E-08 0.62547003E-11 0.21495141E+05 0.38197586E+02                   4
C4H5CO     10/29/96     C   5H   5O   1    0G   300.000  5000.000 1396.000     1
 1.58085169E+01 1.21091896E-02-4.19157321E-06 6.55964091E-10-3.82687739E-14    2
 5.36837386E+03-5.71877022E+01-2.21823023E-01 5.92535187E-02-5.88130628E-05    3
 2.94945976E-08-5.77646233E-12 1.00455214E+04 2.55999547E+01                   4
VINCOC2H2  8/ 2/97 THERMC   5H   5O   1    0G   300.000  5000.000 1392.000     1
 1.49811127E+01 1.29779877E-02-4.52943110E-06 7.12789532E-10-4.17465190E-14    2
 1.80992122E+04-5.04067637E+01 4.97273994E-01 5.08283705E-02-4.37783152E-05    3
```

```
 1.96626145E-08-3.57467555E-12 2.27836549E+04 2.60510972E+01                   4
C3H7-N            P11/94C   3H   7    0    0G   300.000  3000.000             1
 0.77097479E+01 0.16031485E-01-0.52720238E-05 0.75888352E-09-0.38862719E-13    2
 0.79762236E+04-0.15515297E+02 0.10491173E+01 0.26008973E-01 0.23542516E-05    3
-0.19595132E-07 0.93720207E-11 0.10312346E+05 0.21136034E+02                   4
C3H7-I            P11/94C   3H   7    0    0G   300.000  3000.000             1
 0.65192741E+01 0.17220104E-01-0.57364217E-05 0.84130732E-09-0.44565913E-13    2
 0.73227193E+04-0.90830215E+01 0.14449199E+01 0.20999112E-01 0.77036222E-05    3
-0.18476253E-07 0.71282962E-11 0.94223724E+04 0.20116317E+02                   4
CH3CO             T 9/92C   2H   3O   1    0G   200.000  6000.0    1000.0     1
 0.59447731E+01 0.78667205E-02-0.28865882E-05 0.47270875E-09-0.28599861E-13    2
-0.37873075E+04-0.50136751E+01 0.41634257E+01-0.23261610E-03 0.34267820E-04    3
-0.44105227E-07 0.17275612E-10-0.26574529E+04 0.73468280E+01-0.12027167E+04    4
CH3CHCO           MAR94 C   3H   4O   1    0g   300.00   5000.    1392.       1
 9.40386796e 00 9.90994860e-03-3.34130605e-06 5.13787016e-10-2.96102254e-14    2
-1.42771281e 04-2.42902025e 01 2.69187311e 00 2.49761396e-02-1.61712107e-05    3
 5.46391115e-09-7.62496644e-13-1.18758805e 04 1.19898101e 01                   4
CH2CHO            D05/83O   1H   3C   2    0G   300.000  5000.000             1
 0.59756699E+01 0.81305914E-02-0.27436245E-05 0.40703041E-09-0.21760171E-13    2
-0.96950000E+03-0.50320879E+01 0.34090624E+01 0.10738574E-01 0.18914925E-05    3
-0.71585831E-08 0.28673851E-11 0.62000000E+02 0.95714535E+01 0.30474436E+04    4
CH3CHO            L 8/88C   2H   4O   1    0G   200.000  6000.0    1000.0     1
 0.54041108E+01 0.11723059E-01-0.42263137E-05 0.68372451E-09-0.40984863E-13    2
-0.22593122E+05-0.34807917E+01 0.47294595E+01-0.31932858E-02 0.47534921E-04    3
-0.57458611E-07 0.21931112E-10-0.21572878E+05 0.41030159E+01-0.19987949E+05    4
CH3A1CH2          MAR94 C   8H   9    0    0g   300.000  5000.000 1390.000    1
 2.02877023e 01 2.38848411e-02-8.23202298e-06 1.30847851e-09-7.65835818e-14    2
 1.12047828e 04-8.57677163e 01-2.37164288e 00 7.61932716e-02-5.46335287e-05    3
 2.00939215e-08-3.02944543e-12 1.91590196e 04 3.61877664e 01                   4
C2HCHO                  C   3H   2O   1     g  0300.00   5000.00  1383.00     1
 9.53489086e 00 5.27356380e-03-1.86790292e-06 2.96884935e-10-1.75093893e-14    2
 7.94341348e 03-2.51820453e 01 2.96395961e 00 2.11989287e-02-1.69306862e-05    3
 6.91407180e-09-1.15124164e-12 1.01776675e 04 9.92163123e 00                   4
C4H2              D11-99H   2C   4          G     300.0    3000.0  1000.0     1
    9.1576328E0   5.5430518E-3  -1.3591604E-6  1.8780075E-11  2.3189536E-14    2
    5.2588039E4    -2.371146E1    1.0543978E0    4.162696E-2  -6.5871784E-5    3
   5.3257075E-8 -1.6683162E-11    5.4185211E4    1.4866591E1                   4
H2C4O             USC/07C   4H   2O   1    0G   300.000  5000.000             1
 0.84292183E+01 0.10502701E-01-0.42066836E-05 0.71184902E-09-0.35796602E-13    2
 0.22907807E+05-0.16511997E+02 0.31811900E+01 0.29840752E-01-0.32832409E-04    3
 0.20631813E-07-0.54200598E-11 0.24125576E+05 0.94210100E+01                   4
CH2-S             L S/93C   1H   2   00   00G   200.000  3500.000  1000.000    1
```

```
 2.87410113E+00 3.65639292E-03-1.40894597E-06 2.60179549E-10-1.87727567E-14    2
 4.62636040E+04 6.17119324E+00 3.76267867E+00 9.68872143E-04 2.79489841E-06    3
-3.85091153E-09 1.68741719E-12 4.60040401E+04 1.56253185E+00 1.00274170E+04    4
CH2               IU3-03H   2C   1          G     200.0    6000.0  1000.0      1
   3.14631886E0  3.03671259E-3 -9.96474439E-7  1.5048358E-10-8.57335515E-15    2
   4.60412605E4   4.72341711E0   3.71757846E0   1.2739126E-3  2.17347251E-6    3
   -3.488585E-9 1.65208866E-12   4.58723866E4   1.75297945E0                   4
C3H8              P11/94C   3H   8    0    0G   300.000  3000.000              1
 0.75244152E+01 0.18898282E-01-0.62921041E-05 0.92161457E-09-0.48684478E-13    2
-0.16564394E+05-0.17838375E+02 0.92851093E+00 0.26460566E-01 0.60332446E-05    3
-0.21914953E-07 0.94961544E-11-0.14057907E+05 0.19225538E+02                   4
C5H3               20387C   5H   3          g  0300.00   5000.00  1000.00      1
 0.10787622e+02 0.09539619e-01-0.03206744e-04 0.04733323e-08-0.02512135e-12    2
 0.06392904e+06-0.03005444e+03 0.04328720e+02 0.02352480e+00-0.05856723e-04    3
-0.12154494e-07 0.07726478e-10 0.06588531e+06 0.04173258e+02                   4
CH                TPIS79C   1H   1   00   00G   200.000  3500.000  1000.000    1
 2.87846473E+00 9.70913681E-04 1.44445655E-07-1.30687849E-10 1.76079383E-14    2
 7.10124364E+04 5.48497999E+00 3.48981665E+00 3.23835541E-04-1.68899065E-06    3
 3.16217327E-09-1.40609067E-12 7.07972934E+04 2.08401108E+00 8.62500000E+03    4
C5H2               20587C   5H   2          g  0300.00   5000.00  1000.00      1
 0.01132917e+03 0.07424057e-01-0.02628189e-04 0.04082541e-08-0.02301333e-12    2
 0.07878706e+06-0.03617117e+03 0.03062322e+02 0.02709998e+00-0.01009170e-03    3
-0.01272745e-06 0.09167219e-10 0.08114969e+06 0.07071078e+02                   4
C6H2              T 3/92C   6H   2    0    0G  300.000   3000.000  1000.       1
 0.12532801E+02 0.87766321E-02-0.31329616E-05 0.50371820E-09-0.30071921E-13    2
 0.79784338E+05-0.38858580E+02-0.54109216E+00 0.74532628E-01-0.13578252E-03    3
 0.12226630E-06-0.41825207E-10 0.82115132E+05 0.21882710E+02 0.84288792E+05    4
C4H4CHO    8/26/96      C   5H   5O   1    0G   300.000  5000.000 1396.000    1
 1.62360823E+01 1.18297101E-02-4.11454219E-06 6.46026823E-10-3.77767639E-14    2
 1.93499885E+04-5.83498817E+01-5.06628841E-01 6.04671965E-02-5.97396749E-05    3
 2.96804228E-08-5.76240010E-12 2.42765544E+04 2.82994148E+01                   4
C4H3-N            H6W-94H   3C   4          G     300.0    3000.0  1000.0      1
    5.4328279E0   1.6860981E-2  -9.4313109E-6   2.5703895E-9 -2.7456309E-13    2
     6.160068E4   -1.5673981E0  -3.1684113E-1     4.69121E-2   -6.809381E-5    3
   5.3179921E-8 -1.6523005E-11    6.2476199E4    2.4622559E1                   4
C3H5-A            PD5/98C   3H   5    0    0G   300.000  3000.000              1
 0.65007877E+01 0.14324731E-01-0.56781632E-05 0.11080801E-08-0.90363887E-13    2
 0.17482449E+05-0.11243050E+02 0.13631835E+01 0.19813821E-01 0.12497060E-04    3
-0.33355555E-07 0.15846571E-10 0.19245629E+05 0.17173214E+02                   4
C3H4-A            L 8/89C   3H   4    0    0G   200.000  6000.000              1
 0.63168722E+01 0.11133728E-01-0.39629378E-05 0.63564238E-09-0.37875540E-13    2
 0.20117495E+05-0.10995766E+02 0.26130445E+01 0.12122575E-01 0.18539880E-04    3
```

```
-0.34525149E-07 0.15335079E-10 0.21541567E+05 0.10226139E+02 0.22962267E+05    4
HCCOH              SRI91C   2O   1H   20   0G   300.000  5000.000   1000.G     1
 0.59238291E+01 0.67923600E-02-0.25658564E-05 0.44987841E-09-0.29940101E-13    2
 0.72646260E+04-0.76017742E+01 0.12423733E+01 0.31072201E-01-0.50866864E-04    3
 0.43137131E-07-0.14014594E-10 0.80316143E+04 0.13874319E+02                   4
C2HCO                   C   3H   1O   1     g  0300.00   5000.00  1453.00     1
 4.72901298e 00 8.55263742e-03-3.11261630e-06 4.45053019e-10-2.03272018e-14    2
 2.88623722e 04 6.44697916e 00 6.40938042e 00 1.15715116e-02-1.02639923e-05    3
 4.52524382e-09-8.02150325e-13 2.70126564e 04-5.92675057e 00                   4
CHOCHO             tHerM C   2H   2O   2    0g   300.     5000.    1396.       1
 9.75438561e 00 4.97645947e-03-1.74410483e-06 2.75586994e-10-1.61969892e-14    2
-2.95832896e 04-2.48038370e 01 1.88105121e 00 2.36386368e-02-1.83443295e-05    3
 6.84842963e-09-9.92733674e-13-2.69280190e 04 1.72994753e 01                   4
C2                 121286C   2               G  0300.00   5000.00  1000.00     1
 0.04135978E+02 0.06531618E-03 0.01837099E-05-0.05295085E-09 0.04712137E-13    2
 0.09967272E+06 0.07472923E+01 0.06996045E+02-0.07400601E-01 0.03234703E-04    3
 0.04802535E-07-0.03295917E-10 0.09897487E+06-0.13862268E+02                   4
C2O                RUS 79C   2O   1    0    0G   200.000  6000.000             1
 0.51512722E+01 0.23726722E-02-0.76135971E-06 0.11706415E-09-0.70257804E-14    2
 0.33241888E+05-0.22183135E+01 0.28648610E+01 0.11990216E-01-0.18362448E-04    3
 0.15769739E-07-0.53897452E-11 0.33749932E+05 0.88867772E+01 0.35003406E+05    4
CH3O               IU1/03C   1H   3O   1     G   200.000  6000.00              1
 4.75779238E+00 7.44142474E-03-2.69705176E-06 4.38090504E-10-2.63537098E-14    2
 3.78111940E+02-1.96680028E+00 3.71180502E+00-2.80463306E-03 3.76550971E-05    3
-4.73072089E-08 1.86588420E-11 1.29569760E+03 6.57240864E+00 2.52571660E+03    4
HCOH               MAR94 C   1H   2O   1    0g   300.     5000.    1398.       1
 9.18749272e 00 1.52011152e-03-6.27603516e-07 1.09727989e-10-6.89655128e-15    2
 7.81364593e 03-2.73434214e 01-2.82157421e 00 3.57331702e-02-3.80861580e-05    3
 1.86205951e-08-3.45957838e-12 1.12956672e 04 3.48487757e 01                   4
CH3OH              L 8/88C   1H   4O   1   00G   200.000  3500.000  1000.000    1
 1.78970791E+00 1.40938292E-02-6.36500835E-06 1.38171085E-09-1.17060220E-13    2
-2.53748747E+04 1.45023623E+01 5.71539582E+00-1.52309129E-02 6.52441155E-05    3
-7.10806889E-08 2.61352698E-11-2.56427656E+04-1.50409823E+00 1.14352770E+04    4
C9H10      2/26/96 THERMC   9H  10    0    0G   300.000  5000.000 1395.000    1
 2.28149173E+01 2.59004648E-02-8.74436616E-06 1.34774960E-09-7.78601230E-14    2
-4.41762245E+03-1.03131536E+02-9.22089628E+00 1.04472866E-01-8.20101464E-05    3
 3.21662864E-08-5.00494710E-12 6.14702594E+03 6.72855805E+01                   4
A1CH3                   C   7H   8          G   100.000  5000.000 1073.72      1
 9.30667130E+00 3.36713230E-02-1.41158452E-05 2.69973752E-09-1.93204076E-13    2
5.79813528E+02-2.68610894E+01 2.05719474E+00 3.12152776E-02 3.04758250E-05    3
-5.05435593E-08 1.81542493E-11 3.83493690E+03 1.65378111E+01                   4
A1C2H3                  C   8H   8          G   100.000  5000.000  908.14      1
```

```
 1.35644523E+01 2.85577143E-02-9.77956044E-06 1.73692901E-09-1.23055469E-13    2
 1.13341567E+04-4.66993022E+01 1.35925094E+00 3.82561053E-02 4.69783478E-05    3
-9.33553133E-08 4.07624191E-11 1.53678302E+04 2.10109659E+01                   4
A1C2H2-N                C   8H   7    0    0g   300.000  5000.000 1394.000     1
 1.87665766e 01 2.00619262e-02-6.90883699e-06 1.07799789e-09-6.27759176e-14    2
 3.76791153e 04-7.60276228e 01-2.72251268e 00 7.09701368e-02-5.27526320e-05    3
 1.97369835e-08-2.95890798e-12 4.50007235e 04 3.90143531e 01                   4
```

LIST OF PUBLICATIONS

1. Kunal Dhoke, K P J Reddy, and E. Arunan, Shock Tube Ignition Delay Studies of Dicyclopentadiene, International Symposium on Shock Waves 30, Tel-Aviv, Israel.,2015.
2. Kunal Dhoke, K P J Reddy, G. Jagadeesh, and E. Arunan, Shock Tube Thermal Decomposition of Dicyclopentadiene: Experiment and Computation Study (Manuscript under preparation)
3. Kunal Dhoke, K P J Reddy, G. Jagadeesh, and E. Arunan, Shock Tube Ignition Delay Studies of Dicyclopentadiene: Experiment and Kinetic Modelling (Manuscript under preparation)
4. Kunal Dhoke, and E. Arunan, Theoretical Investigation on Dissociation Reaction of dicyclopentadiene to cyclopentadiene conversion (Manuscript under preparation).
5. Kunal Dhoke, Tarandeep Singh, K P J Reddy, G. Jagadeesh, and E. Arunan, Driver Insert: A Strategy to Achieve Near-ideal Behavior Behind Reflected Shock-wave (Manuscript under preparation)